

Programa de Química Orgánica

Tesis Doctoral

**Synthesis, Biological Evaluation and  
Insights into the Mode of Action of  
Quinoxaline Containing Peptides**

Rubí Zamudio Vázquez

Dirigida y revisada por:

Dr. Fernando Albericio

(Universitat de Barcelona)

Dra. Judit Tulla Puche

(Institut de Recerca Biomèdica Barcelona)

Barcelona, 2014



# **Synthesis, Biological Evaluation and Insights into the Mode of Action of Quinoxaline Containing Peptides**

I thankfully acknowledge "la Caixa" Foundation and IRB Barcelona for awarding me a "La Caixa/IRB Barcelona International PhD Programme Fellowship" to undertake this research project within the "Combinatorial Chemistry" group.



Rubí Zamudio Vázquez

Barcelona, 2014



*A mi madre,*

*porque has luchado mil batallas y nunca te has rendido.*



---

|                            |      |
|----------------------------|------|
| Annexes                    | v    |
| Abbreviations and acronyms | viii |

|   |    |
|---|----|
| <b>INTRODUCTION AND OBJECTIVES</b>                                | 1  |
| General introduction  | 3  |
| Objectives  | 7  |
| References  | 8  |
| <br>  |    |
| <b>CHEMICAL SYNTHESIS</b>   | 11 |
| Introduction  | 13 |
| Results and discussion  | 22 |
| Design of the RZ1-RZ12 library                                    | 22 |
| Synthesis of the RZ1-RZ12 library                                 | 25 |
| <i>Protection scheme</i>  | 25 |
| <i>Polymeric support</i>  | 25 |
| <i>Ethylenediamine, first entity attached on the 2-CTC resin</i>  | 26 |
| <i>In situ N-methylation on the solid support</i>                 | 28 |
| <i>Coupling reagents</i>  | 29 |
| Coupling system for peptide elongation on solid phase             | 29 |
| Reagents for the introduction of the QC moieties in solution      | 31 |
| <i>Monitoring</i>   | 31 |
| <i>Peptide cleavage from the solid support</i>                    | 31 |
| <i>General synthetic strategy scheme for peptide elongation</i>   | 33 |
| The designed peptides without QC moieties: Z1-Z12 peptide library | 34 |
| Z1-Z12 peptides with QC moieties: RZ1-RZ12 library                | 35 |
| Fluorescent versions of the compound RZ2                          | 36 |
| <i>Compound RZ2CF</i>   | 37 |

---

|   |     |
|---|-----|
| <i>Compound RZ2_EDAQC</i>   | 38  |
| <i>Compound RZ2_EDACF</i>   | 39  |
| Other simplified analogues based on RZ2: compounds RZV                        | 40  |
| <i>Compound RZV13</i>   | 40  |
| <i>Compound RZV14</i>   | 41  |
| <i>Compound RZV15</i>   | 42  |
| Alloc-NMe-Cys(Me)-OH synthesis  | 43  |
| Positive control for biological assays: triostin A synthesis                  | 45  |
| Alloc-NMe-Val-OH synthesis  | 45  |
| Boc-NMe-Cys(Acm)-OH synthesis   | 46  |
| <i>Triostin A</i>   | 46  |
| Materials and methods   | 48  |
| References  | 103 |
| <br>  |     |
| <b>BIOLOGICAL EVALUATION</b>  | 107 |
| Introduction  | 109 |
| Results and discussion  | 115 |
| Antitumoral activity evaluation   | 115 |
| <i>Preliminari studies to determine the best conditions for the MTT assay</i> | 117 |
| Detection limits  | 117 |
| Exponential growth phase  | 119 |
| Doubling time   | 130 |
| <i>Preliminari chemosensitivity test using only</i>                           |     |
| <i>one concentration of compound</i>  | 131 |
| <i>IC50 values for the library RZ1-RZ12 against tumor cells</i>               | 133 |
| <i>IC50 value for most active compound, RZ2, against non-tumor cells</i>      | 137 |
| <i>Cytotoxic activity of peptides Z1-Z12</i>                                  | 138 |
| <i>Cytotoxic activity of compounds RZV</i>                                    | 138 |

---

|   |     |
|---|-----|
| <i>Cytotoxic activity of the fluorescent versions of compound RZ2</i> | 139 |
| Stability assays of compound RZ2                                      | 140 |
| Enhancing RZ2 cytotoxicity through a liposomal formulation            | 142 |
| Antibacterial activity evaluation                                     | 144 |
| Antiviral activity evaluation   | 145 |
| Antiplasmodial activity evaluation                                    | 146 |
| <i>Hemocompatibility of compound RZ2</i>                              | 147 |
| Materials and methods   | 148 |
| References  | 154 |
| <br>  |     |
| <b>INSIGHTS INTO THE MODE OF ACTION</b>                               | 159 |
| Introduction  | 161 |
| Results and discussion  | 166 |
| DNA-binding assays  | 166 |
| <i>Circular dichroism spectroscopy</i>                                | 167 |
| <i>Band shift experiment</i>  | 170 |
| <i>DNase I footprinting</i>   | 171 |
| Molecular dynamics simulations  | 179 |
| Topoisomerase inhibition assay  | 187 |
| <i>Topoisomerase I activity assay</i>                                 | 188 |
| <i>Topoisomerase II activity assay</i>                                | 189 |
| Studies on the mechanism of cell death                                | 191 |
| <i>Does RZ2 cause necrosis to cancer cells?</i>                       | 191 |
| <i>Does RZ2 cause apoptosis to cancer cells?</i>                      | 194 |
| <i>Does RZ2 cause a cell-cycle arrest?</i>                            | 197 |
| <i>Does RZ2 trigger autophagy?</i>                                    | 199 |
| <i>RZ2 is internalized into the cell in acidic compartments</i>       | 200 |
| Gene expression microarray  | 203 |

|  |            |
|--|------------|
| Effects of RZ2 on mitochondria   | 207        |
| Materials and methods  | 210        |
| References   | 222        |
| <br>   |            |
| <b>GENERAL CONCLUSIONS</b>   | <b>226</b> |
| <br>   |            |
| <b>RESUMEN EN ESPAÑOL</b>  | <b>231</b> |
| SÍNTESIS, EVALUACIÓN BIOLÓGICA Y ESTUDIOS SOBRE EL<br>MODO DE ACCIÓN DE PÉPTIDOS UNIDOS A QUINOXALINAS | 233        |

| Amino acid*                 | Code**     | Chemical structure |
|-----------------------------|------------|--------------------|
| $\alpha$ -aminobutyric acid | Abu        |                    |
| Alanine                     | Ala<br>A   |                    |
| Aspartic acid               | Asp<br>D   |                    |
| Cysteine                    | Cys<br>C   |                    |
| Glycine                     | Gly<br>G   |                    |
| Isoleucine                  | Ile<br>I   |                    |
| D-Proline                   | D-Pro<br>p |                    |
| Serine                      | Ser<br>S   |                    |
| D-Serine                    | D-Ser<br>S |                    |
| Threonine                   | Thr<br>T   |                    |
| Valine                      | Val<br>V   |                    |

\* Amino acids are represented on the L-configuration unless otherwise indicated.

\*\* In this table, lower case letters describe D-amino acids. When possible, the three-letter code for each amino acid is expressed.

| Protecting group            | Symbol | Chemical structure |
|-----------------------------|--------|--------------------|
| Acetamidomethyl             | Acm    |                    |
| Allyl                       | All    |                    |
| Allyloxycarbonyl            | Alloc  |                    |
| <i>tert</i> -butoxycarbonyl | Boc    |                    |
| <i>tert</i> -butyl          | tBu    |                    |
| 9-fluorenylmethoxycarbonyl  | Fmoc   |                    |
| Trityl                      | Trt    |                    |

| Reagent   | Abbreviation | Chemical structure |
|---|--------------|--------------------|
| <i>N,N'</i> -diisopropylcarbodiimide  | DIPCDI       |                    |
| 4-dimethylaminopyridine   | DMAP         |                    |
| 1-[(1-(cyano-2-ethoxy-2-oxoethylideneaminoxy)-dimethylaminomorpholinomethylene)methanaminium hexafluorophosphate  | COMU         |                    |
| 2-cyano-2-(hydroxyimino)acetate   | Oxyma        |                    |
| <i>N</i> -[(dimethylamino)-1 <i>H</i> -1,2,3-triazolo[4,5- <i>b</i> ]pyridin-1-yl-methylene)- <i>N</i> -methylmethanaminium hexafluorophosphate <i>N</i> -oxide | HATU         |                    |
| 1-hydroxy-7-azabenzotriazole  | HOAt         |                    |
| Benzotriazol-1-yl- <i>N</i> -oxytris(pyrrolidino)phosphonium hexafluorophosphate  | PyBOP        |                    |
| <i>N,N</i> -diisopropylethylamine   | DIEA         |                    |

|                |   |
|----------------|---|
| 11b-HSD1       | 11b-Hydroxysteroid dehydrogenase type 1 |
| 2-CTC          | 2-Chlorotritly chloride                 |
| A (nucleobase) | Adenine                                 |
| a2AR           | a2-Adrenergic receptor                  |
| ACH            | a-Cyano-4-hydroxycinnamic acid          |
| ACN            | Acetonitrile                            |
| ADP            | Adenosine diphosphate                   |
| ATP            | Adenosine triphosphate                  |
| Baf            | Bafilomycin A <sub>1</sub>              |
| Bak            | BH3-homologous agonist killer           |
| Bax            | Bcl-2-associated X protein              |
| Bcl-2          | B-cell lymphoma 2                       |
| BH             | Bcl-2 homology                          |
| Bid            | BH3-interacting domain death agonist    |
| Bik            | Bcl-2 interacting killer                |
| Bim            | Bcl-2 interacting mediator              |
| Bzl            | Benzyl                                  |
| C (nucleobase) | Cytosine                                |
| cAMP           | Cyclic adenosine monophosphate          |
| CD             | Circular dichroism                      |
| CDK            | Cyclin-Dependent Kinase                 |
| CF             | 5-Carboxyfluorescein                    |
| CFU            | Colony-forming units                    |
| cGMP           | Cyclic guanosine monophosphate          |
| Chol           | Cholesterol                             |
| CK2            | Casein kinase II                        |
| CNS            | Central nervous system                  |
| CPD buffer     | Citrate-phosphate-dextrose buffer       |
| CSC            | Cancer stem cells                       |
| Da             | Dalton                                  |
| DCM            | Dichloromethane                         |
| DKP            | Diketopiperazine                        |
| DMEM           | Dulbecco's modified eagle medium        |
| DMF            | Dimethylformamide                       |
| DMSO           | Dimethyl sulfoxide                      |
| DNA            | Deoxyribonucleic acid                   |
| DNase          | Deoxyribonuclease                       |
| EBV-EA         | Epstein-Barr virus early antigen        |
| EDA            | Ethylenediamine                         |
| EDTA           | Ethylenediaminetetraacetic acid         |

|                  |   |
|------------------|---|
| EtOAc            | Ethyl acetate   |
| EtOH             | Ethanol   |
| FACS             | Fluorescence-assisted cell sorting                            |
| FADD             | Fas-associated protein with death domain                      |
| FasL             | Fas ligand  |
| FCS              | Fetal calf serum  |
| <i>g</i>         | Earth's gravitational acceleration                            |
| G (nucleobase)   | Guanine   |
| GSEA             | Gene Set Enrichment Analysis                                  |
| GSK-3            | Glycogen synthase kinase 3                                    |
| h                | Hour  |
| HCoV             | Human coronavirus   |
| HPLC             | High-pressure liquid chromatography                           |
| IC <sub>50</sub> | 50% inhibitory concentration                                  |
| JAK              | Janus kinase  |
| kDNA             | Kinetoplast DNA   |
| lag phase        | Initial growth phase  |
| LC3              | Microtubule-associated protein 1A/1B-light chain 3            |
| LC50             | 50% lethal concentration                                      |
| log phase        | Exponential phase of growth                                   |
| LUV              | Large unilamellar vesicle                                     |
| MALDI-TOF        | Matrix-assisted laser desorption/ionization–time-of-flight    |
| Mcl-1            | Myeloid cell leukaemia-1                                      |
| MeOH             | Methanol  |
| MIC              | Minimum inhibitory concentration                              |
| min              | Minutes   |
| MLV              | Multilamellar vesicle   |
| MMP-2            | Matrix metalloproteinase-2                                    |
| MPE              | Methidiumpropyl-EDTA·Fe(II)                                   |
| MS               | Mass spectrometry   |
| MTT              | 3-[4,5-Dimethylthiazol-2-yl]-2,5 diphenyl tetrazolium bromide |
| MW               | Microwave   |
| NAD(P)H          | Reduced form of nicotinamide adenine dinucleotide phosphate   |
| NCCD             | Nomenclature Committee on Cell Death                          |
| nm               | Nanometer   |
| NMR              | Nuclear magnetic resonance                                    |
| NRPS             | Nonribosomal peptide synthetase                               |
| OD               | Optical density   |
| ORL-1            | Opioid receptor like-1  |
| PARP             | Poly(ADP-ribose) polymerase                                   |
| PBS              | Phosphate buffered saline                                     |

---

---

|                       |   |
|-----------------------|---|
| PDA                   | Photodiode array                                      |
| PDE                   | Phosphodiesterase                                     |
| PDGFR                 | Platelet-derived growth factor receptors              |
| PI                    | Propidium iodide                                      |
| PI3K                  | Phosphatidylinositol 3-kinase                         |
| PS                    | Phosphatidyl serine                                   |
| PUMA                  | p53 upregulated modulator of apoptosis                |
| QC                    | 2-quinoxalinecarboxilic acid                          |
| RafK                  | Rapidly accelerated fibrosarcoma kinase               |
| RBC                   | Red blood cells                                       |
| REMD                  | Replica exchange molecular dynamics                   |
| RIPK1                 | Receptor-interacting protein kinase 1                 |
| RNA                   | Ribonucleic acid                                      |
| ROS                   | Reactive oxygen species                               |
| RP-HPLC               | Reversed-phase high-performance liquid chromatography |
| rpm                   | Revolutions per minute                                |
| RPMI medium           | Roswell Park Memorial Institute complete medium       |
| RSV                   | Respiratory syncytial virus                           |
| RU                    | Relative units  |
| s                     | Second  |
| SPPS                  | Solid-phase peptide synthesis                         |
| SUV                   | Small unilamellar vesicle                             |
| Syk                   | Spleen tyrosine kinase                                |
| T (nucleobase)        | Thymine   |
| <sup>t</sup> Bu       | <i>tert</i> -Butyl                                    |
| TFA                   | Trifluoroacetic acid                                  |
| TFE                   | Trifluoroethanol                                      |
| THF                   | Tetrahydrofuran                                       |
| TIS                   | Triisopropylsilane                                    |
| TMRE                  | Tetramethylrhodamine ethyl ester                      |
| TNF                   | Tumor necrosis factor                                 |
| <i>t</i> <sub>R</sub> | Retention time  |
| TRAF2                 | Tumor necrosis factor receptor-associated factor 2    |
| tRNA                  | Transfer RNA  |
| U                     | Enzyme unit   |
| δ                     | Chemical shifts                                       |
| Δψ <sub>m</sub>       | Inner mitochondrial transmembrane potential           |

# **Introduction and objectives**

---

---



## GENERAL INTRODUCTION

### Peptides in cancer treatment

Cancer is a global concern that accounts for 13% of all deaths worldwide,<sup>1</sup> and it is estimated that there will be more than 16 million new cancer cases every year by 2020.<sup>2</sup> It affects almost any part of the body and involves an uncontrolled proliferation and spread of abnormal cells, leading to the formation of a tumor mass.<sup>3</sup> Cancer cells acquire biological capabilities during the development of tumors: ability for continual proliferation evading growth suppressors, resistance to cell death enabling replicative immortality, promotion of angiogenesis, invasion and metastasis, reprogramming of energy metabolism and immune destruction evasion.<sup>4</sup>

Chemotherapy, the delivery of a cytotoxic agent to cancer cells, is one of the most effective ways to treat cancer among the various approaches. It was in 1945 that wartime research on chemicals related to mustard gas proved these agents as potential drugs for treating leukaemias and other types of cancer. The US Army discovered that a compound called "nitrogen mustard" kills rapidly-growing cancer cells, and this agent became the model for a series of similar compounds aimed to treat cancer (Figure 1). Since that discovery, many researchers started to develop a number of drugs that could block cell replication and growth, and the era of chemotherapy begun.<sup>5</sup>

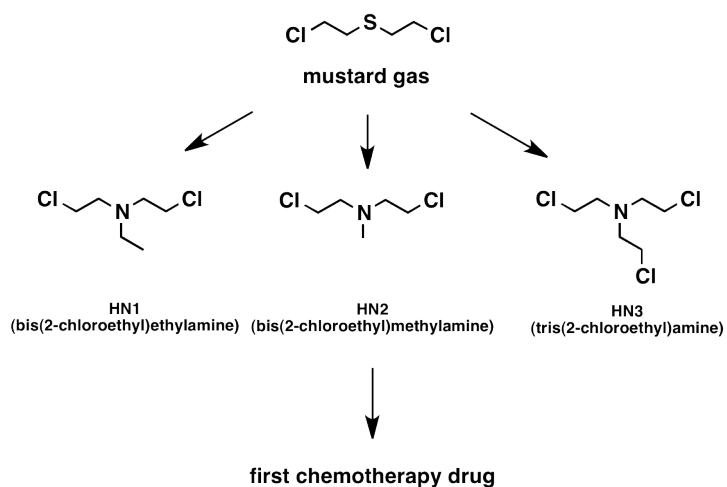


**Figure 1.** Chemical warfare agents that became the first chemical treatment for cancer.

However, conventional chemotherapy presents certain disadvantages, such as the inability to kill cancer cells in a specific manner without affecting normal cells, altered biodistribution and biotransformation, and the appearance of multidrug resistance by tumor cells.<sup>6</sup>

Discovery of diverse protein/peptide receptors and tumor-related peptides and proteins has leaded to an option in cancer treatment that includes the use of these kind of biomolecules.<sup>7,8</sup> Furthermore, the use of peptides has certain advantages: good delivery to tumors due to their small size, tumor-penetrating ability, good biocompatibility, and ease of synthesis and modification.<sup>9</sup> In addition, therapeutic peptides are generally less immunogenic than recombinant proteins and antibodies,<sup>10</sup> and since they are the smallest functional part of a protein, they are better in terms of efficacy, selectivity and specificity than small organic molecules.<sup>11</sup> Besides, the risk of systemic toxicity due to degradation of peptides into amino acids is very low.<sup>12</sup>

In recent years, peptides have emerged again as potential drug candidates despite their low oral bioavailability and propensity to be rapidly metabolized. Plasma, gastrointestinal and tissue peptidases are involved in peptide degradation, limiting their therapeutic use. Moreover, peptides can be cleared from the circulation through hepatic and renal clearance in few minutes.<sup>13</sup>

Absorption, transport, and passage of biological membranes and cellular barriers of peptide drug candidates are determined by a combination of their physicochemical properties, such as aqueous solubility, lipophilicity, H-bond formation, chemical stability and metabolic stability. Thus, peptides composed of natural amino acids are not very good drug candidates because of their intrinsic physicochemical properties and pharmacokinetic profiles. Nonetheless, chemical modifications such as incorporation of D-amino acids, N-methylations or cyclization may overcome these drawbacks.<sup>14</sup>

In spite of that peptides were considered in the past to be poor drug candidates, new synthetic strategies have been developed in recent years to improve productivity with reduced costs. Additionally, alternative routes of administration besides the oral one, and modifications in the structure of peptides aimed to reduce their metabolism and low bioavailability have revived the interest in peptides as potential drugs.<sup>15</sup>

There are three main sources of therapeutic peptides: (1) peptides from natural sources, such as plants, animals or humans; (2) peptides isolated from genetic or recombinant libraries, and (3) peptides from chemical libraries.<sup>16,17</sup> In this last concern, over hundred years of knowledge in peptide chemistry and two Nobel Prizes in the field —Vincet du Vigneaud for the discovery and synthesis of oxytocin<sup>18</sup> and Robert Bruce Merrifield for the invention of solid phase peptide synthesis (SPPS)<sup>19</sup>— allow chemists to synthesize at will almost any desired peptide sequence.

Chemical synthesis offers access to multigram amounts of natural occurring peptides, and the use of unnatural amino acids and pseudo-peptide bonds enables the access to a much wider chemical diversity of compounds for early clinical research. Likewise, it is often necessary to

optimize the chemical structure of a model peptide of interest in order to obtain a compound that can be used therapeutically.

Anticancer activity of different peptides may be due to a number of mechanisms that hamper tumor growth. Some peptides act as antagonists that bind to a receptor,<sup>20</sup> pro-apoptotic peptides point to induction of apoptosis,<sup>21,22</sup> and others inhibit protein-protein interactions, enzymes, signal transduction pathways, angiogenesis or gene expression.<sup>23–25</sup>

The outstanding recent development in peptide therapeutics has led to an unprecedented number of marketing approvals for this kind of drugs. On top of that, the majority of peptides undergoing phase III clinical trials are those evaluated for the oncology therapeutic area, along with infectious diseases.<sup>26</sup>

Between 2009 and 2011, the FDA approved eight peptides to enter into the market, which represent the 11% of the total molecules that were accepted. Among them, two compounds are anticancer drugs: romidepsin and brentuximab vedotin (Figure 2).

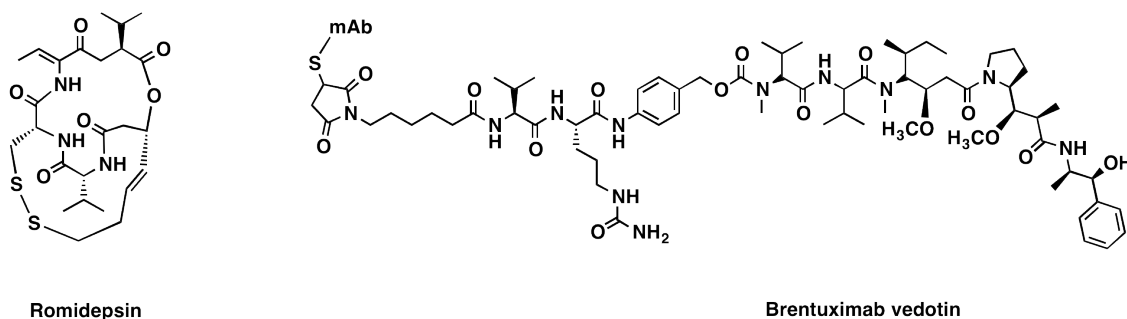


**Figure 2.** Anticancer peptides approved by the FDA between 2009 and 2011.

Romidepsin is a natural bicyclic depsipeptide with a disulfide bridge, whereas brentuximab vedotin is an antibody-drug conjugate between the monoclonal antibody brentuximab and the antimitotic peptide monomethyl auristatin E.<sup>27</sup>

Other peptide that is in phase III studies against malignant pleural mesothelioma is NGR-hTNF, which is a conjugate between the tumor-homing peptide (Asn-Gly-Arg; NGR), a ligand of an aminopeptidase overexpressed by endothelial cells of newly formed tumor blood vessels,<sup>28</sup> and the human tumor necrosis factor (hTNF).<sup>29</sup> The same molecule is being evaluated in phase II studies for non-small-cell lung cancer, soft tissue sarcomas and ovarian cancer.<sup>26</sup>

Furthermore, two cell-targeting peptides conjugated to an anticancer drug are being evaluated in phase II clinical trials. The first one, zoqtarelin doxorubicin, comprises a peptide analogue of the luteinizing-hormone-releasing hormone (LHRH) receptor, which is expressed in the majority of ovarian and prostate cancers, in half of breast cancer cases, as well as in bladder, colorectal,

renal and pancreatic cancers.<sup>30</sup> This peptide is coupled to the well-known anticancer drug doxorubicin. The other compound, EP-100, is a targeted anticancer drug comprised of LHRH fused to the lytic peptide CLIP 71, which disrupts cell membranes. Clinical studies are being conducted to determine the effect of a combination of EP-100 with paclitaxel in multi-drug resistant LHRH receptor positive uterine sarcoma, ovarian, prostate and breast cancer.<sup>31</sup>

Other two peptides that are currently in phase II studies are prodrugs used for prostate cancer. G202 is a carboxypeptidase prostate-specific membrane antigen (PSMA) specific peptide coupled to an analogue of the sarcoplasmic/endoplasmic reticulum calcium adenosine triphosphatase (SERCA) pump inhibitor thapsigargin. This molecule achieves targeted inhibition through the unique expression of PSMA by tumor endothelial cells, which hydrolyzes the prodrug at the tumor site, releasing the drug.<sup>32</sup> PRX302 is a modified form of proaerolysin, the inactive precursor of a bacterial cytoytic pore-forming protein, which is cleaved by the active prostate-specific antigen (PSA), a serine protease secreted at high levels in prostate tissue, and produces cytolytic aerolysin that remains localized in PSA expressing cells.<sup>33</sup>

Although few peptides have entered clinical trials in the last years and a decreased number of drugs are currently being approved besides the growing expenses for R&D, there are several peptide molecules with great potential to reach approval for marketing as anticancer treatments. Many research groups around the world are doing considerable efforts towards the development of peptides with groundbreaking compositions and specific mechanisms of action, auguring a promising future for innovative synthetic therapeutic peptides.

## OBJECTIVES

The general objective of the present thesis was the solid-phase synthesis of simplified analogues of the natural bisintercalator molecule triostin A. These analogues should display better antineoplastic activity than the parent compound.

In order to achieve this objective, various specific objectives arose during the development of this PhD project:

- Design, synthesis and characterization of a small library of quinoxaline-containing peptides inspired in the chemical structure of triostin A.
- Development of an efficient synthetic route for the obtention of peptidic scaffolds rich in consecutive *N*-methylations and  $\beta$ -branched amino acid residues.
- Establishment of the optimal experimental conditions for the *in vitro* antitumor evaluation of the synthesized compounds on four different human cancer cell lines.
- Cytotoxic evaluation of the synthesized compounds against tumor and non-tumor cells, using the parent compound, triostin A, or the well-known antineoplastic drug doxorubicin as positive controls for comparison purposes.
- Biological evaluation of the most cytotoxic compounds on bacteria, a human parasite and viruses.
- Evaluation of the DNA-binding properties of the most cytotoxic analogues through different techniques, principally by DNase I footprinting.
- Determination of the death pathway followed by cancer cells treated with the most cytotoxic compound, RZ2.
- Synthesis of a fluorescent version of compound RZ2 to perform colocalization assays through confocal microscopy.
- Evaluation of global perturbations in genome-wide RNA expression in cancer cells treated with compound RZ2 by a gene expression microarray.
- Analysis of the effect of RZ2 on mitochondrial membrane potential and superoxide mitochondrial levels.

## REFERENCES

- (1) World Health Organization <http://www.who.int/topics/cancer/en/>.
- (2) Jemal, A.; Bray, F.; Center, M. M.; Ferlay, J.; Ward, E.; Forman, D. *CA. Cancer J. Clin.* **61**, 69–90.
- (3) World Health Organization [http://www.who.int/gho/ncd/mortality\\_morbidity/cancer/en/](http://www.who.int/gho/ncd/mortality_morbidity/cancer/en/).
- (4) Hanahan, D.; Weinberg, R. A. *Cell* **2011**, *144*, 646–674.
- (5) American Cancer Society. <http://www.cancer.org/cancer/cancerbasics/thehistoryofcancer/the-history-of-cancer-cancer-treatment-chemo>
- (6) Kakde, D.; Jain, D.; Shrivastava, V.; Kakde, R.; Patil, A. T. *J. Appl. Pharm. Sci.* **2011**, *1*, 1–10.
- (7) Aina, O. H.; Sroka, T. C.; Chen, M.-L.; Lam, K. S. *Biopolymers* **2002**, *66*, 184–199.
- (8) Vlieghe, P.; Lisowski, V.; Martinez, J.; Khrestchatsky, M. *Drug Discov. Today* **2010**, *15*, 40–56.
- (9) Borghouts, C.; Kunz, C.; Groner, B. *J. Pept. Sci.* **2005**, *11*, 713–726.
- (10) McGregor, D. P. *Curr. Opin. Pharmacol.* **2008**, *8*, 616–619.
- (11) Hummel, G.; Reineke, U.; Reimer, U. *Mol. Biosyst.* **2006**, *2*, 499–508.
- (12) Loffet, A. *J. Pept. Sci.* **2002**, *8*, 1–7.
- (13) Pichereau, C.; Allary, C. *Eur. Biopharm. Rev.* **2005**, *5*, 1–4.
- (14) Thayer, A. M. *Chem. Eng. News* **2011**, *89*, 13–20.
- (15) Marx, V. *Chem. Eng. News* **2005**, *83*, 17–24.
- (16) Latham, P. W. *Nat. Biotechnol.* **1999**, *17*, 755–757.
- (17) Sato, A. K.; Viswanathan, M.; Kent, R. B.; Wood, C. R. *Curr. Opin. Biotechnol.* **2006**, *17*, 638–642.
- (18) Du Vigneaud, V.; Ressler, C.; Swan, J. M.; Roberts, C. W.; Katsoyannis, P. G. *J. Am. Chem. Soc.* **1954**, *76*, 3115–3121.
- (19) Merrifield, R. B. *J. Am. Chem. Soc.* **1963**, *85*, 2149–2154.
- (20) Sotomayor, S.; Muñoz-Moreno, L.; Carmena, M. J.; Schally, A. V.; Sánchez-Chapado, M.; Prieto, J. C.; Bajo, A. M. *Int. J. Cancer* **2010**, *127*, 1813–1822.
- (21) Ellerby, H. M.; Arap, W.; Ellerby, L. M.; Kain, R.; Andrusiak, R.; Rio, G. D.; Krajewski, S.; Lombardo, C. R.; Rao, R.; Ruoslahti, E.; Bredesen, D. E.; Pasqualini, R. *Nat. Med.* **1999**, *5*, 1032–1038.
- (22) Walensky, L. D.; Kung, A. L.; Escher, I.; Malia, T. J.; Barbuto, S.; Wright, R. D.; Wagner, G.; Verdine, G. L.; Korsmeyer, S. J. *Science* **2004**, *305*, 1466–1470.
- (23) Rosca, E. V.; Koskimaki, J. E.; Rivera, C. G.; Pandey, N. B.; Tamiz, A. P.; Popel, A. S. *Curr. Pharm. Biotechnol.* **2011**, *12*, 1101–1116.
- (24) Kritzer, J. A.; Stephens, O. M.; Guerracino, D. A.; Reznik, S. K.; Schepartz, A. *Bioorg. Med. Chem.* **2005**, *13*, 11–16.
- (25) Eldar-Finkelman, H.; Eisenstein, M. *Curr. Pharm. Des.* **2009**, *15*, 2463–2470.
- (26) Kaspar, A. a; Reichert, J. M. *Drug Discov. Today* **2013**, *18*, 807–817.
- (27) Albericio, F.; Kruger, H. G. *Future Med. Chem.* **2012**, *4*, 1527–1531.

- (28) Svensen, N.; Walton, J. G. A.; Bradley, M. *Trends Pharmacol. Sci.* **2012**, *33*, 186–192.
- (29) Curnis, F.; Arrigoni, G.; Sacchi, A.; Fischetti, L.; Arap, W.; Pasqualini, R.; Corti, A. *Cancer Res.* **2002**, *62*, 867–874.
- (30) Engel, J.; Emons, G.; Pinski, J.; Schally, A. V. *Expert Opin. Investig. Drugs* **2012**, *21*, 891–899.
- (31) Leuschner, C.; Giardina, C.; Alila, H. W. *Cancer Res.* **2012**, *72*, 3715.
- (32) Denmeade, S. R.; Mhaka, A. M.; Rosen, D. M.; Brennen, W. N.; Dalrymple, S.; Dach, I.; Olesen, C.; Gurel, B.; Demarzo, A. M.; Wilding, G.; Carducci, M. A.; Dionne, C. A.; Møller, J. V; Nissen, P.; Christensen, S. B.; Isaacs, J. T. *Sci. Transl. Med.* **2012**, *4*, 140ra86, 1–22.
- (33) Williams, S. A.; Merchant, R. F.; Garrett-Mayer, E.; Isaacs, J. T.; Buckley, J. T.; Denmeade, S. R. *J. Natl. Cancer Inst.* **2007**, *99*, 376–385.



# **Chemical synthesis**

---

---

Work presented in this chapter, as well as results from chapters 2 and 3 have been submitted to the *Chemistry & Biology Journal* for publication.

## INTRODUCTION

### Echinomycin and triostin A: staple-shaped quinoxaline antibiotics

Some organisms in nature have developed the capacity of synthesizing secondary metabolites that play an essential role in survival since most of them act as a defense system that protects the hosts against their habitats, that is, from microbes or competing organisms within their vicinity. These chemical arsenals have been perfected through natural selection over hundreds of years, therefore, they typically possess excellent properties and great potency. Interestingly, a plethora of these secondary metabolites isolated from various organisms have been found to possess useful biological activities, making them potential therapeutic leads for clinical use as novel antibiotics, anticancer, and antiviral agents.<sup>1</sup>

Echinomycin was originally discovered in culture filtrates from *Streptomyces echinatus* sp. in 1957.<sup>2</sup> Other quinoxaline antibiotics isolated from other sources, named compound X-948, actinoleukin, levomycin and quinomycin A,<sup>3–5</sup> were chemically identical to echinomycin.<sup>6</sup> This molecule is a cyclic depsipeptide containing L-alanine, N-methyl-L-valine, N-methyl-L-cysteine and N-methyl-D-serine. Its structure contains 2-quinoxalinecarbonyl chromophores attached to the  $\alpha$ -amino group of the N-methyl-D-serine residues through an amide bond, while the side-chain of these amino acids forms an ester with the N-methyl-L-valine residues. Echinomycin possesses an imperfect twofold axis of rotational symmetry due to an unusual dithioacetal bridge between the cysteines (Figure 3).<sup>7</sup>

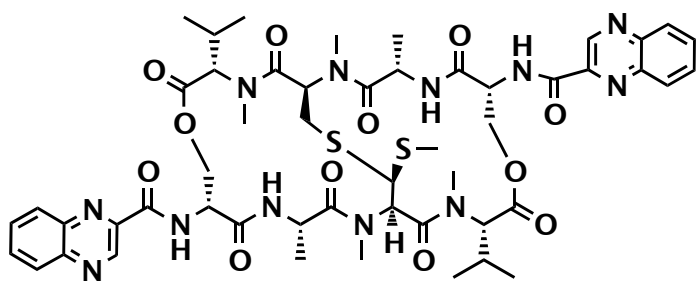


Figure 3. Chemical structure of echinomycin.

This natural product was found to be a potent antibacterial agent against Gram-positive bacteria, whereas Gram-negative bacteria and fungi are generally resistant.<sup>8,9</sup> Moderate activity against protozoa and viruses has also been reported,<sup>2,10</sup> but most interest in quinoxaline antibiotics has been focused on their cytotoxicity.<sup>11,12</sup>

Echinomycin is a potent antitumour agent brought into clinical trials by the National Cancer Institute. Phase I studies carried out in mice and dogs found toxic effects in the gastrointestinal, hepatic, and lymphoreticular systems, but these were reversible at all but the highest dose.<sup>13</sup>

Some years latter, echinomycin was administered to 43 patients with advanced cancer in escalating doses ranging from 60 to 2128  $\mu\text{g}/\text{m}^2$ . The dose-limiting toxicity of echinomycin administered as a 24 h continuous infusion every 28 days was nausea and vomiting beginning at the end of the 24 h infusion and lasting from 3 to 8 days, reversible liver abnormalities and allergic reactions. The maximally tolerated dose of echinomycin was 2128  $\mu\text{g}/\text{m}^2$ .<sup>14</sup> However, minimal to no activity was observed in phase II clinical trials against soft tissue sarcomas,<sup>15</sup> advanced ovarian<sup>16</sup> and breast cancers,<sup>17</sup> cervical squamous cell carcinoma<sup>18</sup> and central nervous system malignancies.<sup>19</sup> Nonetheless, in more recent years, it was observed that echinomycin selectively eliminates lymphoma cancer stem cells (CSC) with a long-lasting effect. Treated mice with this compound, with as little as 200 ng of the natural product, showed complete lack of lymphoma recurrence.<sup>20</sup> It was also demonstrated that echinomycin inhibited colony-forming units (CFU) of lymphoma CSC without affecting the CFU of normal hematopoietic progenitor cells in mice. Moreover, the doses used in this study were 50-fold lower than the maximally tolerated dose in humans. This remarkable efficacy opens a new possibility for echinomycin to reenter into clinical trials based on the concept of cancer stem cells involved in leukemia.

In 1974, it was demonstrated that echinomycin binds to duplex DNA by inserting its two planar chromophores between the base pairs of duplex DNA, placing its cyclic depsipeptide backbone in the minor groove.<sup>21</sup> This novel mode of action converted echinomycin into the "prototypical bisintercalator", the first DNA bisintercalator identified. However, echinomycin was originally shown to exert its biological effects through RNA polymerase inhibition.<sup>22</sup> Hence, it was suggested that the natural bisintercalator forms a complex with the duplex DNA that blocks the progression of the enzyme, thus acting as an inhibitor of transcription.

The interaction between echinomycin and a variety of natural and synthetic poly-deoxynucleotides through thermal-denaturation and viscometry experiments was studied. The aim was to determine what selectivity the antibiotic may display with respect to its capacity to bind to different types of nucleotide sequence and to define the general character of the interaction.<sup>23</sup> The results showed that echinomycin strongly interacts with certain synthetic poly-deoxynucleotides, the binding constant decreasing in the order poly(dG)-poly(dC) greater than poly(dG-dC), and poorly to poly(dA-dT), with little binding to poly(dA)-poly(dT).

This sequence selectivity has been confirmed through the use of footprinting, possibly the most powerful technique for the study of ligand-DNA interactions, and one that has been developed extensively in the studies of bisintercalator natural products. Footprinting is essentially a protection assay in which the digestion of double-stranded DNA by a cleavage agent, either enzymatic or chemical, is locally inhibited by the binding of a ligand at specific binding sites within a DNA fragment. The DNA fragment, which is labeled at one end of one strand, is cut so that, on average, each DNA molecule is only cleaved once (*i.e.* single-hit kinetics). If the

cleavage agent does not possess any sequence selectivity, then it will produce a random distribution of products that can be resolved on a denaturing polyacrylamide gel. When the digestion is repeated in the presence of a sequence selective ligand, this ligand will protect from cleavage at the regions to which it is bound, and these products will therefore be missing from the reaction and will be evident as a gap ("footprint") in the gel. By running control and ligand-treated digestion alongside suitable markers the exact binding sites for the ligand can be easily determined.<sup>24</sup>

The DNase I and DNase II footprinting technique was firstly applied in 1984 to study the sequence selectivity of echinomycin.<sup>25</sup> All the binding sites contained the dinucleotide sequence CpG and the preferred high affinity flanking base pairs were A and T, such that the best binding sites were 5'-ACGT and 5'-TCGT. Moreover, it was also observed that certain sequences, mainly runs of A or runs of T, switch from nuclease-resistant to nuclease-sensitive when echinomycin binds nearby, due to an altered helix conformation in the vicinity of the bisintercalated ligand. Homologous series of footprinting experiments on the binding of echinomycin were performed to a 133 base pair DNA restriction fragment containing a small number of discrete binding sites. Two of those sites each contained a pair of closely clustered CpG steps, the cognate dinucleotide sequence recognized by echinomycin. Evidence of binding to both CpG steps in the clustered pair was obtained, with indications of possible cooperativity.<sup>26</sup>

NMR experiments<sup>27-29</sup> have corroborated that echinomycin is selective for the dinucleotide CpG. Specificity is achieved by the formation of hydrogen bonds between the 2-amino group of guanine and the carbonyl oxygens of the alanines and between the guanine N3 and alanine NH groups.

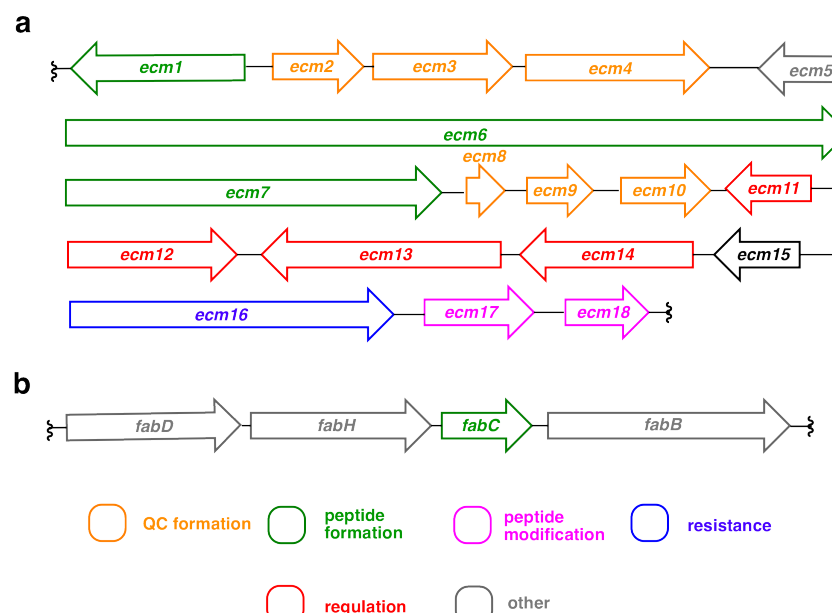
However, it was shown that echinomycin is unable to target nucleosomal DNA, meaning that it will have little effect on inactive chromatin, which is highly condensed and inaccessible to intercalation. In contrast, it may have a greater effect on active chromatin, in which the DNA may transiently dissociate from the protein. In these regions echinomycin will prevent nucleosome reassembly.<sup>30</sup>

Probably because of the presence of a synthetically challenging thioacetal in echinomycin's structure, no chemical synthesis has been described. To date, this natural product is commercially available from a fermentation progress in *Streptomyces echinatus*. However, several modifications of the natural product structure have been performed. The first analogue of echinomycin (named quinazomycin) was described in 1969. This molecule was produced by feeding bacteria with quinazol-4-on-3 acetic acid so that it replaced one of the quinoxaline chromophores when biosynthesized.<sup>31</sup> The first analogue in which both chromophores were replaced was biquinazomycin, obtained by a cell-free synthesis.<sup>32</sup> New antibiotics produced by *Streptomyces echinatus A8331* cultured in the presence of 2-quinoxalinecarboxylic acid or 2-

quinolinecarboxylic acid rendered echinomycin and certain quinoline derivatives.<sup>33</sup> Additionally, modifications in the peptidic core rendered the *S*-methylated sulfonium perchlorate of echinomycin, monosulfoxide, disulfoxide and sulfone analogues.<sup>34</sup>

Furthermore, the role of the chromophores in determining the mechanism and specificity of their interaction with DNA was studied. The results showed that the capacity to bisintercalate into DNA was not altered by the replacement of one or both 2-quinoxalinecarboxylic acids by quinoline moieties, and indeed the substitution may render analogues with enhanced binding affinity as well as altered sequence recognition, resulting in changes in its biological effect.<sup>35</sup>

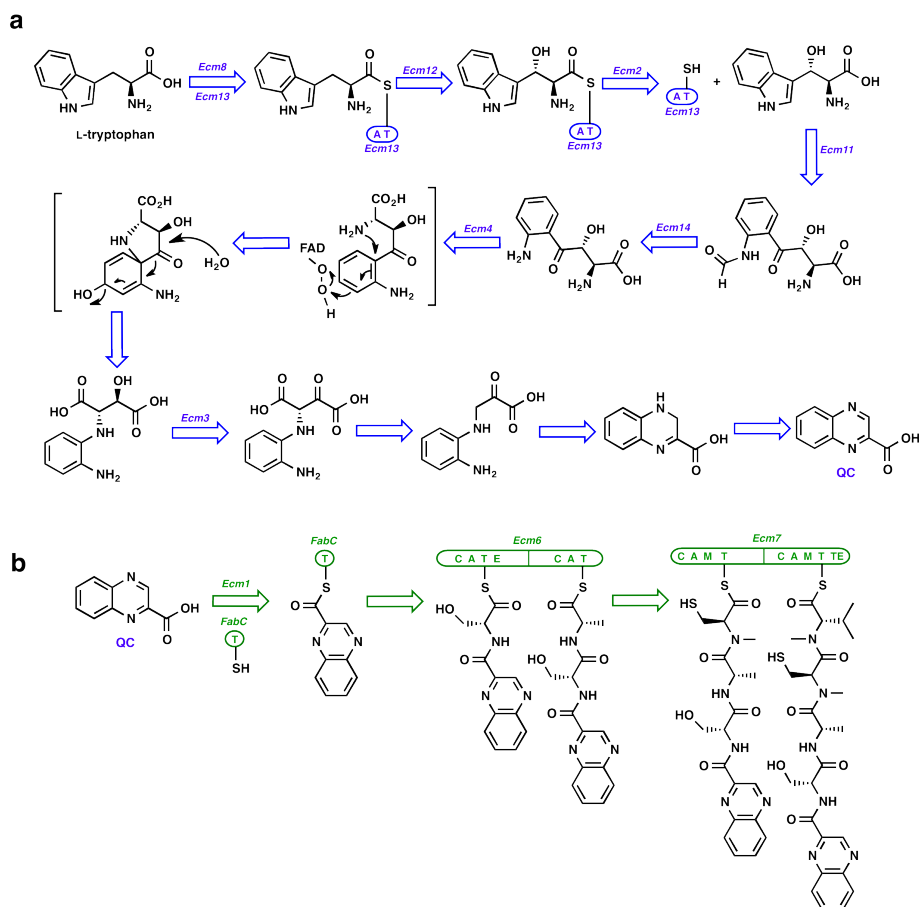
The core structure of echinomycin is biosynthesized by nonribosomal peptide synthetases (NRPSs) in streptomycetes.<sup>1</sup> A 36-kilobase-long cluster isolated from *S. lasaliensis* revealed the presence of eight genes responsible for 2-quinoxalinecarboxylic acid (QC) biosynthesis (*ecm2*, *ecm3*, *ecm4*, *ecm8*, *ecm11*, *ecm12*, *ecm13* and *ecm14*), five genes for peptide backbone formation and modifications (*ecm1*, *ecm6*, *ecm7*, *ecm17* and *ecm18*) and a resistance gene (*ecm16*) (Figure 4).<sup>36</sup>



| ORF          | Amino acids | Sequence homolog (conserved domain code or protein accession number) | Expected value       | Putative function             |
|--------------|-------------|--|----------------------|-------------------------------|
| <i>ecm1</i>  | 527         | Peptide arylation enzyme <i>entE</i> (COG1021)                       | $2 \times 10^{-160}$ | QC activation                 |
| <i>ecm2</i>  | 248         | Type II thioesterase <i>grsT</i> (COG3208)                           | $3 \times 10^{-151}$ | QC biosynthesis               |
| <i>ecm3</i>  | 362         | Isopropylmalate deshydrogenase <i>leuB</i> (COG0473)                 | $10^{-85}$           | QC biosynthesis               |
| <i>ecm4</i>  | 472         | FAD-dependent oxidoreductase <i>ubiH</i> (COG0654)                   | $2 \times 10^{-30}$  | QC biosynthesis               |
| <i>ecm5</i>  | n.a.        | Transposase (inactive)   | n.a.                 | Unknown                       |
| <i>ecm6</i>  | 2608        | Nonribosomal peptide synthetase <i>telC</i> (CAG15011)               | 0                    | Peptide synthesis modules 1-2 |
| <i>ecm7</i>  | 3135        | Nonribosomal peptide synthetase <i>acmC</i> (AAF42473)               | 0                    | Peptide synthesis modules 3-4 |
| <i>ecm8</i>  | 70          | MbtH-like protein <i>mbtH</i> (pfam03621)                            | $2 \times 10^{-24}$  | Unknown                       |
| <i>ecm9</i>  | 181         | DNA-binding response regulator <i>ompR</i> (COG0745)                 | $3 \times 10^{-12}$  | Regulation                    |
| <i>ecm10</i> | 252         | TetR-family transcriptional regulator <i>pip</i> (AAG31690)          | $2 \times 10^{-80}$  | Regulation                    |
| <i>ecm11</i> | 220         | Tryptophan 2,3-dioxygenase <i>tdo2</i> (COG3483)                     | $4 \times 10^{-14}$  | QC biosynthesis               |
| <i>ecm12</i> | 395         | Cytochrome P450 oxidase <i>cypX</i> (COG2124)                        | $6 \times 10^{-59}$  | QC biosynthesis               |
| <i>ecm13</i> | 598         | Mannopeptimycin peptide synthetase <i>mppB</i> (AAU34203)            | $10^{-118}$          | QC biosynthesis               |
| <i>ecm14</i> | 402         | Erythromycin esterase <i>ereB</i> (pfam05139)                        | $3 \times 10^{-24}$  | QC biosynthesis               |
| <i>ecm15</i> | 285         | Helix-turn-helix transcription regulator <i>marR</i> (Cd00592)       | $2 \times 10^{-10}$  | Regulation                    |
| <i>ecm16</i> | 806         | Exonuclease ATPase <i>uvrA</i> (COG0178)                             | 0                    | Self resistance               |
| <i>ecm17</i> | 313         | Thioredoxin reductase <i>trxB</i> (COG0492)                          | $6 \times 10^{-14}$  | Disulfide formation           |
| <i>ecm18</i> | 224         | SAM-dependent methyltransferase <i>smtA</i> (COG0500)                | $10^{-4}$            | Thioacetal formation          |
| <i>fabC</i>  | 82          | Fatty acid synthase acyl carrier protein <i>acpP</i> (COG0236)       | $3 \times 10^{-9}$   | QC carrier protein            |

**Figure 4.** The echinomycin biosynthetic cluster from *S. lasaliensis*. **(a)** The organization of the echinomycin biosynthetic gene cluster isolated from *S. lasaliensis*. **(b)** Predicted fatty acid synthase gene organization in *S. lasaliensis*. **(Table)** Deduced functions of the ORFs of the *S. lasaliensis* echinomycin biosynthetic gene cluster and fatty acid synthase acyl carrier protein. Expected value is the number of matches expected to be found purely by chance for a given query sequence in a database; n.a., not applicable. Adapted from ref. 36.

Selective feeding experiments using unlabelled L-tryptophan-supplemented media showed that N1 and N4 of the quinoxaline rings have their origins in the indole and amino groups of tryptophan, respectively.<sup>37</sup> More recently, it was demonstrated for the first time that the quinoxaline chromophore is activated and condensed with serine through a functional interaction between non-ribosomal peptide synthesis and fatty acid biosynthesis.<sup>38</sup> It has also been proven that triostin A is the natural precursor to echinomycin, as it was firstly proposed by Nolan and co-workers (Figure 5).<sup>39</sup>



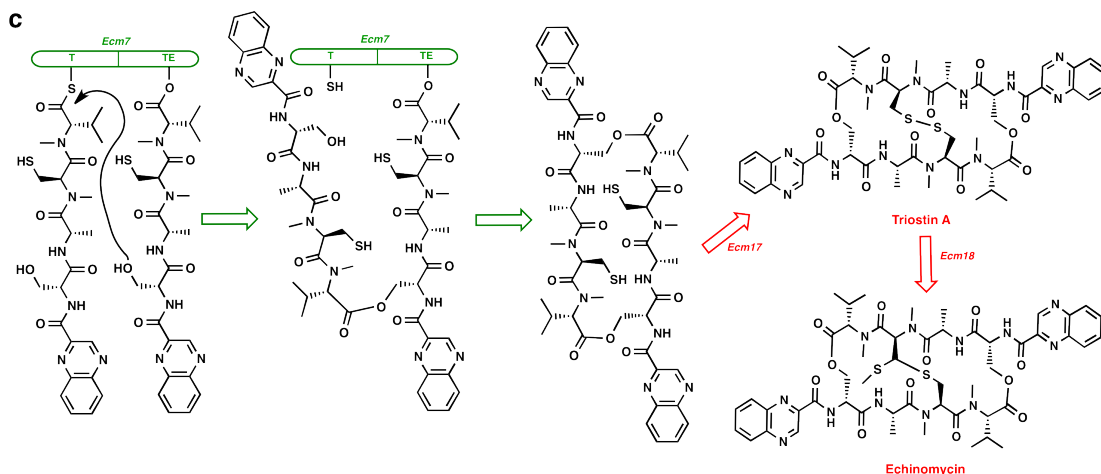


**Figure 5.** Mechanism for echinomycin biosynthesis. **(a)** Pathway for QC biosynthesis (blue). **(b)** Pathway for octadepsipeptide core-structure biosynthesis (green). **(c)** Proposed mechanism for peptide chain homodimerization and cyclorelease from *Ecm7* (green) and subsequent modifications for the formation of the quinoxaline antibiotics (red). Adapted from ref. 39.

Triostins are also members of the quinoxaline antibiotic family.<sup>11</sup> They were isolated from *Streptomyces aureus* S-2-210 and it was discovered through chromatographic separation that the isolated mixture contained three similar quinoxaline components that were named triostins A, B and C (Figure 6).<sup>9</sup>

The first structure to be elucidated was that of triostin C, since it was the most abundant of the three triostins in the isolated mixture. NMR and infrared spectroscopy experiments showed the presence of 2-quinoxalinecarboxylic acid, D-serine, L-alanine, *N*-methyl-L-cysteine and *N*- $\gamma$ -dimethyl-L-*allo*-isoleucine.<sup>40,41</sup> Thus, a cyclic octadepsipeptide structure with a disulfide cross-link was proposed. The other triostins differ only in one of the *N*-methylated residues. Triostin A bears an *N*-methyl-L-valine, whereas triostin B contains an *N*-methyl-L-*allo*-isoleucine.<sup>42</sup>

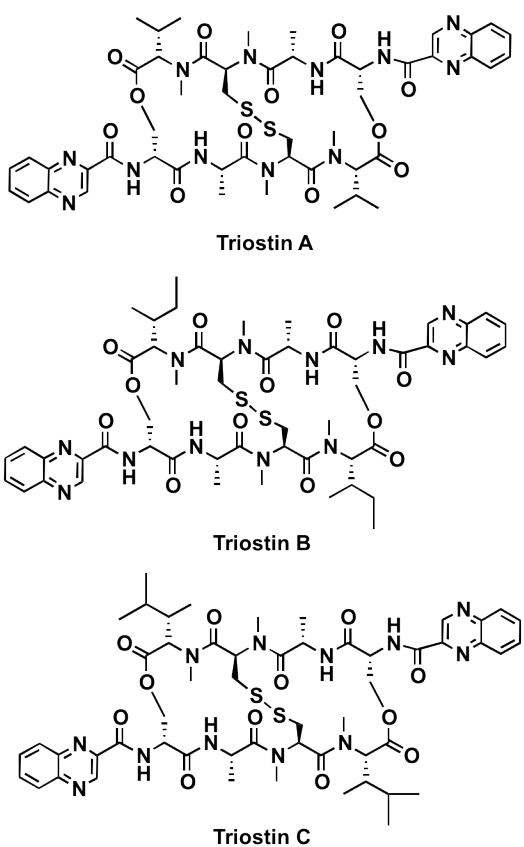


**Figure 6.** Chemical structures of triostins A, B and C.

After the isolation of quinoxaline antibiotics, a number of research groups began investigations in the synthesis and biological activity of these compounds and related analogues. In 1977, Olsen and co-workers reported the linear synthesis of the *N*-demethylated triostin A analogue, TANDEM.<sup>43</sup> Some years latter, they also obtained TANDEM through a convergent approach.<sup>44</sup> Moreover, they also completed the first chemical synthesis of the natural compound triostin A using a similar strategy to the one developed for TANDEM, but with significant modifications due to the incorporation of *N*-methyl amino acids.<sup>45</sup>

In the 80's, more syntheses of triostin A and TANDEM were reported, as well as the synthesis of an *S,S*-dibenzyl analogue of triostin A lacking the disulfide bridge. NMR experiments in weakly polar solvents with these molecules revealed the presence of two conformers of triostin A and its *S*-benzyl derivative, while TANDEM, which lacks the *N*-methyl groups, gave just one conformer. Therefore, it was demonstrated that there was not a reversal of the chirality around the *S-S* bond, but a *cis-trans* isomerization of the *N*-methyl peptide bonds. It was also reported that only one of the two conformers of triostin A interacts with purine derivatives.<sup>46</sup>

More than 15 years latter, an analogue of triostin A in which the D-serine residues were replaced by 1,3-diaminopropionic acid (Dap), azatriostin, was reported.<sup>47</sup> This solution phase

synthesis was suitable for the preparation of combinatorial libraries in which each intermediate could be isolated and purified only by liquid-liquid acid/base extractions.

However, the introduction of the solid-phase methodology gave a new burst to the combinatorial synthesis of triostin A analogues, since it allows the rapid production of compounds with "point mutations" at every site. In 2005, the first solid-phase synthesis of TANDEM was described. The approach involved the SPPS of the linear peptide using HBTU and HOBr, in the presence of DIEA, and removal from the solid phase prior to disulfide bond formation. The macrolactamization under mild conditions was done in solution followed by disulfide bond formation.<sup>48</sup> The solid-phase approach was also used to synthesize a demethylated analogue of azatriostin and several analogues in which the quinoxaline chromophores were substituted by nucleobases.<sup>49</sup>

The synthetic challenges encountered during triostin A synthesis are associated with the presence of consecutive *N*-methylated amino acids and two ester bonds that favor diketopiperazine (DKP) formation. These difficulties were overcome by a solid-phase synthesis, developed in our research group, employing a number of coupling reagents, various orthogonal protecting groups, and a new concept of protection referred to as conformationally restricted mobility, in which the minimization of DKP formation is achieved by the formation of an interchain disulfide bridge that restricts the mobility of the peptide chain.<sup>50</sup>

Nucleobase-functionalized triostin A analogues were synthesized by solution-phase peptide chemistry in order to obtain new ds-DNA binding motifs. UV and FID experiments corroborated DNA binding of these molecules, but through a recognition that differs from bisintercalation.<sup>51</sup>

The first studies carried out on quinoxaline antibiotics demonstrated that triostins, as echinomycin, possess antibacterial and antitumour activities.<sup>11</sup> Ten years latter, Waring and co-workers developed a novel solvent-partition method for measuring the DNA-drug interactions for non-water-soluble drugs and applied it to study triostin A. Based on their results they proposed a bisintercalation mechanism as mode of action for triostin A.<sup>52</sup> In addition, this conclusion was confirmed by measurements of changes in the viscosity of sonicated rod-like DNA fragments in which the helix extension was found to be almost double that expected for a monofunctional intercalator.<sup>53</sup> Furthermore, footprinting experiments showed that, even though triostin A binding sites are practically the same as those reported for echinomycin, it displays less preference for CpG steps. TANDEM was also tested in these experiments and it was reported that this demethylated analogue binds to ATA or TAT sequences,<sup>54</sup> leading to the proposal that not only the quinoxaline chromophores are important for specificity in DNA-binding, but also the peptidic scaffold plays an important role.

The molecular structure of triostin A complexed to the DNA sequence CGTACG was solved, showing that the two planar quinoxaline rings of triostin A bisintercalate into the minor groove of the DNA double helix surrounding the CG base pairs at either ends, while the depsipeptide ring adopts an U-shape with the disulfide bridge pointing away from the binding site. The orientation of the D-Ser amino group allows the chromophores to project parallel to each other at right angles from the peptide backbone, bracketing a CG base-pair in the minor groove of DNA. Later, the two members of the quinoxaline antibiotic family, echinomycin and triostin A, were complexed to a DNA fragment with the aforementioned sequence, CGTACG, and crystalized. Both complexes were solved by X-ray diffraction to near-atomic resolution. It was found that the two structures are similar to each other with minor differences due to the shorter cross bridge of echinomycin.<sup>56</sup>

Both molecules act as bisintercalators surrounding the d(CpG) sequence. The alanine residues form hydrogen bonds to the guanines in the minor groove. The adenine residues in the center are in the *syn* conformation and are paired to thymine through Hoogsteen base pairing in both complexes. Base stacking in the DNA is perturbed, and the major binding interaction involves a large number of Van der Waals contacts between the peptides and the nucleic acid. An octahedrally hydrated magnesium ion is found in the crystal lattice and plays an important role in organizing the lattice. This ion also stabilizes the complex by hydrogen bonding both to base pairs of DNA and to the quinoxaline ring nitrogen atoms in the major groove side of the DNA double helix. More recent crystal structures have demonstrated the formation of Hoogsteen pairing for the base pairs flanking the intercalating chromophores on the outside and Watson-Crick pairing for both base pairs enclosed by the bisintercalators.<sup>57</sup>

## RESULTS AND DISCUSSION

### Design of the RZ1-RZ12 library

Echinomycin is the parent member of a big variety of natural products that bisintercalate on duplex DNA.<sup>58</sup> The structural variety in these compounds include cyclic peptides, depsipeptides and thiodepsipeptides which act as linkers of two planar chromophores that are inserted into the genetic material spanning two base pairs while the peptide backbone is placed in the minor groove.

As previously mentioned in the introduction of this chapter, it was found that triostin A and echinomycin display an U-shape when bisintercalating.<sup>56</sup> Moreover, this conformation was also observed in NMR experiments and crystal structure determinations without DNA.<sup>59,60</sup> Interestingly, the crystal structure of thiocoraline revealed stacked arrays of docked pairs of staple-shaped molecules,<sup>61</sup> resembling the characteristic shape of quinoxaline antibiotics. Furthermore, other natural antineoplastic bisintercalators such as sandramycin and luzopeptin also display a staple conformation when binding to DNA.<sup>62,63</sup>

So, in continuation of the efforts of our research group on the design and synthesis of novel anticancer agents, a small library of peptides inspired in the peptidic scaffolds of echinomycin, triostin A and TANDEM was envisioned. Our main purpose was to develop simplified analogues whose synthesis was easier and more scalable than those reported for the natural product, in order to obtain enough quantities to perform biological assays. Furthermore, our biggest concern was to obtain a compound with better biological activity than the one displayed by triostin A and, if possible, with better pharmacokinetic properties.

It was thought that having the peptidic scaffold in the U-shape displayed by the majority of the natural bisintercalators would improve the DNA binding affinity of our compounds. However, avoiding the presence of ester bonds and disulfide bridges, very common entities in the chemical structure of the natural compounds, would facilitate the synthesis, thus improving final yields. So, the design of short peptides defined by a  $\beta$ -hairpin motif with two quinoxaline units covalently attached to both ends was a plausible option.

It has been reported that the two-residue loop D-Pro-Gly is a very strong promoter for induction of  $\beta$ -hairpin folding,<sup>64</sup> in which two antiparallel strands are connected by a short loop. Furthermore, side chain-side chain interactions are critical determinants of antiparallel  $\beta$ -sheet stability. Thus, even though the D-Pro-Gly loop segment is a strong promoter of  $\beta$ -hairpin folding, the favorability of this loop segment needs the contribution given by the interactions between hydrophobic side chains laterally paired on adjacent strands and diagonal side chain-side chain interactions that stabilize the antiparallel  $\beta$ -sheet (Figure 7).<sup>65</sup>

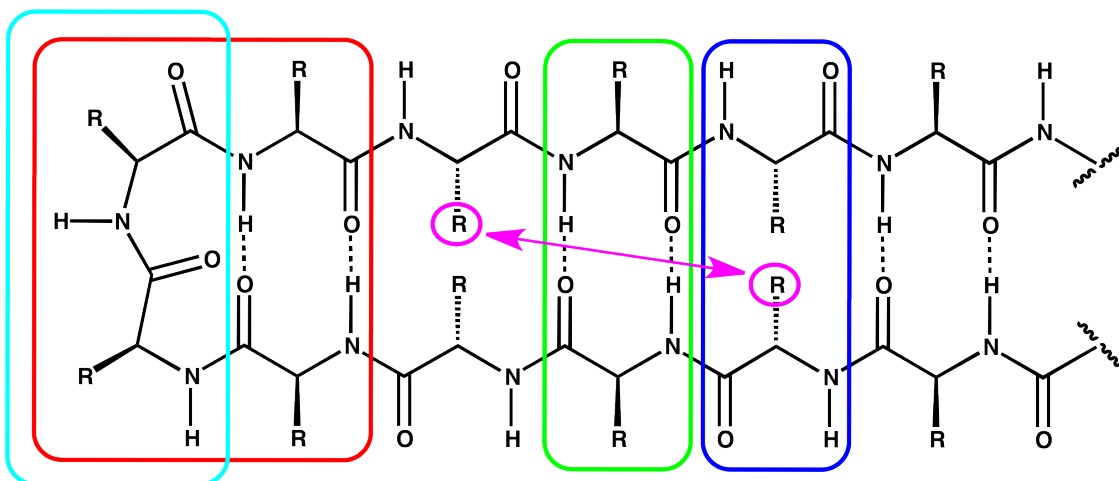
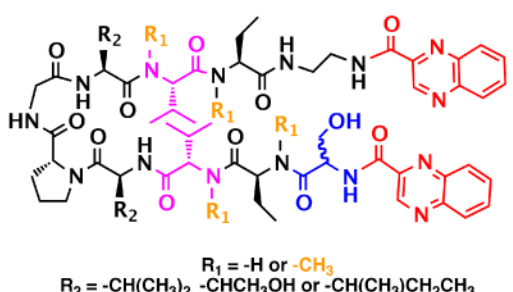
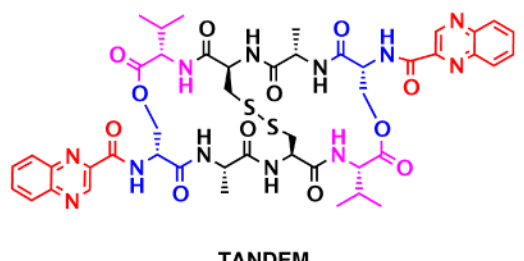
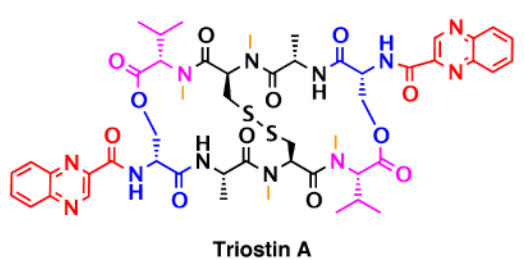
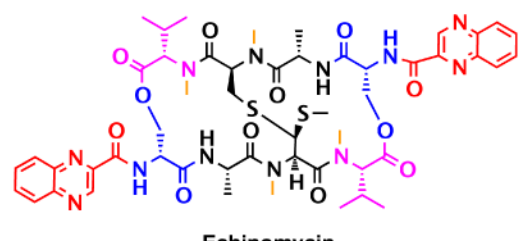


**Figure 7.** Graphic definitions of the interactions that stabilize a  $\beta$ -sheet. (Cyan) the two residues that define a loop in a tight  $\beta$ -hairpin, (red) the four residues that define a  $\beta$ -turn, (green) hydrogen bonded interstrand pairing in antiparallel  $\beta$ -sheet, (blue) non-hydrogen bonded interstrand pairing in antiparallel  $\beta$ -sheet, (fuchsia) diagonal interactions in the antiparallel  $\beta$ -sheet.

Based on all the aforementioned reasons, the new library of compounds herein presented shows the following characteristics: (1) a two-residue short loop formed by D-Pro-Gly, (2) the adjoining presence of  $\beta$ -branched amino acids next to the  $\beta$ -loop to define a four residue  $\beta$ -turn, (3) two valines, which are also present in echinomycin, triostin A and TANDEM, (4) two  $\alpha$ -aminobutyric acid residues mimicking the cysteine residues present in the aforementioned natural compounds, (5) a serine residue that holds a D configuration in half of the new compounds and that is changed to L-serine in the other half, (6) an ethylenediamine (EDA) at the C-terminus, (7) two quinoxaline moieties linked to both N-terminus of the formed  $\beta$ -hairpin, and (8) four N-methylated amino acids as in the chemical structure of echinomycin and triostin. The corresponding demethylated analogues were also synthesized, as TANDEM is for triostin A (see Figure 8).

The D-Pro in the  $\beta$ -loop was never replaced by L-Pro, since the local twist of the common type I and type II  $\beta$ -turns is left-handed, which is not compatible with the strand twist for L-residues. Indeed, replacing D-Pro with L-Pro appears to be antithetical to formation of two-residue  $\beta$ -hairpin loops.<sup>64</sup>



RZ1-RZ12 library

**Figure 8.** Structures of echinomycin, triostin A, TANDEM and general structure for the novel RZ1-RZ12 library. Common features between all chemical structures are shown in color. Quinoxaline moieties are highlighted in red. Serine residues are shown in blue and valine residues in fuchsia. Orange color depicts *N*-methylations.

## Synthesis of the RZ1-RZ12 library

The solid-phase peptide synthesis (SPPS) is an advantageous and versatile technique that allows the rapid preparation of peptides and is, nowadays, the method of choice over the time-consuming and, perhaps, more tedious solution-phase synthesis. The fact that work-ups between amino acid couplings involve only filtration and washing steps to remove the excess of reagents and soluble by-products enables the synthesis of peptides and small proteins in good yields without the undesired losses when performing typical solution-phase work-ups and purifications. Moreover, the SPPS facilitates the attempt of a variety of coupling conditions and enables an easy access to analogues and combinatorial libraries.

The most convenient way to synthesize small peptides, such as the RZ1-RZ12 peptidic scaffolds, is by a combination of solid-phase and solution methods. So, the chosen approach was a stepwise solid phase peptide synthesis with the introduction of the 2-quinoxalinecarboxylic acids and the side-chains deprotection as final stages carried out in solution.

### **Protection scheme**

All the SPPS was done following a 9-fluorenylmethoxycarbonyl/*tert*-butyl (Fmoc/*t*Bu) strategy, which enables peptide synthesis under milder conditions than the Boc/Bzl strategy. Moreover, for the preparation on *N*Me-containing peptides, the Boc strategy could lead to the formation of a Boc-oxazolonium ion that decomposes into an *N*-carboxyanhydride derivative, which tends to polymerize.<sup>66</sup> Thus, the safer Fmoc amino-protecting group was chosen accompanied by the acid-labile *t*Bu side-chain protecting group for threonines and serines.

### **Polymeric support**

The synthesis of peptides with consecutive *N*-methyl amino acids represents a challenge because couplings between them are difficult to achieve and they can undergo internal diketopiperazine (DKP) formation.<sup>66</sup> So it was decided to use the 2-chlorotriptyl chloride (2-CTC) resin<sup>67</sup> (Figure 9) as solid support since it tolerates *in situ* *N*-methylations under Mitsunobu conditions when performed after the first residue, it minimizes the formation of DKP<sup>68</sup> and it allows the release of the peptide under mild acidic conditions<sup>69</sup> allowing us to keep the *tert*-butyl side-chain protection for further reactions performed in solution.

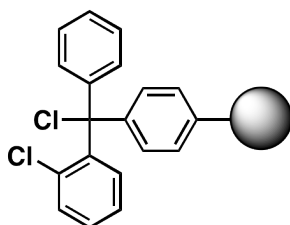


**Figure 9.** Structure of polystyrene-based 2-chlorotriyl chloride resin.

### **Ethylenediamine, first entity attached on the 2-CTC resin**

2-CTC resin is one of the most widely used resins for the solid-phase synthesis of *C*-terminal peptides. However, because of the design of our library in which two 2-quinoxalinecarboxylic acids are introduced at both ends of the peptidic scaffold, peptides with two *N*-terminus were required in order to be able to attach both chromophores via an amide bond as a final stage prior to total side-chain deprotection. For this reason, an ethylenediamine group was firstly coupled to the resin so that further cleavage would render the required peptide with both *N*-terminus free to react with the quinoxalinecarboxylic acids.

Two options were explored for the incorporation of the ethylenediamine on the solid support:

- 1) An excess of unprotected ethane-1,2-diamine (10 eq) was added to the resin using CH<sub>2</sub>Cl<sub>2</sub> as solvent. Employing so many equivalents of the reactant avoids the incorporation of both free amines on the polymeric support.

Different reaction times were evaluated in terms of loading. For this, nine syringes with 20 mg of 2-CTC resin each were washed with DMF and CH<sub>2</sub>Cl<sub>2</sub> and ethylenediamine (10 eq) was anchored to the resin, allowing the mixture to react for different times. No capping step with MeOH was carried out. Next, Fmoc-Val-OH (3 eq) in the presence of COMU (3 eq), Oxyma Pure (3 eq) and DIEA (6 eq) was added to the resin and the loading was calculated by spectrometric quantification of the *N*-fluorenylmethylpiperidine adduct. The reaction times and the corresponding calculated loadings are detailed in Table 1.

Based on the results of this loading study, it was concluded that the incorporation of the diamine takes place almost immediately after addition on the resin. The maximum incorporation that can be achieved using an excess of 10 eq at room temperature is 1 mmol/g of 2-CTC resin.

This strategy was followed in the first syntheses, allowing this first reaction to proceed over 30 min. However, whereas the syntheses of non *N*-methylated peptides were achieved without any problems, the syntheses of *N*-methylated peptides, as expected, were much more complicated. After several modifications in the attempt to optimize the purity and yields of these synthetically

demanding peptides, it was decided to employ another strategy for the incorporation of the ethylenediamine moiety.

| Reaction time | Loading |
|---------------|---------|
| 5 min         | 1.0     |
| 10 min        | 0.95    |
| 30 min        | 1.0     |
| 1 h           | 0.9     |
| 2 h           | 0.95    |
| 3 h           | 0.95    |
| 5 h           | 0.95    |
| 10 h          | 1.0     |
| 20 h          | 0.9     |

**Table 1.** Ethylenediamine incorporation on 2-CTC resin over time.

**2)** Fmoc-1,2-ethylenediamine\*HCl in the presence of DIEA was anchored to the resin using CH<sub>2</sub>Cl<sub>2</sub> as solvent, allowing the mixture to react for 45 min.

In this case, the loading is controlled by the mmol of reactant that are added to the resin. Since decreasing the loading of commercial 2-CTC resin (1.56 mmol/g) is necessary to avoid aggregation problems when growing the peptidic chains and to diminish further steric hindrances between the vicinal elongated peptides, it was decided to anchor 0.7 mmol of Fmoc-1,2-ethylenediamine\*HCl per gram of 2-CTC resin. Next, a capping step with MeOH was carried out, followed by Fmoc-removal. The piperidine-DMF (1:4) solution and consecutive DMF washings were collected and the loading calculated. The obtained value was corroborated as 0.7 mmol/g resin.

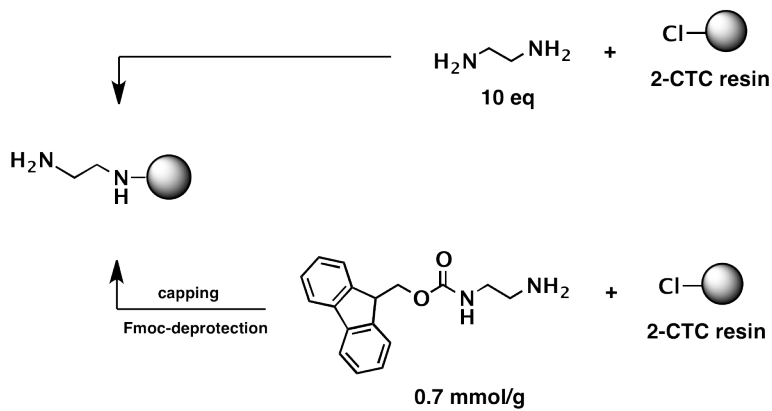


**Figure 10.** The two explored options for the incorporation of ethylenediamine on the resin.

After Fmoc-1,2-ethylenediamine\*HCl incorporation and following deprotection, the *N*-methylated peptides were further elongated on the solid support and the final products were obtained with better purities than the cases in which ethane-1,2-diamine was used.

Given the high price of Fmoc-1,2-ethylenediamine\*HCl in comparison to ethane-1,2-diamine, it was considered to use the former for the synthesis of *N*-methylated peptides and the latter for non-*N*-methylated peptides.

#### ***In situ N-methylation on the solid support***

As illustrated in Figure 8, half of the designed compounds bear two *N*-methylated amino acid residues: *N*Me-Val and *N*Me-Abu. Whereas the former is commercially available as an Fmoc *N*-protected amino acid, the latter is purchased as Fmoc-Abu-OH and *in situ N*-methylation were carried out on the solid support following an efficient, practical and selective three-step procedure.<sup>70</sup> This optimized procedure reported by Kessler and co-workers is a three-step sequence that involves amine activation by an *o*-nitrobenzenesulfonyl group (*o*-NBS), *N*-methylation via Mitsunobu reaction, followed by removal of the sulfonamide group.

Protection of the resin-bound free amine peptide is achieved by treatment with *o*-nitrobenzenesulfonyl chloride (3 eq) in the presence of 2,4,6-collidine (5 eq) in CH<sub>2</sub>Cl<sub>2</sub> at room temperature for 1 h. Completeness of the reaction is monitored by HPLC and *N*-methylation of the resin-bound *N*<sub>α</sub>-*o*-NBS-amino acid is achieved under Mitsunobu conditions with 5 eq of triphenylphosphine, 10 eq of methanol and 5 eq of diisopropyl azodicarboxylate (DIAD) in anhydrous THF under N<sub>2</sub> atmosphere in 20 min. Removal of the *o*-NBS protecting group is accomplished with 10 eq of mercaptoethanol and 5 eq of DBU in DMF. Three treatments of 15 min each ensure a complete deprotection.

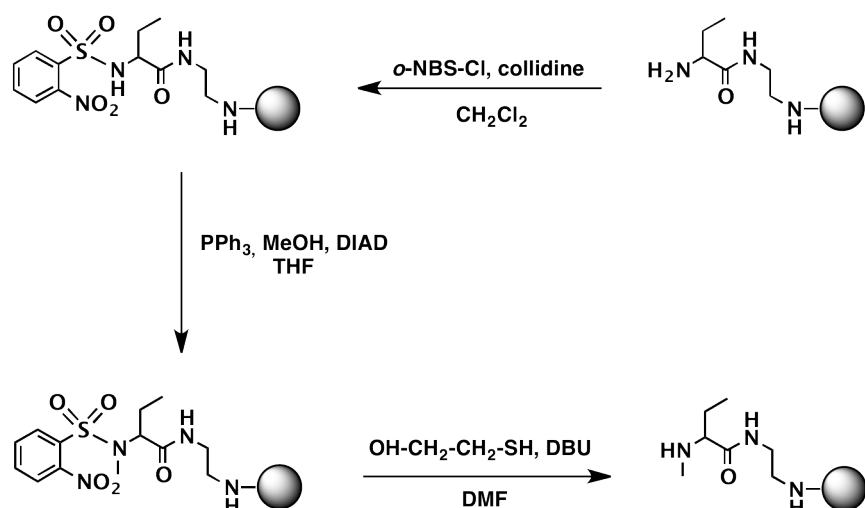


**Figure 11.** Three-step procedure for site-selective *N*-methylation on the solid support.

It is worth to highlight that the o-NBS group provides a selective deprotection for *N*-methylated derivatives since mercaptoethanol does not react under these conditions when the protected amine is not alkylated.

Despite the fact that *N*-methylation steps are known to give partial cleavage on 2-CTC resin when performed on the first residue, the *in situ* *N*-methylation of the Abu residue that was incorporated after the ethylenediamine was well tolerated without a significant percentage of cleavage from the resin. The same happened with the other *N*-methylation that was carried out at the final stages of the peptide elongation.

### Coupling reagents

#### Coupling system for peptide elongation on solid phase

The controlled formation of the amide bond requires activation of the carboxylic group prior to reaction with the amino component. During this process, the possibility of racemization is often a big concern. Thus, the experimental conditions, such as solvent, temperature, time, concentration, preactivation (if applicable) and the presence of base, should be rationalized when a difficult coupling is attempted.

Since our peptide library is not only characterized by consecutive *N*-methyl amino acids but also by consecutive  $\beta$ -branched amino acids whose couplings are very difficult to achieve, the choice of the coupling reagents was another important issue.

HOAt-based onium salts, such as HATU, have been shown to be very favorable for the coupling of hindered amino acids since the activation step occurs in a faster way than with carbodiimides.<sup>71</sup> However, this aminium salt can lead to the formation of a non-desired guanidino non-desired derivative when reacting with an *N*-terminal amino component.<sup>72</sup> To avoid this, preactivation of the reactive amino acid with the coupling reagent and DIEA is conducted. Moreover, HOAt has been described as superior to HOBr as an additive and reduces the risk of racemization.<sup>73</sup> So, the efficacy of the coupling system HATU-HOAt-DIEA was evaluated.

On the other hand, an efficient combination of the third generation uronium salt COMU<sup>74</sup> and Oxyma<sup>75</sup> in the presence of diisopropylethylamine (DIEA) was also evaluated, since it has been reported that Oxyma-containing reagents allow an outstanding epimerization suppression and superior coupling efficiency than HATU, specially when the sterical hindrance at the coupling junction is significant.<sup>76</sup>

For the determination of the best coupling system that would be used for all the designed compounds, the coupling of the commercially available Fmoc-*N*Me-Val-OH on the *in situ*

methylated aminobutyric acid residue, previously attached to the ethylenediamine on the 2-CTC resin, was performed using the conditions detailed in Table 2 and DMF as solvent. Next, Fmoc removal was performed, followed by cleavage from the resin by treatment with TFA–CH<sub>2</sub>Cl<sub>2</sub> (95:5). Percentages of the target "tripeptide" were analyzed by HPLC.

| Entry | Coupling reagents         | Equivalents | Coupling time | Temperature | Recoupling | % Coupling |
|-------|---------------------------|-------------|---------------|-------------|------------|------------|
| 1     | HATU<br>HOAt<br>DIEA      | 3<br>3<br>6 | 60 min        | 25 °C       | No         | 21         |
| 2     | HATU<br>HOAt<br>DIEA      | 3<br>3<br>6 | 60 min        | 25 °C       | Yes        | 64         |
| 3     | HATU<br>HOAt<br>DIEA      | 4<br>4<br>8 | 90 min        | 25 °C       | No         | 28         |
| 4     | HATU<br>HOAt<br>DIEA      | 4<br>4<br>8 | 90 min        | 25 °C       | Yes        | 71         |
| 5     | HATU<br>HOAt<br>DIEA      | 4<br>4<br>8 | 90 min        | 40 °C       | Yes        | 79         |
| 6     | HATU<br>HOAt<br>DIEA      | 4<br>4<br>8 | 90 min        | 50 °C       | Yes        | 86         |
| 7     | COMU<br>OxymaPure<br>DIEA | 3<br>3<br>6 | 60 min        | 25 °C       | No         | 34         |
| 8     | COMU<br>OxymaPure<br>DIEA | 3<br>3<br>6 | 60 min        | 25 °C       | Yes        | 75         |
| 9     | COMU<br>OxymaPure<br>DIEA | 4<br>4<br>8 | 90 min        | 25 °C       | No         | 43         |
| 10    | COMU<br>OxymaPure<br>DIEA | 4<br>4<br>8 | 90 min        | 25 °C       | Yes        | 82         |
| 11    | COMU<br>OxymaPure<br>DIEA | 4<br>4<br>8 | 90 min        | 40 °C       | Yes        | 91         |
| 12    | COMU<br>OxymaPure<br>DIEA | 4<br>4<br>8 | 90 min        | 50 °C       | Yes        | 97         |

**Table 2.** Extend of NMe-Val coupling over NMe-Abu using various coupling conditions.

Additionally, the use of microwave irradiation was also evaluated on the basis of previous reports on the synthesis of difficult peptide sequences with microwave (MW)-assisted chemistry where improvement in terms of yields and purities were achieved.<sup>77,78</sup>

A small study was carried out using specialized equipment for MW applications with direct temperature and intermediate cooling control. Again, the same coupling was attempted using COMU (4 eq) and OxymaPure (4 eq) in the presence of DIEA (8 eq) using DMF as solvent, since the superiority of this system over the HATU-HOAt-DIEA coupling system was demonstrated in the study detailed in Table 2. Because MW irradiation has been reported to reduce the reaction time of difficult couplings, the reaction time employed in this MW-SPPS was

reduced to 20 min and the reaction temperature was kept below 50 °C to prevent undesired side reactions. All the tested conditions are detailed in Table 3.

| Potency | Temperature | Cooling | % Coupling |
|---------|-------------|---------|------------|
| 150 W   | 35 °C       | Yes     | 47         |
| 200 W   | 35 °C       | Yes     | 56         |
| 200 W   | 35 °C       | No      | 59         |
| 200 W   | 35 °C       | Yes     | 58         |
| 200 W   | 40 °C       | Yes     | 60         |
| 200 W   | 50 °C       | Yes     | 72         |
| 300 W   | 50 °C       | Yes     | 76         |

**Table 3.** Results for the MW solid-phase NMe-Val coupling over NMe-Abu using different conditions.

The results obtained following a MW assisted SPPS for the specific coupling of Fmoc-NMe-Val-OH on the *in situ* methylated aminobutyric acid residue were disappointing, and it was decided to adopt the COMU-Oxyma-DIEA coupling system for our syntheses on solid phase, performing double or triple couplings at 50 °C when required.

#### Reagents for the introduction of the QC moieties in solution

Phosphonium salts are slightly more stable in the presence of a base, than aminium derivatives, and they are used during slow activation processes since they do not form guanidino derivatives when reacting with the amino component.<sup>79</sup> Thus, after cleavage from the resin, the QC moieties were introduced using PyBOP (2.4 eq), HOAt (2.4 eq) and DIEA (to adjust pH 8).

#### **Monitoring**

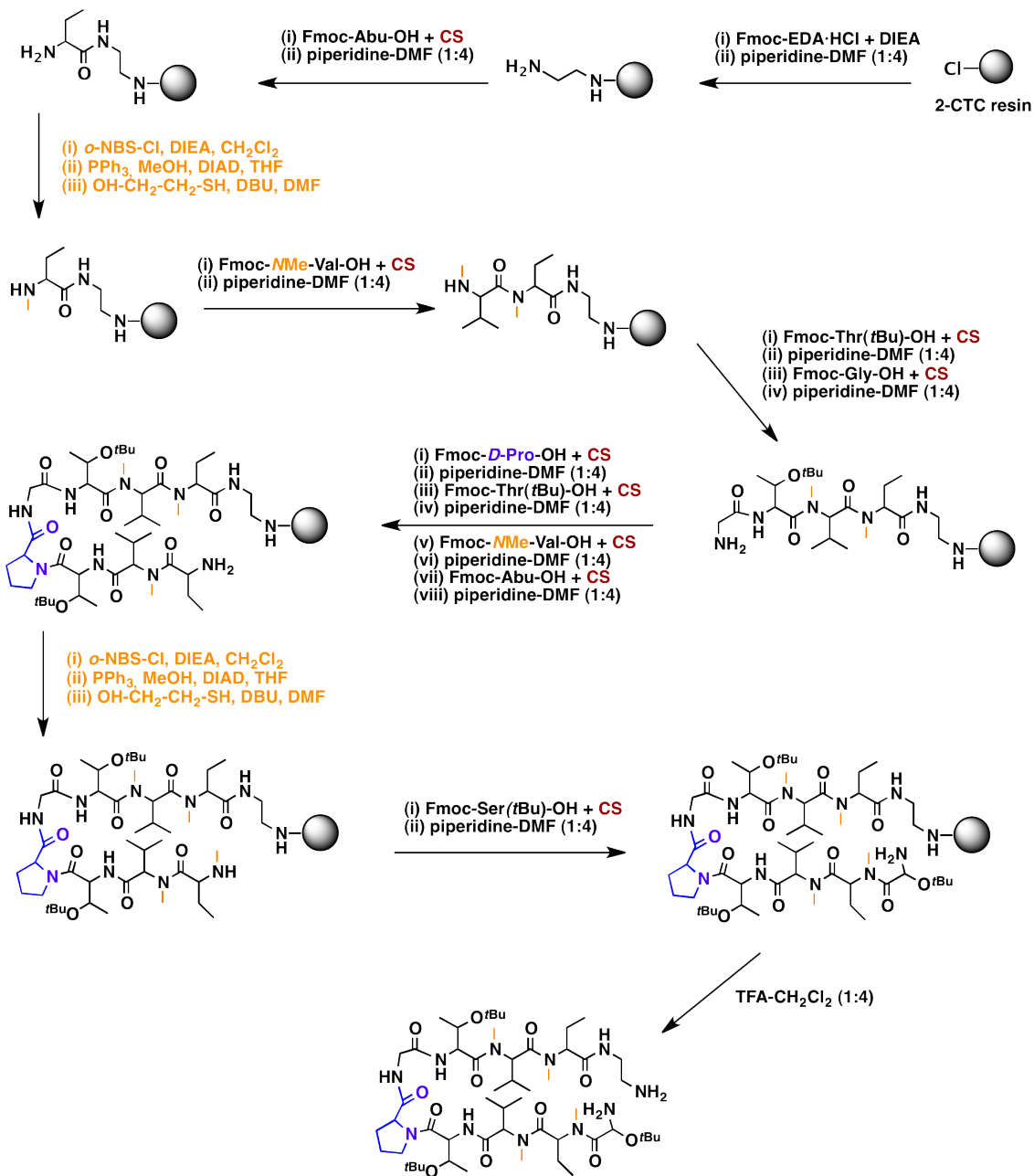
The amino acid couplings and deprotection steps were monitored by the qualitative ninhydrin test,<sup>80</sup> chloranil test,<sup>81</sup> or De Clercq test,<sup>82</sup> depending on the type of amine that was to be detected. Additionally, monitoring of difficult couplings was performed by HPLC-PDA, so as to evaluate their completeness in a quantitative manner.

#### **Peptide cleavage from the solid support**

Cleavage from 2-CTC resin is achieved by acidolytic treatment in very mild TFA conditions. However, it was observed that several treatments with 2% TFA in CH<sub>2</sub>Cl<sub>2</sub> were not enough for total cleavage from the resin. It seems that the attachment of the ethylenediamine entity as the first anchoring point for peptide elongation modifies the lability of this resin. Therefore, several generations of cleavage treatments with increasing percentages of TFA were carried out with the same batch of peptidyl resin and collected separately. The solvent was evaporated and analyzed by RP-HPLC so as to identify the occurrence of peptide.

In the first round of cleavage, the peptidyl resin was treated with 5 washes of 1 min each of 2% TFA in CH<sub>2</sub>Cl<sub>2</sub> and further washed with CH<sub>2</sub>Cl<sub>2</sub> until the resin's red color went back to light yellow. The treatments and the washes were directly poured over H<sub>2</sub>O–ACN (1:1) to avoid *t*Bu side-chains deprotection, and the next round of treatment with 5% TFA in CH<sub>2</sub>Cl<sub>2</sub> was performed under the same conditions. The process was repeated with 10%, 20% and 30% TFA in CH<sub>2</sub>Cl<sub>2</sub>.

After RP-HPLC and MS-HPLC characterization of the cleaved crudes, it was observed that a very little amount of peptide remained attached to the resin before the last treatment but such percentage of TFA provoked some *t*Bu deprotection, whereas this did not happen using 20% of TFA. So it was decided to perform the peptides cleavage using 20% TFA in CH<sub>2</sub>Cl<sub>2</sub>.

**General synthetic strategy scheme for peptide elongation**

**Figure 12.** Example of general SPPS procedure for peptide elongation. Reaction conditions for the *N*-methylated analogues are colored in orange, and are omitted for the non-*N*-methylated peptides. CS stands for the coupling system COMU-Oxyma-DIEA. Amino acid residues with D-configuration are colored in blue.

**The designed peptides without QC moieties: Z1-Z12 peptide library**

So as to evaluate the biological activity of the peptidic scaffolds and the role that they might play, it was decided to isolate an aliquot of the elongated peptides after cleavage from the resin. Global deprotection of the twelve peptides (Figure 13) was carried out with trifluoroacetic acid (TFA)-H<sub>2</sub>O (95:5) in 2 hours. The crudes were purified by semi-preparative reversed-phase high-performance liquid chromatography (RP-HPLC) to furnish purities over 95% as shown by analytical HPLC.

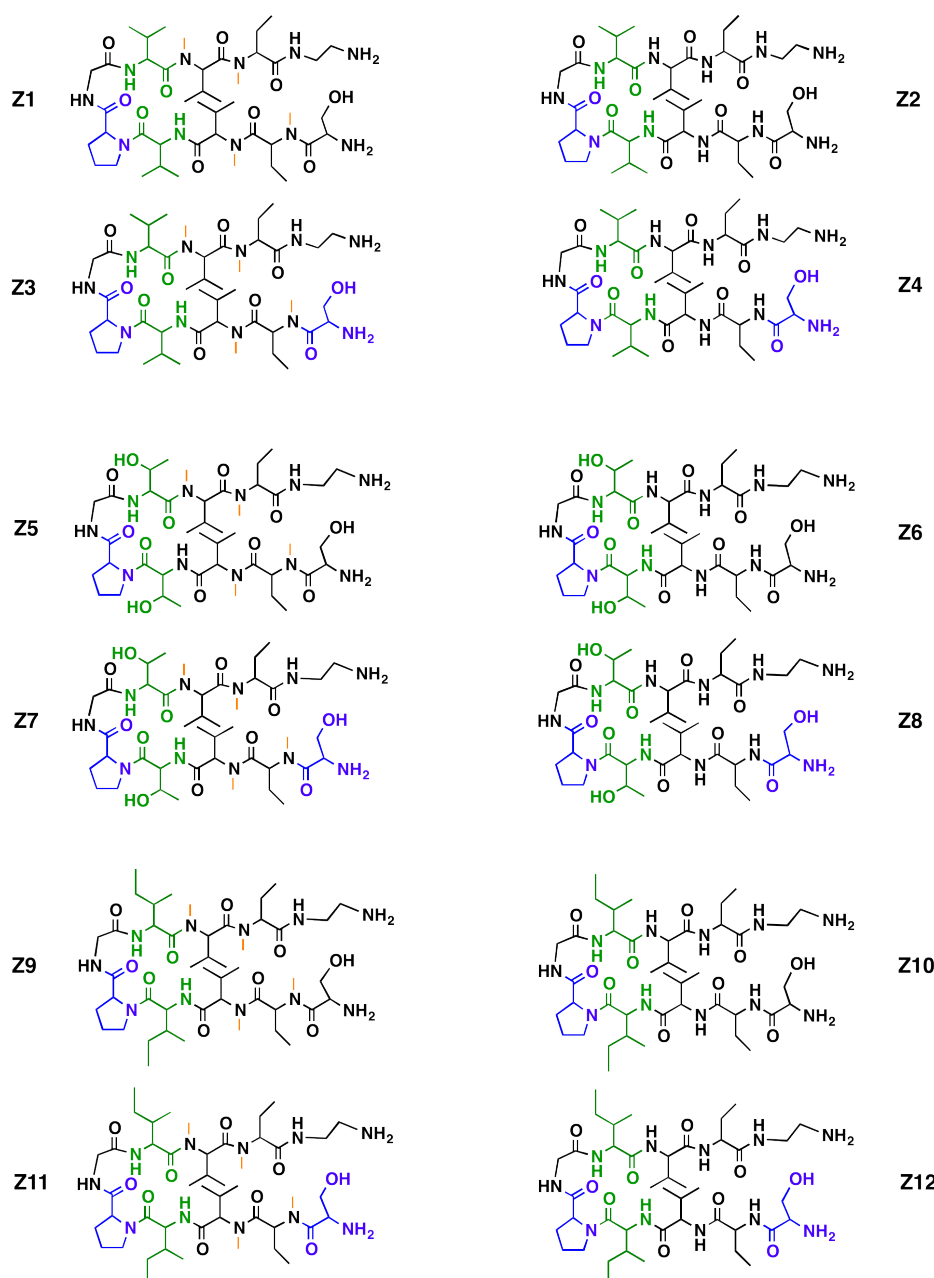


**Figure 13.** Chemical structures of the Z1-Z12 peptide library. For identification purposes D-amino acids are shown in blue and N-methylations in orange. The β-branched amino acids (valine, threonine or isoleucine) next to the β-loop that define the four residue β-turn are shown in green.

### Z1-Z12 peptides with QC moieties: RZ1-RZ12 library

Long coupling reactions were run between the side-chains protected peptides and 2-quinoxalinecarboxylic acid using the efficient coupling system PyBOP–HOAt–DIEA in DMF–CH<sub>2</sub>Cl<sub>2</sub> (1:1), to afford the designed library of analogues RZ1–RZ12 (Figure 14). Global deprotection of the twelve quinoxaline-containing peptides was carried out with trifluoroacetic acid TFA–H<sub>2</sub>O (95:5) in 2 hours. The crudes were purified by semi-preparative RP-HPLC to furnish purities over 90%.

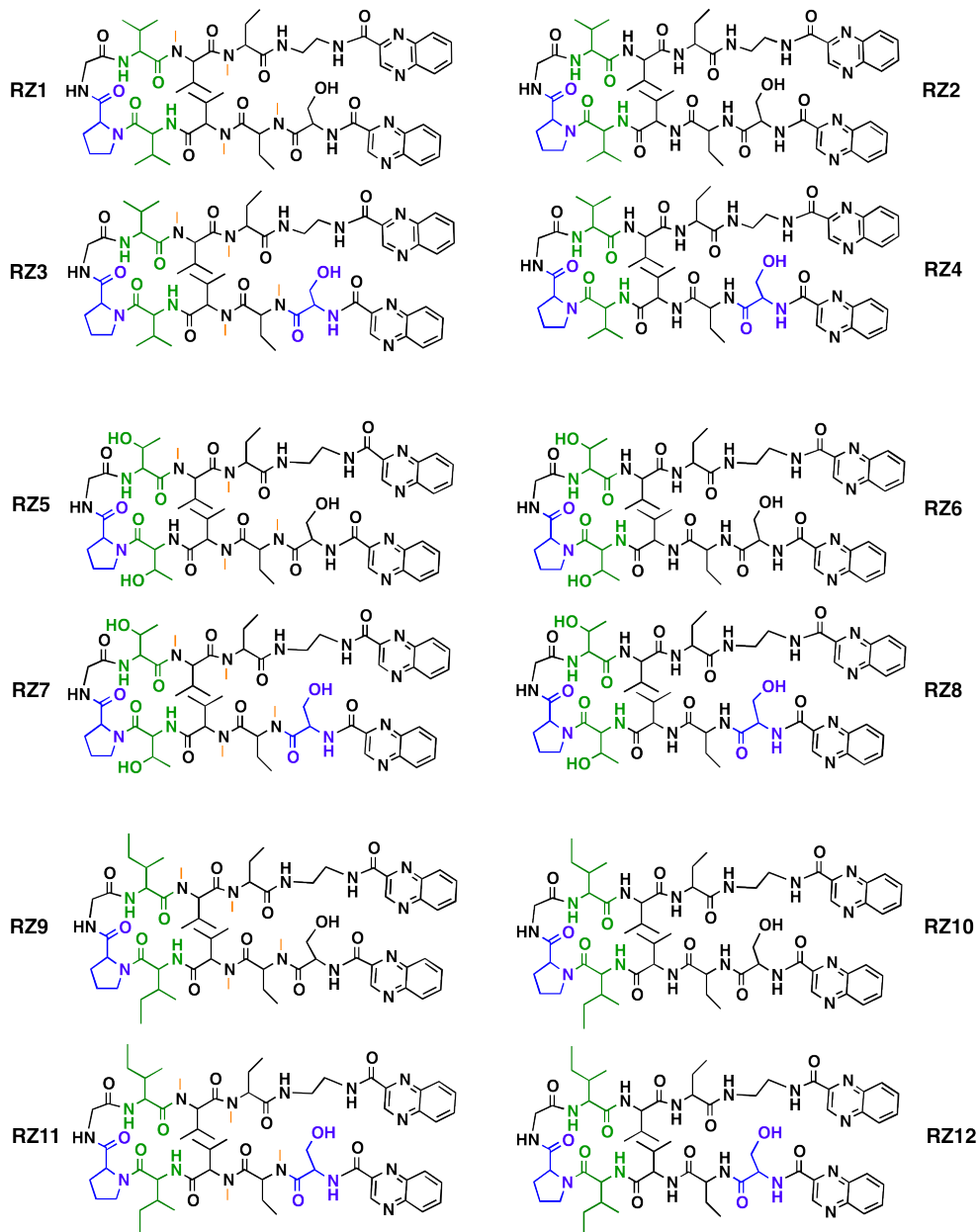


**Figure 14.** Chemical structures of the RZ1–RZ12 library. For identification purposes D-amino acids are shown in blue and *N*-methylation in orange. The  $\beta$ -branched amino acids (valine, threonine or isoleucine) next to the  $\beta$ -loop that define the four residue  $\beta$ -turn are shown in green.

### Fluorescent versions of the compound RZ2

As further described in the second chapter of the present thesis, the most active compound of the RZ1-RZ12 library against four different human cancer cell lines was compound RZ2.

Since RZ2's fluorescence properties ( $\lambda_{\text{ex}}$  323 nm;  $\lambda_{\text{em}}$  418) due to the presence of two quinoxaline moieties in its structure were not bright enough for visualization under the confocal microscope without overlapping with cells' autofluorescence, 5-carboxyfluorescein (CF) ( $\lambda_{\text{ex}}$  492 nm;  $\lambda_{\text{em}}$  517 nm) was used for labeling the compound.

After several unsuccessful attempts of attaching the CF via an ester bond between its carboxylic acid and the unprotected secondary alcohol of the serine's side chain, it was decided to synthesize the three fluorescent analogues illustrated in Figure 15.

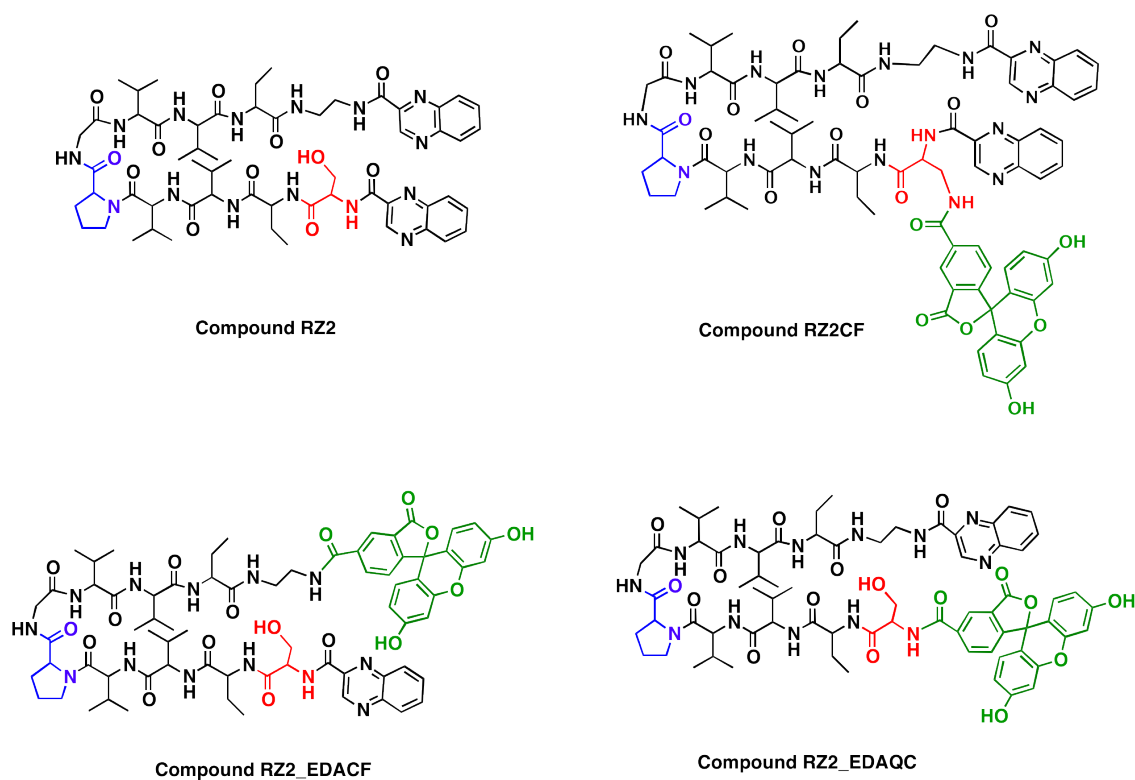


**Figure 15.** Fluorescent synthesized versions of compound RZ2. For identification purposes D-amino acids are shown in blue and CF moieties in green. The Ser residue from RZ2 that is substituted by Dap in RZ2CF is highlighted in red.

### Compound RZ2CF

The peptide chain is elongated in the same fashion than peptide Z2 besides the incorporation of Fmoc-EDA\*HCl as the first moiety attached to the 2-CTC resin to ensure a controlled loading of 0.7 mmol/g resin. Diminishing the maximum loading capacity of the resin ensures an easier coupling of the bulky 5-carboxyfluorescein dye, which may be impeded in very steric hindered environments.

Towards the peptide assembly, the serine residue is substituted by diaminopropionic acid (Dap), so that the CF moiety can be coupled to its side-chain through an amide bond while the peptide is still attached to the resin. Further attachment of the two quinoxalines is performed in solution, followed by work-up and purification by semi-preparative RP-HPLC. The final compound is obtained in a 5.3% overall yield.

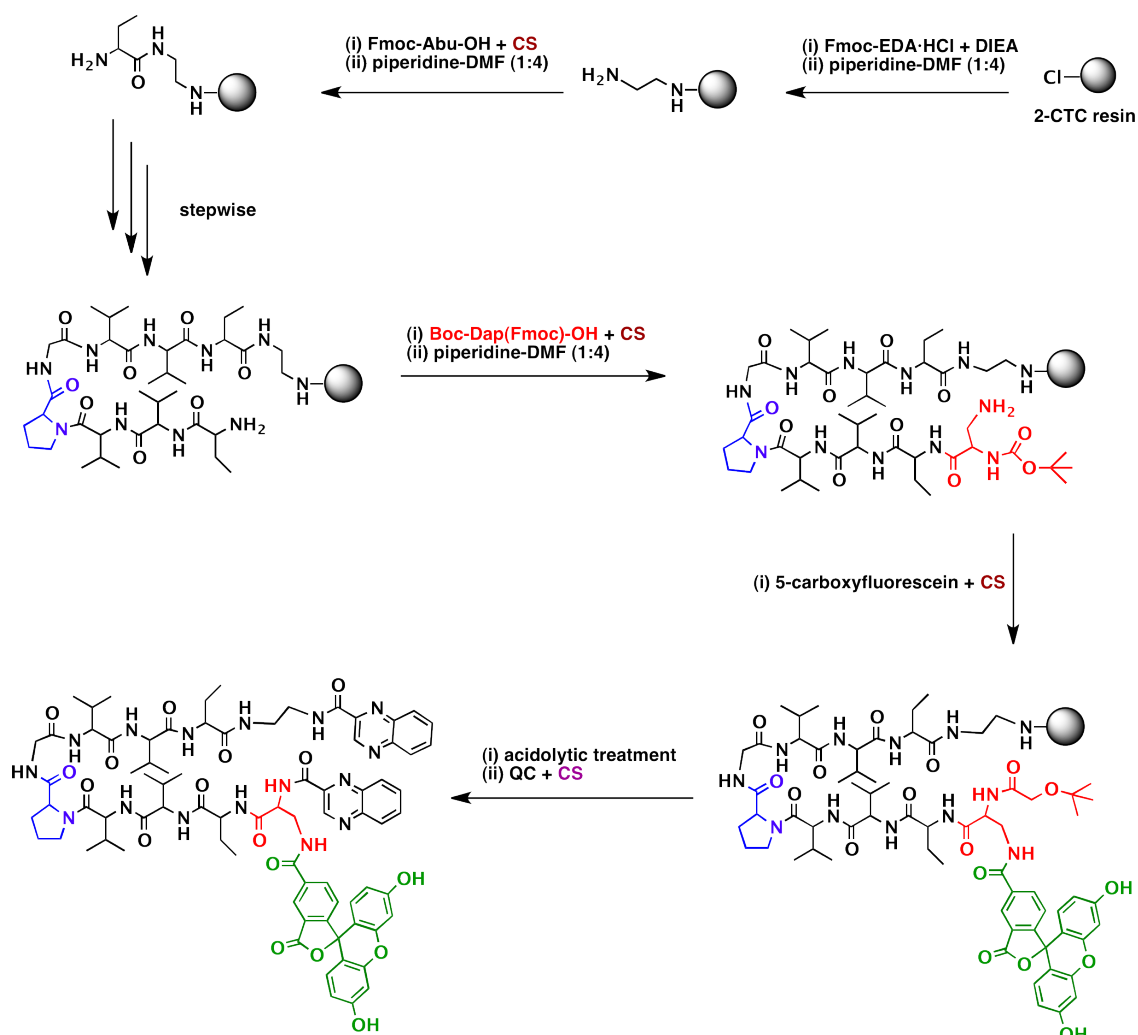


**Figure 16.** Synthetic strategy for the synthesis of compound RZ2CF. Amino acid residues with D-configuration are colored in blue, CF in green and the Dap residue that substitutes the Ser residue from the RZ2 compound is highlighted in red. CS stands for coupling system (COMU-Oxyma-DIEA for couplings on solid phase and PyBOP-HOAt-DIEA for the introduction of the quinoxalines in solution).

**Compound RZ2\_EDAQC**

Peptide Z2 is synthesized and the CF moiety is attached to the serine residue on solid-phase. The labeled peptide is cleaved and just one quinoxaline unit is attached to the free *N*-terminus of the ethylenediamine in solution. Further deprotection of the side-chain of the serine residue, work-up and purification by semi-preparative RP-HPLC renders the final product in 4.6% yield.

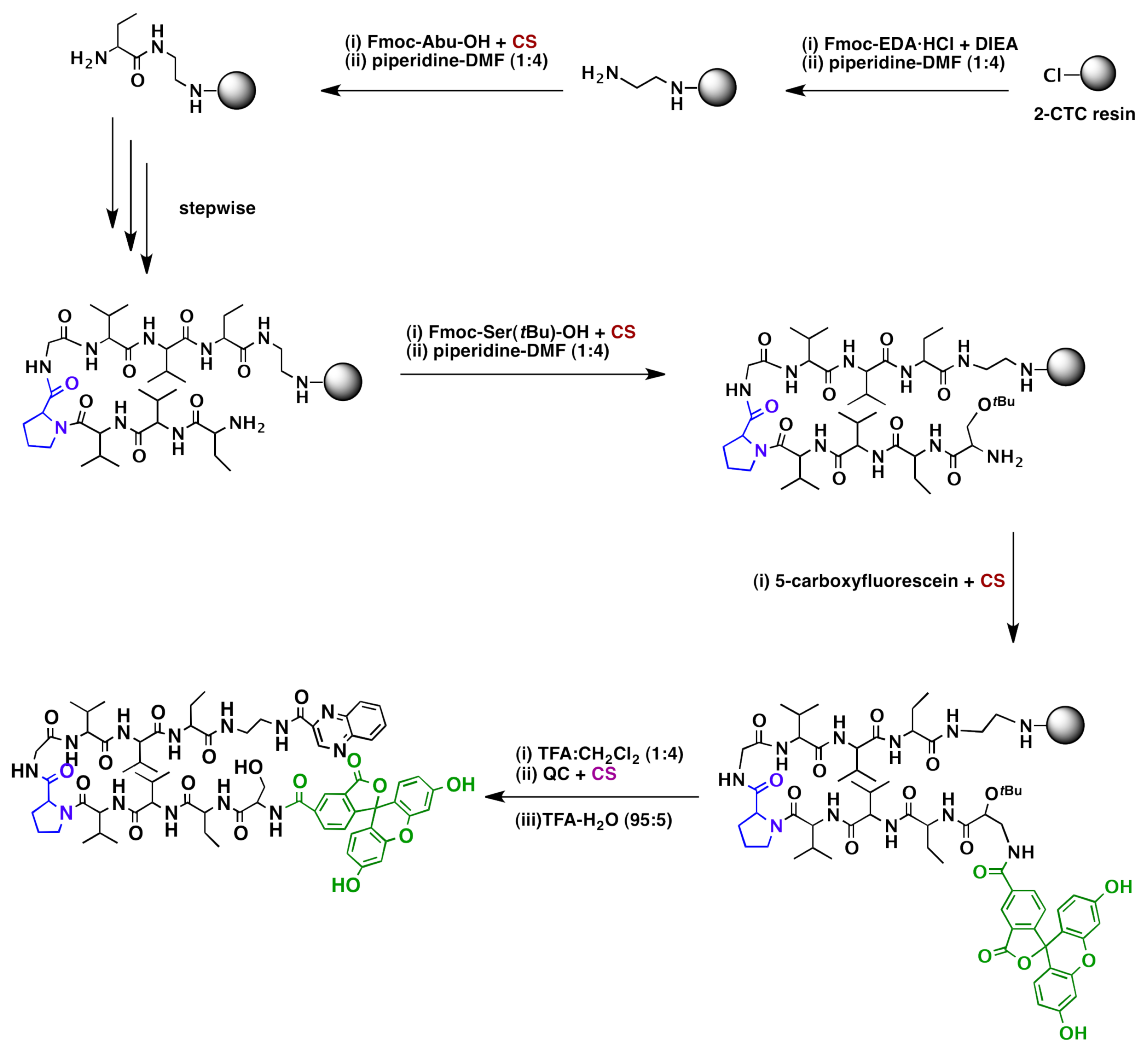


**Figure 17.** Synthetic strategy for the synthesis of compound RZ2\_EDAQC. Amino acid residues with D-configuration are colored in blue and CF in green. CS stands for coupling system (COMU-Oxyma-DIEA for couplings on solid phase and PyBOP-HOAt-DIEA for the introduction of the quinoxaline moiety in solution).

**Compound RZ2\_EDACF**

The only difference between this compound and RZ2\_EDAQC is that the quinoxaline moiety is coupled to the serine residue on solid-phase and the free *N*-terminus of the ethylenediamine after resin cleavage is coupled to CF through an amide bond.

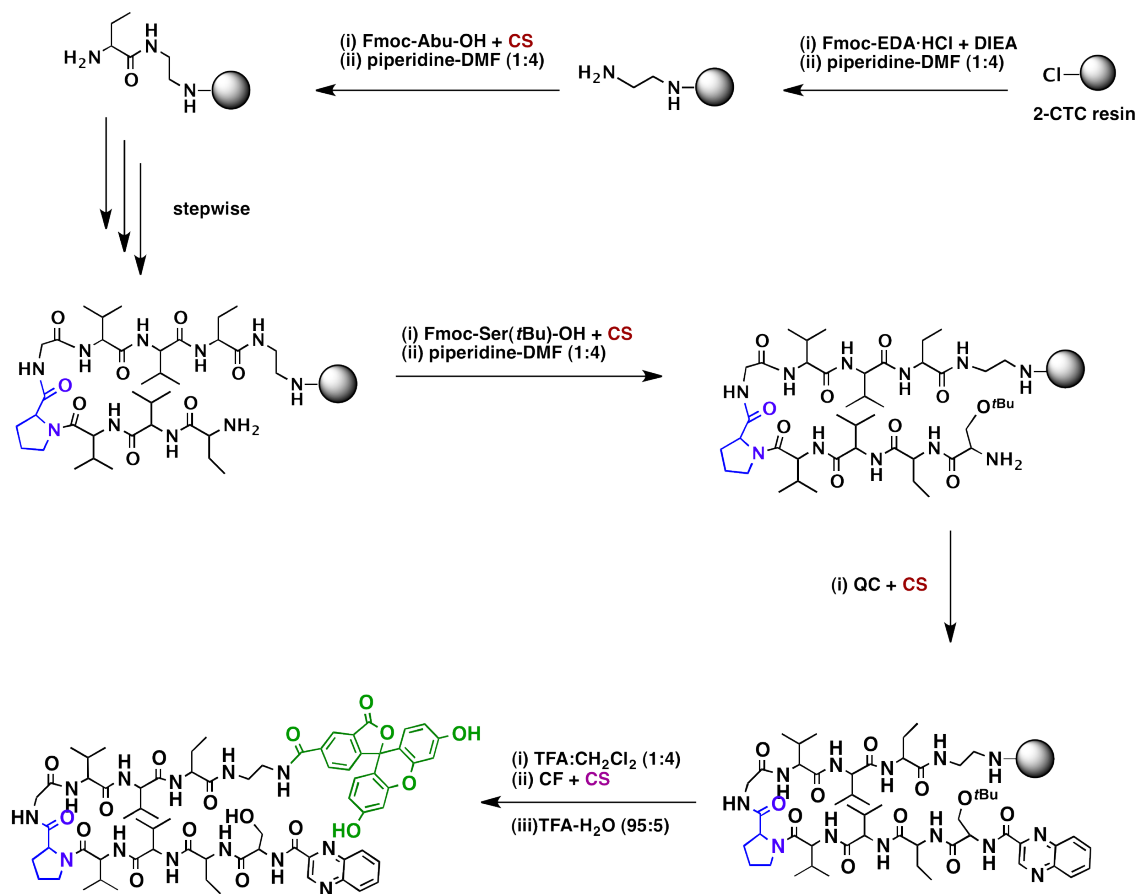


**Figure 18.** Synthetic strategy for the synthesis of compound RZ2-EDACF. Amino acid residues with D-configuration are colored in blue and CF in green. CS stands for coupling system (COMU-Oxyma-DIEA for couplings on solid phase and PyBOP-HOAt-DIEA for the introduction of the CF dye in solution).

For the last two compounds, it was thought that the stacking interactions between the heterocyclic units (quinoxaline and CF) would maintain the secondary structure of the original compound RZ2, so that the biological activity would be maintained.

The three CF labeled RZ2 analogues were obtained in excellent purity, as shown by their HPLC profiles.

### Other simplified analogues based on RZ2: compounds RZV

On the basis that compound RZ2 displayed the best biological activity among the RZ1-RZ12 library, another three analogues were designed and synthesized for further biological evaluation, based on the chemical structure of bisintercalator molecules, such as thiocoraline<sup>83</sup> and triostin A<sup>9</sup> (Figure 19). The efficient coupling system COMU-Oxyma-DIEA was used for the peptides' elongation, and PyBOP-HOAt-DIEA for the incorporation of the quinoxaline moieties in solution.

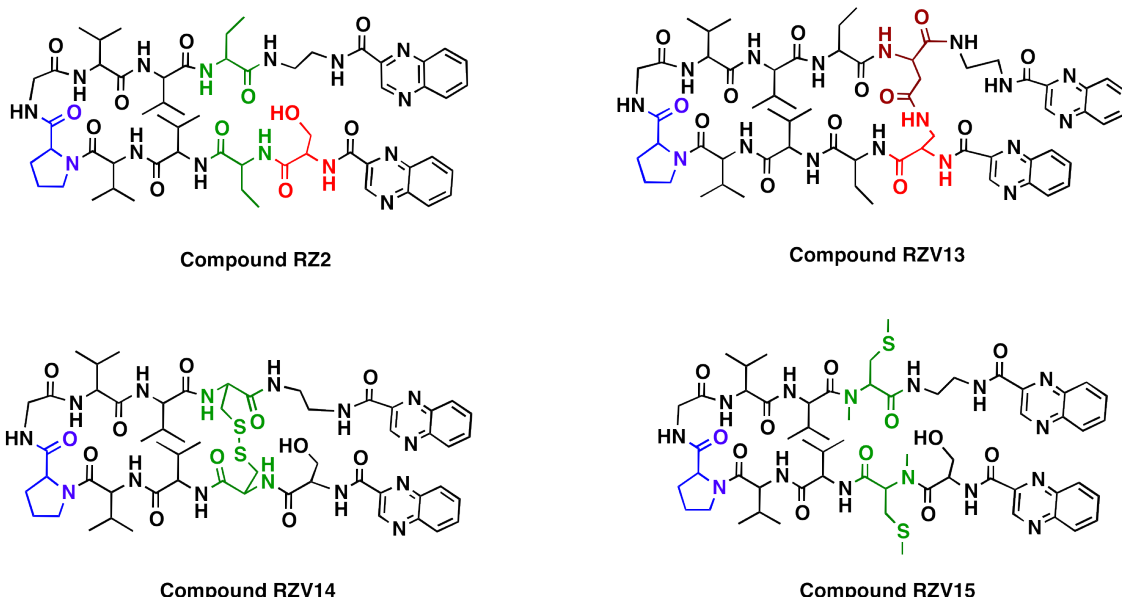


**Figure 19.** Chemical structures of compounds RZV. For identification purposes D-amino acids are shown in blue. Substitutions of the Abu residues from compound RZ2 are highlighted in green. Substitution of the Ser residue is highlighted in red. The additional residue that was not present in the chemical structure of RZ2 is displayed in brown.

#### Compound RZV13

This analogue is a cyclic version of compound RZ2. The  $\beta$ -sheet secondary structure of the original molecule is maintained but closed via an amide bond just next to both quinoxaline moieties.

After anchoring 0.7 mmol/g of Fmoc-EDA\*HCl to 2-CTC, Fmoc-Asp(Allyl)-OH was coupled and its side-chain remained protected during peptide assembly. The serine residue of RZ2 was replaced by Boc-Dap(Fmoc)-OH to form an amide bond between its Fmoc-deprotected side-chain and the previously deprotected hydroxyl function of the Asp residue. After the cyclization step, the peptide was cleaved from the solid support and the quinoxalines were attached in solution. Further semi-preparative RP-HPLC purification afforded the final compound in 95% purity and 11% yield.

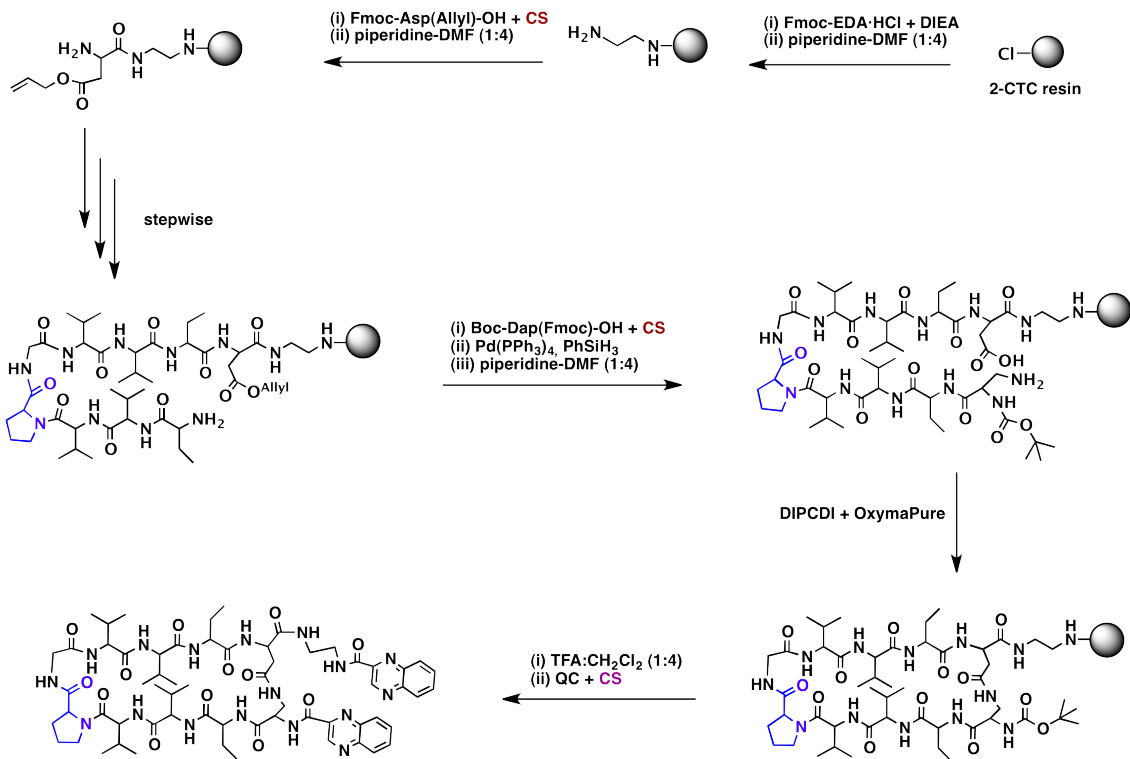


**Figure 20.** Synthetic strategy for the synthesis of compound RZV13. Amino acid residues with D-configuration are colored in blue. CS stands for coupling system (COMU-Oxyma-DIEA for couplings on solid phase and PyBOP-HOAt-DIEA for the introduction of the QC moieties in solution).

### Compound RZV14

This analogue bears a disulfide bridge, as the natural bisintercalator triostin A does. In this case, the Abu residues of RZ2 are replaced by the commercially available Fmoc-Cys(Acm)-OH at both strands of the antiparallel  $\beta$ -sheet. The whole peptide elongation is performed and after incorporation of the final Ser residue, concomitant removal of both S-Acm side-chain protecting groups and formation of the disulfide bridge is performed in a single step by treatment with iodine. The peptide is then cleaved from the resin and both quinoxalines are attached in solution. Final serine's side-chain deprotection is performed using TFA-H<sub>2</sub>O (95:5) and the crude peptide is purified by semi-preparative RP-HPLC, affording RZV14 with a purity of 96% and 5% yield.

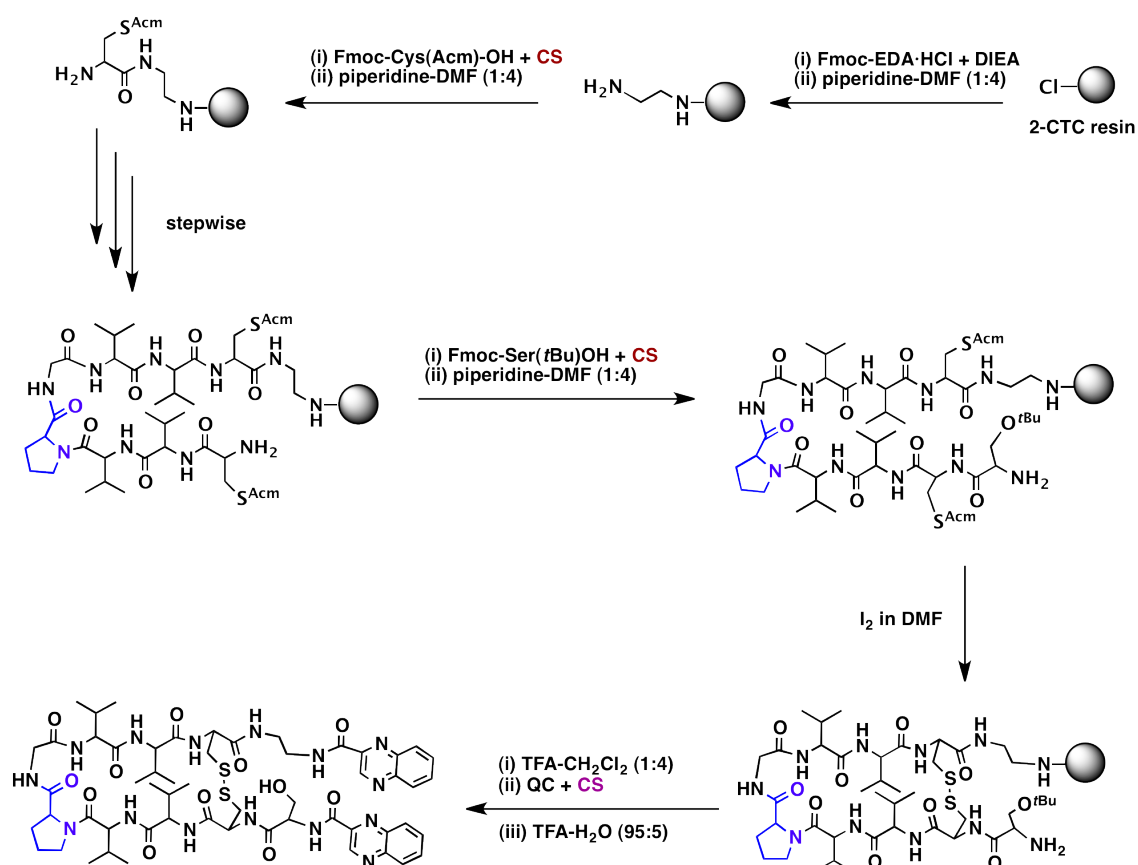


**Figure 21.** Synthetic strategy for the synthesis of compound RZV14. Amino acid residues with D-configuration are colored in blue. CS stands for coupling system (COMU-Oxyma-DIEA for couplings on solid phase and PyBOP-HOAt-DIEA for the introduction of the QC moieties in solution).

### Compound RZV15

Based on thiocoraline's chemical structure, that exhibits two NMe-Cys(Me) residues, it was decided to synthesize this RZ2 analogue in which both Abu residues are replaced by this N-methylated Cys (Figure 22).

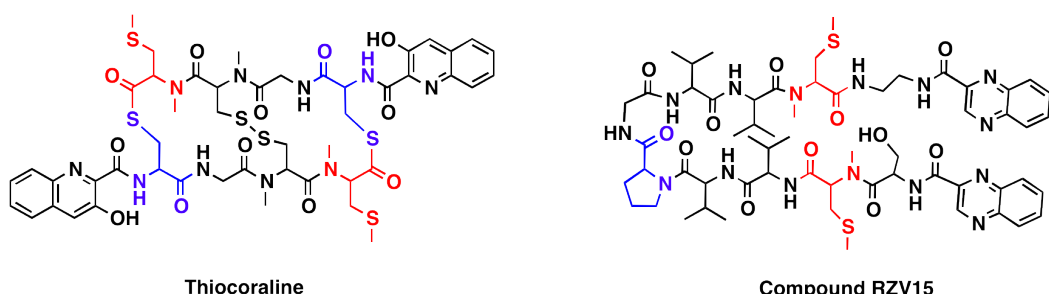


**Figure 22.** Compound RZV15 bears the same NMe-Cys(Me) residue as thiocoraline. For identification purposes D-amino acids are shown in blue and the NMe-Cys(Me) residues are shown in red.

Firstly, the synthesis of the allyloxycarbonyl (Alloc)-protected *N*-methylated Cys was undertaken from commercially available Fmoc-Cys(Trt)-OH using reported procedures developed in our research group.<sup>84</sup>

#### Alloc-NMe-Cys(Me)-OH synthesis

Alloc-Cys(Trt)-OH is obtained by attaching Fmoc-Cys(Trt)-OH on 2-CTC resin, followed by removal and re-protection of the amino function with Alloc-Cl. After cleavage from the solid support, Alloc-Cys(Trt)-OH is subjected to standard procedures of *N*-methylation. Next, the Trt group is removed under acidic conditions in the presence of TIS to avoid realkylation of this protecting group. Me side-chain protection was introduced without previous purification of the free thiol derivative since the remaining triphenylmethane and TIS do not interfere in the protection reaction. Alloc-NMe-Cys(Me)-OH was obtained in 78% yield under mild conditions with a slight excess of Mel in aqueous medium, maintaining neutral pH. The synthetic Cys residue was used without further purification.

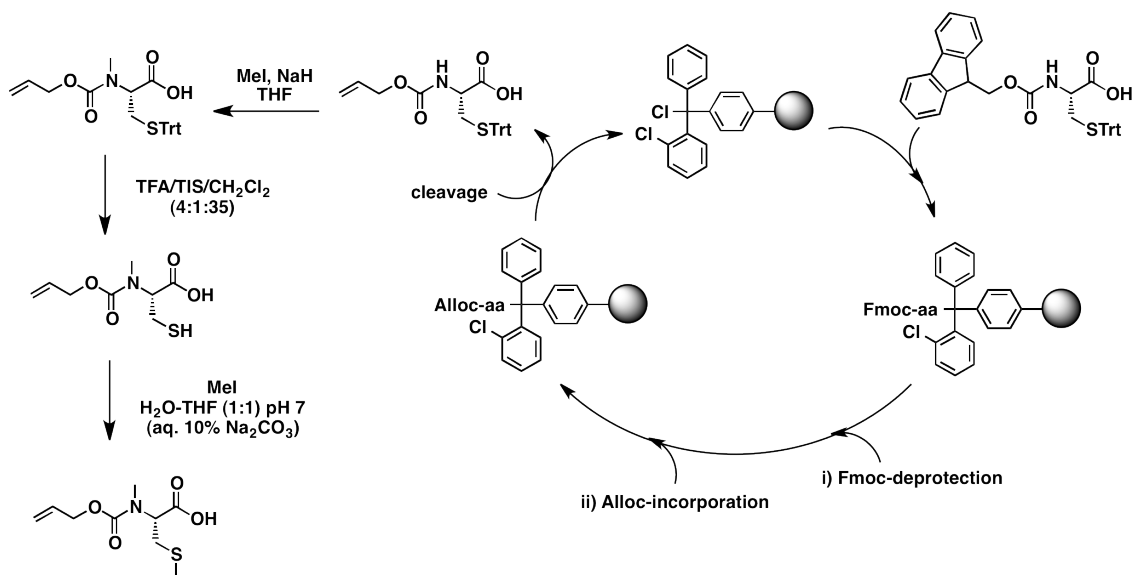
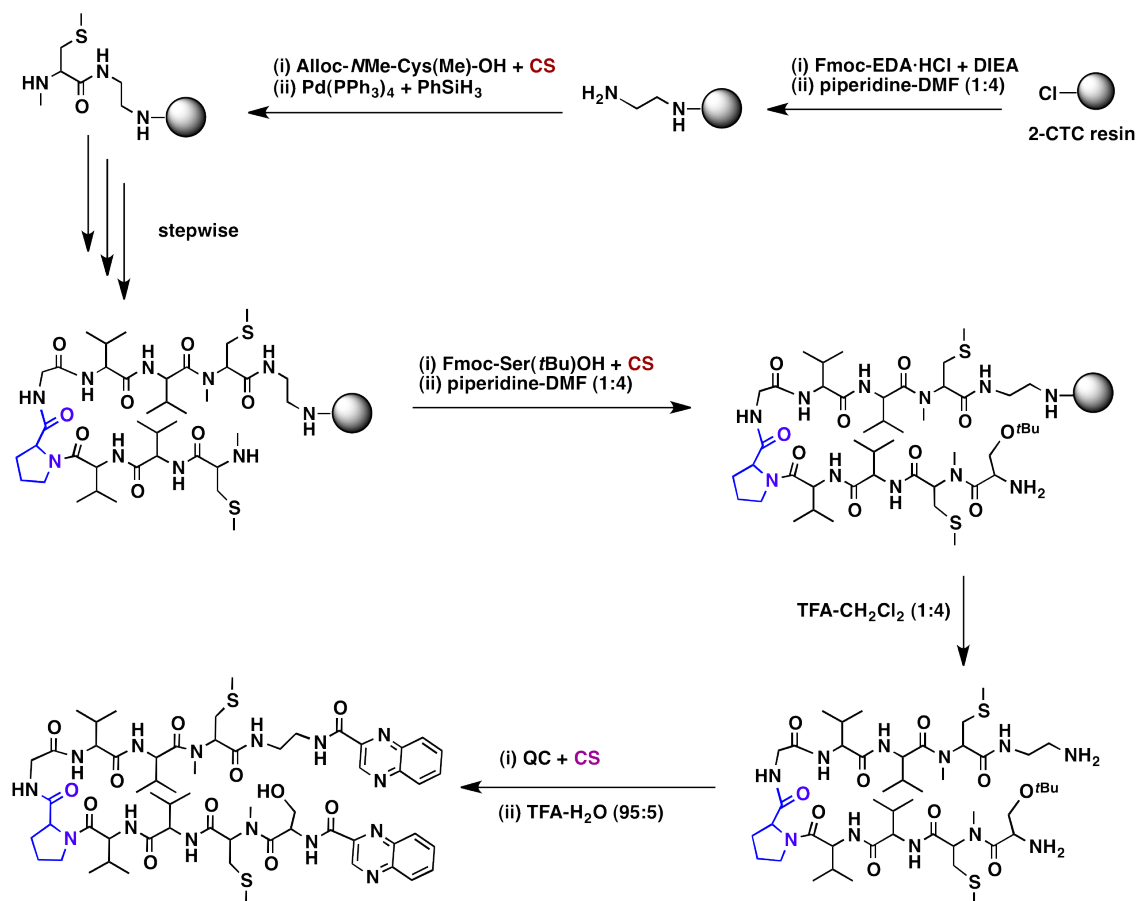


Figure 23. Synthetic strategy for the synthesis of the Alloc-NMe-Cys(Me)-OH residue.

The solid-phase synthesis of compound RZV15 began by anchoring Fmoc-1,2-ethylenediamine\*HCl onto the 2-CTC resin, followed by the incorporation of the synthesized Alloc-NMe-Cys(Me)-OH. Removal of the Alloc group was achieved by treatment with Pd(PPh<sub>3</sub>)<sub>4</sub> and PhSiH<sub>3</sub> and peptide elongation was achieved following a stepwise strategy, performing the other Alloc group removal under the same described conditions for the final incorporation of the protected Fmoc-Ser(*i*Bu)-OH amino acid. Cleavage from the resin with 20% TFA was performed after the last Fmoc removal and the incorporation of the QC moieties was performed prior to side-chain deprotection. The resulting crude was purified by semi-preparative RP-HPLC.



**Figure 24.** Synthetic strategy for the synthesis of compound RZV15. Amino acid residues with D-configuration are colored in blue. CS stands for coupling system (COMU-Oxyma-DIEA for couplings on solid phase and PyBOP-HOAt-DIEA for the introduction of the QC moieties in solution).

The three RZV analogues were obtained in excellent purity, as shown by their HPLC profiles.

### Positive control for biological assays: triostin A synthesis.

This natural bisintecalator was synthesized on solid-phase using reported procedures developed in our research group, which make use of a number of coupling reagents, several orthogonal protecting groups and conformationally restricted mobility, a new concept of protection described in the first solid-phase synthesis of triostin A reported.<sup>50</sup>

For this synthetic strategy, two non-commercially available suitable protected amino acids must be firstly synthesized: Alloc-NMe-Val-OH and Boc-NMe-Cys(Acm)-OH (Figure 25).

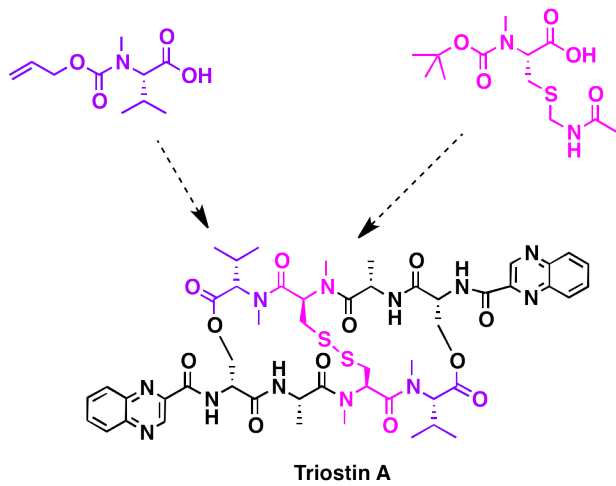


**Figure 25.** Non-commercial protected amino acids obtained for the synthesis of triostin A.

#### *Alloc-NMe-Val-OH synthesis*

Alloc-NMe-Val-OH was synthesized from Boc-NMe-Val-OH by using TFA-CH<sub>2</sub>Cl<sub>2</sub> (1:1) to remove the Boc group and allyl chloroformate in dioxane to introduce the Alloc group, using standard procedures (100% yield, 90% purity).

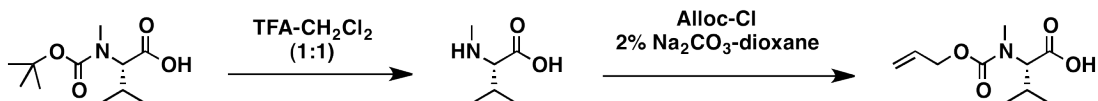


**Figure 26.** Alloc-NMe-Val-OH obtained from Boc-NMe-Val-OH.

Boc-NMe-Cys(Acm)-OH synthesis

This amino acid was prepared from Boc-Cys(Trt)-OH using reported procedures developed in our research group.<sup>84</sup>

Specifically, Boc-Cys(Trt)-OH was *N*-Methylated by using regular conditions (NaH, MeI) to obtain Boc-NMe-Cys(Trt)-OH. Then, reaction with acetamidomethanol (Acm-OH) under acidic conditions and in the presence of TIS simultaneously removed the Trt and Boc groups and introduced the Acm moiety in a single step. The Boc derivative of the intermediate obtained, H-NMe-Cys(Acm)-OH, was easily obtained by reaction with (Boc)<sub>2</sub>O in 76% yield.

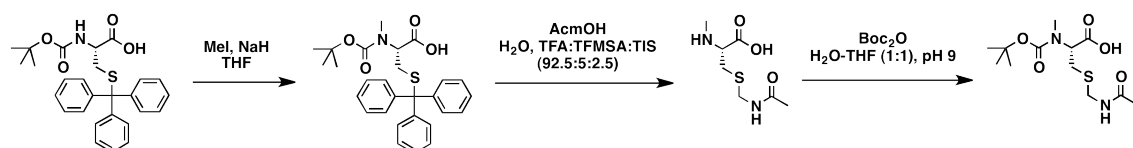


**Figure 27.** Boc-NMe-Cys(Acm)-OH obtained from Boc-Cys(Trt)-OH.

**Triostin A**

The synthetic strategy followed is a [4+4] convergent approach, taking advantage of the C<sub>2</sub> symmetry of the molecule.

A Wang-type resin (Figure 28) substitutes the use of 2-CTC resin since the latter is incompatible with the temporary protecting Trt group of the hydroxyl function of the D-Ser.

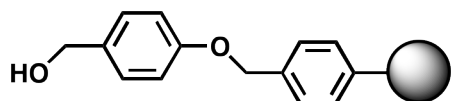


**Figure 28.** Structure of the polystyrene-based Wang resin.

The starting point for the synthesis is the Ala anchoring to the resin, followed by the introduction of the Fmoc-D-Ser(Trt)-OH. After Fmoc deprotection, the 2-quinoxalinecarboxylic acid coupling takes place, and the two remaining residues *N*Me-Val and *N*Me-Cys are introduced through the side-chain of the D-Ser residue. At this point, the formation of the inter-chain disulfide bridge is built in order to restrict the mobility of the peptide chain so as to prevent the formation of DKP between these last two *N*-methylated amino acid residues. Then, cleavage from the resin with

concomitant Boc group removal was performed followed by the final double cyclization to obtain the natural product.

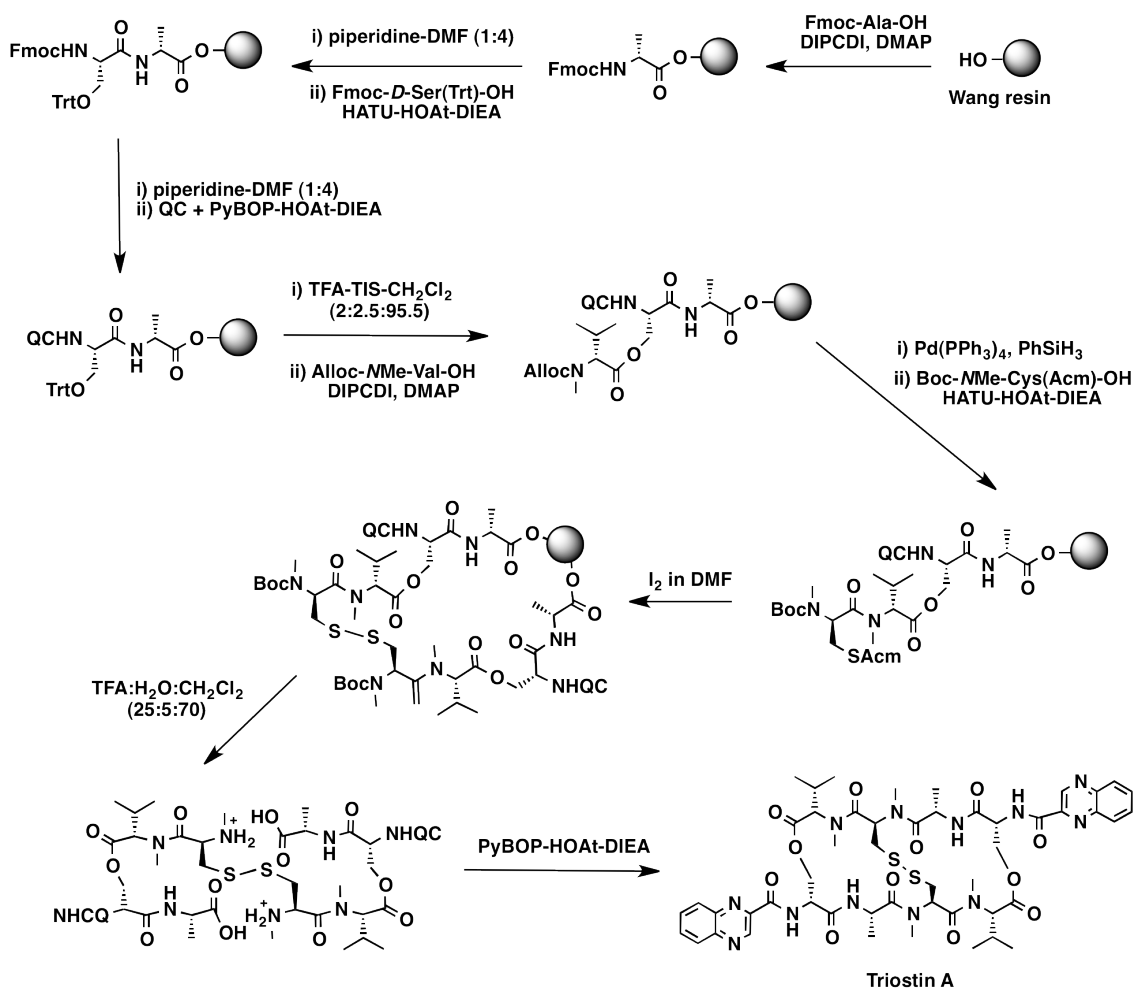


**Figure 29.** Solid-phase synthesis of triostin A.

## MATERIALS AND METHODS

### Solvents

Toluene and methyl *tert*-butyl ether were purchased from Scharlau; acetone, DMF, CH<sub>2</sub>Cl<sub>2</sub>, acetonitrile (HPLC grade), and methanol (HPLC grade) were obtained from SDS; EtOAc and DMSO were from Panreac; THF was obtained from Scharlau and purified using a Pure-Solv MD-2 solvent system (Innovative Technology, Inc.). TFA was obtained from Sigma-Aldrich.

### Reagents

Protected amino acid derivatives and 2-CTC resin were obtained from Iris Biotech. DIEA, DIPCDI, piperidine, collidine, 2-quinoxalinecarboxylic acid, 1,8-diazabicyclo[5.4.0]undec-7-ene, *N,N*-diisopropylethylamine, diisopropylcarbodiimide, 4-(dimethylamino)pyridine, β-mercaptoethanol, *o*-nitrobenzenesulfonyl chloride, ninhydrin, triisopropylsilane and 5-carboxyfluorescein were obtained from Sigma-Aldrich; PyBOP was from Shanghai Medpep; HOAt, COMU and OxymaPure were from Luxembourg Industries. All commercial reagents were used as received.

### General basic instrumentation

|                          |   |
|--------------------------|---|
| Balances                 | METTLER TOLEDO<br>MS 303-S. 3 significant figures<br>AB 204-S. 4 significant figures<br>AT 261 DeltaRange®. 5 significant figures<br>MX5. 6 significant figures |
| Lyophilizers             | Freezemobile 25 EL, VirTis  |
| Orbital shakers          | Unimax 1010, Heidolph   |
| Rotary evaporators       | Laborota 4003 Control, Heidolph   |
| Ultrasonic bath          | BRANSON   |
| UV-Vis spectrophotometer | UV-2501PC, Shimadzu   |
| Vortex mixers            | MERCK® eurolab  |

## High-performance liquid chromatography

### **Analytical HPLC**

Analytical HPLC was performed on a Waters instrument comprising a Waters 2695 (Waters, MA, USA) separation module, an automatic injector, a photodiode array detector (Waters 996 or Waters 2998), and a Millenium<sup>32</sup> login system controller. The columns used were a Xbridge<sup>TM</sup> C18 reversed-phase analytical column (2.5 µm x 4.6 mm x 75 mm), a Xbridge<sup>TM</sup> BEH130 C18 reversed-phase analytical column (3.5 µm x 4.6 mm x 100 mm) and a SunFire<sup>TM</sup> C18 reversed-phase analytical column (3.5 µm x 4.6 mm x 100 mm) run with linear gradients of ACN (0.036% TFA) into H<sub>2</sub>O (0.045% TFA) over 8 min or a Symmetry<sup>®</sup> C18 reversed phase analytical column (5 µm x 4.6 mm x 150 mm) run with linear gradients over 15 min. UV detection was at 220, 242 and 320 nm and the system was run at a flow rate of 1.0 mL/min.

### **Semi-analytical HPLC**

Semi-analytical HPLC was performed on a Waters instrument comprising two solvent delivery pumps (Waters 1525), an automatic injector (Waters 717 autosampler), a Waters 2487 dual wavelength detector, a Breeze v3.20 system controller, a Symmetry<sup>®</sup> C18 reversed phase column (5 µm x 7.8 mm x 100 mm) or a XBridge<sup>TM</sup> Prep BEH130 C18 reversed-phase column (5 µm x 10 mm x 100 mm) and linear gradients of ACN (0.036% TFA) into H<sub>2</sub>O (0.045%TFA) over 20 min. The system was run at a flow rate of 3 mL/min. UV detection was at 220, 242 and 320 nm.

### **Semi-preparative HPLC**

Semi-preparative RP-HPLC was carried on a Waters instrument comprising two solvent delivery pumps (Waters Delta 600), an automatic injector (Waters 2700 Sample Manager), a Waters 2487 dual wavelength absorbance detector, an automatic sample collector (Waters Fraction Collector II), a Masslinx v3.5 system controller and three different columns, obtained also from Waters: a Symmetry<sup>®</sup> C8 reversed-phase column (5 µm x 30 mm x 100 mm), a Symmetry<sup>®</sup> C18 reversed-phase column (5 µm x 30 mm x 100 mm) and a SunFire<sup>TM</sup> Prep C18 OBD<sup>TM</sup> reversed-phase column (5 µm x 19 mm x 100 mm). Linear gradients of ACN (0.5% TFA) into H<sub>2</sub>O (1% TFA) with a flow rate of 10 mL/min or 15 mL/min were used.

### **HPLC-MS**

HPLC-MS analysis was performed on a Waters instrument comprising a Waters 2695 separation module, an automatic injector, a Waters 2998 photodiode array detector, a Waters

ESI-MS Micromass ZQ spectrometer, a Masslynx v4.1 system controller and a Sunfire<sup>TM</sup> C18 reversed-phase analytical column (3.5 µm x 2.1 mm x 100 mm). UV detection was at 220 and 242 nm, and linear gradients of ACN (0.07% formic acid) into H<sub>2</sub>O (0.1% formic acid) were run at a 0.3 mL/min flow rate over 8 min.

### MALDI-TOF

Mass spectra were recorded on a MALDI-TOF Applied Biosystem 4700 with a N<sub>2</sub> laser of 337 nm using α-cyano-4-hydroxycinnamic acid (ACH) matrix (20 mg/ mL ACH in 50% / 49.9% H<sub>2</sub>O / 0.1% TFA).

Sample preparation: a mixture of sample solution (1 µL) and matrix (1 µL) is prepared, placed on a MALDI-TOF plate and dried by air.

### Amino acids analysis

After hydrolysis and derivatization (AccQ-Tag<sup>TM</sup> Chemistry Kit, Waters) of the peptidic sample, the concentration of each amino acid was found using a Waters 600 instrument provided with a delta 600 pump, a Waters 717 automatic injector, a Waters 2487 UV detector, a Masslynx system controller and a Waters AccQ-Tag<sup>TM</sup> amino acid analysis Nova-pak C18 column (4 µm x 3.9 mm x 150 mm). Linear gradients of AccQ-Tag<sup>TM</sup> eluent A (Waters) and ACN at a flow rate of 1 mL/min were used.

### Nuclear magnetic resonance (NMR)

<sup>1</sup>H NMR and <sup>13</sup>C NMR spectroscopy was performed on a Bruker Digital Avance 600. Chemical shifts ( $\delta$ ) are expressed in parts per million downfield from tetramethylsilyl chloride. Coupling constants are expressed in Hertz. Homonuclear and heteronuclear NMR experiments were carried out on a Bruker Digital Avance 600 spectrometer at 298 °K.

### Solid phase peptide synthesis (SPPS)

#### *General considerations*

Solid-phase syntheses were performed in polypropylene syringes fitted with a polyethylene porous disc. Solvents and soluble reagents were removed by suction. Washings between deprotection and coupling steps were carried out with DMF (5 x 1 min) and CH<sub>2</sub>Cl<sub>2</sub> (5 x 1 min) using 5 mL solvent·g<sup>-1</sup> resin for each wash. Peptide synthesis transformations and washes were performed at 25 °C unless indicated otherwise. All peptides were synthesized by SPPS using the 9-fluorenylmethoxycarbonyl/*tert*-butyl (Fmoc/*t*Bu) strategy. Syntheses carried out on solid

phase were controlled by colorimetric tests and/or by HPLC of the intermediates obtained after cleaving an aliquot (~2 mg) of the peptidyl resin with TFA–TIS–H<sub>2</sub>O (95:2.5:2.5) for 1 h.

### **Colorimetric tests**

#### Kaiser test

The Kaiser test, also known as ninhydrin test, allows the qualitative confirmation of the presence of free primary amines on the resin. This test was used as a control in the coupling and deprotection steps during the elongation of the peptide in solid phase.<sup>80</sup>

The peptidyl-resin is washed with CH<sub>2</sub>Cl<sub>2</sub> and vacuum dried. A few beads are transferred to a small glass tube. Six drops of reagent solution A and 2 drops of reagent solution B are added to the tube and the mixture is heated at 110 °C for 3 min. When the appearance of the resin or the solution is blue, it means that primary amines are present (positive ninhydrin). Conversely, when their color is yellow there is absence of primary amines (negative ninhydrin). The method is highly sensitive and a negative test assures a coupling rate higher than 99%.

*Reagent solution A:* 400 g of phenol are dissolved in 100 mL of absolute EtOH and the mixture is heated until complete dissolution. 20 mL of 10 mM KCN (65 mg in 100 mL of H<sub>2</sub>O) are added to 1 L of freshly distilled pyridine over ninhydrin. Both solutions are stirred for 45 min with 40 g of Amberlite MB-3 resin ion exchange resin, filtered, and mixed.

*Reagent solution B:* 2.5 g of ninhydrin are dissolved in 50 mL of absolute EtOH; the resulting solution is kept in a flask protected from light.

#### Chloranil test

Chloranil test detects the presence of secondary amines during solid-phase chain assembly and it is used to evaluate couplings onto proline or *N*-alkyl residues.<sup>81</sup>

The peptide-resin is washed with CH<sub>2</sub>Cl<sub>2</sub> and vacuum dried. A small portion of peptidyl-resin beads is transferred to a small glass tube and 20 drops of acetone plus 5 drops of a saturated chloranil solution (0.75 mg of 2,3,5,6-tetrachloro-1,4-benzoquinone in 25 mL of toluene) are added. The resulting solution is shaken in a vortex mixer for 5 min at room temperature. A greenish color indicates the presence of free secondary amines and is thus considered a positive test. Negative samples display yellow, amber or brown color. This method is less sensitive than the De Clercq test.

### De Clercq test

The De Clercq test, also known as the *p*-nitrophenyl ester test, is a colorimetric test used in SPPS that enables qualitative detection of free secondary and primary amines with higher sensitivity than the chloranil test.<sup>82</sup>

The resin is washed with CH<sub>2</sub>Cl<sub>2</sub>, and then an amount between 0.5–2 mg of peptidyl-resin is placed in a glass tube and 5 drops of De Clercq reagent are added. After, the mixture is incubated at 70 °C for 10 min and cooled. The resin beads are washed with MeOH (3 times), DMF (3 times), and CH<sub>2</sub>Cl<sub>2</sub> (3 times). The presence of free amines is indicated by red-colored beads (positive test), whereas the absence of coloration (negative test) ensures a quantitative coupling.

*De Clercq reagent:* A three-step synthesis enables ready access to the red disperse 1 *p*-nitrophenyl ester:

- a) To a solution of 20 mmol of disperse red 1 (6.28 mg) and 0.34 mmol of Rh<sub>2</sub>(OAc)<sub>4</sub> (150 mg) in a mixture of CH<sub>2</sub>Cl<sub>2</sub> (100 mL) and toluene (100 mL), a solution of 80 mmol of ethyl diazoacetate (8.4 mL) in toluene (40 mL) is added at 40°C over a 1 h period. The reaction mixture is stirred overnight at room temperature and purified by flash chromatography.
- b) 62.5 mmol of KOH (4.062 g) and 12.5 mmol (5 g) of the product obtained in step (a) are dissolved in MeOH (300 mL) and toluene (70 mL) and refluxed under N<sub>2</sub> for 1.5 h. The product is purified by a series of extractions.
- c) The product obtained in step (b) (2.322 g) and *p*-nitrophenol (0.834 g) are dissolved in a solution of pyridine (100 mL) and CH<sub>2</sub>Cl<sub>2</sub> (120 mL). The mixture is cooled down to -15 °C and 10.8 mmol of POCl<sub>3</sub> (1.006 mL in 10 mL CH<sub>2</sub>Cl<sub>2</sub>) are slowly added over 1 h. The product is purified by a series of extractions.

The disperse red 1 *p*-nitrophenyl ester is used at a concentration of 0.02 M in acetonitrile.

### Solid-supported hydroxyl group detection

The test is adapted from the known staining method of amines using *p*-nitrophenyl ester. It is a sensitive and highly practical colorimetric test for resin-bound alcohols, phenols, and thiols and the general monitoring of the attachment of a first synthetic building block onto popular hydroxyl-derivatized solid supports.<sup>85</sup>

To a small amount of resin (1 mg) are added 100 µL of a 0.2 M DMAP solution in acetonitrile and 100 µL of a 0.002 M disperse red 1 *p*-nitrophenyl ester solution in acetonitrile. The suspension is allowed to stand for 10 min at room temperature after which the supernatant is removed, and the resin washed with DMF and methanol. In case of the presence of a reactive

functionality, the color of the resin turns pink to red. Due to the lower stability after *p*-nitrophenyl ester acylation, thiol and oxime resins are only washed with DMF.

### Initial conditioning of the resin

Conditioning of the 2-CTC and Wang resins consists on washes with DMF (5 x 1 min) and with CH<sub>2</sub>Cl<sub>2</sub> (5 x 1 min) to obtain an optimal swollen of the resin before incorporation of the first amino acid. In the case of 2-CTC resin, which is extremely acid labile, the initial DMF washes are also meant to eliminate hydrochloric acid traces.

### Incorporation of ethylenediamine on 2-CTC resin

In the case of non *N*-methylated peptides, ethane-1,2-diamine (10 equiv) was dissolved in CH<sub>2</sub>Cl<sub>2</sub> (15 mL/g resin) and added to the resin. The reaction was shaken at 25 °C for 30 min, and then washed with CH<sub>2</sub>Cl<sub>2</sub> (5 x 1 min) and with DMF (5 x 1 min).

In the case of *N*-methylated peptides, Fmoc-1,2-ethylenediamine\*HCl (0.7 mmol/g resin) was dissolved in CH<sub>2</sub>Cl<sub>2</sub> (10 mL/g resin) and DIEA (9 mmol/g resin) and was added to the resin. The reaction was shaken at 25 °C for 45 min. Next, the resin was capped by the addition of MeOH (0.8 µL/mg resin) for 10 min at 25 °C, and the resin was washed with CH<sub>2</sub>Cl<sub>2</sub> (5 x 1 min) and with DMF (5 x 1 min). Fmoc quantitation gave a loading of 0.7 mmol/g.

### Incorporation of the first amino acid onto Wang resin

For the synthesis of the natural product triostin A, a Wang-type resin was used for the synthesis because the 2-CTC resin is incompatible with Trt protection, used for temporary protecting group of the hydroxyl function of the D-Ser. The incorporation of the first amino acid is carried out forming an ester bond.

Fmoc-Ala-OH (10 eq) was coupled onto Wang resin (1.1 mmol/g resin) by treatment with DIPCDI (10 eq) and DMAP (1 eq) in CH<sub>2</sub>Cl<sub>2</sub>–DMF (9:1) and the reaction was shaken at 25 °C overnight. Next, the resin was capped by the addition of DIEA (10 eq) and acetic anhydride (10 eq) in CH<sub>2</sub>Cl<sub>2</sub> for 30 min at 25 °C, and the resin was washed with CH<sub>2</sub>Cl<sub>2</sub> (5 x 1 min) and with DMF (5 x 1 min).

### Removal of the Fmoc group

The Fmoc group was removed with piperidine–DMF (1:4, v/v) (10 mL/g resin) (2 x 1 min, 2 x 5 min). In order to remove the Fmoc group from Fmoc-*N*Me-AA-OH or Fmoc-D-Pro-OH an additional treatment with a DBU–toluene–piperidine–DMF (5:5:20:70) solution (1 x 5 min) was performed when complete deprotection was not accomplished with the usual methodology.

### Fmoc group quantification

The loading capacity of the resin can be found by quantifying the Fmoc group from the first amino acid anchored into the resin. Thus, when deprotecting, all the treatments with the piperidine–DMF (1:4) solution and the DMF washes (3 x 1 min) are collected in a volumetric flask, and measured by UV spectroscopy ( $\lambda = 290$  nm). The loading capacity is calculated according to the equation:

$$Z = \frac{A \cdot X}{\varepsilon \cdot Y \cdot l}$$

Where:

- $Z$  Loading of the resin
- $A$  Absorbance
- $X$  Volume of solvent (mL)
- $\varepsilon$  Molar absorbance coefficient (5800 L·mol<sup>-1</sup>·cm<sup>-1</sup>)
- $Y$  Resin weight (g)
- $l$  Length of the cell (cm)

### Peptide chain elongation

The assembly of the peptidic chain can be achieved by using several different coupling conditions. In the present thesis, all the peptides have been synthesized using one or a combination of the following protocols:

| HATU–HOAt–DIEA |                   |  |
|----------------|-------------------|--|
| Step           | Treatment         | Conditions   |
| 1              | Washes            | CH <sub>2</sub> Cl <sub>2</sub> (3 x 1 min)                    |
| 2              | Fmoc deprotection | piperidine–DMF (1:4) (2 x 1 min) + (2 x 5 min)                 |
| 3              | Washes            | DMF (3 x 1 min)<br>CH <sub>2</sub> Cl <sub>2</sub> (3 x 1 min) |
| 4              | Coupling          | Fmoc-AA-OH–HATU–HOAt–DIEA (x:x:x:2x) in DMF                    |
| 5              | Washes            | DMF (3 x 1 min)<br>CH <sub>2</sub> Cl <sub>2</sub> (3 x 1 min) |
| 6              | Colorimetric test | Kaiser test, chloranil test or De Clercq test, as needed       |

| COMU–OxymaPure–DIEA |                   |  |
|---------------------|-------------------|--|
| Step                | Treatment         | Conditions   |
| 1                   | Washes            | CH <sub>2</sub> Cl <sub>2</sub> (3 x 1 min)                    |
| 2                   | Fmoc deprotection | piperidine–DMF (1:4) (2 x 1 min) + (2 x 5 min)                 |
| 3                   | Washes            | DMF (3 x 1 min)<br>CH <sub>2</sub> Cl <sub>2</sub> (3 x 1 min) |
| 4                   | Coupling          | Fmoc-AA-OH-COMU–Oxyma–DIEA (x:x:x:2x) in DMF                   |
| 5                   | Washes            | DMF (3 x 1 min)<br>CH <sub>2</sub> Cl <sub>2</sub> (3 x 1 min) |
| 6                   | Colorimetric test | Kaiser test, chloranil test or De Clercq test, as needed       |

### Amino acid N-alkylation

This process was divided into 3 steps<sup>70</sup>:

#### a) Protection and activation with o-NBS

o-NBS-Cl (4 equiv) and 2,4,6-collidine (10 equiv) in CH<sub>2</sub>Cl<sub>2</sub> were added to the resin. The reaction was gently stirred for 1.5 h. The reaction was monitored by the ninhydrin test.

#### b) Deprotonation and methylation

Triphenylphosphine (5 equiv) in MeOH (10 equiv) and anhydrous THF (5 mL/g resin) were added to the resin and left for 1 min under N<sub>2</sub> atmosphere. Then, DIAD (5 equiv) was carefully added and left for 20 min under N<sub>2</sub> atmosphere.

#### c) o-NBS removal

To remove the o-NBS group, β-mercaptopropanoic acid (10 equiv) and DBU (5 equiv) in DMF were added to the resin and the mixture was left to react for 15 min. This operation was repeated twice.

### Allyl and Alloc group elimination

The allyl ester and the Alloc group are removed by treatment with a catalytic amount of Pd(PPh<sub>3</sub>)<sub>4</sub> (0.1 equiv) in the presence of the scavenger PhSiH<sub>3</sub> (10 equiv) in CH<sub>2</sub>Cl<sub>2</sub> and under

Ar or N<sub>2</sub> atmosphere (3 x 15 min). After the treatments, the resin is washed with CH<sub>2</sub>Cl<sub>2</sub> (5 x 1 min), DMF (5 x 1 min) and CH<sub>2</sub>Cl<sub>2</sub> (5 x 1 min).

### **Cleavage of the peptides from the resin**

After washing the resin with CH<sub>2</sub>Cl<sub>2</sub> (3 x 1 min), it is treated with a TFA–CH<sub>2</sub>Cl<sub>2</sub> (20:80) solution (5 x 2 min) and then washed again with CH<sub>2</sub>Cl<sub>2</sub> until the resin color changes from red to the original yellow. All washes are collected in a round-bottomed flask and the solvents are removed under reduced pressure. For complete side-chain deprotection the peptide is treated with the appropriate percentage of TFA in the presence of the scavengers required by the peptide sequence. Although cleavage from the resin and complete side-chain deprotection could be performed in one step by increasing the TFA percentage, it is recommended to carry out the two treatments stepwise in order to obtain cleaner crudes.

### **Cleavage from the resin without peptide's side-chains deprotection**

After CH<sub>2</sub>Cl<sub>2</sub> washing, the resin is cleaved using 20% TFA in CH<sub>2</sub>Cl<sub>2</sub> (10 mL/g resin, 10 x 30 s) at 25 °C and poured over H<sub>2</sub>O–ACN (1:1) to avoid cleavage of tBu groups. The resulting solution is evaporated until reducing half of the volume, and lyophilized.

### **2-quinoxalinecarboxylic acid introduction in solution and final deprotection**

2-quinoxalinecarboxylic acid (2.4 equiv), PyBOP (2.4 equiv), HOAt (2.4 equiv) and DIEA (until pH 8) were dissolved in DMF–CH<sub>2</sub>Cl<sub>2</sub> (1:1) and stirred at 25 °C for 35 hours. The solvent was evaporated, redissolved in CH<sub>2</sub>Cl<sub>2</sub> and washed with saturated solutions of NH<sub>4</sub>Cl, NaHCO<sub>3</sub> and NaCl, dried (MgSO<sub>4</sub>), and evaporated. The side-chain' deprotection was accomplished by treatment with TFA–H<sub>2</sub>O (95:5) at 25 °C for 2 h. After global deprotection, the resulting solution was evaporated and lyophilized.

### **Peptide purification**

All peptides were purified using a reversed-phase HPLC equipment. The instrument and the column were chosen depending on the amount of crude, the degree of purity and the complexity of the chromatographic profile of the crude. All the samples were dissolved in the minimum amount of a H<sub>2</sub>O–ACN solution, whose ACN percentage depended on the solubility of the peptide crude, and filtered through a 0.45 mm nylon filter. The fractions were analyzed by HPLC-PDA, combined and lyophilized.

## Peptide characterization

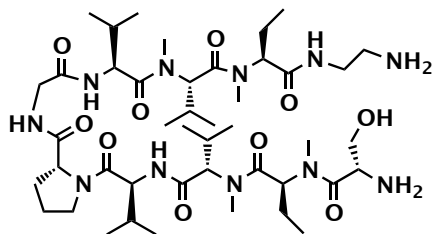
Peptides identity was confirmed by MALDI-TOF, HPLC-ESMS and/or HRMS analysis, and their purity was checked by HPLC-PDA.

## Synthesis and characterization of compounds

### Example: Synthesis of peptide Z1

2-CTC resin (150 mg, 1.56 mmol/g) was placed in a 10-mL polypropylene syringe fitted with a polyethylene filter disc. It was then washed with DMF (5 x 1 min) and CH<sub>2</sub>Cl<sub>2</sub> (5 x 1 min). Fmoc-1,2-ethylenediamine\*HCl (33.5 mg, 0.105 mmol) and DIEA (230 µL) in CH<sub>2</sub>Cl<sub>2</sub> (1.5 mL) was added to the resin. The mixture was shaken at 25 °C for 45 min. The reaction was quenched by addition of MeOH (120 µL) and the mixture was stirred for 10 min at 25 °C. After filtration, the resin was washed with CH<sub>2</sub>Cl<sub>2</sub> (5 x 1 min) and with DMF (5 x 1 min) and cleavage of the Fmoc group was done by treatment with piperidine-DMF (1:4) (3.75 mL) (2 x 1 min, 2 x 5 min). The filtrates were collected and quantified by UV (290 nm) obtaining a loading of 0.70 mmol/g. Based on this loading, Fmoc-Abu-OH (136.7 mg, 0.42 mmol) was incorporated with COMU (179.9 mg, 0.42 mmol), OxymaPure (59.7 mg, 0.42 mmol) and DIEA (142.9 µL, 0.84 mmol) in DMF (10 mL/g resin) with preactivation for 30 s at 25 °C and stirred for 1.5 h. After resin filtration and washings with DMF (5 x 1 min) and CH<sub>2</sub>Cl<sub>2</sub> (5 x 1 min) the Fmoc group was removed as described above and the resin was washed again. A solution of *o*-NBS-Cl (93 mg, 0.42 mmol) and 2,4,6-collidine (138.8 µL, 1.05 mmol) in CH<sub>2</sub>Cl<sub>2</sub> was added to the resin and the mixture stirred for 90 min. After filtration and washings with CH<sub>2</sub>Cl<sub>2</sub> (5 x 1 min), DMF (5 x 1 min), CH<sub>2</sub>Cl<sub>2</sub> (5 x 1 min) and THF (5 x 1 min), a solution of PPh<sub>3</sub> (137.7 mg, 0.525 mmol) and MeOH (42.6 µL, 1.05 mmol) in THF, and a solution of DIAD (101.8 µL, 0.525 mmol) in THF were mixed and added to the resin under N<sub>2</sub> atmosphere. After stirring the resin for 20 min, it was filtered and washed with THF (5 x 1 min), CH<sub>2</sub>Cl<sub>2</sub> (5 x 1 min) and DMF (5 x 1 min). After removal of the *o*-NBS group with DBU (78.7 µL, 0.525 mmol) and 2-mercaptoethanol (73.6 µL, 1.05 mmol) in DMF (3 x 15 min), the resin was washed with DMF (5 x 1 min), CH<sub>2</sub>Cl<sub>2</sub> (5 x 1 min), and DMF (5 x 1 min). Fmoc-NMe-Val-OH (148.4 mg, 0.42 mmol) was incorporated with COMU (179.9 mg, 0.42 mmol), OxymaPure (59.7 mg, 0.42 mmol) and DIEA (142.9 µL, 0.84 mmol) in DMF (10 mL/g resin) at 50 °C. After stirring for 90 min, the resin was filtered and washed with DMF (5 x 1 min) and CH<sub>2</sub>Cl<sub>2</sub> (5 x 1 min) and one recoupling was performed under the same conditions. After resin filtration, and further removal of the Fmoc group, the resin was washed again. Next, Fmoc-Val-OH (142.6 mg, 0.42 mmol) was incorporated with COMU (179.9 mg, 0.42 mmol), OxymaPure (59.7 mg, 0.42 mmol) and DIEA (142.9 µL, 0.84 mmol) in DMF (10 mL/g resin) at 50 °C. After stirring for 90 min, the resin was filtered and washed with DMF (5 x 1 min) and CH<sub>2</sub>Cl<sub>2</sub> (5 x 1 min) and one recoupling was carried out under the same conditions. After resin

filtration, the Fmoc group was removed and the resin was washed again. The following protected amino acids (Fmoc-Gly-OH, Fmoc-D-Pro-OH, Fmoc-Val-OH, Fmoc-NMe-Val-OH) were incorporated with COMU (4 equiv), OxymaPure (4 equiv) and DIEA (8 equiv) in DMF stirring for 90 min at room temperature. Fmoc-Abu-OH (136.7 mg, 0.42 mmol) was incorporated with COMU (179.9 mg, 0.42 mmol), OxymaPure (59.7 mg, 0.42 mmol) and DIEA (142.9  $\mu$ L, 0.84 mmol) in DMF (10 mL/g resin) with preactivation for 30 s at 50 °C and stirred for 1.5 h. One recoupling was done. The N-alkylation of this residue was accomplished under the same conditions described above and after removal of the *o*-NBS group, the resin was washed, and Fmoc-Ser(*t*Bu) (161.1 mg, 0.42 mmol) was incorporated with COMU (179.9 mg, 0.42 mmol), OxymaPure (59.7 mg, 0.42 mmol) and DIEA (142.9  $\mu$ L, 0.84 mmol) in DMF (10 mL/g resin) at 50 °C. No recoupling was necessary at this time. After finishing the elongation, the peptide was cleaved with 20% TFA in CH<sub>2</sub>Cl<sub>2</sub> (4.5 mL, 10 x 30 s) at 25 °C and the solvent was evaporated under reduced pressure. To fully remove the side-chain protecting groups, the protected peptide was treated with a TFA-H<sub>2</sub>O solution (95:5; 50 mL) for 2 hours at 25 °C. The HPLC-PDA showed completion of the deprotection. The TFA was removed under reduced pressure and the resulting aqueous suspension was redissolved adding H<sub>2</sub>O-ACN (3:7; 15 mL) and lyophilized. The product was then purified by semipreparative RP-HPLC.

**Peptide Z1**

Purification column: XBridge® BEH130 C18 column, (10 mm x 100 mm, 5  $\mu$ m)

Purification gradient: 20% to 35% of ACN over 8 min with a flow of 3 mL/min

Yield: 99%

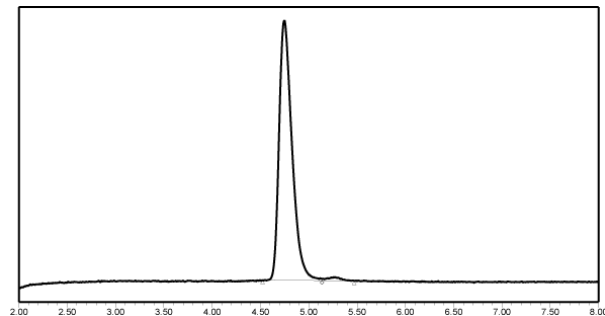
Analytical column: SunFire® C18 (4.6 mm x 100 mm, 3.5  $\mu$ m)

**Peptide Z1**

HPLC-PDA  $t_h = 4.748$

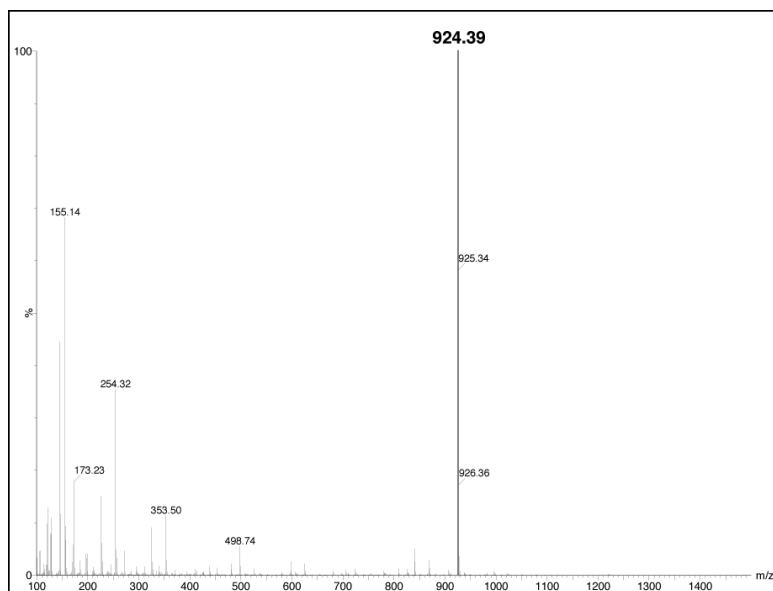
Gradient: 15% to 40% of ACN over 8 min

Purity ( $\lambda=220$ ): 99%

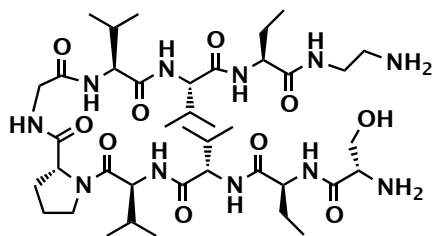


$m/z$  calculated for  $C_{44}H_{81}N_{11}O_{10}$ : 923.62 Da

HPLC-ESMS(+),  $[M+H]^+$ : 924.39 Da



### Peptide Z2



Purification column: XBridge® BEH130 C18 column, (10 mm x 100 mm, 5  $\mu$ m)

Purification gradient: 22% to 23% of ACN over 8 min with a flow of 3 mL/min

Yield: 85%

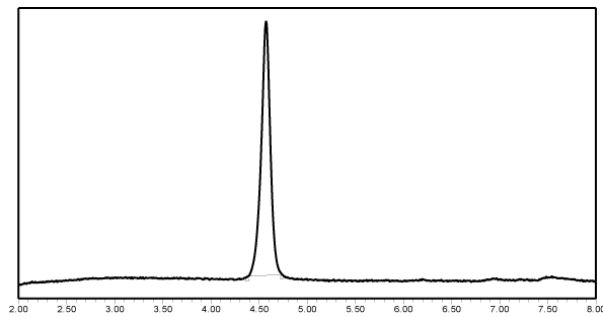
Analytical column: SunFire® C18 (4.6 mm x 100 mm, 3.5  $\mu$ m)

### Peptide Z2

HPLC-PDA  $t_R$  = 4.573

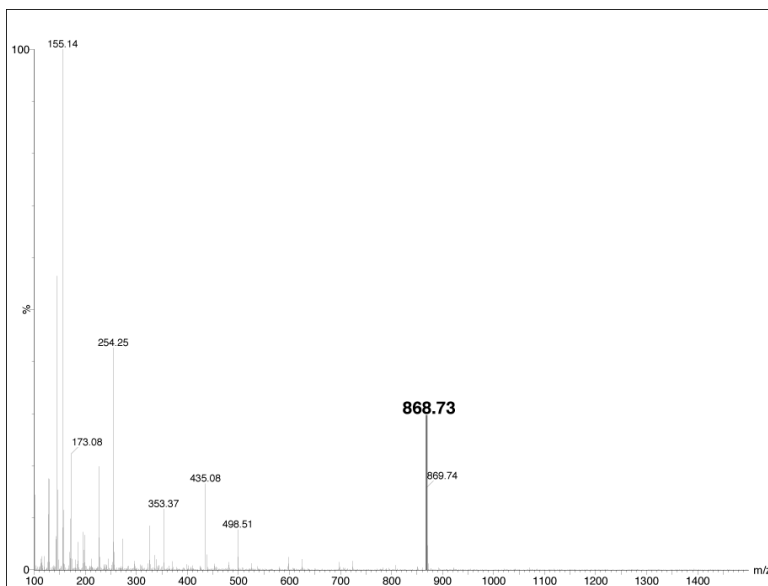
Gradient: 10% to 50% of ACN over 8 min

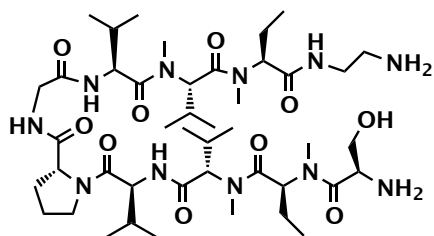
Purity ( $\lambda=220$ ): 99%



$m/z$  calculated for  $C_{40}H_{73}N_{11}O_{10}$ : 867.55 Da

HPLC-ESMS(+),  $[M+H]^+$ : 868.73 Da



**Peptide Z3**

Purification column: XBridge® BEH130 C18 column, (10 mm x 100 mm, 5  $\mu$ m)

Purification gradient: 22% to 30% of ACN over 8 min with a flow of 3 mL/min

Yield: 71%

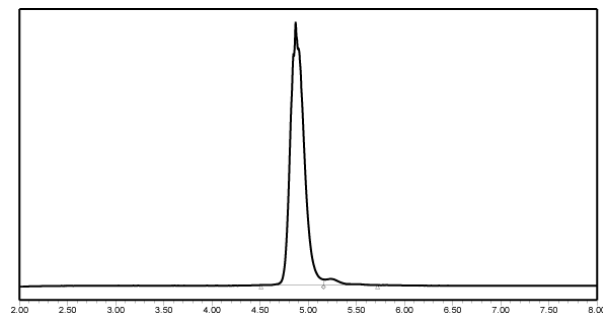
Analytical column: SunFire® C18 (4.6 mm x 100 mm, 3.5  $\mu$ m)

**Peptide Z3**

HPLC-PDA  $t_R$  = 4.869

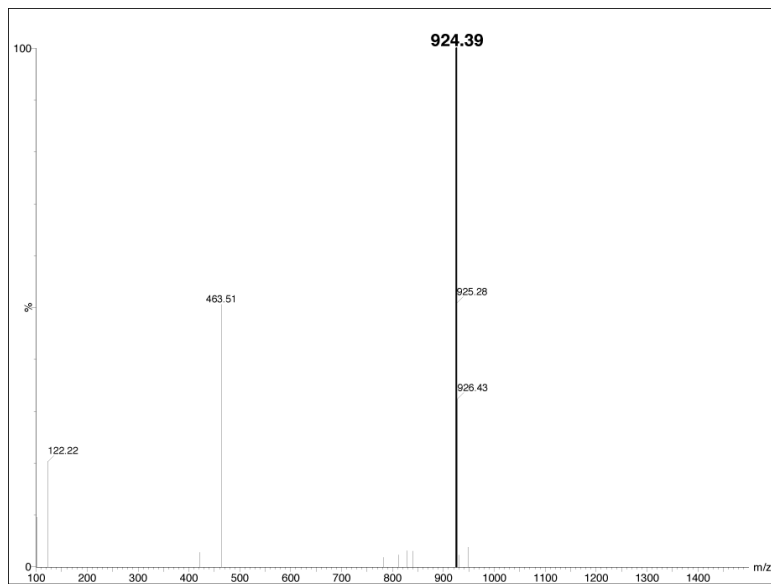
Gradient: 15% to 40% of ACN over 8 min

Purity ( $\lambda=220$ ): 97%

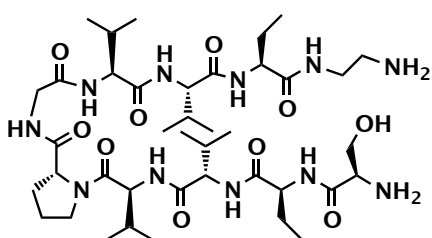


$m/z$  calculated for  $C_{44}H_{81}N_{11}O_{10}$ : 923.62 Da

HPLC-ESMS(+),  $[M+H]^+$ : 924.39 Da



**Peptide Z4**



Purification column: XBridge® BEH130 C18 column, (10 mm x 100 mm, 5  $\mu$ m)

Purification gradient: 22% to 23% of ACN over 8 min with a flow of 3 mL/min

Yield: 82%

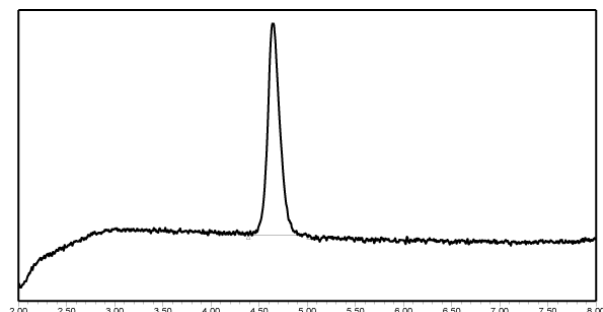
Analytical column: SunFire® C18 (4.6 mm x 100 mm, 3.5  $\mu$ m)

**Peptide Z4**

HPLC-PDA  $t_R$  = 4.640

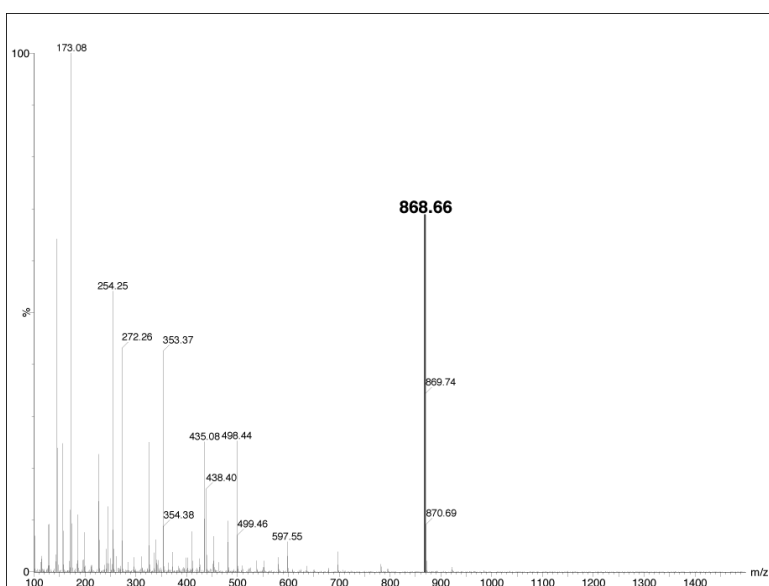
Gradient: 10% to 50% of ACN over 8 min

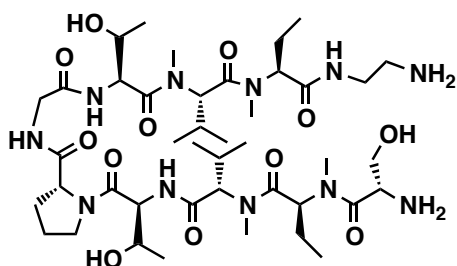
Purity ( $\lambda=220$ ): 100%



$m/z$  calculated for  $C_{40}H_{73}N_{11}O_{10}$ : 867.55 Da

HPLC-ESMS(+),  $[M+H]^+$ : 868.66 Da



**Peptide Z5**

Purification column: XBridge® BEH130 C18 column,  
(10 mm x 100 mm, 5  $\mu$ m)

Purification gradient: 15% to 25% of ACN over 8 min  
with a flow of 3 mL/min

Yield: 70%

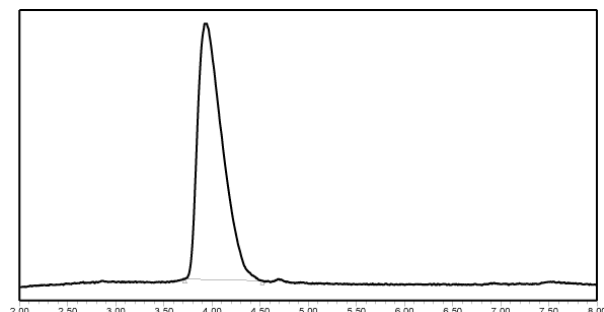
Analytical column: SunFire® C18 (4.6 mm x 100 mm,  
3.5  $\mu$ m)

**Peptide Z5**

HPLC-PDA  $t_R$  = 3.929

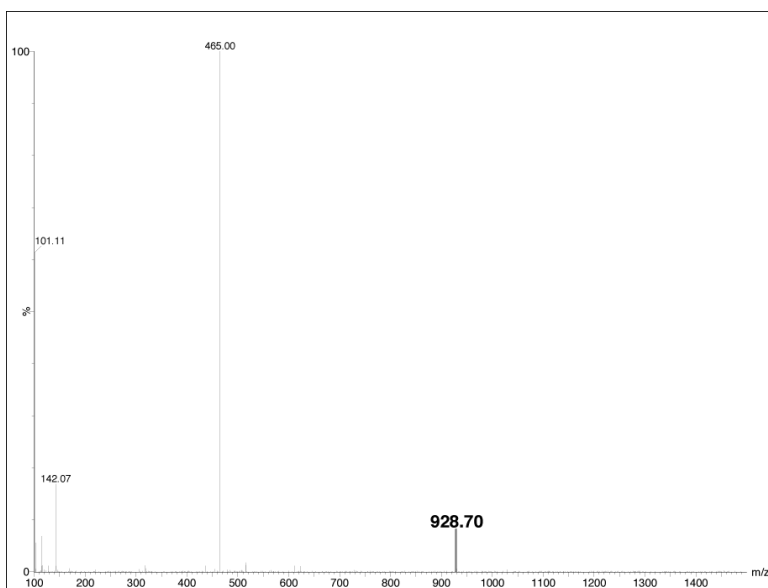
Gradient: 10% to 50% of ACN over 8 min

Purity ( $\lambda=220$ ): 99%

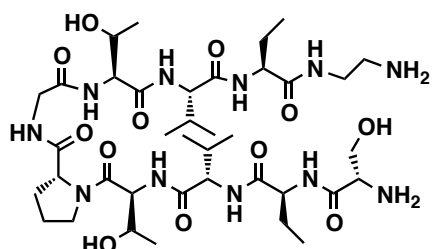


$m/z$  calculated for  $C_{42}H_{77}N_{11}O_{12}$ : 927.58 Da

HPLC-ESMS(+),  $[M+H]^+$ : 928.70 Da



## Peptide Z6



Purification column: XBridge® BEH130 C18 column, (10 mm x 100 mm, 5 µm)

Purification gradient: 22% to 40% of ACN over 8 min with a flow of 3 ml /min

**Yield:** 93%

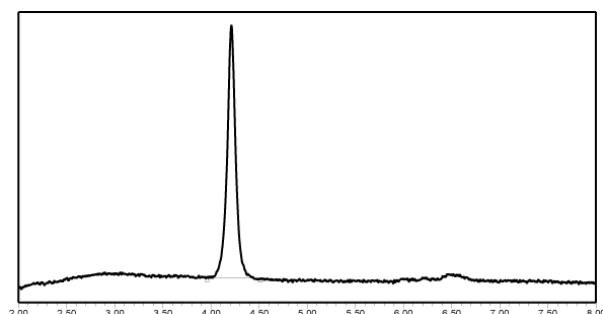
Analytical column: SunFire® C18 (4.6 mm x 100 mm, 3.5 µm)

## Peptide Z6

HPLC-PDA  $t_R = 4.212$

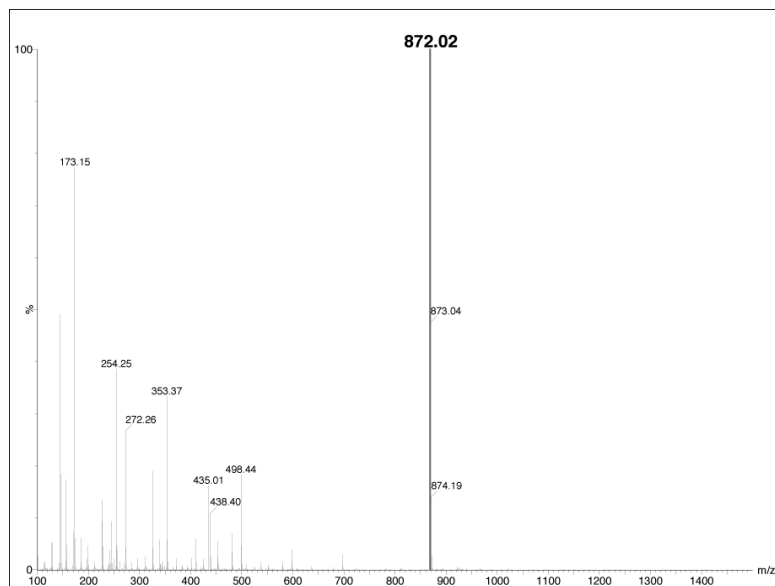
Gradient: 10% to 60% of ACN over 8 min

Purity ( $\lambda=220$ ): 99%

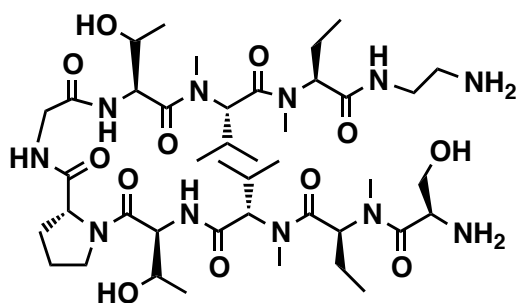


*m/z* calculated for C<sub>38</sub>H<sub>69</sub>N<sub>11</sub>O<sub>12</sub>: 871.51Da

HPLC-ESMS(+),  $[M+H]^+$ : 872.02 Da



## Peptide Z7



Purification column: XBridge® BEH130 C18 column, (10 mm x 100 mm, 5 µm)

Purification gradient: 15% to 25% of ACN over 8 min with a flow of 3 mL/min

**Yield: 81%**

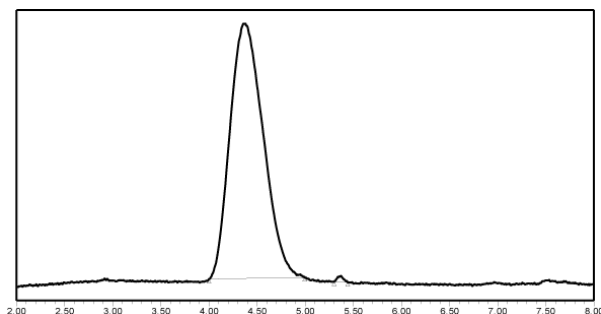
Analytical column: SunFire® C18 (4.6 mm x 100 mm, 3.5 µm)

## Peptide Z7

HPLC-PDA  $t_R = 4.376$

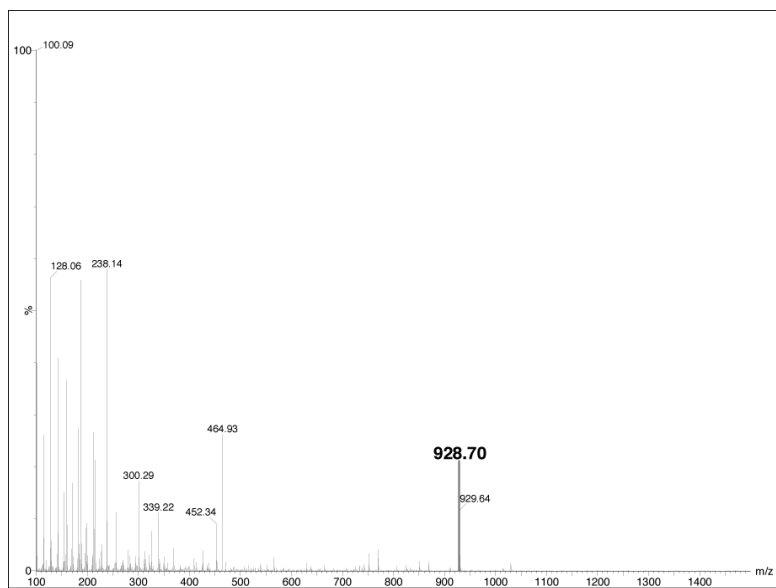
Gradient: 10% to 50% of ACN over 8 min

Purity ( $\lambda=220$ ): 99%

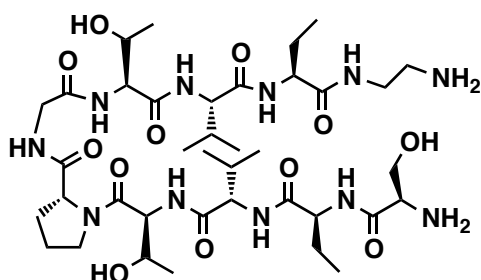


*m/z* calculated for C<sub>42</sub>H<sub>77</sub>N<sub>11</sub>O<sub>12</sub>: 927.58 Da

HPLC-ESMS(+),  $[M+H]^+$ : 928.70 Da



**Peptide Z8**



Purification column: XBridge® BEH130 C18 column, (10 mm x 100 mm, 5  $\mu$ m)

Purification gradient: 20% to 21% of ACN over 15 min with a flow of 3 mL/min

Yield: 92%

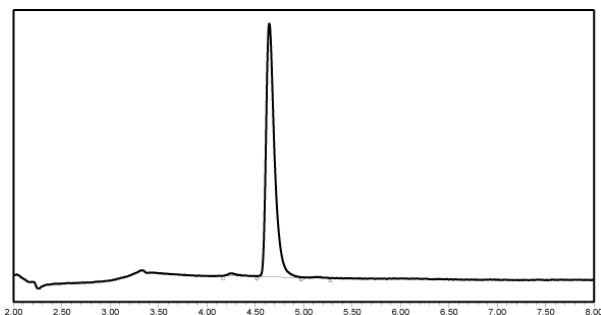
Analytical column: SunFire® C18 (4.6 mm x 100 mm, 3.5 $\mu$ m)

**Peptide Z8**

HPLC-PDA  $t_R$  = 4.643

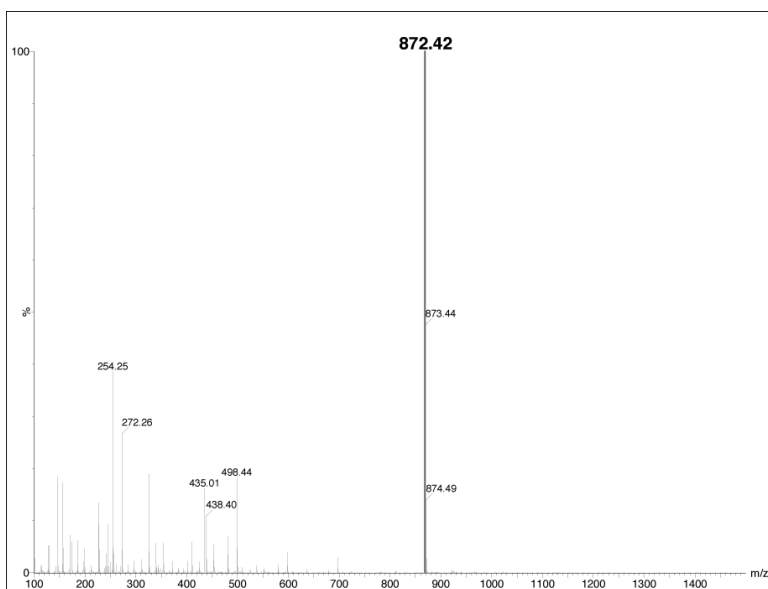
Gradient: 0% to 60% of ACN over 8 min

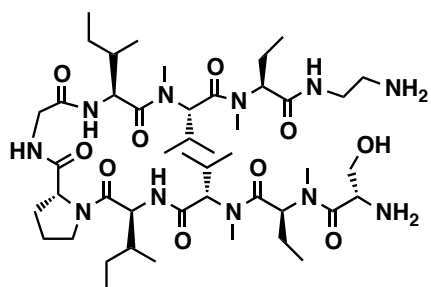
Purity ( $\lambda=220$ ): 98%



$m/z$  calculated for C<sub>38</sub>H<sub>69</sub>N<sub>11</sub>O<sub>12</sub>: 871.51 Da

HPLC-ESMS(+), [M+H]<sup>+</sup>: 872.42 Da



**Peptide Z9**

Purification column: XBridge® BEH130 C18 column, (10 mm x 100 mm, 5  $\mu$ m)

Purification gradient: 25% to 31% of ACN over 10 min with a flow of 3 mL/min

Yield: 53%

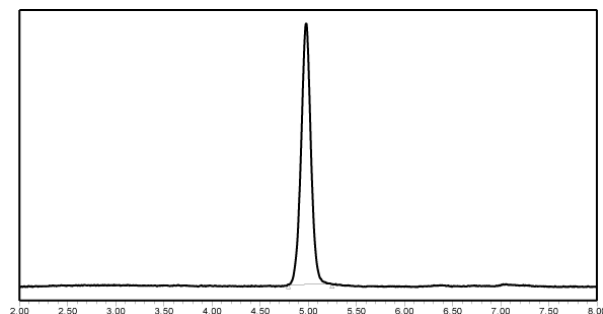
Analytical column: SunFire® C18 (4.6 mm x 100 mm, 3.5  $\mu$ m)

**Peptide Z9**

HPLC-PDA  $t_R$  = 4.979

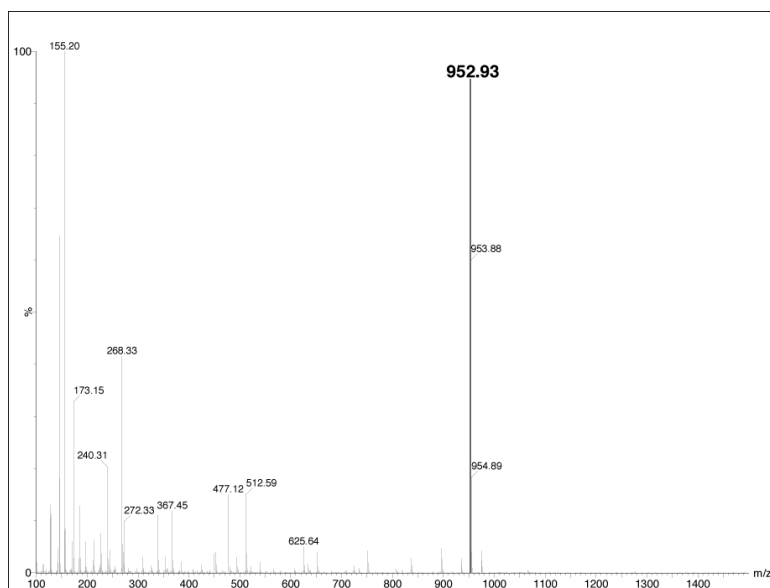
Gradient: 15% to 50% of ACN over 8 min

Purity ( $\lambda=220$ ): 100%

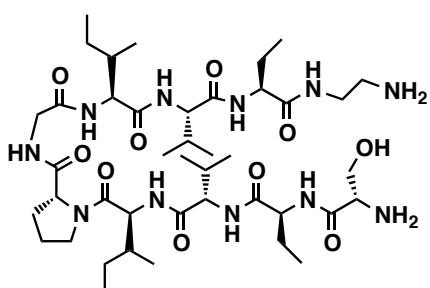


$m/z$  calculated for  $C_{46}H_{85}N_{11}O_{10}$ : 951.65 Da

HPLC-ESMS(+),  $[M+H]^+$ : 952.93 Da



### Peptide Z10



Purification column: XBridge® BEH130 C18 column, (10 mm x 100 mm, 5  $\mu$ m)

Purification gradient: 27% to 28% of ACN over 20 min with a flow of 3 mL/min

Yield: 84%

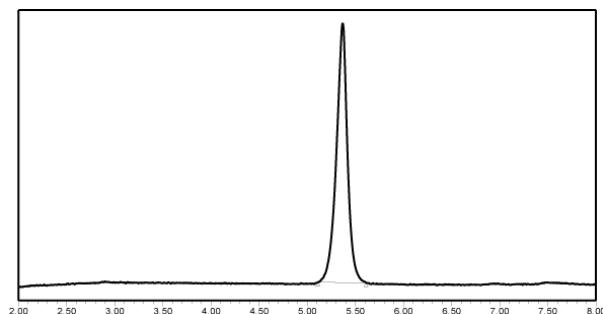
Analytical column: SunFire® C18 (4.6 mm x 100 mm, 3.5  $\mu$ m)

### Peptide Z10

HPLC-PDA  $t_R$  = 5.368

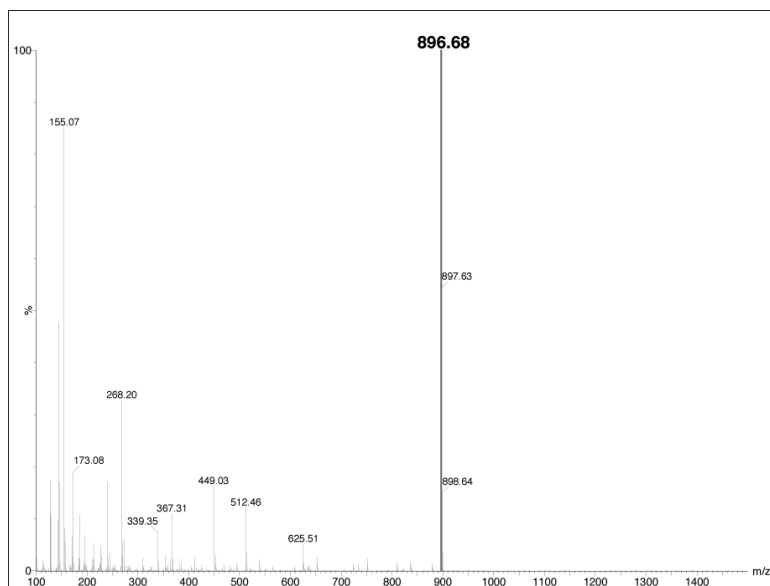
Gradient: 10% to 50% of ACN over 8 min

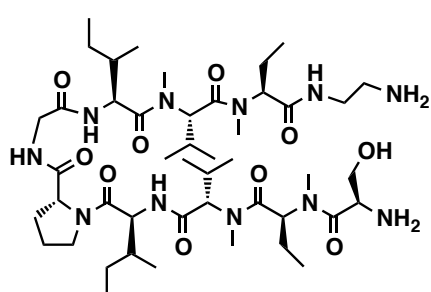
Purity ( $\lambda=220$ ): 100%



$m/z$  calculated for  $C_{42}H_{77}N_{11}O_{10}$ : 895.59Da

HPLC-ESMS(+),  $[M+H]^+$ : 896.68 Da



**Peptide Z11**

Purification column: XBridge® BEH130 C18 column, (10 mm x 100 mm, 5  $\mu$ m)

Purification gradient: 25% to 29% of ACN over 10 min with a flow of 3 mL/min

Yield: 76%

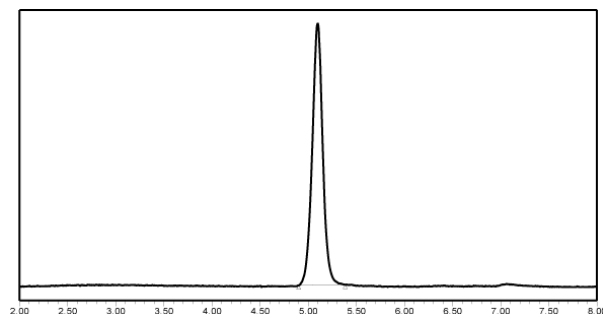
Analytical column: SunFire® C18 (4.6 mm x 100 mm, 3.5  $\mu$ m)

**Peptide Z11**

HPLC-PDA  $t_R$  = 5.099

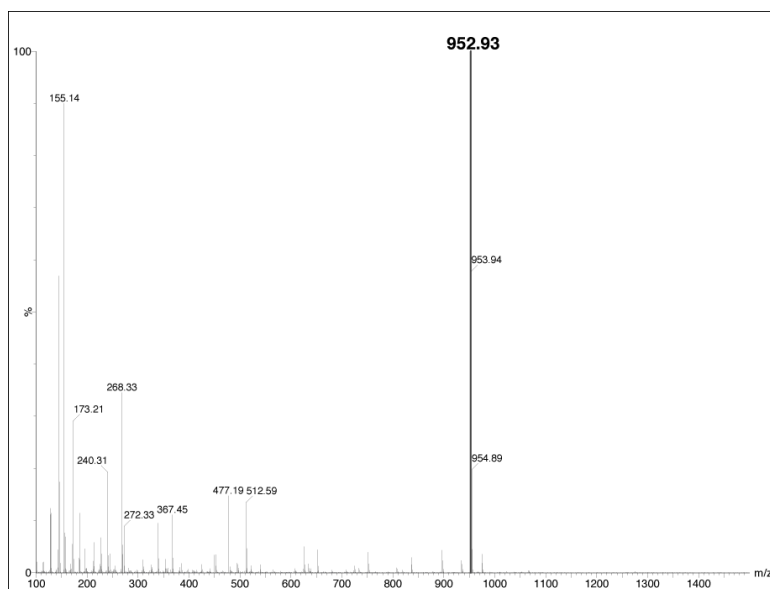
Gradient: 15% to 50% of ACN over 8 min

Purity ( $\lambda=220$ ): 100%

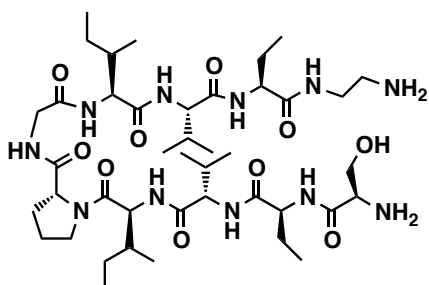


$m/z$  calculated for  $C_{46}H_{85}N_{11}O_{10}$ : 951.65 Da

HPLC-ESMS(+),  $[M+H]^+$ : 952.93 Da



### Peptide Z12



Purification column: XBridge® BEH130 C18 column, (10 mm x 100 mm, 5  $\mu$ m)

Purification gradient: 27% to 28% of ACN over 20 min with a flow of 3 mL/min

Yield: 86%

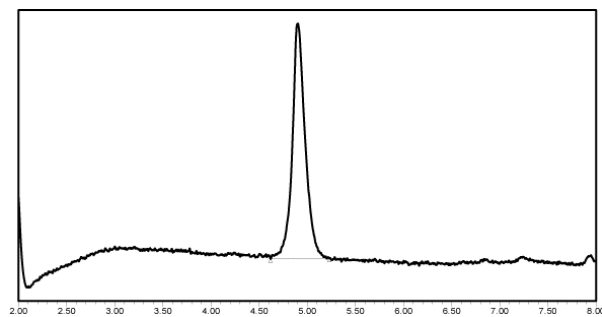
Analytical column: SunFire® C18 (4.6 mm x 100 mm, 3.5  $\mu$ m)

### Peptide Z12

HPLC-PDA  $t_R$  = 4.903

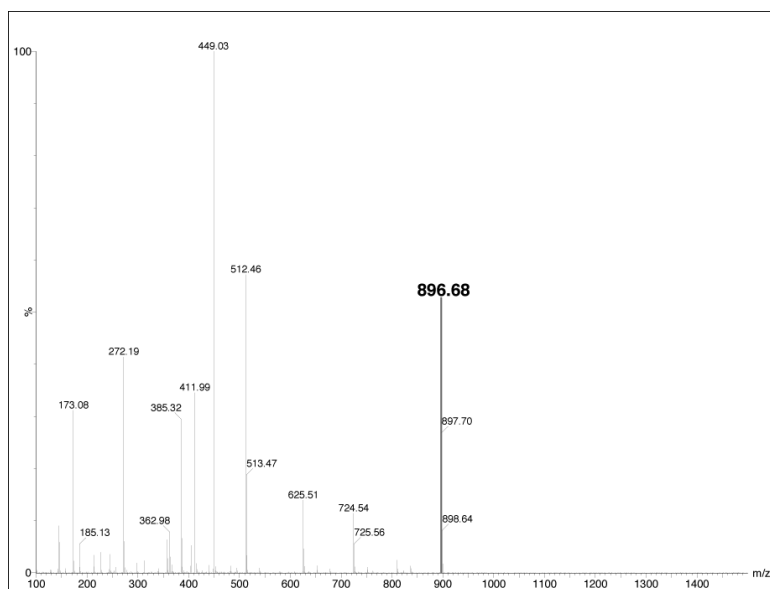
Gradient: 10% to 60% of ACN over 8 min

Purity ( $\lambda=220$ ): 99%



$m/z$  calculated for  $C_{42}H_{77}N_{11}O_{10}$ : 895.59 Da

HPLC-ESMS(+),  $[M+H]^+$ : 896.68 Da

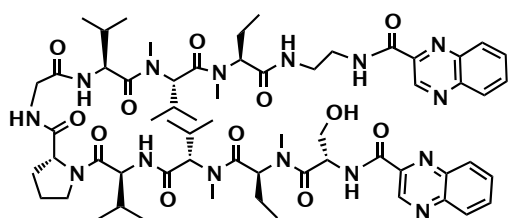


**Example: Synthesis of compound RZ1**

Peptide Z1 was synthesized through SPPS as previously described (see page 57).

After finishing the elongation, the peptide was cleaved with 20% TFA in  $\text{CH}_2\text{Cl}_2$  (4.5 mL, 10 x 30 s) at 25 °C and poured over  $\text{H}_2\text{O}$ -ACN (1:1) (50 mL) to avoid cleavage of the *t*Bu groups. The resulting solution was partially evaporated and lyophilized (102.4 mg; 99.5% yield). The peptide (0.1 mmol) was dissolved in DMF- $\text{CH}_2\text{Cl}_2$  (1:1) (10 mL), and PyBOP (124.9 mg, 0.24 mmol), HOAt (32.7 mg, 0.24 mmol) and 2-quinoxalinecarboxylic acid (41.8 mg, 0.24 mmol) were added to the solution. The pH was adjusted to 8 by adding DIEA and the mixture was stirred until HPLC analysis indicated the completion of the reaction. The solvent was evaporated under reduced pressure and the peptide was redissolved in  $\text{CH}_2\text{Cl}_2$  (30 mL). The organic layer was washed with saturated solutions of  $\text{NH}_4\text{Cl}$  (1 x 20 mL),  $\text{NaHCO}_3$  (1 x 20 mL) and brine (1 x 20 mL, dried with  $\text{MgSO}_4$  and evaporated under vacuum. Total deprotection was accomplished by treatment with TFA- $\text{H}_2\text{O}$  (95:5; 40 mL) at 25 °C for 2 h. After global deprotection, the resulting solution was evaporated to 5 mL and lyophilized. The crude peptide was purified by semi-preparative RP-HPLC.

**Compound RZ1**



Purification column: Symmetry® C18 column (19 mm x 100 mm, 5  $\mu$ m)

Purification gradient: 40% to 45% of ACN over 10 min with a flow of 3 mL/min; T = 30°C

Yield: 15%

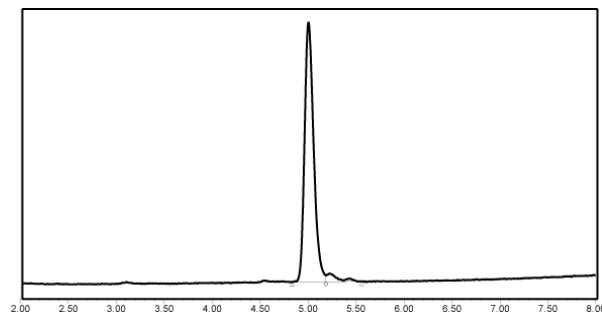
Analytical column: SunFire® C18 (4.6 mm x 100 mm, 3.5  $\mu$ m)

**Compound RZ1**

HPLC-PDA  $t_R$  = 5.005

Gradient: 30% to 100% of ACN over 8 min

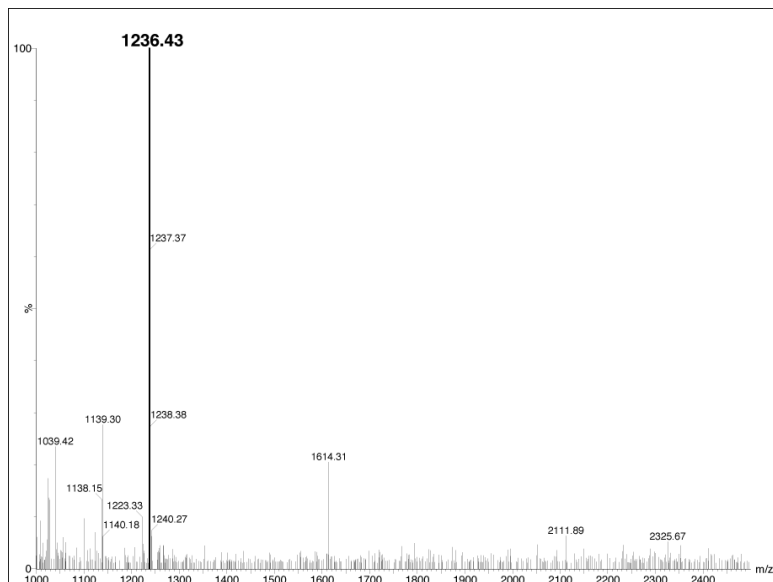
Purity ( $\lambda=220$ ): 96.03%

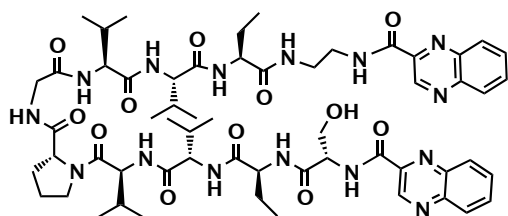


$m/z$  calculated for  $C_{62}H_{89}N_{15}O_{12}$ : 1235.68097 Da

HRMS (NanoESI): 1235.68006 Da

HPLC-ESMS(+),  $[M+H]^+$ : 1236.43 Da



**Compound RZ2**

Purification column: Symmetry® C18 column (19 mm x 100 mm, 5  $\mu$ m)

Purification gradient: 38% to 40% of ACN over 10 min with a flow of 3 mL/min; T = 50 °C

Yield: 12.1%

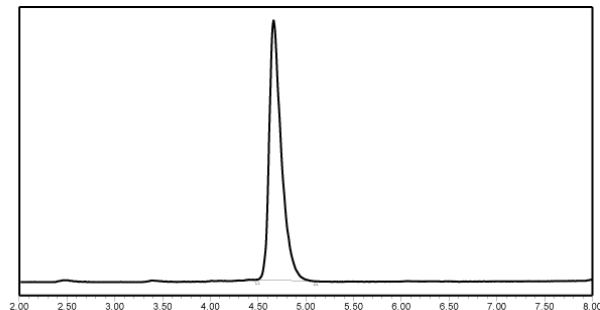
Analytical column: SunFire® C18 (4.6 mm x 100 mm, 3.5  $\mu$ m)

**Compound RZ2**

HPLC-PDA  $t_R$  = 4.663

Gradient: 30% to 100% of ACN over 8 min

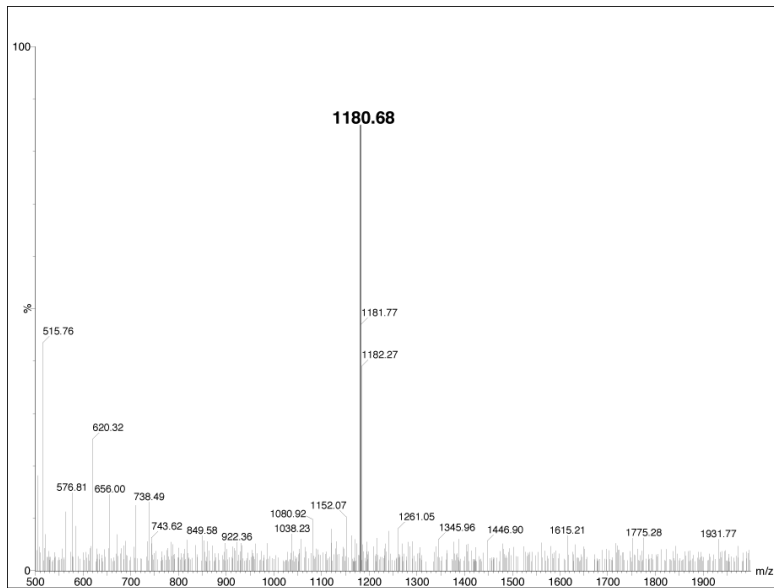
Purity ( $\lambda=220$ ): 100%



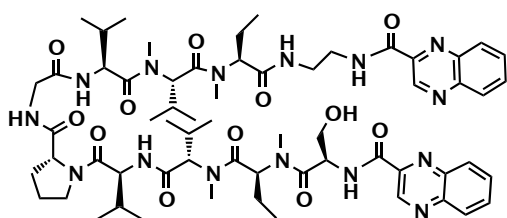
$m/z$  calculated for  $C_{58}H_{81}N_{15}O_{12}$ : 1179.61836 Da

HRMS (NanoESI): 1179.61954 Da

HPLC-ESMS(+),  $[M+H]^+$ : 1180.68 Da



**Compound RZ3**



Purification column: Symmetry® C18 column (19 mm x 100 mm, 5  $\mu$ m)

Purification gradient: 40% to 41% of ACN over 10 min with a flow of 3 mL/min; T = 50 °C

Yield: 0.5%

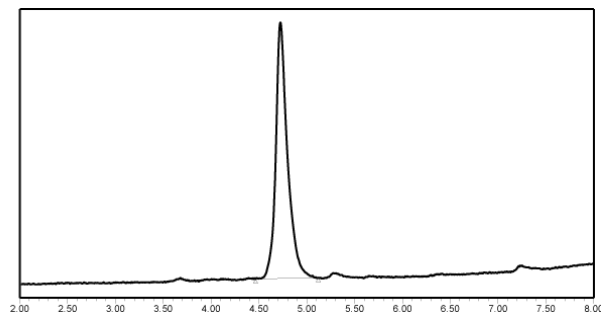
Analytical column: SunFire® C18 (4.6 mm x 100 mm, 3.5  $\mu$ m)

**Compound RZ3**

HPLC-PDA  $t_R$  = 4.729

Gradient: 30% to 100% of ACN over 8 min

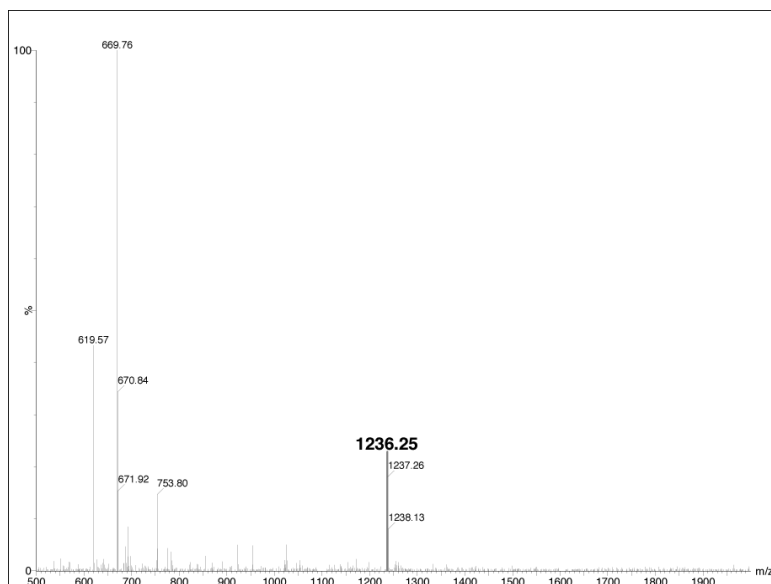
Purity ( $\lambda=220$ ): 95%

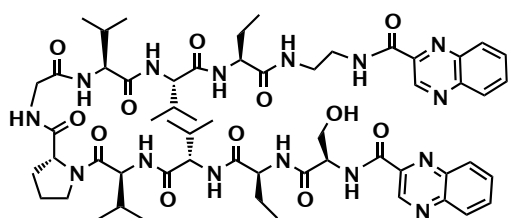


$m/z$  calculated for  $C_{62}H_{89}N_{15}O_{12}$ : 1235.68097 Da

HRMS (NanoESI): 1235.6780 Da

HPLC-ESMS(+),  $[M+H]^+$ : 1236.25 Da



**Compound RZ4**

Purification column: Symmetry® C18 column (19 mm x 100 mm, 5  $\mu$ m)

Purification gradient: 38% to 39% of ACN over 10 min with a flow of 3 mL/min

Yield: 1.5%

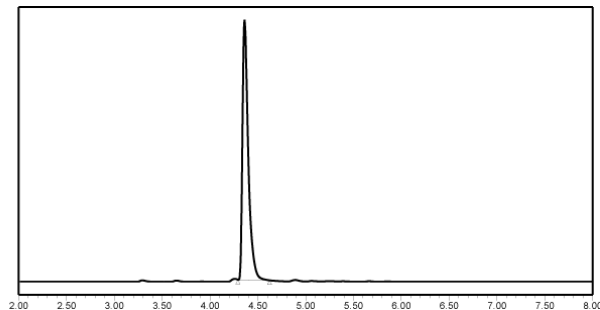
Analytical column: SunFire® C18 (4.6 mm x 100 mm, 3.5  $\mu$ m)

**Compound RZ4**

HPLC-PDA  $t_R$  = 4.361

Gradient: 30% to 100% of ACN over 8 min

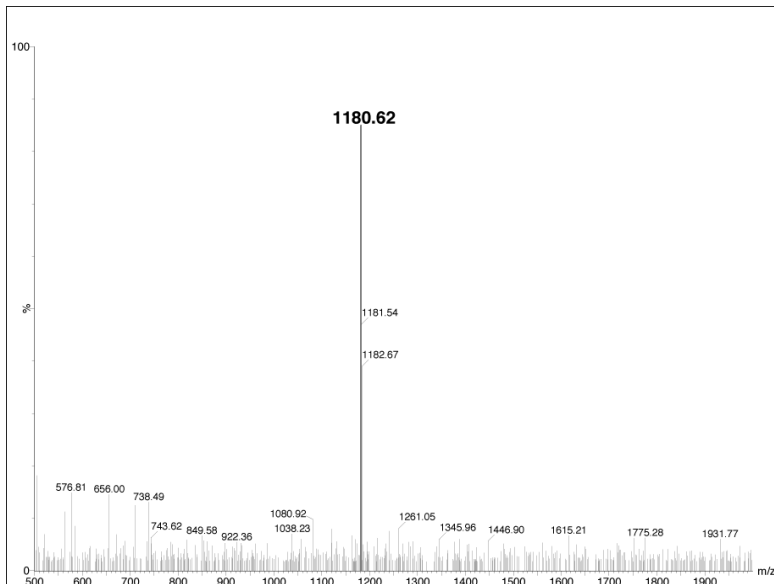
Purity ( $\lambda=220$ ): 97%



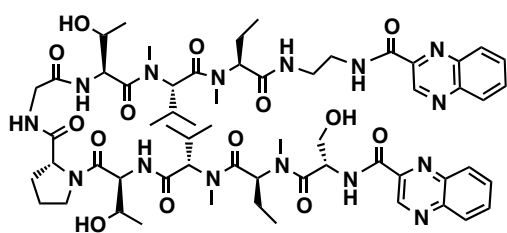
$m/z$  calculated for  $C_{58}H_{81}N_{15}O_{12}$ : 1179.61836 Da

HRMS (NanoESI): 1179.61917 Da

HPLC-ESMS(+),  $[M+H]^+$ : 1180.62 Da



**Compound RZ5**



Purification column: Symmetry® C18 column (19 mm x 100 mm, 5  $\mu$ m)

Purification gradient: 30% to 50% of ACN over 10 min with a flow of 3 mL/min

Yield: 11.7%

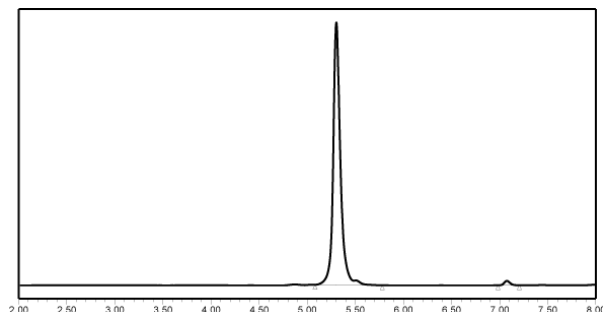
Analytical column: SunFire® C18 (4.6 mm x 100 mm, 3.5  $\mu$ m)

**Compound RZ5**

HPLC-PDA  $t_R$  = 5.303

Gradient: 20% to 80% of ACN over 8 min

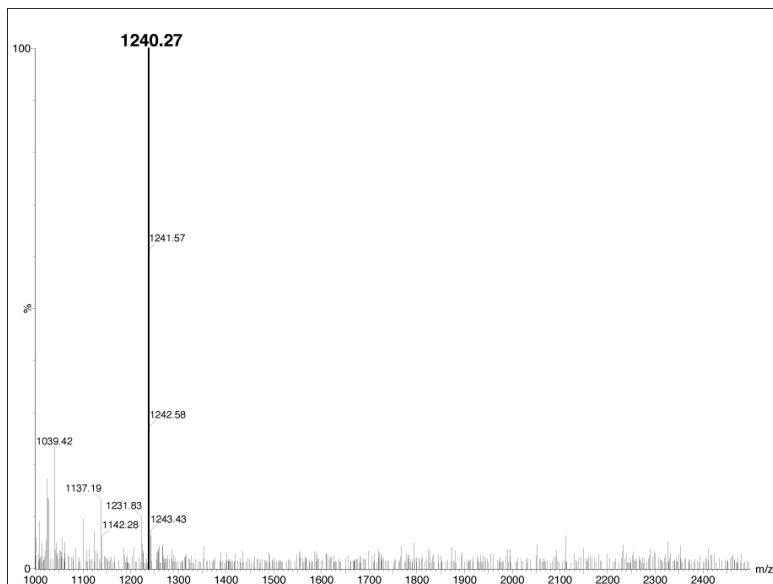
Purity ( $\lambda=220$ ): 96%

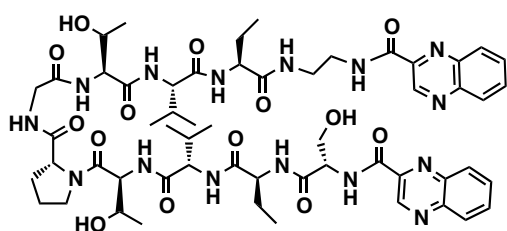


$m/z$  calculated for  $C_{60}H_{85}N_{15}O_{14}$ : 1239.63949 Da

HRMS (NanoESI): 1239.63906 Da

HPLC-ESMS(+),  $[M+H]^+$ : 1240.27 Da



**Compound RZ6**

Purification column: Symmetry® C18 column (19 mm x 100 mm, 5  $\mu$ m)

Purification gradient: 45% to 50% of ACN over 10 min with a flow of 3 mL/min; T = 50 °C

Yield: 0.2%

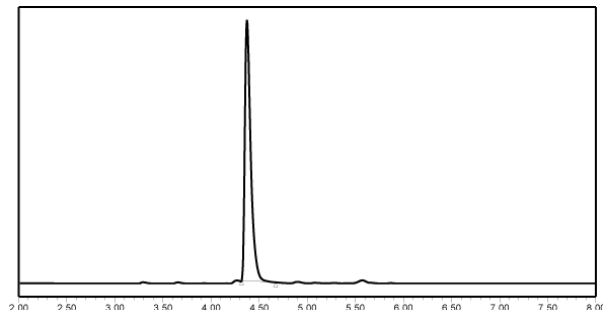
Analytical column: SunFire® C18 (4.6 mm x 100 mm, 3.5  $\mu$ m)

**Compound RZ6**

HPLC-PDA  $t_R$  = 4.373

Gradient: 20% to 80% of ACN over 8 min

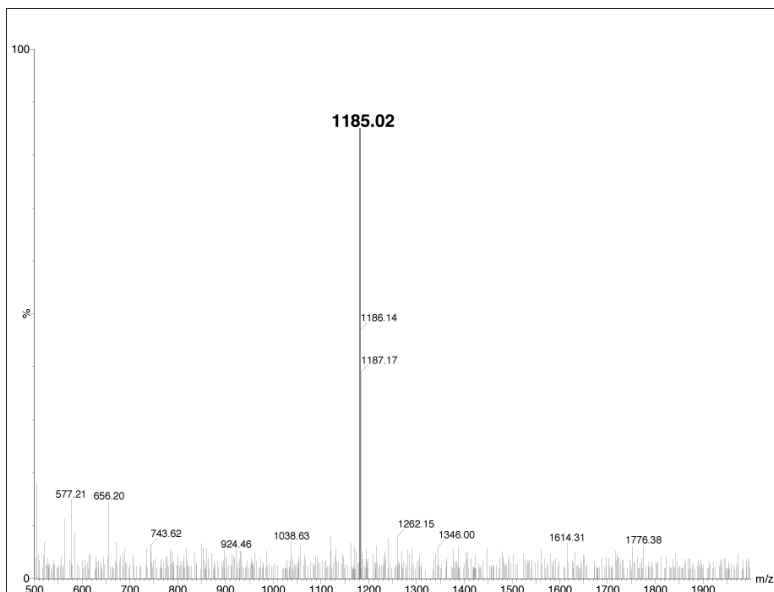
Purity ( $\lambda=220$ ): 96%



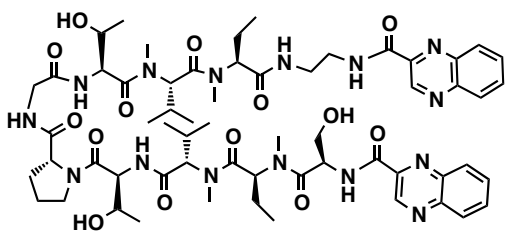
$m/z$  calculated for  $C_{56}H_{77}N_{15}O_{14}$ : 1183.57689 Da

HRMS (NanoESI): 1183.57278 Da

HPLC-ESMS(+),  $[M+H]^+$ : 1185.02 Da



**Compound RZ7**



Purification column: Symmetry® C18 column (19 mm x 100 mm, 5  $\mu$ m)

Purification gradient: 25% to 40% of ACN over 15 min with a flow of 3 mL/min

Yield: 3%

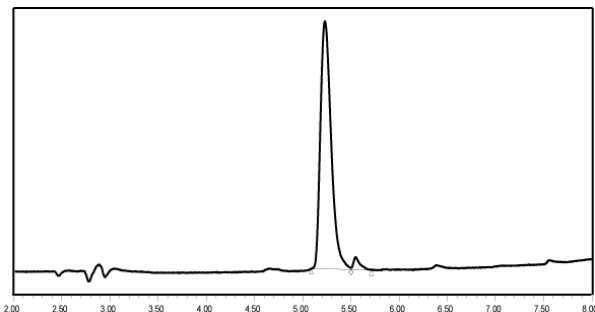
Analytical column: SunFire® C18 (4.6 mm x 100 mm, 3.5  $\mu$ m)

**Compound RZ7**

HPLC-PDA  $t_R$  = 5.247

Gradient: 20% to 80% of ACN over 8 min

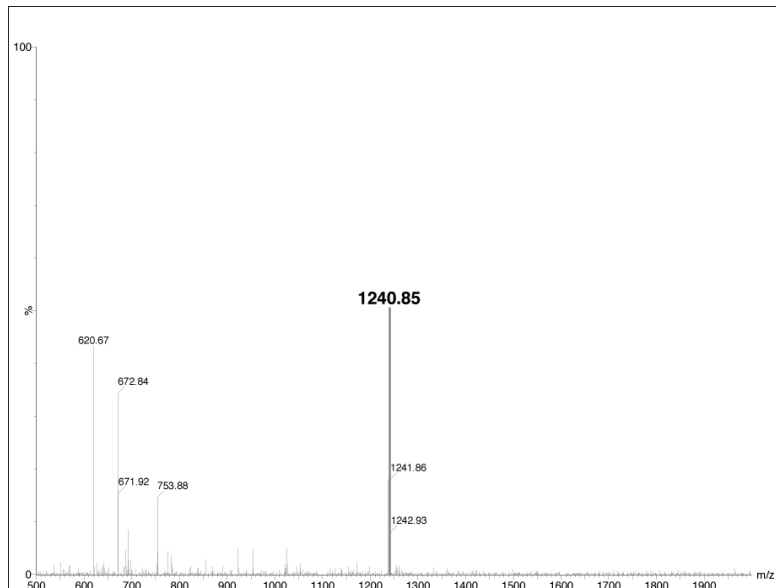
Purity ( $\lambda=220$ ): 94%

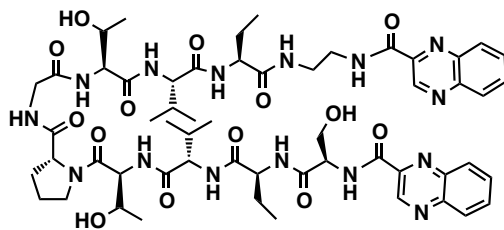


$m/z$  calculated for  $C_{60}H_{85}N_{15}O_{14}$ : 1239.63949 Da

HRMS (NanoESI): 1239.63764 Da

HPLC-ESMS(+),  $[M+H]^+$ : 1240.85 Da



**Compound RZ8**

Purification column: Symmetry® C18 column (19 mm x 100 mm, 5  $\mu$ m)

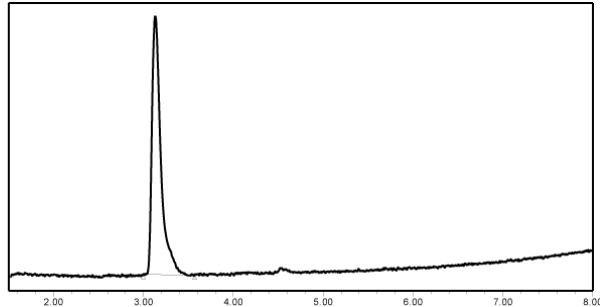
Purification gradient: 38% to 39% of ACN over 10 min with a flow of 3 mL/min; T = 50 °C

Yield: 5.6%

Analytical column: SunFire® C18 (4.6 mm x 100 mm, 3.5  $\mu$ m)

**Compound RZ8**HPLC-PDA  $t_R$  = 3.131

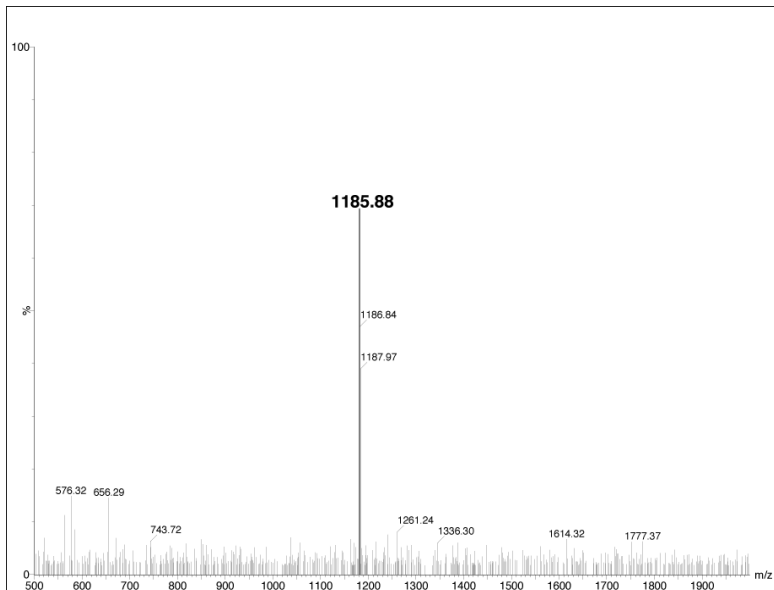
Gradient: 30% to 100% of ACN over 8 min

Purity ( $\lambda=220$ ): 99%

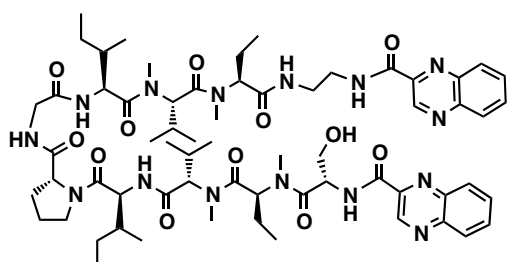
*m/z* calculated for  $C_{56}H_{77}N_{15}O_{14}$ : 1183.57689 Da

HRMS (NanoESI): 1183.57781 Da

HPLC-ESMS(+),  $[M+H]^+$ : 1185.88 Da



**Compound RZ9**



Purification column: Symmetry® C18 column (19 mm x 100 mm, 5  $\mu$ m)

Purification gradient: 46% to 47% of ACN over 10 min with a flow of 3 mL/min; T = 50 °C

Yield: 4%

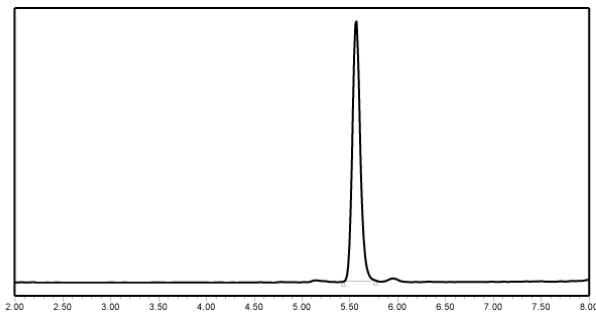
Analytical column: SunFire® C18 (4.6 mm x 100 mm, 3.5  $\mu$ m)

**Compound RZ9**

HPLC-PDA  $t_R$  = 5.586

Gradient: 30% to 100% of ACN over 8 min

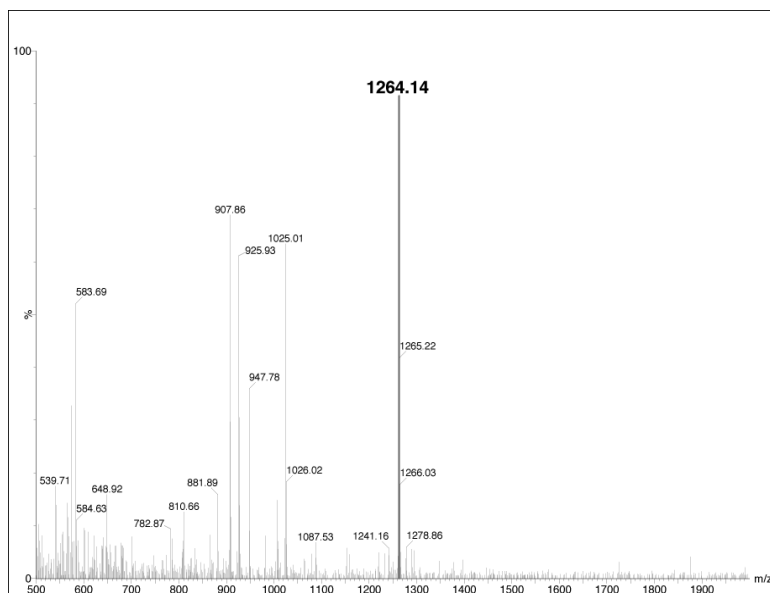
Purity ( $\lambda=220$ ): 98%

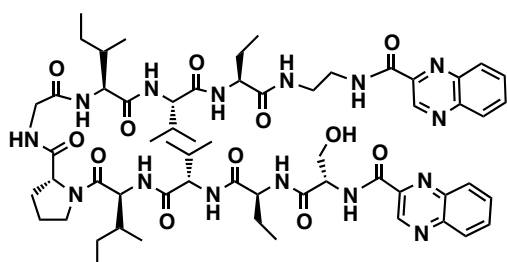


$m/z$  calculated for  $C_{64}H_{93}N_{15}O_{12}$ : 1263.71227 Da

HRMS (NanoESI): 1263.71240 Da

HPLC-ESMS(+),  $[M+H]^+$ : 1264.14 Da



**Compound RZ10**

Purification column: Symmetry® C18 column (19 mm x 100 mm, 5  $\mu$ m)

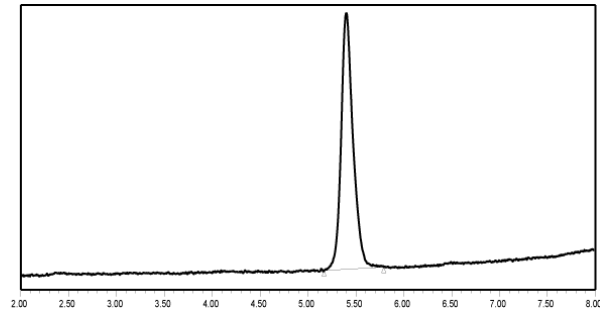
Purification gradient: 50% to 51% of ACN over 10 min with a flow of 3 mL/min

Yield: 7%

Analytical column: SunFire® C18 (4.6 mm x 100 mm, 3.5  $\mu$ m)

**Compound RZ10**

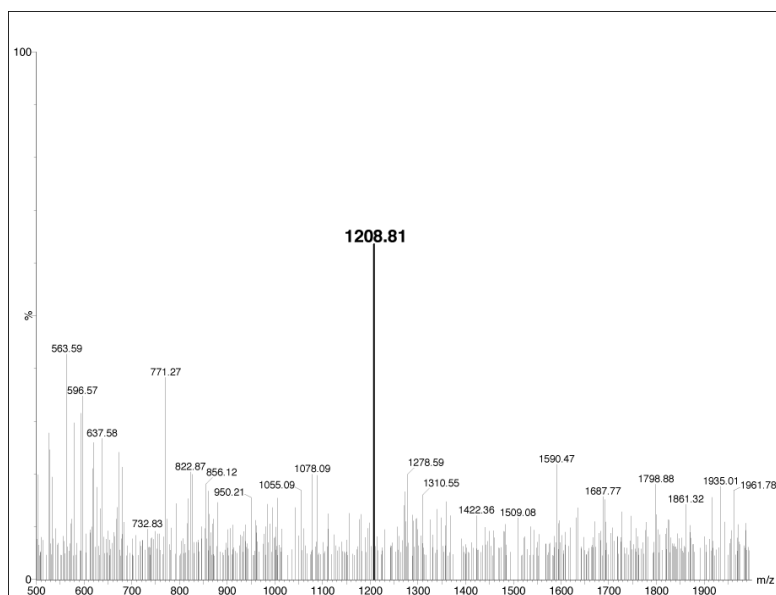
HPLC-PDA  $t_R$  = 5.409  
Gradient: 30% to 100% of ACN over 8 min  
Purity ( $\lambda=220$ ): 100%



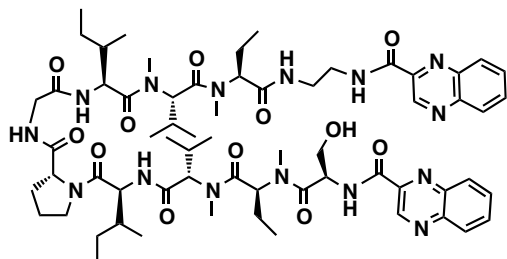
$m/z$  calculated for  $C_{60}H_{85}N_{15}O_{12}$ : 1207.64967 Da

HRMS (NanoESI): 1207.65062 Da

HPLC-ESMS(+),  $[M+H]^+$ : 1208.81 Da



### Compound RZ11



Purification column: Symmetry® C18 column (19 mm x 100 mm, 5  $\mu$ m)

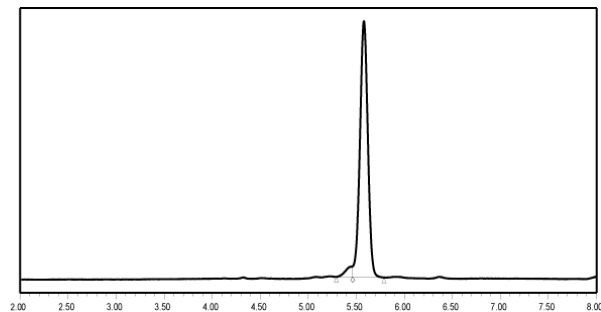
Purification gradient: 46% to 47% of ACN over 10 min with a flow of 3 mL/min; T = 50 °C

Yield: 0.7%

Analytical column: SunFire® C18 (4.6 mm x 100 mm, 3.5  $\mu$ m)

**Compound RZ11**

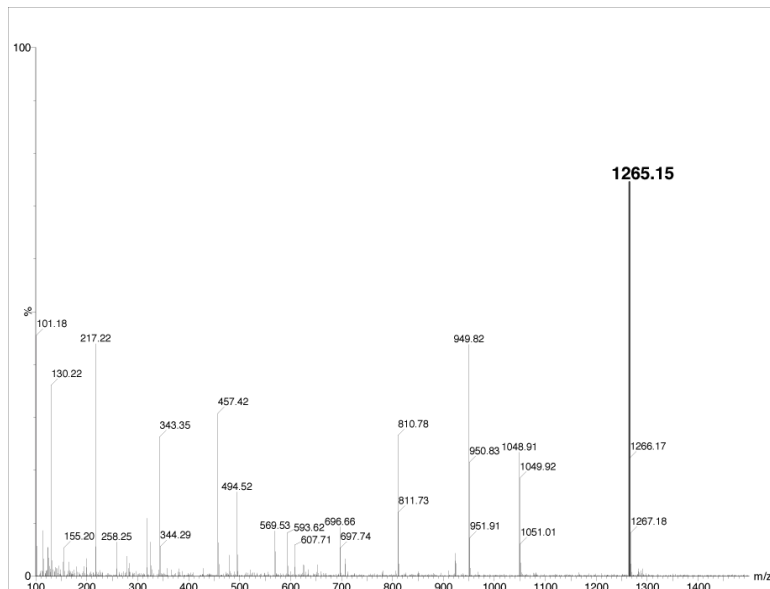
HPLC-PDA  $t_R$  = 5.577  
Gradient: 30% to 100% of ACN over 8 min  
Purity ( $\lambda=220$ ): 96%

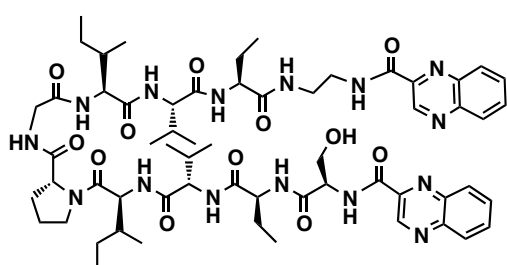


$m/z$  calculated for  $C_{64}H_{93}N_{15}O_{12}$ : 1263.71227 Da

HRMS (NanoESI): 1263.71376 Da

HPLC-ESMS(+),  $[M+H]^+$ : 1265.15 Da



**Compound RZ12**

Purification column: Symmetry® C18 column (19 mm x 100 mm, 5  $\mu$ m)

Purification gradient: 50% to 51% of ACN over 10 min with a flow of 3 mL/min; T = 50 °C

Yield: 0.2%

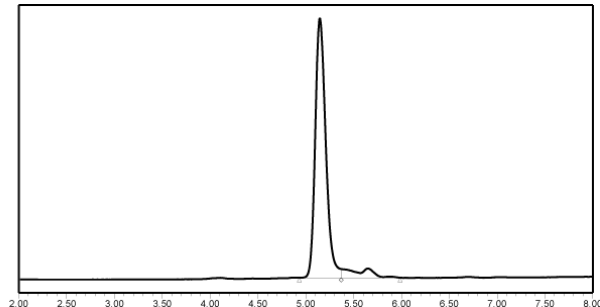
Analytical column: SunFire® C18 (4.6 mm x 100 mm, 3.5  $\mu$ m)

**Compound RZ12**

HPLC-PDA  $t_R$  = 5.146

Gradient: 30% to 100% of ACN over 8 min

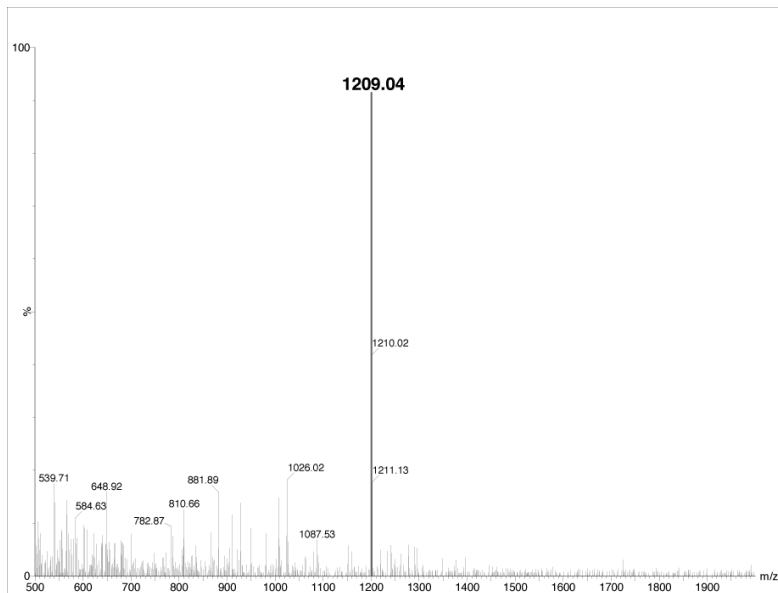
Purity ( $\lambda=220$ ): 92%

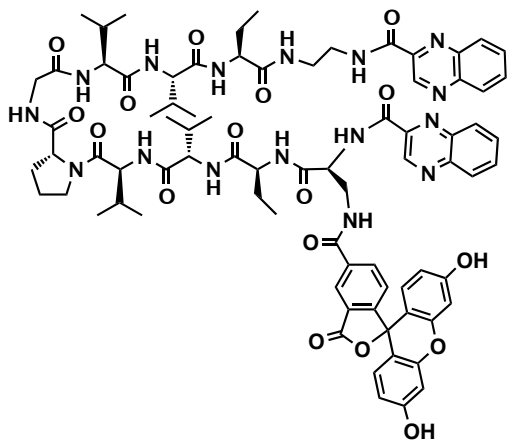


$m/z$  calculated for  $C_{60}H_{85}N_{15}O_{12}$ : 1207.64967 Da

HRMS (NanoESI): 1207.65076 Da

HPLC-ESMS(+),  $[M+H]^+$ : 1209.04 Da



**Compound RZ2CF**

2-CTC resin (300 mg, 1.56 mmol/g) was placed in a 10-mL polypropylene syringe fitted with a polyethylene filter disc. It was then washed with DMF (5 x 1 min) and CH<sub>2</sub>Cl<sub>2</sub> (5 x 1 min). Ethane-1,2-diamine (315 µL, 4.68 mmol) in CH<sub>2</sub>Cl<sub>2</sub> (3 mL) was added to the resin. The mixture was shaken at 25 °C for 30 min. After filtration, the resin was washed with CH<sub>2</sub>Cl<sub>2</sub> (5 x 1 min) and with DMF (5 x 1 min). Fmoc-Abu-OH (390.6 mg, 1.2 mmol) was incorporated with COMU (514 mg, 1.2 mmol),

OxymaPure (170.6 mg, 1.2 mmol) and DIEA (408.3 µL, 2.4 mmol) in DMF (10 mL/g resin) with preactivation for 30 s at 25 °C and stirred for 1.5 h. After filtration, the resin was washed with CH<sub>2</sub>Cl<sub>2</sub> (5 x 1 min) and with DMF (5 x 1 min) and the Fmoc group was removed by treatment with piperidine-DMF (1:4) (7.5 mL) (2 x 1 min, 2 x 5 min). The resin was washed with DMF (5 x 1 min) and CH<sub>2</sub>Cl<sub>2</sub> (5 x 1 min), and Fmoc-Val-OH (407 mg, 1.2 mmol) was incorporated with COMU (514 mg, 1.2 mmol), OxymaPure (170.6 mg, 1.2 mmol) and DIEA (408.3 µL, 2.4 mmol) in DMF (10 mL/g resin) at 25 °C. After stirring for 90 min, the resin was filtered and washed with DMF (5 x 1 min) and CH<sub>2</sub>Cl<sub>2</sub> (5 x 1 min) and one recoupling was performed under the same conditions. After resin filtration, and further removal of the Fmoc group, the resin was washed again. Next, Fmoc-Val-OH (407 mg, 1.2 mmol) was incorporated with COMU (514 mg, 1.2 mmol), OxymaPure (170.6 mg, 1.2 mmol) and DIEA (408.3 µL, 2.4 mmol) in DMF (10 mL/g resin) at 25 °C. After stirring for 90 min, the resin was filtered and washed with DMF (5 x 1 min) and CH<sub>2</sub>Cl<sub>2</sub> (5 x 1 min) and one recoupling was carried out under the same conditions. After resin filtration, the Fmoc group was removed and the resin was washed again. The following protected amino acids (Fmoc-Gly-OH, Fmoc-D-Pro-OH, Fmoc-Val-OH, Fmoc-Val-OH) were incorporated with COMU (4 equiv), OxymaPure (4 equiv) and DIEA (8 equiv) in DMF stirring for 90 min at room temperature. Fmoc-Abu-OH (390.6 mg, 1.2 mmol) was incorporated with COMU (514 mg, 1.2 mmol), OxymaPure (170.6 mg, 1.2 mmol) and DIEA (408.3 µL, 2.4 mmol) in DMF (10 mL/g resin) with preactivation for 30 s at 50 °C and stirred for 1 h. One recoupling was done and Boc-Dap(Fmoc)-OH (511.8 mg, 1.2 mmol) was incorporated with COMU (514 mg, 1.2 mmol), OxymaPure (170.6 mg, 1.2 mmol) and DIEA (408.3 µL, 2.4 mmol) in DMF at 25 °C. No recoupling was necessary at this time. The side-chain Fmoc group was removed by treatment with piperidine-DMF (1:4) (7.5 mL) (2 x 1 min, 2 x 5 min) and 5-carboxyfluorescein (451.6 mg, 1.2 mmol) was attached using COMU (514 mg, 1.2 mmol), OxymaPure (170.6 mg, 1.2 mmol) and DIEA (408.3 µL, 2.4 mmol) in DMF at 25 °C. After washing the resin, it was treated with a TFA-CH<sub>2</sub>Cl<sub>2</sub> (20:80) solution (5 x 2 min) and then washed again with CH<sub>2</sub>Cl<sub>2</sub> until the resin color changed from red to its original yellow color. All washes were collected in a round-bottom flask

and the solvents were removed under reduced pressure. To fully remove the Boc protecting group, the peptide was treated with a TFA-H<sub>2</sub>O-CH<sub>2</sub>Cl<sub>2</sub> (55:5:40; 25 mL) solution for 1 hour at 25 °C. The HPLC-PDA showed completion of the deprotection. The TFA and CH<sub>2</sub>Cl<sub>2</sub> were removed under reduced pressure and the resulting aqueous suspension was redissolved adding H<sub>2</sub>O-ACN (3:7; 15 mL) and lyophilized.

The peptide (0.16 mmol) was dissolved in DMF-CH<sub>2</sub>Cl<sub>2</sub> (1:1) (10 mL), and PyBOP (206.8 mg, 0.4 mmol), HOAt (54.1 mg, 0.4 mmol) and 2-quinoxalinecarboxylic acid (69.2 mg, 0.4 mmol) were added to the solution. The pH was adjusted to 8 by adding DIEA and the mixture was stirred until HPLC analysis indicated the completion of the reaction. The solvent was evaporated under reduced pressure and the peptide was redissolved in CH<sub>2</sub>Cl<sub>2</sub> (30 mL). The organic layer was washed with saturated solutions of NH<sub>4</sub>Cl (1 x 20 mL), NaHCO<sub>3</sub> (1 x 20 mL) and brine (1 x 20 mL, dried with MgSO<sub>4</sub> and evaporated under vacuum. The crude peptide was purified by semi-preparative RP-HPLC.

Purification column: Sunfire™ Prep18 column (10 mm x 150 mm, 5 µm)

Purification gradient: 30% to 100% of ACN over 15 min with a flow of 15 mL/min

Yield: 5.3%

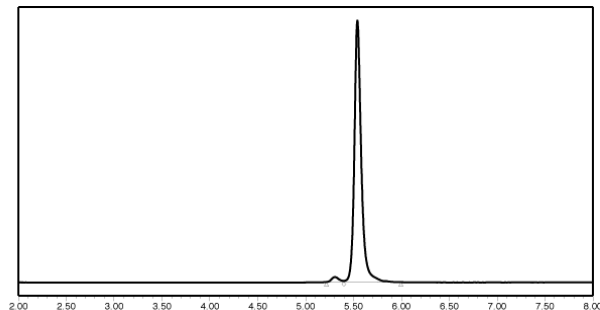
Analytical column: SunFire® C18 (4.6 mm x 100 mm, 3.5 µm)

**Compound RZ2CF**

HPLC-PDA  $t_R$  = 5.540

Gradient: 20% to 100% of ACN over 8 min

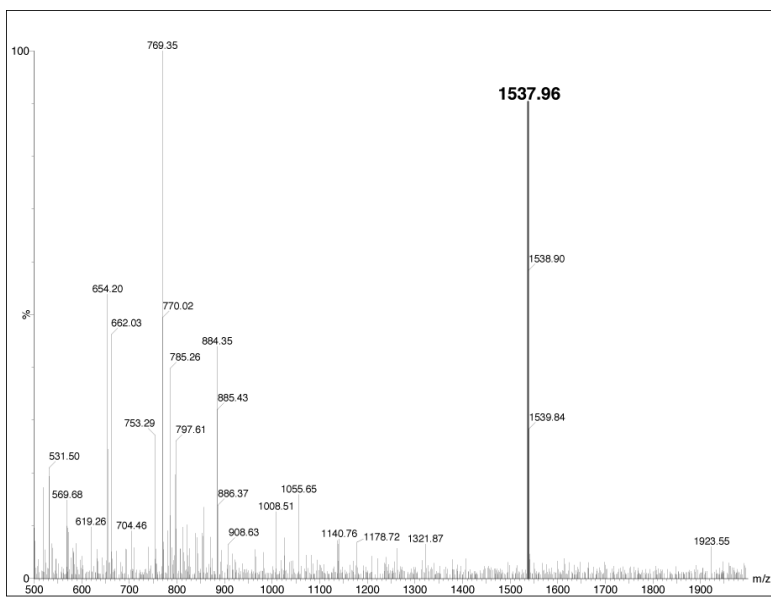
Purity ( $\lambda=220$ ): 98%



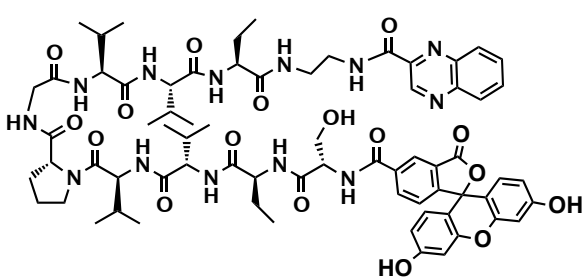
*m/z* calculated for C<sub>79</sub>H<sub>92</sub>N<sub>16</sub>O<sub>17</sub>: 1536,68264 Da

HRMS (NanoESI): 1537.6899 Da

HPLC-ESMS(+), [M+H]<sup>+</sup>: 1537.96 Da



### Compound RZ2\_EDAQC



2-CTC resin (300 mg, 1.56 mmol/g) was placed in a 10-mL polypropylene syringe fitted with a polyethylene filter disc. It was then washed with DMF (5 x 1 min) and CH<sub>2</sub>Cl<sub>2</sub> (5 x 1 min). Ethane-1,2-diamine (315 µL, 4.68 mmol) in CH<sub>2</sub>Cl<sub>2</sub> (3 mL) was added to the resin. The mixture was shaken

at 25 °C for 30 min. After filtration, the resin was washed with CH<sub>2</sub>Cl<sub>2</sub> (5 x 1 min) and with DMF (5 x 1 min). Fmoc-Abu-OH (390.6 mg, 1.2 mmol) was incorporated with COMU (514 mg, 1.2 mmol), OxymaPure (170.6 mg, 1.2 mmol) and DIEA (408.3 µL, 2.4 mmol) in DMF (10 mL/g resin) with preactivation for 30 s at 25 °C and stirred for 1.5 h. After filtration, the resin was washed with CH<sub>2</sub>Cl<sub>2</sub> (5 x 1 min) and with DMF (5 x 1 min) and the Fmoc group was removed by treatment with piperidine-DMF (1:4) (7.5 mL) (2 x 1 min, 2 x 5 min). The resin was washed with DMF (5 x 1 min) and CH<sub>2</sub>Cl<sub>2</sub> (5 x 1 min), and Fmoc-Val-OH (407 mg, 1.2 mmol) was incorporated with COMU (514 mg, 1.2 mmol), OxymaPure (170.6 mg, 1.2 mmol) and DIEA (408.3 µL, 2.4 mmol) in DMF (10 mL/g resin) at 25 °C. After stirring for 90 min, the resin was filtered and washed with DMF (5 x 1 min) and CH<sub>2</sub>Cl<sub>2</sub> (5 x 1 min) and one recoupling was performed under the same conditions. After resin filtration, and further removal of the Fmoc group, the resin was washed again. Next, Fmoc-Val-OH (407 mg, 1.2 mmol) was incorporated with COMU (514 mg, 1.2 mmol), OxymaPure (170.6 mg, 1.2 mmol) and DIEA (408.3 µL, 2.4 mmol) in DMF (10 mL/g resin) at 25 °C. After stirring for 90 min, the resin was filtered and washed with DMF (5 x 1 min) and CH<sub>2</sub>Cl<sub>2</sub> (5 x 1 min) and one recoupling was carried out under

the same conditions. After resin filtration, the Fmoc group was removed and the resin was washed again. The following protected amino acids (Fmoc-Gly-OH, Fmoc-D-Pro-OH, Fmoc-Val-OH, Fmoc-Val-OH) were incorporated with COMU (4 equiv), OxymaPure (4 equiv) and DIEA (8 equiv) in DMF stirring for 90 min at room temperature. Fmoc-Abu-OH (390.6 mg, 1.2 mmol) was incorporated with COMU (514 mg, 1.2 mmol), OxymaPure (170.6 mg, 1.2 mmol) and DIEA (408.3  $\mu$ L, 2.4 mmol) in DMF (10 mL/g resin) with preactivation for 30 s at 50 °C and stirred for 1 h. One recoupling was done and Fmoc-Ser(*t*Bu) (460 mg, 1.2 mmol) was incorporated with COMU (514 mg, 1.2 mmol), OxymaPure (170.6 mg, 1.2 mmol) and DIEA (408.3  $\mu$ L, 2.4 mmol) in DMF (10 mL/g resin) at 50 °C. No recoupling was necessary at this time. After resin filtration, the Fmoc group was removed and the resin was washed again. 5-carboxyfluorescein (451.6 mg, 1.2 mmol) was attached using COMU (514 mg, 1.2 mmol), OxymaPure (170.6 mg, 1.2 mmol) and DIEA (408.3  $\mu$ L, 2.4 mmol) in DMF at 25 °C. The peptide was cleaved with 20% TFA in CH<sub>2</sub>Cl<sub>2</sub> (4.5 mL, 10 x 30 s) at 25 °C and poured over H<sub>2</sub>O-ACN (1:1) (50 mL) to avoid cleavage of the *t*Bu groups. The resulting solution was partially evaporated and lyophilized.

The peptide (0.42 mmol) was dissolved in DMF-CH<sub>2</sub>Cl<sub>2</sub> (1:1) (20 mL), and PyBOP (265.6 mg, 0.5 mmol), HOAt (70 mg, 0.5 mmol) and 2-quinoxalinecarboxylic acid (88.9 mg, 0.5 mmol) were added to the solution. The pH was adjusted to 8 by adding DIEA and the mixture was stirred until HPLC analysis indicated the completion of the reaction. The solvent was evaporated under reduced pressure and the peptide was redissolved in CH<sub>2</sub>Cl<sub>2</sub> (40 mL). The organic layer was washed with saturated solutions of NH<sub>4</sub>Cl (1 x 20 mL), NaHCO<sub>3</sub> (1 x 20 mL) and brine (1 x 20 mL, dried with MgSO<sub>4</sub> and evaporated under vacuum. Total deprotection was accomplished by treatment with TFA-H<sub>2</sub>O (95:5; 50 mL) at 25 °C for 2 h. After global deprotection, the resulting solution was evaporated to 5 mL and lyophilized. The crude peptide was purified by semi-preparative RP-HPLC.

Purification column: Sunfire™ Prep18 column (10 mm x 150 mm, 5  $\mu$ m)

Purification gradient: 35% to 55% of ACN over 15 min with a flow of 15 mL/min

Yield: 4.6%

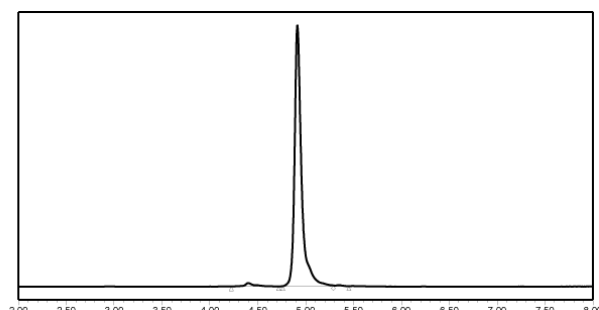
Analytical column: SunFire® C18 (4.6 mm x 100 mm, 3.5  $\mu$ m)

#### Compound RZ2\_EDAQC

HPLC-PDA  $t_r$  = 4.913

Gradient: 20% to 100% of ACN over 8 min

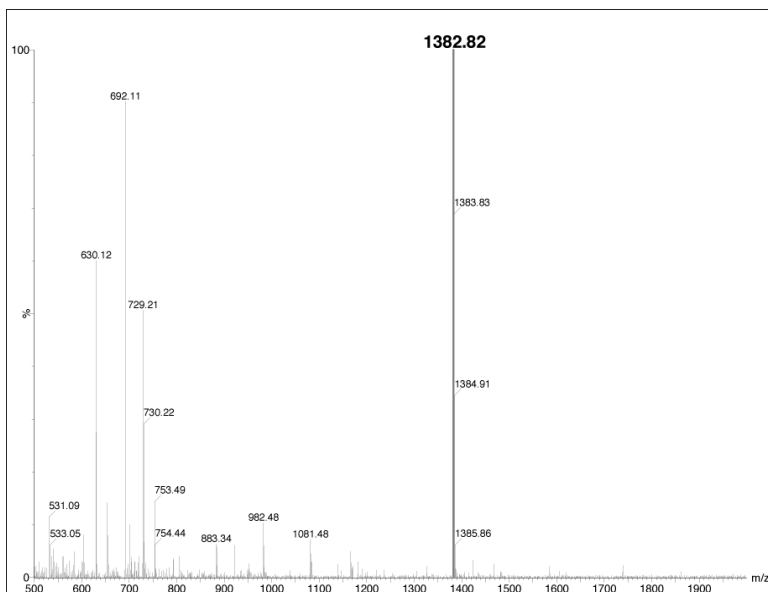
Purity ( $\lambda=220$ ): 98%



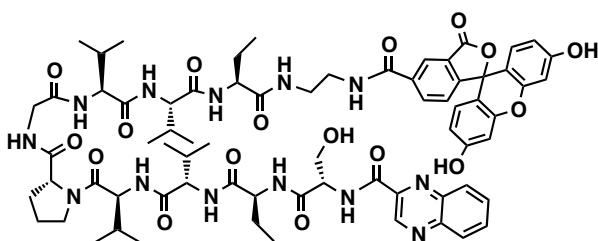
*m/z* calculated for C<sub>70</sub>H<sub>87</sub>N<sub>13</sub>O<sub>17</sub>: 1381.6343 Da

HRMS (NanoESI): 1381.6363 Da

HPLC-ESMS(+), [M+H]<sup>+</sup>: 1382.82 Da



### Compound RZ2\_EDACF



2-CTC resin (300 mg, 1.56 mmol/g) was placed in a 10-mL polypropylene syringe fitted with a polyethylene filter disc. It was then washed with DMF (5 x 1 min) and CH<sub>2</sub>Cl<sub>2</sub> (5 x 1 min). Ethane-1,2-diamine (315  $\mu$ L, 4.68 mmol) in CH<sub>2</sub>Cl<sub>2</sub> (3 mL) was

added to the resin. The mixture was shaken at 25 °C for 30 min. After filtration, the resin was washed with CH<sub>2</sub>Cl<sub>2</sub> (5 x 1 min) and with DMF (5 x 1 min). Fmoc-Abu-OH (390.6 mg, 1.2 mmol) was incorporated with COMU (514 mg, 1.2 mmol), OxymaPure (170.6 mg, 1.2 mmol) and DIEA (408.3  $\mu$ L, 2.4 mmol) in DMF (10 mL/g resin) with preactivation for 30 s at 25 °C and stirred for 1.5 h. After filtration, the resin was washed with CH<sub>2</sub>Cl<sub>2</sub> (5 x 1 min) and with DMF (5 x 1 min) and the Fmoc group was removed by treatment with piperidine-DMF (1:4) (7.5 mL) (2 x 1 min, 2 x 5 min). The resin was washed with DMF (5 x 1 min) and CH<sub>2</sub>Cl<sub>2</sub> (5 x 1 min), and Fmoc-Val-OH (407 mg, 1.2 mmol) was incorporated with COMU (514 mg, 1.2 mmol), OxymaPure (170.6 mg, 1.2 mmol) and DIEA (408.3  $\mu$ L, 2.4 mmol) in DMF (10 mL/g resin) at 25 °C. After stirring for 90 min, the resin was filtered and washed with DMF (5 x 1 min) and CH<sub>2</sub>Cl<sub>2</sub> (5 x 1 min) and one recoupling was performed under the same conditions. After resin filtration, and further removal

of the Fmoc group, the resin was washed again. Next, Fmoc-Val-OH (407 mg, 1.2 mmol) was incorporated with COMU (514 mg, 1.2 mmol), OxymaPure (170.6 mg, 1.2 mmol) and DIEA (408.3  $\mu$ L, 2.4 mmol) in DMF (10 mL/g resin) at 25 °C. After stirring for 90 min, the resin was filtered and washed with DMF (5 x 1 min) and CH<sub>2</sub>Cl<sub>2</sub> (5 x 1 min) and one recoupling was carried out under the same conditions. After resin filtration, the Fmoc group was removed and the resin was washed again. The following protected amino acids (Fmoc-Gly-OH, Fmoc-D-Pro-OH, Fmoc-Val-OH, Fmoc-Val-OH) were incorporated with COMU (4 equiv), OxymaPure (4 equiv) and DIEA (8 equiv) in DMF stirring for 90 min at room temperature. Fmoc-Abu-OH (390.6 mg, 1.2 mmol) was incorporated with COMU (514 mg, 1.2 mmol), OxymaPure (170.6 mg, 1.2 mmol) and DIEA (408.3  $\mu$ L, 2.4 mmol) in DMF (10 mL/g resin) with preactivation for 30 s at 50 °C and stirred for 1 h. One recoupling was done and Fmoc-Ser(*t*Bu) (460 mg, 1.2 mmol) was incorporated with COMU (514 mg, 1.2 mmol), OxymaPure (170.6 mg, 1.2 mmol) and DIEA (408.3  $\mu$ L, 2.4 mmol) in DMF (10 mL/g resin) at 50 °C. No recoupling was necessary at this time. After resin filtration, the Fmoc group was removed and the resin was washed again. 2-quinoxalinecarboxylic acid (230 mg, 1.2 mmol) was attached using COMU (514 mg, 1.2 mmol), OxymaPure (170.6 mg, 1.2 mmol) and DIEA (408.3  $\mu$ L, 2.4 mmol) in DMF at 25 °C. The peptide was cleaved with 20% TFA in CH<sub>2</sub>Cl<sub>2</sub> (4.5 mL, 10 x 30 s) at 25 °C and poured over H<sub>2</sub>O-ACN (1:1) (50 mL) to avoid cleavage of the *t*Bu groups. The resulting solution was partially evaporated and lyophilized.

The peptide (0.39 mmol) was dissolved in DMF-CH<sub>2</sub>Cl<sub>2</sub> (1:1) (20 mL), and PyBOP (243.7 mg, 0.47 mmol), HOAt (63.8 mg, 0.47 mmol) and 5-carboxyfluorescein (176.2 mg, 0.47 mmol) were added to the solution. The pH was adjusted to 8 by adding DIEA and the mixture was stirred until HPLC analysis indicated the completion of the reaction. The solvent was evaporated under reduced pressure and the peptide was redissolved in CH<sub>2</sub>Cl<sub>2</sub> (40 mL). The organic layer was washed with saturated solutions of NH<sub>4</sub>Cl (1 x 20 mL), NaHCO<sub>3</sub> (1 x 20 mL) and brine (1 x 20 mL, dried with MgSO<sub>4</sub> and evaporated under vacuum. Total deprotection was accomplished by treatment with TFA-H<sub>2</sub>O (95:5; 50 mL) at 25 °C for 2 h. After global deprotection, the resulting solution was evaporated to 5 mL and lyophilized. The crude peptide was purified by semi-preparative RP-HPLC.

Purification column: Sunfire™ Prep18 column (10 mm x 150 mm, 5  $\mu$ m)

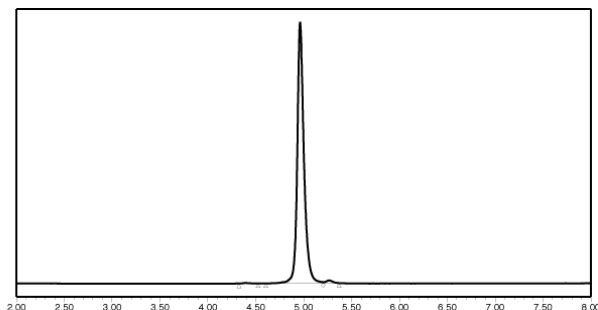
Purification gradient: 35% to 50% of ACN over 15 min with a flow of 15 mL/min

Yield: 2.1%

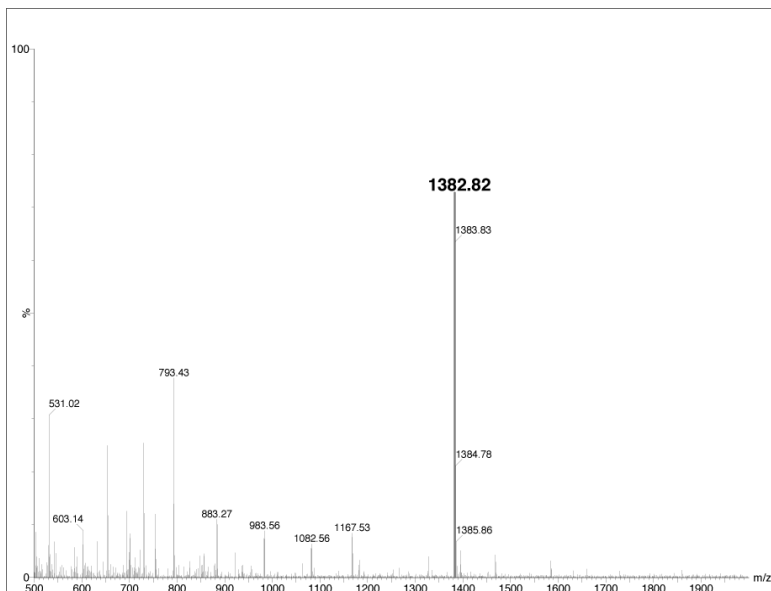
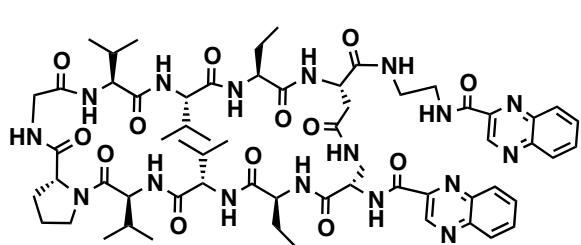
Analytical column: SunFire® C18 (4.6 mm x 100 mm, 3.5  $\mu$ m)

**Compound RZ2\_EDACF**HPLC-PDA  $t_R = 4.963$ 

Gradient: 20% to 100% of ACN over 8 min

Purity ( $\lambda=220$ ): 99% $m/z$  calculated for  $C_{70}H_{87}N_{13}O_{17}$ : 1381.6343 Da

HRMS (NanoESI): 1381.6349 Da

HPLC-ESMS(+),  $[M+H]^+$ : 1382.82 Da**Compound RZV13**

2-CTC resin (100 mg, 1.56 mmol/g) was placed in a 10-mL polypropylene syringe fitted with a polyethylene filter disc. It was then washed with DMF (5 x 1 min) and  $CH_2Cl_2$  (5 x 1 min). Fmoc-1,2-ethylenediamine\*HCl (22.3 mg, 0.07 mmol)

and DIEA (15.3  $\mu$ L) in  $CH_2Cl_2$  (1 mL) was added to the resin. The mixture was shaken at 25 °C for 45 min. The reaction was quenched by addition of MeOH (80  $\mu$ L) and the mixture was stirred for 10 min at 25 °C. After filtration, the resin was washed with  $CH_2Cl_2$  (5 x 1 min) and with DMF (5 x 1 min) and cleavage of the Fmoc group was done by treatment with piperidine-DMF (1:4)

(2.5 mL) (2 x 1 min, 2 x 5 min). The filtrates were collected and quantified by UV (290 nm) obtaining a loading of 0.70 mmol/g. Based on this loading, Fmoc-Asp(Allyl)-OH (110.7 mg, 0.28 mmol) was incorporated with COMU (120 mg, 0.28 mmol), OxymaPure (40 mg, 0.28 mmol) and DIEA (95  $\mu$ L, 0.56 mmol) in DMF (10 mL/g resin) with preactivation for 30 s at 25 °C and stirred for 1 h. After filtration, the resin was washed with CH<sub>2</sub>Cl<sub>2</sub> (5 x 1 min) and with DMF (5 x 1 min) and the Fmoc group was removed by treatment with piperidine-DMF (1:4) (7.5 mL) (2 x 1 min, 2 x 5 min). Fmoc-Abu-OH (91.2 mg, 0.28 mmol) was incorporated with COMU (120 mg, 0.28 mmol), OxymaPure (40 mg, 0.28 mmol) and DIEA (95  $\mu$ L, 0.56 mmol) in DMF (10 mL/g resin) with preactivation for 30 s at 25 °C and stirred for 1.5 h. After the Fmoc group removal, the resin was washed with DMF (5 x 1 min) and CH<sub>2</sub>Cl<sub>2</sub> (5 x 1 min), and Fmoc-Val-OH (95.1 mg, 0.28 mmol) was incorporated with COMU (120 mg, 0.28 mmol), OxymaPure (40 mg, 0.28 mmol) and DIEA (95  $\mu$ L, 0.56 mmol) in DMF (10 mL/g resin) at 25 °C. After resin filtration, and further removal of the Fmoc group, the resin was washed again. Next, Fmoc-Val-OH (95.1 mg, 0.28 mmol) was incorporated with COMU (120 mg, 0.28 mmol), OxymaPure (40 mg, 0.28 mmol) and DIEA (95  $\mu$ L, 0.56 mmol) in DMF (10 mL/g resin) at 25 °C. After resin filtration, the Fmoc group was removed and the resin was washed again. The following protected amino acids (Fmoc-Gly-OH, Fmoc-D-Pro-OH, Fmoc-Val-OH, Fmoc-Val-OH) were incorporated with COMU (4 equiv), OxymaPure (4 equiv) and DIEA (8 equiv) in DMF stirring for 90 min at room temperature. Fmoc-Abu-OH (91.2 mg, 0.28 mmol) was incorporated with COMU (120 mg, 0.28 mmol), OxymaPure (40 mg, 0.28 mmol) and DIEA (95  $\mu$ L, 0.56 mmol) in DMF (10 mL/g resin) with preactivation for 30 s and stirred for 1 h. Boc-Dap(Fmoc)-OH (119.4 mg, 0.28 mmol) was incorporated with COMU (120 mg, 0.28 mmol), OxymaPure (40 mg, 0.28 mmol) and DIEA (95  $\mu$ L, 0.56 mmol) in DMF at 25 °C. Next, to remove the Allyl group, the peptide-resin was treated with Pd(PPh<sub>3</sub>)<sub>4</sub> (8 mg, 7  $\mu$ mol) and PhSiH<sub>3</sub> (86.3  $\mu$ L, 0.7 mmol) dissolved in CH<sub>2</sub>Cl<sub>2</sub> for 15 min under Ar, and was then washed with CH<sub>2</sub>Cl<sub>2</sub> (3 x 1 min). The process was repeated three times and the side-chain Fmoc group was removed by treatment with piperidine-DMF (1:4) (7.5 mL) (2 x 1 min, 2 x 5 min). Then, DIPCDI (32.5  $\mu$ L, 0.21 mmol) and OxymaPure (29.8 mg, 0.21 mmol) in CH<sub>2</sub>Cl<sub>2</sub> were added and the stirred overnight at 25 °C. The reaction was monitored by HPLC-PDA. After the completion of the cyclization, the peptide was cleaved with 20% TFA in CH<sub>2</sub>Cl<sub>2</sub> (4.5 mL, 5 x 2 min). All washes were collected in a round-bottom flask and the solvents were removed under reduced pressure.

The peptide (0.035 mmol) was dissolved in DMF-CH<sub>2</sub>Cl<sub>2</sub> (1:1) (10 mL), and PyBOP (43.7 mg, 0.084 mmol), HOAt (11.44 mg, 0.084 mmol) and 2-quinoxalinecarboxylic acid (14.6 mg, 0.084 mmol) were added to the solution. The pH was adjusted to 7-8 by adding DIEA and the mixture was stirred until HPLC analysis indicated the completion of the reaction. The solvent was evaporated under reduced pressure and the peptide was redissolved in CH<sub>2</sub>Cl<sub>2</sub> (10 mL). The organic layer was washed with saturated solutions of NH<sub>4</sub>Cl (1 x 20 mL), NaHCO<sub>3</sub> (1 x 20

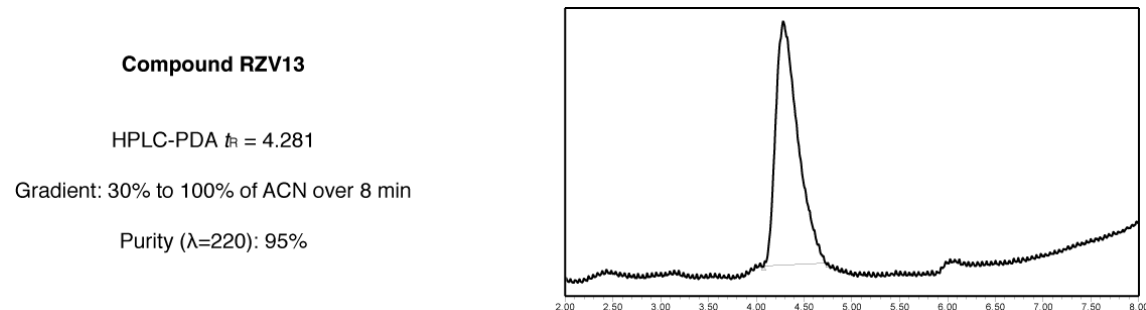
mL) and brine (1 x 20 mL), dried with MgSO<sub>4</sub> and evaporated under vacuum. The crude peptide was purified by semi-preparative RP-HPLC.

Purification column: Symmetry® C18 column (19 mm x 100 mm, 5 µm)

Purification gradient: 35% to 45% of ACN over 15 min with a flow of 3 mL/min

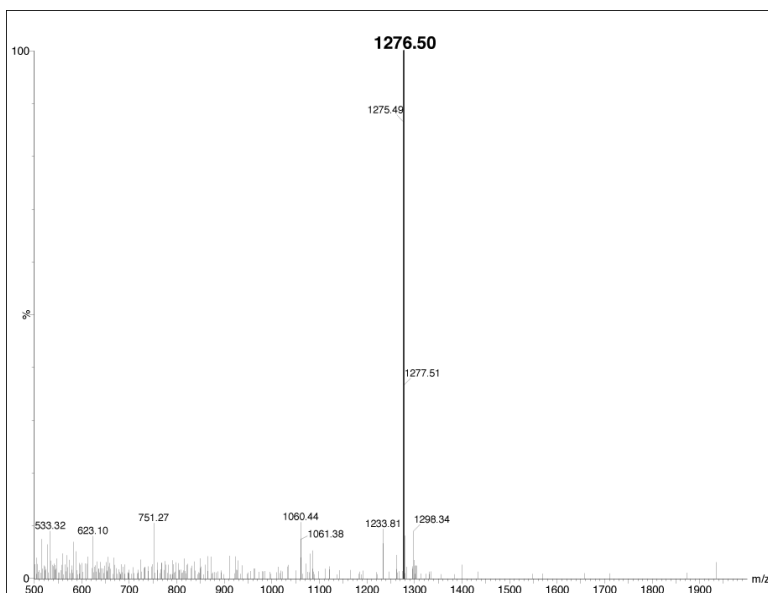
Yield: 10.8%

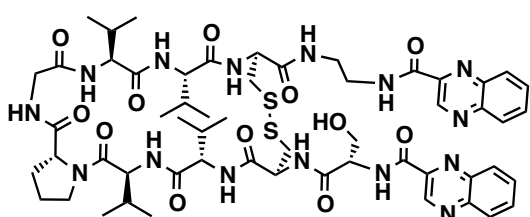
Analytical column: SunFire® C18 (4.6 mm x 100 mm, 3.5 µm)



*m/z* calculated for C<sub>62</sub>H<sub>85</sub>N<sub>17</sub>O<sub>13</sub>: 1275.65 Da

HPLC-ESMS(+), [M+H]<sup>+</sup>: 1276.50 Da



**Compound RZV14**

2-CTC resin (100 mg, 1.56 mmol/g) was placed in a 10-mL polypropylene syringe fitted with a polyethylene filter disc. It was then washed with DMF (5 x 1 min) and CH<sub>2</sub>Cl<sub>2</sub> (5 x 1 min). Fmoc-1,2-ethylenediamine\*HCl (22.3 mg, 0.07 mmol)

and DIEA (15.3 µL) in CH<sub>2</sub>Cl<sub>2</sub> (1 mL) was added to the resin. The mixture was shaken at 25 °C for 45 min. The reaction was quenched by addition of MeOH (80 µL) and the mixture was stirred for 10 min at 25 °C. After filtration, the resin was washed with CH<sub>2</sub>Cl<sub>2</sub> (5 x 1 min) and with DMF (5 x 1 min) and cleavage of the Fmoc group was done by treatment with piperidine-DMF (1:4) (2.5 mL) (2 x 1 min, 2 x 5 min). The filtrates were collected and quantified by UV (290 nm) obtaining a loading of 0.70 mmol/g. Based on this loading, Fmoc-Cys(Acm)-OH (116.6 mg, 0.28 mmol) was incorporated with COMU (120 mg, 0.28 mmol), OxymaPure (40 mg, 0.28 mmol) and DIEA (95 µL, 0.56 mmol) in DMF (10 mL/g resin) with preactivation for 30 s at 25 °C and stirred for 1 h. After filtration, the resin was washed with CH<sub>2</sub>Cl<sub>2</sub> (5 x 1 min) and with DMF (5 x 1 min) and the Fmoc group was removed by treatment with piperidine-DMF (1:4) (7.5 mL) (2 x 1 min, 2 x 5 min). Fmoc-Val-OH (95.1 mg, 0.28 mmol) was incorporated with COMU (120 mg, 0.28 mmol), OxymaPure (40 mg, 0.28 mmol) and DIEA (95 µL, 0.56 mmol) in DMF (10 mL/g resin) at 25 °C. After resin filtration, and further removal of the Fmoc group, the resin was washed again. The following protected amino acids (Fmoc-Val-OH, Fmoc-Gly-OH, Fmoc-D-Pro-OH, Fmoc-Val-OH, Fmoc-Val-OH) were incorporated with COMU (4 equiv), OxymaPure (4 equiv) and DIEA (8 equiv) in DMF stirring for 90 min at room temperature. Fmoc-Cys(Acm)-OH (116.6 mg, 0.28 mmol) was incorporated with COMU (120 mg, 0.28 mmol), OxymaPure (40 mg, 0.28 mmol) and DIEA (95 µL, 0.56 mmol) in DMF (10 mL/g resin) with preactivation for 30 s and stirred for 1 h. The resin was then filtered and washed with DMF (5 x 1 min) and CH<sub>2</sub>Cl<sub>2</sub> (5 x 1 min) and one recoupling was carried out under the same conditions. After resin filtration, and further removal of the Fmoc group, the resin was washed again. Next, Fmoc-Ser(iBu) (107.4 mg, 0.28 mmol) was incorporated with COMU (120 mg, 0.28 mmol), OxymaPure (40 mg, 0.28 mmol) and DIEA (95 µL, 0.56 mmol) in DMF at 25 °C. Fmoc group was removed by treatment with piperidine-DMF (1:4) (7.5 mL) (2 x 1 min, 2 x 5 min). Removal of S-Acm and formation of the intermolecular disulfide bridge were obtained by treatment of the peptidyl resin with iodine (0.89 g, 0.35 mmol, 0.1 M) in DMF at 25 °C for 10 minutes and the treatment was repeated two more times. The resin was repeatedly washed with CH<sub>2</sub>Cl<sub>2</sub> (10 x 1 min), DMF (10 x 1 min), and CH<sub>2</sub>Cl<sub>2</sub> (10 x 1 min). The peptide was then cleaved from the resin by treatment with 20% TFA in CH<sub>2</sub>Cl<sub>2</sub> (4.5 mL, 5 x 2 min). All washes were collected in a round-bottom flask and the solvents were removed under reduced pressure.

The peptide (0.035 mmol) was dissolved in DMF-CH<sub>2</sub>Cl<sub>2</sub> (1:1) (10 mL), and PyBOP (43.7 mg, 0.084 mmol), HOAt (11.44 mg, 0.084 mmol) and 2-quinoxalinecarboxylic acid (14.6 mg, 0.084 mmol) were added to the solution. The pH was adjusted to 7-8 by adding DIEA and the mixture was stirred until HPLC analysis indicated the completion of the reaction. The solvent was evaporated under reduced pressure and the peptide was redissolved in CH<sub>2</sub>Cl<sub>2</sub> (10 mL). The organic layer was washed with saturated solutions of NH<sub>4</sub>Cl (1 x 20 mL), NaHCO<sub>3</sub> (1 x 20 mL) and brine (1 x 20 mL), dried with MgSO<sub>4</sub> and evaporated under vacuum. Total deprotection was accomplished by treatment with TFA-H<sub>2</sub>O (95:5; 40 mL) at 25 °C for 2 h. After global deprotection, the resulting solution was evaporated to 5 mL and lyophilized. The crude peptide was purified by semi-preparative RP-HPLC.

Purification column: Symmetry® C18 column (19 mm x 100 mm, 5 µm)

Purification gradient: 38% to 45% of ACN over 15 min with a flow of 3 mL/min

Yield: 5.1%

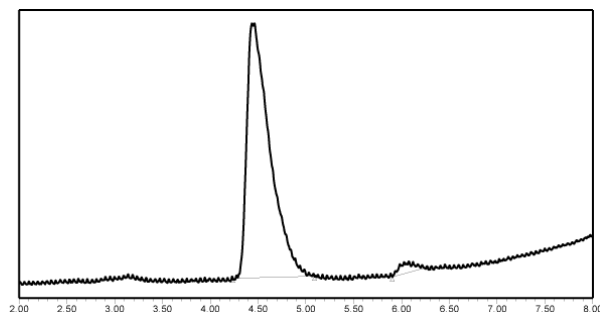
Analytical column: SunFire® C18 (4.6 mm x 100 mm, 3.5 µm)

**Compound RZV14**

HPLC-PDA  $t_R$  = 4.436

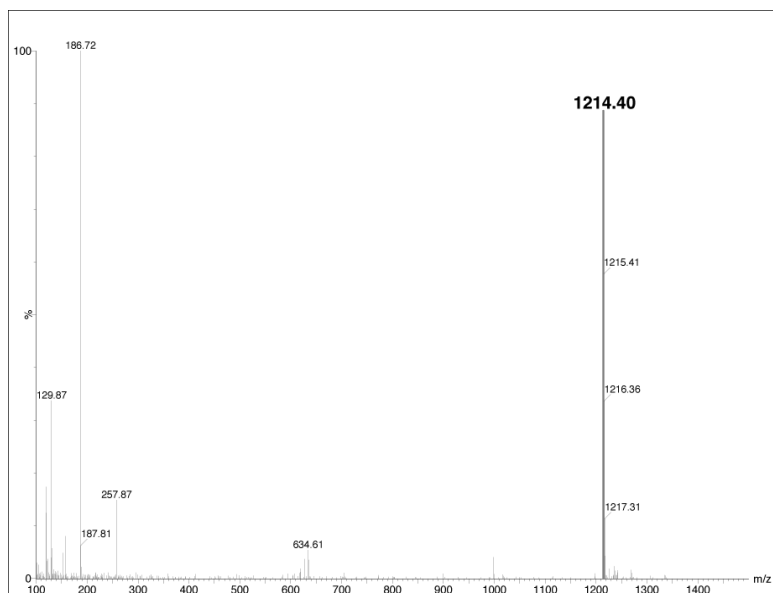
Gradient: 30% to 100% of ACN over 8 min

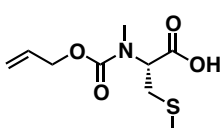
Purity ( $\lambda=220$ ): 97%



*m/z* calculated for C<sub>56</sub>H<sub>75</sub>N<sub>15</sub>O<sub>12</sub>S<sub>2</sub>: 1213.51 Da

HPLC-ESMS(+), [M+H]<sup>+</sup>: 1214.40 Da



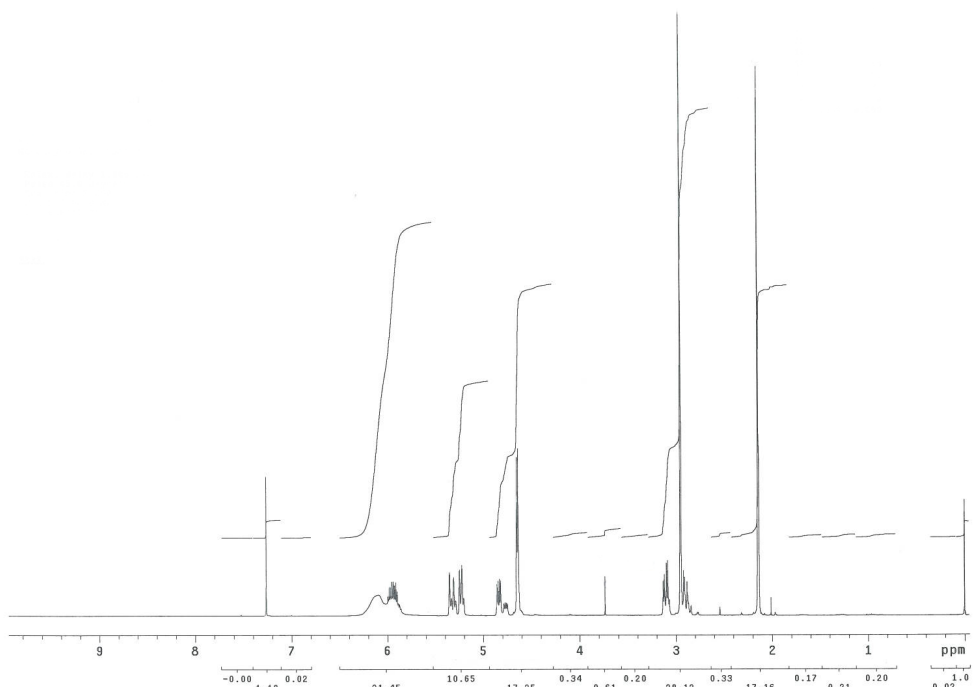
**RZV15 non-commercial building block*****Alloc-NMe-Cys(Me)-OH***

2-CTC resin (500 mg, 1.56 mmol/g) was placed in a 10-mL polypropylene syringe fitted with a polyethylene filter disc. It was then washed with DMF (5 x 1 min) and CH<sub>2</sub>Cl<sub>2</sub> (5 x 1 min). Commercially available Fmoc-Cys(Trt)-OH (2 equiv) was attached to the resin with DIEA (10 equiv) as base in DMF, allowing the mixture to react for 90 min. Next, a capping step with MeOH was carried out, followed by removal of the Fmoc group by treatment with piperidine-DMF (1:4) (7.5 mL) (2 x 1 min, 2 x 5 min). Then, Alloc-Cl (3 equiv) was incorporated with DIEA (15 equiv) for 50 min in order to obtain Alloc-Cys(Trt)-OH. The cleavage was made using TFA-CH<sub>2</sub>Cl<sub>2</sub> (1:99) (5 x 1 min). Several washings with CH<sub>2</sub>Cl<sub>2</sub> were performed until the resin recovered its initial pale yellow color. The solvent was evaporated to give 306 mg of product as a white solid (88% yield; 85% purity). Analytical HPLC (linear gradient from 0 to 100% ACN over 15 min, 1 mL/min): *t*<sub>R</sub> = 13.9 min. HPLC-ESMS: *m/z* calcd for C<sub>26</sub>H<sub>25</sub>NO<sub>4</sub>S, 447.2; found, 445.5 [M - H]<sup>+</sup>.

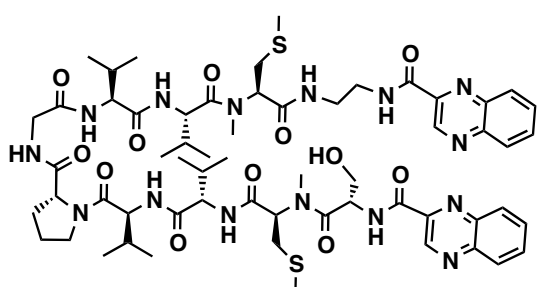
Next, in a round-bottomed flask, NaH (60% in mineral oil) (61.7 mg, 1.54 mmol) was suspended in anhydrous THF (20 mL) under a nitrogen atmosphere and the suspension was cooled at 4 °C. Alloc-Cys(Trt)-OH (287 mg, 0.64 mmol) was dissolved in THF (4 mL), and the solution was added slowly. MeI (133 µL, 2.12 mmol) was dropped, and the mixture was stirred for 2 h at 4 °C and for 10 h at room temperature. MeOH and H<sub>2</sub>O were added to quench the reaction, and the THF was removed under vacuum. The aqueous solution was washed with TBME (3 x 20 mL) and acidified with 1 N HCl to pH 6-7, and the product was extracted with EtOAc (3 x 30 mL). The solvent was dried with Na<sub>2</sub>SO<sub>4</sub> and removed under vacuum. The product was redissolved in ACN and H<sub>2</sub>O and lyophilized to give 234 mg of Alloc-NMe-Cys(Trt)-OH as a white powder (79% yield; 97% purity). Analytical HPLC (linear gradient from 0 to 100% ACN for 15 min, 1 mL/min): *t*<sub>R</sub> = 14.5 min. HPLC-ESMS: *m/z* calcd for C<sub>27</sub>H<sub>27</sub>NO<sub>4</sub>S, 461.2; found 459.4 [M - H]<sup>+</sup>. HRMS: *m/z* calcd for C<sub>27</sub>H<sub>26</sub>NO<sub>4</sub>S, 460.1577 [M - H]<sup>+</sup>; found, 460.1572.

Finally, to a round-bottomed flask containing Alloc-NMe-Cys(Trt)-OH (0.22 mmol, 100 mg) a solution of TFA and TIS in CH<sub>2</sub>Cl<sub>2</sub> (4:1:35, 2 mL) was added dropwise. The solution was stirred for 1 h at room temperature, and the solvent evaporated under reduced pressure and coevaporated with toluene. The product was dissolved in H<sub>2</sub>O-THF (1:1, 2.8 mL), and the solution was cooled to 4 °C. Maintaining the pH at 7, MeI (0.31 mmol, 20 µL) was added to the solution. The mixture was stirred for 4 h at room temperature and THF evaporated under vacuum. The aqueous layer was basified to pH 9, washed with TBME (3 x 5 mL), and acidified to pH 3.5. Then, the product was extracted with EtOAc (3 x 7 mL), dried (MgSO<sub>4</sub>), and evaporated to obtain 40.0 mg of colorless oil (78% yield, 80% purity). Analytical HPLC (linear gradient from 0 to 100% ACN for 15 min): *t*<sub>R</sub> = 9.2 min. ESMS: *m/z* calcd for C<sub>9</sub>H<sub>15</sub>NO<sub>4</sub>S, 233.07; found, 234.3 [M + H]<sup>+</sup>.

<sup>1</sup>H NMR (CDCl<sub>3</sub>, 400 MHz): δ 5.93 (m, 1H), 5.35 (dd, 1H), 5.22 (dd, 1H), 4.88 (m, 1H), 4.65 (d, 2H), 3.12 (dd, 1H), 2.95 (s, 3H), 2.92 (dd, 1H), 2.15 (s, 3H). <sup>13</sup>C NMR (CDCl<sub>3</sub>, 100 MHz): δ 174.8, 157.2, 136.8, 117.9, 67.1, 58.8, 33.1, 32.0, 17.9.



### Compound RZV15



2-CTC resin (100 mg, 1.56 mmol/g) was placed in a 10-mL polypropylene syringe fitted with a polyethylene filter disc. It was then washed with DMF (5 x 1 min) and CH<sub>2</sub>Cl<sub>2</sub> (5 x 1 min). Fmoc-1,2-ethylenediamine\*HCl (22.3 mg, 0.07 mmol) and DIEA (15.3 μL) in CH<sub>2</sub>Cl<sub>2</sub> (1 mL) was added to the resin. The mixture was shaken at

25 °C for 45 min. The reaction was quenched by addition of MeOH (80 μL) and the mixture was stirred for 10 min at 25 °C. After filtration, the resin was washed with CH<sub>2</sub>Cl<sub>2</sub> (5 x 1 min) and with DMF (5 x 1 min) and cleavage of the Fmoc group was done by treatment with piperidine-DMF (1:4) (2.5 mL) (2 x 1 min, 2 x 5 min). The filtrates were collected and quantified by UV (290 nm) obtaining a loading of 0.70 mmol/g. Based on this loading, Alloc-NMe-Cys(Me)-OH (53 mg, 0.28 mmol) was incorporated with COMU (120 mg, 0.28 mmol), OxymaPure (40 mg, 0.28 mmol) and DIEA (95 μL, 0.56 mmol) in DMF (10 mL/g resin) with preactivation for 30 s at 25 °C and stirred for 1 h. After filtration, the resin was washed with CH<sub>2</sub>Cl<sub>2</sub> (5 x 1 min) and with DMF (5 x 1 min) and the Alloc group was removed by treatment with Pd(PPh<sub>3</sub>)<sub>4</sub> (8 mg, 7 μmol) and

PhSiH<sub>3</sub> (86.3 µL, 0.7 mmol) dissolved in CH<sub>2</sub>Cl<sub>2</sub> for 15 min under Ar. The resin was then washed with CH<sub>2</sub>Cl<sub>2</sub> (3 × 1 min) and the process was repeated twice. Fmoc-Val-OH (95.1 mg, 0.28 mmol) was incorporated with COMU (120 mg, 0.28 mmol), OxymaPure (40 mg, 0.28 mmol) and DIEA (95 µL, 0.56 mmol) in DMF (10 mL/g resin) at 25 °C. After resin filtration, and further removal of the Fmoc group, the resin was washed again. The following protected amino acids (Fmoc-Val-OH, Fmoc-Gly-OH, Fmoc-D-Pro-OH, Fmoc-Val-OH, Fmoc-Val-OH) were incorporated with COMU (4 equiv), OxymaPure (4 equiv) and DIEA (8 equiv) in DMF stirring for 90 min at room temperature. Alloc-NMe-Cys(Me)-OH (53 mg, 0.28 mmol) was incorporated with COMU (120 mg, 0.28 mmol), OxymaPure (40 mg, 0.28 mmol) and DIEA (95 µL, 0.56 mmol) in DMF (10 mL/g resin) with preactivation for 30 s at 25 °C and stirred for 1.5 h. After filtration, the resin was washed with CH<sub>2</sub>Cl<sub>2</sub> (5 × 1 min) and with DMF (5 × 1 min) and the Alloc group was removed by treatment with Pd(PPh<sub>3</sub>)<sub>4</sub> (8 mg, 7 µmol) and PhSiH<sub>3</sub> (86.3 µL, 0.7 mmol) dissolved in CH<sub>2</sub>Cl<sub>2</sub> for 15 min under Ar. The resin was then washed with CH<sub>2</sub>Cl<sub>2</sub> (3 × 1 min) and the process was repeated twice. Next, Fmoc-Ser(*t*Bu) (107.4 mg, 0.28 mmol) was incorporated with COMU (120 mg, 0.28 mmol), OxymaPure (40 mg, 0.28 mmol) and DIEA (95 µL, 0.56 mmol) in DMF at 25 °C. The Fmoc group was removed by treatment with piperidine-DMF (1:4) (7.5 mL) (2 × 1 min, 2 × 5 min). The peptide was cleaved with 20% TFA in CH<sub>2</sub>Cl<sub>2</sub> (4.5 mL, 10 × 30 s) at 25 °C and poured over H<sub>2</sub>O-ACN (1:1) (30 mL) to avoid cleavage of the *t*Bu groups. The resulting solution was partially evaporated and lyophilized.

The peptide (0.035 mmol) was dissolved in DMF-CH<sub>2</sub>Cl<sub>2</sub> (1:1) (10 mL), and PyBOP (43.7 mg, 0.084 mmol), HOAt (11.44 mg, 0.084 mmol) and 2-quinoxalinecarboxylic acid (14.6 mg, 0.084 mmol) were added to the solution. The pH was adjusted to 7-8 by adding DIEA and the mixture was stirred until HPLC analysis indicated the completion of the reaction. The solvent was evaporated under reduced pressure and the peptide was redissolved in CH<sub>2</sub>Cl<sub>2</sub> (10 mL). The organic layer was washed with saturated solutions of NH<sub>4</sub>Cl (1 × 20 mL), NaHCO<sub>3</sub> (1 × 20 mL) and brine (1 × 20 mL), dried with MgSO<sub>4</sub> and evaporated under vacuum. Total deprotection was accomplished by treatment with TFA-H<sub>2</sub>O (95:5; 40 mL) at 25 °C for 2 h. After global deprotection, the resulting solution was evaporated to 5 mL and lyophilized. The crude peptide was purified by semi-preparative RP-HPLC.

Purification column: Symmetry® C18 column (19 mm x 100 mm, 5 µm)

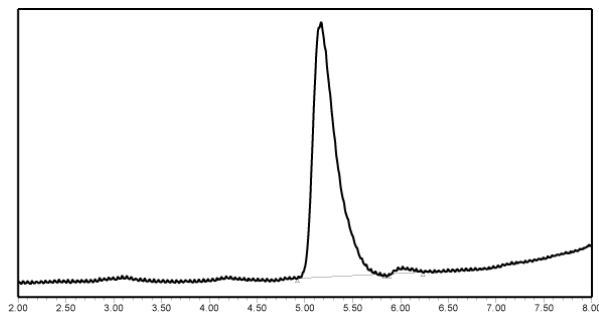
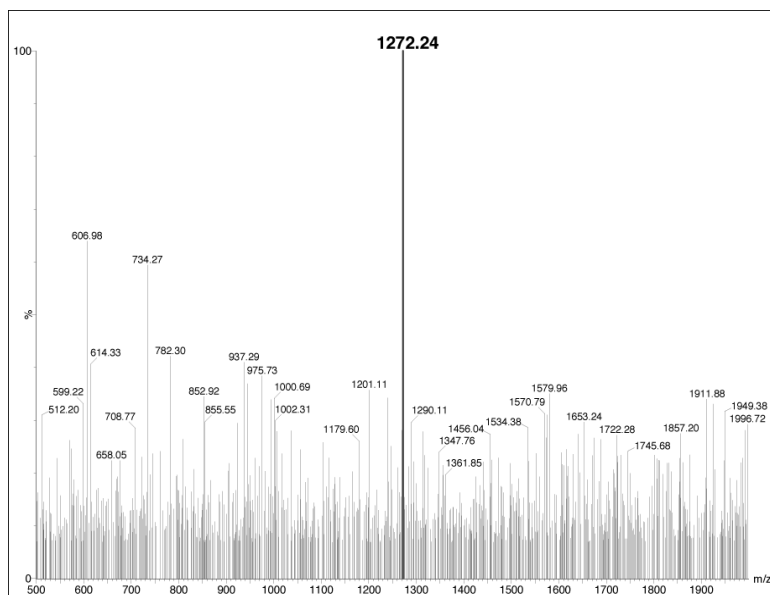
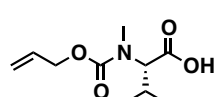
Purification gradient: 35% to 40% of ACN over 15 min with a flow of 3 mL/min

Yield: 3.1%

Analytical column: SunFire® C18 (4.6 mm x 100 mm, 3.5 µm)

**Compound RZV15**HPLC-PDA  $t_R = 5.170$ 

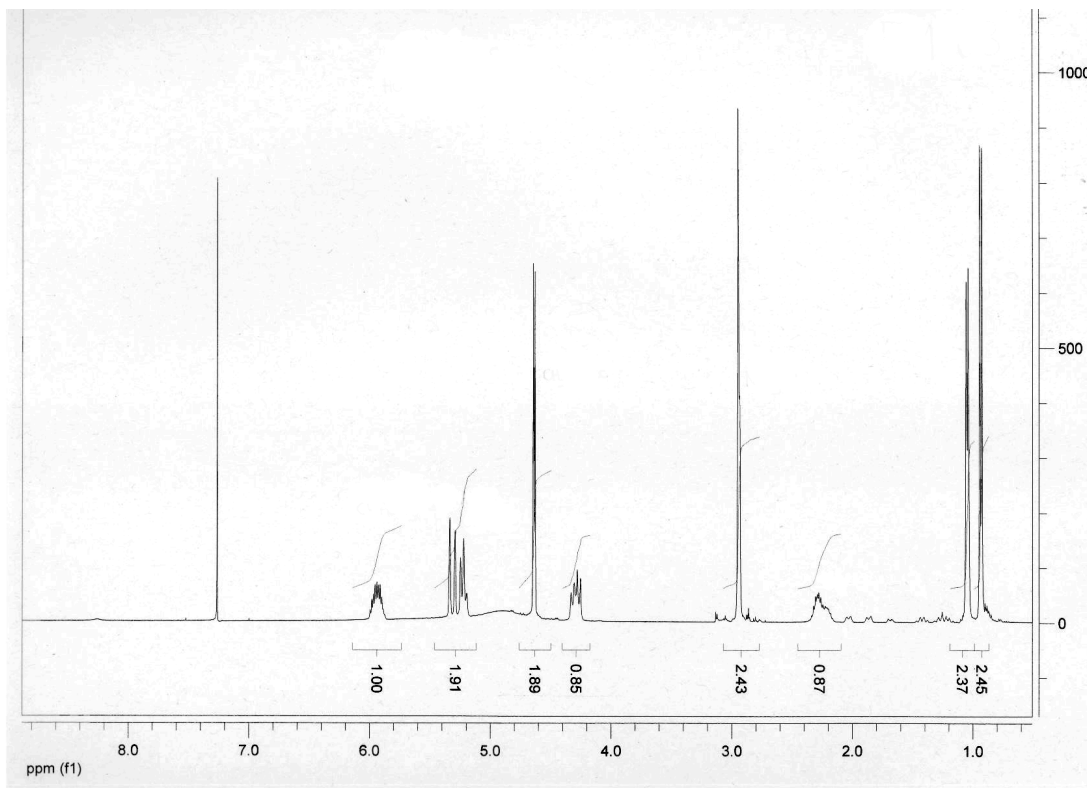
Gradient: 30% to 100% of ACN over 8 min

Purity ( $\lambda=220$ ): 98% $m/z$  calculated for  $C_{60}H_{85}N_{15}O_{12}S_2$ : 1271.5944 DaHPLC-ESMS(+),  $[M+H]^+$ : 1272.39 Da**Triostin A non-commercial building blocks*****Alloc-NMe-Val-OH synthesis***

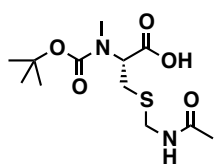
Alloc-NMe-Val-OH was synthesized from Boc-NMe-Val-OH (2.45 g, 10.63 mmol) by using 30 mL of TFA-CH<sub>2</sub>Cl<sub>2</sub> (1:1) to remove the Boc group. After 2 h the solvent was evaporated and two additional coevaporations with CH<sub>2</sub>Cl<sub>2</sub> were done to eliminate the remaining TFA. The white-yellowish solid obtained was dissolved in 2% aqueous solution of Na<sub>2</sub>CO<sub>3</sub>-dioxane (60 mL). Allyl chloroformate (1.7 mL, 15.94 mmol) was added and after adjusting to pH 9 by adding 1 M NaOH, the mixture was stirred for 16 h at 25 °C after which time it was adjusted again to pH 9 by adding 1 M NaOH. The dioxane was evaporated, and the aqueous phase extracted with TBME (3 x 50 mL). Next, the aqueous phase was acidified to pH 3.5 and extracted with EtOAc (4 x 50 mL). The organic

layer was dried ( $\text{MgSO}_4$ ) and evaporated to obtain 2.2 g of final product (100% yield; 90% purity). HPLC-ESMS:  $m/z$  calcd for  $\text{C}_{10}\text{H}_{17}\text{NO}_4$ , 215.12; found, 216.34 [ $\text{M} + \text{H}]^+$ .

$^1\text{H}$  NMR ( $\text{CDCl}_3$ , 400 MHz):  $\delta$  5.95 (m, 1H, CH Alloc), 5.31 (dd, 1H,  $\text{CHH}'$  Alloc,  $J = 17.2$  Hz), 5.22 (dd, 1H,  $\text{CHH}'$  Alloc,  $J = 10.4$  Hz), 4.64 (dt, 2H,  $\text{CH}_2$  Alloc,  $J = 5.6$  Hz,  $J = 1.6$  Hz), 4.29 (dd, 1H,  $\text{CH}\alpha$ ,  $J = 10.4$  Hz), 2.95 (broad s, 3H,  $\text{NMe}$ ), 2.26 (m, 1H,  $\text{CH}\beta$ ), 1.05 (d, 3H,  $\text{CH}_3$ ,  $J = 6.4$  Hz), 0.94 (d, 3H,  $\text{CH}_3$ ,  $J = 6.8$  Hz).  $^{13}\text{C}$  NMR ( $\text{CDCl}_3$ , 100 MHz):  $\delta$  174.3, 157.5, 132.8, 117.9, 66.9, 65.5, 31.7, 27.7, 19.9, 19.3.



### Boc-NMe-Cys(Acm)-OH synthesis

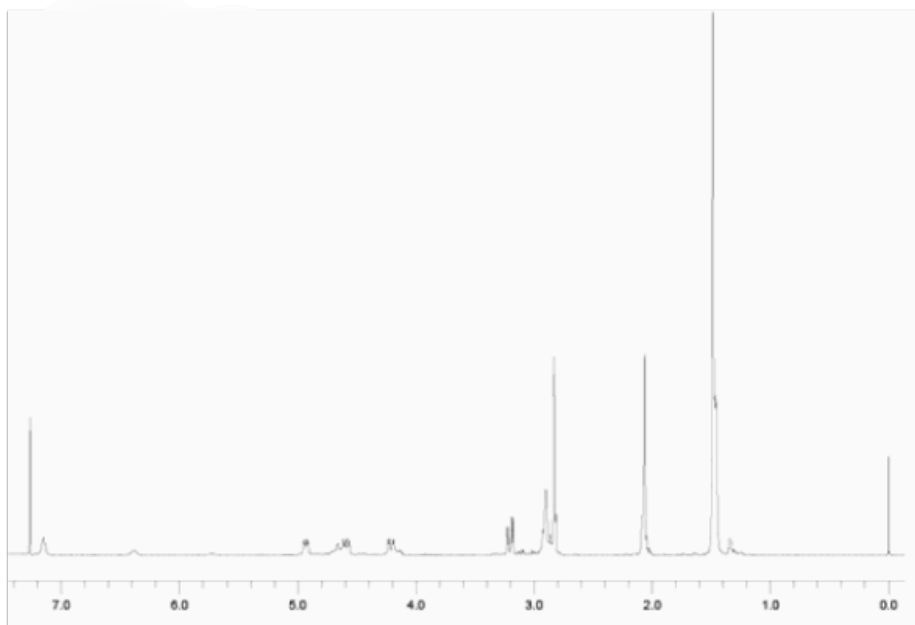


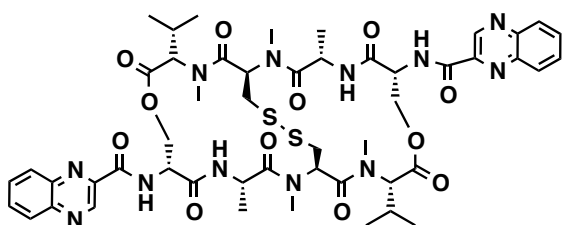
Boc-Cys(Trt)-OH (5.0 g, 10.8 mmol) was dissolved in anhydrous THF (10 mL). The amino acid solution was transferred to a NaH suspension in mineral oil 60% (0.87 g, 25.9 mmol) in anhydrous THF (35 mL) cooled in an ice-water bath. Mel (2 mL, 32.4 mmol) was then added dropwise, and the reaction was stirred overnight (0-25 °C). The next morning, more NaH (0.42 g, 13 mmol) and Mel (1.1 mL, 17.8 mmol) were added and the reaction was stirred for another 24 h (0-25 °C). MeOH and  $\text{H}_2\text{O}$  were added to the reaction mixture to quench excess NaH, and the solution was then evaporated. The residue was dissolved in  $\text{H}_2\text{O}$  (400 mL), and the aqueous layer was washed with TBME (3 x 150 mL), acidified to pH 4.5, extracted with EtOAc (4 x 100 mL), dried ( $\text{MgSO}_4$ ), and evaporated to afford 4.2 g of a white solid (82% yield; 100% purity). Analytical

HPLC (linear gradient from 50 to 100% ACN for 8 min, 1 mL/min):  $t_R = 7.0$  min. HPLC-ESMS:  $m/z$  calcd for  $C_{28}H_{31}NO_3S$ , 477.20; found, 477.12 [M - H].

Boc-NMe-Cys(Trt)-OH (4.2 g, 8.9 mmol) was dissolved in  $H_2O$  (40 mL), cooled in an ice-water bath, and acetamidomethanol (1.03 g, 11.5 mmol) was added followed by a solution of TFA-TFMSA-TIS (92.5:5:2.5; 50 mL). The solution was stirred overnight (0-25 °C), and then, it was evaporated. After coevaporations with TBME (4 x 50 mL) to remove excess TFA, the residue was dissolved in  $H_2O$  (20 mL) and lyophilized. The yellow solid, H-NMe-Cys(Acm)-OH, was dissolved in  $H_2O$  (35 mL) and THF (80 mL), and the pH was adjusted to 8-9 by adding 50% NaOH. Next,  $(Boc)_2O$  (3.8 g, 17.8 mmol) was added and the mixture kept to pH 9 by adding 50% NaOH. The reaction was stirred for 24 h at 25 °C. The solvent was evaporated, and the aqueous layer was washed with TBME (3 x 100 mL), brought to pH 4 by adding 1 N HCl and extracted with EtOAc (4 x 100 mL). The organic phase was dried ( $MgSO_4$ ) and evaporated to afford 1.14 g of colorless oil (76% yield, 86% purity). Analytical HPLC (linear gradient from 5 to 100% ACN for 8 min, 1 mL/min)  $t_R = 4.15$  min. HPLC-ESMS:  $m/z$  calcd for  $C_{12}H_{22}N_2O_5S$ , 306.12; found, 307.4 [M + H]<sup>+</sup>.

<sup>1</sup>H NMR ( $CDCl_3$ , 400 MHz):  $\delta$  6.72 (br s, 1H), 4.92 (m, 1H), 4.56 (m, 1H), 4.21 (m, 1H), 3.21 (m, 1H), 2.89 and 2.82 (m, 4H), 2.05 (m, 3H), 1.50 (s, 9H). <sup>13</sup>C NMR ( $CDCl_3$ , 100 MHz):  $\delta$  172.6, 159.1, 153.5, 80.9, 59.3, 40.6, 32.3, 31.4, 28.3, 22.9.



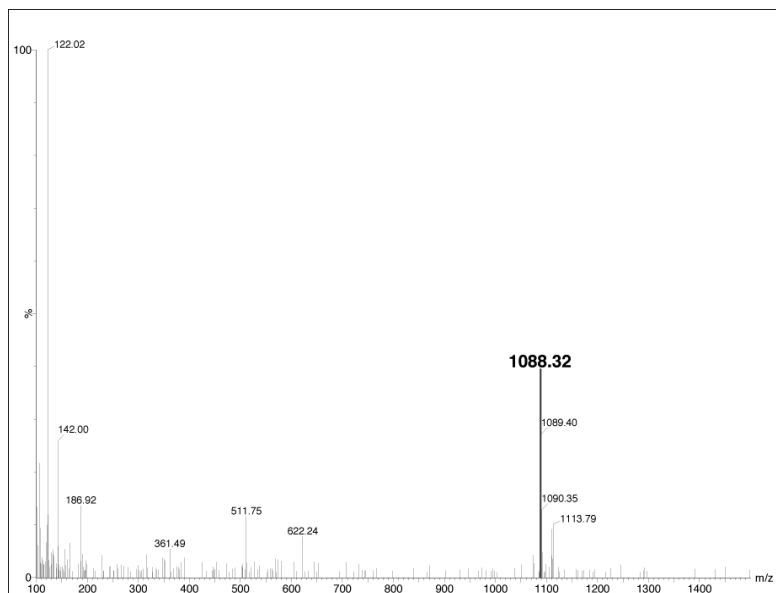
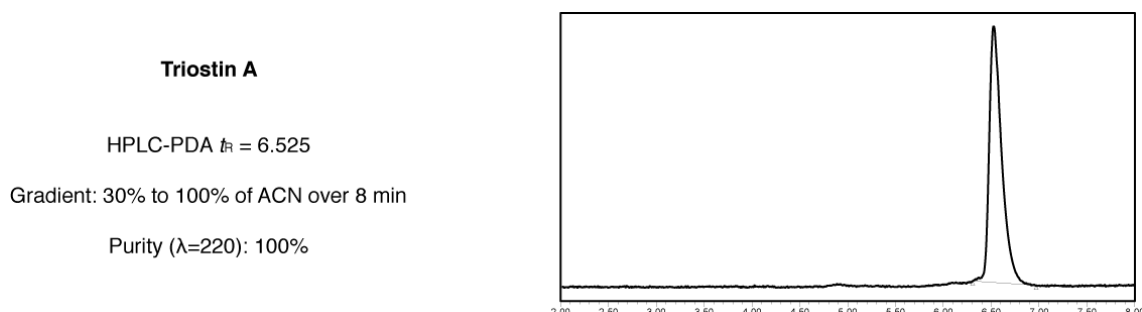
**Triostin A**

Wang resin (200 mg, 1.1 mmol/g) was placed in a 5 mL-polypropylene syringe fitted with a polyethylene filter disc. The resin was then washed with DMF (3 x 1 min) and CH<sub>2</sub>Cl<sub>2</sub> (3 x 1 min). Fmoc-Ala-OH\*H<sub>2</sub>O (444 mg, 2.0

mmol) was dissolved in CH<sub>2</sub>Cl<sub>2</sub>-DMF (9:1) and DIPCDI (310 µL, 2.0 mmol) was added. The mixture was then added to the resin and DMAP (24 mg, 0.2 mmol) in DMF (0.5 mL) was finally added and the mixture was reacted overnight at 25 °C. The Fmoc-Ala-O-Wang resin was subjected to filtration and washings with CH<sub>2</sub>Cl<sub>2</sub> (3 x 1 min) and DMF (3 x 1 min) and capped through acetylation with DIEA (374 µL, 2.2 mmol) and acetic anhydride (208 µL, 2.2 mmol) in CH<sub>2</sub>Cl<sub>2</sub> for 30 min. A solid-supported hydroxyl group detection was done for monitoring of the attachment (see page 52) and colorless beads were obtained. Fmoc deprotection was done with piperidine-DMF (1:4) (2 x 1 min, 2 x 5 min). Next, Fmoc-D-Ser(*Trit*)-OH (0.376 g, 0.66 mmol) was introduced with HATU (0.251 g, 0.66 mmol) and HOAt (90 mg, 0.66 mmol) as coupling reagents in DMF in the presence of DIEA (0.225 mL, 1.32 mmol) to the peptide resin. The mixture was stirred for 1 h and after filtration Kaiser test indicated the completion of the coupling reaction. The peptide resin was then washed with DMF (3 x 1 min), CH<sub>2</sub>Cl<sub>2</sub> (3 x 1 min), and treated with piperidine-DMF (1:4) (2 x 1 min, 2 x 5 min) to remove the Fmoc group. In order to introduce the heterocyclic moiety, the resin was treated with 2-quinoxaline carboxylic acid (76.8 mg, 0.44 mmol) and DIEA (150 µL, 0.88 mmol) in DMF for 45 min. Removal of the trityl group was accomplished by washings with TFA-TIS-CH<sub>2</sub>Cl<sub>2</sub> (2:2.5:95.5) until a colourless filtrate was obtained. The peptide-resin was then washed with CH<sub>2</sub>Cl<sub>2</sub> (3 x 1 min) and Alloc-NMe-Val-OH (0.473 g, 2.2 mmol) was introduced by reaction with DIPCDI (0.34 mL, 2.2 mmol) and DMAP (26.8 mg, 0.22 mmol) in DMF-CH<sub>2</sub>Cl<sub>2</sub> (1:9) for 14 h at 25 °C. Next, to remove the Alloc group, the peptide-resin was treated with Pd(PPh<sub>3</sub>)<sub>4</sub> (25.4 mg, 22 µmol) and PhSiH<sub>3</sub> (0.27 mL, 2.2 mmol) dissolved in CH<sub>2</sub>Cl<sub>2</sub> under Ar, and was then washed with CH<sub>2</sub>Cl<sub>2</sub> (3 x 1 min). The process was repeated three times and Boc-NMe-Cys(Acm)-OH (0.21 g, 0.7 mmol) was introduced with HATU (0.27 mg, 0.7 mmol), HOAt (95.2 mg, 0.7 mmol), and DIEA (0.25 mL, 1.4 mmol) as coupling system for 1 h. The coupling was repeated once with using PyAOP (0.36 g, 0.7 mmol), HOAt (95.2 mg, 0.7 mmol), and DIEA (0.25 mL, 1.4 mmol). Formation of the intermolecular disulfide bridge was obtained by treatment of the resin-bound tetrapeptide with I<sub>2</sub> (0.28 g, 1.1 mmol, 0.1 M) in DMF (2 x 10 min). The resin was repeatedly washed with CH<sub>2</sub>Cl<sub>2</sub> (10 x 1 min), DMF (10 x 1 min), CH<sub>2</sub>Cl<sub>2</sub> (10 x 1 min). The dimerized peptide was then cleaved from the resin by treatment with TFA-H<sub>2</sub>O-CH<sub>2</sub>Cl<sub>2</sub> (25:5:70) (10 mL, 30 min), and the mixture was evaporated with N<sub>2</sub>, and lyophilized. Removal of the Boc groups was accomplished by treatment with TFA-CH<sub>2</sub>Cl<sub>2</sub> (1:1) (10 mL, 30 min), and the mixture was evaporated with N<sub>2</sub>, and lyophilized again. The dimer (50.4 mg, 40 µmol) was dissolved in CH<sub>2</sub>Cl<sub>2</sub> and added to a

solution of HOAt (16.3 mg, 0.12 mmol) in DMF-CH<sub>2</sub>Cl<sub>2</sub> (1:9), and the mixture was stirred for 30 min. Further addition of PyBOP (62.5 mg, 0.12 mmol) and DIEA (18 µL) to adjust to pH 8.0 allowed the cyclization reaction to start, which was stirred for 4 h. Then, the solvent was evaporated and the crude bicycle was redissolved in CH<sub>2</sub>Cl<sub>2</sub> (40 mL), and washed with 5% aqueous NaHCO<sub>3</sub> (3 × 50 mL), dried (MgSO<sub>4</sub>), and evaporated to obtain 53 mg of crude triostin.

An aliquot was analyzed by analytical HPLC (linear gradient from 30 to 100% ACN for 8 min, 1 mL/min):  $t_R = 6.5$  min, 51% purity. The compound was purified by semi-preparative reversed HPLC. Conditions: linear gradient (59% to 60%) of CH<sub>3</sub>CN (0.036% TFA) into H<sub>2</sub>O (0.045%) over 10 min, with a flow rate of 3.0 mL/min ( $t_R = 4.3$  min) to obtain 5.7 mg (5.6% overall yield) of pure triostin A. HPLC-ESMS:  $m/z$  calcd for C<sub>50</sub>H<sub>62</sub>N<sub>12</sub>O<sub>12</sub>S<sub>2</sub> 1086.41; found, 1088.32 [M+H]<sup>+</sup>. MALDI-TOF: found 1088.5439 [M+H]<sup>+</sup>. HR-ESMS:  $m/z$  calcd for C<sub>50</sub>H<sub>62</sub>N<sub>12</sub>O<sub>12</sub>S<sub>2</sub> 1086.4124, found 1086.4046.



## REFERENCES

- (1) Sato, M.; Nakazawa, T.; Tsunematsu, Y.; Hotta, K.; Watanabe, K. *Curr. Opin. Chem. Biol.* **2013**, *17*, 537–545.
- (2) Corbaz, R.; Ettlinger, L.; Gaumann, E.; Keller-Schierlein, W.; Kradolfer, F.; Neipp, L.; Prelog, V.; Reusser, P.; Zahner, H. *Helv. Chim. Acta* **1957**, *40*, 199–204.
- (3) Berger, J.; La Sala, E. R.; Scott, W. E.; Meltsner, B. R.; Sternbach, L. H.; Kaiser, S.; Teitel, S.; Mach, E.; Goldberg, M. W. *Experientia* **1957**, *13*, 434–436.
- (4) Ishihara, S.; Utahara, R.; Suzuki, M.; Okami, Y.; Umezawa, H. *J. Antibiot. (Tokyo)* **1958**, *11*, 160–161.
- (5) Katagiri, K.; Shoji, J.; Yoshisa, T. *J. Antibiot. (Tokyo)* **1962**, *15*, 273.
- (6) Martin, D. G.; Mizsak, S. a; Biles, C.; Stewart, J. C.; Bacynsky, L.; Meulman, P. a. *J. Antibiot. (Tokyo)* **1975**, *28*, 332–336.
- (7) Dell, A.; Williams, D. H.; Morris, H. R.; Smith, G. A.; Feeney, J.; Roberts, G. C. *J. Am. Chem. Soc.* **1975**, *97*, 2497–2502.
- (8) Yoshida, T.; Katagiri, K.; Yokozawa, S. *J. Antibiot. (Tokyo)* **1961**, *14*, 330–4.
- (9) Shoji, J. I.; Katagiri, K. *J. Antibiot. (Tokyo)* **1961**, *14*, 335–339.
- (10) Ueda, M.; Tanigawa, Y.; Okami, Y.; Umezawa, H. *J. Antibiot. (Tokyo)* **1954**, *7*, 125–126.
- (11) Matsuura, S. *J. Antibiot. (Tokyo)* **1965**, *18*, 43–46.
- (12) Katagiri, K.; Yoshida, T.; Sato, K. *Antibiotics III: Mechanism of Action of Antimicrobial and Antitumour Agents*; Corcoran, F. W.; Hahn, F. E., Eds.; Berlin, 1975; pp. 234–251.
- (13) Foster, B. J.; Clagett-Carr, K.; Shoemaker, D. D.; Suffness, M.; Plowman, J.; Trissel, L. A.; Grieshaber, C. K.; Leyland-Jones, B. *Invest. New Drugs* **1985**, *3*, 403–410.
- (14) Kuhn, J. G.; Von Hoff, D. D.; Hersh, M.; Melink, T.; Clark, G. M.; Weiss, G. R.; Coltman, C. A. *Eur. J. Cancer Clin. Oncol.* **1989**, *25*, 797–803.
- (15) Taylor, S. A.; Metch, B.; Balcerzak, S. P.; Hanson, K. H. *Invest. New Drugs* **1990**, *8*, 381–383.
- (16) Muss, H. B.; Blessing, J. A.; Baker, V. V.; Barnhill, D. R.; Adelson, M. D. *Am. J. Clin. Oncol.* **1990**, *13*, 299–301.
- (17) Schilsky, R. L.; Faraggi, D.; Korzun, A.; Vogelzang, N.; Ellerton, J.; Wood, W.; Henderson, I. C. *Invest. New Drugs* **1991**, *9*, 269–272.
- (18) Muss, H. B.; Blessing, J. A.; Malfetano, J. *Am. J. Clin. Oncol.* **1990**, *13*, 191–193.
- (19) Taylor, S. A.; Crowley, J.; Townsend, J.; Vogel, F. S.; Eyre, H.; Braun, J. J.; Goodwin, J. W. *J. Neurooncology* **1993**, *15*, 181.
- (20) Wang, Y.; Liu, Y.; Malek, S. N.; Zheng, P.; Liu, Y. *Cell Stem Cell* **2011**, *8*, 399–411.
- (21) Waring, M. J.; Wakelin, L. P. *Nature* **1974**, *252*, 653–657.
- (22) Gause, G. G.; Loshkareva, N. P.; Zbarsky, I. B. *Biochim. Biophys. Acta* **1968**, *166*, 752–754.
- (23) Wakelin, L. P. G.; Waring, M. J. *Biochem. J.* **1976**, *157*, 721–740.
- (24) Hampshire, A. J.; Rusling, D. A.; Broughton-Head, V. J.; Fox, K. R. *Methods* **2007**, *42*, 128–140.
- (25) Low, C. M.; Drew, H. R.; Waring, M. J. *Nucleic Acids Res.* **1984**, *12*, 4865–4879.
- (26) Bailly, C.; Waring, M. J. *J. Biomol. Struct. Dyn.* **1995**, *12*, 869–898.
- (27) Gao, X. L.; Patel, D. J. *Biochemistry* **1988**, *27*, 1744–1751.

- (28) Gilbert, D. E.; Feigon, J. *Biochemistry* **1991**, *30*, 2483–2494.
- (29) Gilbert, D. E.; van der Marel, G. A.; van Boom, J. H.; Feigon, J. *Proc. Natl. Acad. Sci. U. S. A.* **1989**, *86*, 3006–3010.
- (30) Leslie, K. D.; Fox, K. R. *Biochemistry* **2002**, *41*, 3484–3497.
- (31) Khan, A. W.; Bhaduri, A. P.; Gupta, C. M.; Dhar, M. M. *Indian J. Biochem.* **1969**, *6*, 220–221.
- (32) Arif, A. J.; Singh, C.; Bhaduri, A. P.; Gupta, C. M.; Khan, A. W.; Dhar, M. M. *Indian J. Biochem.* **1970**, *7*, 193–195.
- (33) Gauvreau, D.; Waring, M. J. *Can. J. Microbiol.* **1984**, *30*, 730–738.
- (34) Park, Y. S.; Kim, Y. H.; Kim, S. K.; Choi, S. J. *Bioorg. Med. Chem. Lett.* **1998**, *8*, 731–734.
- (35) Fox, K. R.; Gauvreau, D.; Goodwin, D. C.; Waring, M. J. *Biochem. J.* **1980**, *191*, 729–742.
- (36) Watanabe, K.; Hotta, K.; Praseuth, A. P.; Koketsu, K.; Migita, A.; Boddy, C. N.; Wang, C. C. C.; Oguri, H.; Oikawa, H. *Nat. Chem. Biol.* **2006**, *2*, 423–428.
- (37) Reid, D. G.; Doddrell, D. M.; Williams, D. H.; Fox, K. R. *Biochim. Biophys. Acta* **1984**, *798*, 111–114.
- (38) Schmoock, G.; Pfennig, F.; Jewiarz, J.; Schlumbohm, W.; Laubinger, W.; Schauwecker, F.; Keller, U. *J. Biol. Chem.* **2005**, *280*, 4339–4349.
- (39) Cornish, A.; Waring, M. J.; Nolan, R. D. *J. Antibiot. (Tokyo)* **1983**, *36*, 1664–1670.
- (40) Otsuka, H.; Shoji, J. *Tetrahedron* **1965**, *21*, 2931–2938.
- (41) Shoji, J. I.; Tori, K.; Otsuka, H. *J. Org. Chem.* **1965**, *30*, 2772–2776.
- (42) Otsuka, H.; Shoji, J. *J. Antibiot. (Tokyo)* **1965**, *18*, 134.
- (43) Ciardelli, T. L.; Olsen, R. K. *J. Am. Chem. Soc.* **1977**, *99*, 2806–2807.
- (44) Viswamitra, M. A.; Kennard, O.; Cruse, W. B.; Egert, E.; Sheldrick, G. M.; Jones, P. G.; Waring, M. J.; Wakelin, L. P.; Olsen, R. K. *Nature* **1981**, *289*, 817–819.
- (45) Chakravarty, P. K.; Olsen, R. K. *Tetrahedron Lett.* **1978**, *19*, 1613–1616.
- (46) Higuchi, N.; Kyogoku, Y.; Shin, M.; Inouye, K. *Int. J. Pept. Protein Res.* **1983**, *21*, 541–545.
- (47) Boger, D. L.; Lee, J. K. *J. Org. Chem.* **2000**, *65*, 5996–6000.
- (48) Malkinson, J. P.; Anim, M. K.; Zloh, M.; Searcey, M.; Hampshire, A. J.; Fox, K. R. *J. Org. Chem.* **2005**, *70*, 7654–7661.
- (49) Dietrich, B.; Diederichsen, U. *European J. Org. Chem.* **2005**, 147–153.
- (50) Tulla-Puche, J.; Marcucci, E.; Fermin, M.; Bayó-Puxan, N.; Albericio, F. *Chemistry* **2008**, *14*, 4475–4478.
- (51) Kumar Ray, A.; Diederichsen, U. *European J. Org. Chem.* **2009**, *2009*, 4801–4809.
- (52) Waring, M. J.; Wakelin, L. P.; Lee, J. S. *Biochim. Biophys. Acta* **1975**, *407*, 200–212.
- (53) Lee, J. S.; Waring, M. J. *Biochem. J.* **1978**, *173*, 115–128.
- (54) Low, C. M.; Olsen, R. K.; Waring, M. J. *FEBS Lett.* **1984**, *176*, 414–420.
- (55) Wang, a H.; Ughetto, G.; Quigley, G. J.; Hakoshima, T.; van der Marel, G. a; van Boom, J. H.; Rich, A. *Science* **1984**, *225*, 1115–1121.
- (56) Ughetto, G.; Wang, A. H.; Quigley, G. J.; van der Marel, G. A.; van Boom, J. H.; Rich, A. *Nucleic Acids Res.* **1985**, *13*, 2305–2323.

- (57) Cuesta-Seijo, J. A.; Sheldrick, G. M. *Acta Crystallogr. D. Biol. Crystallogr.* **2005**, *61*, 442–448.
- (58) Dawson, S.; Malkinson, J. P.; Paumier, D.; Searcey, M. *Nat. Prod. Rep.* **2007**, *24*, 109–126.
- (59) Kalman, J. R.; Blake, T. J.; Williams, D. H.; Feeney, J.; Roberts, G. C. K. *J. Chem. Soc. Perkin Trans. 1* **1979**, 1313–1321.
- (60) Sheldrick, G. M.; Heine, A.; Schmidt-Bäse, K.; Pohl, E.; Jones, P. G.; Paulus, E.; Waring, M. J. *Acta Crystallogr. Sect. B* **1995**, *51*, 987–999.
- (61) Negri, A.; Marco, E.; García-Hernández, V.; Domingo, A.; Llamas-Saiz, A. L.; Porto-Sandá, S.; Riguera, R.; Laine, W.; David-Cordonnier, M.-H.; Bailly, C.; García-Fernández, L. F.; Vaquero, J. J.; Gago, F. *J. Med. Chem.* **2007**, *50*, 3322–3333.
- (62) Boger, D. L.; Chen, J.; Saionz, K. W. *Society* **1996**, *1629*, 1629–1644.
- (63) Zhang, X. L.; Patel, D. J. *Biochemistry* **1991**, *30*, 4026–4041.
- (64) Stanger, H. E.; Gellman, S. H. *J. Am. Chem. Soc.* **1998**, *120*, 4236–4237.
- (65) Syud, F. A.; Stanger, H. E.; Gellman, S. H. *J. Am. Chem. Soc.* **2001**, *123*, 8667–8677.
- (66) Teixidó, M.; Albericio, F.; Giralt, E. *J. Pept. Res.* **2005**, *65*, 153–166.
- (67) Barlos, K.; Gatos, D.; Schäfer, W. *Angew. Chemie Int. Ed. English* **1991**, *30*, 590–593.
- (68) Chiva, C.; Vilaseca, M.; Giralt, E.; Albericio, F. *J. Pept. Sci.* **1999**, *5*, 131–140.
- (69) Barlos, K.; Chatzi, O.; Gatos, D.; Stavropoulos, G. *Int. J. Pept. Protein Res.* **1991**, *37*, 513–520.
- (70) Biron, E.; Chatterjee, J.; Kessler, H. *J. Pept. Sci.* **2006**, *12*, 213–219.
- (71) Carpino, L. A.; El-Faham, A.; Minor, C. A.; Albericio, F. *J. Chem. Soc. Chem. Commun.* **1994**, 201–203.
- (72) Story, S. C.; Aldrich, J. V. *Int. J. Pept. Protein Res.* **1994**, *43*, 292–296.
- (73) Carpino, L. A.; El-Faham, A.; Albericio, F. *Tetrahedron Lett.* **1994**, *35*, 2279–2282.
- (74) El-Faham, A.; Albericio, F. *J. Pept. Sci.* **2010**, *16*, 6–9.
- (75) Subirós-Funosas, R.; Prohens, R.; Barbas, R.; El-Faham, A.; Albericio, F. *Chemistry (Easton)* **2009**, *15*, 9394–9403.
- (76) Subirós-Funosas, R.; Nieto-Rodríguez, L.; Jensen, K. J.; Albericio, F. *J. Pept. Sci.* **2013**, *19*, 408–414.
- (77) Rodríguez, H.; Suárez, M.; Albericio, F. *J. Pept. Sci.* **2010**, *16*, 136–140.
- (78) Pedersen, S. L.; Tofteng, A. P.; Malik, L.; Jensen, K. J. *Chem. Soc. Rev.* **2012**, *41*, 1826–1844.
- (79) Albericio, F.; Bofill, J. M.; El-Faham, A.; Kates, S. A. *J. Org. Chem.* **1998**, *63*, 9678–9683.
- (80) Kaiser, E.; Colescott, R. L.; Bossinger, C. D.; Cook, P. I. *Anal. Biochem.* **1970**, *34*, 595–598.
- (81) Christensen, T. *Acta Chem. Scand. B* **1979**, *33*, 763–766.
- (82) Madder, A.; Farcy, N.; Hosten, N. G. C.; Muynck, H. De; De Clercq, P. J.; Barry, J.; Davis, A. P. *European J. Org. Chem.* **1999**, 2787–2791.
- (83) Pérez Baz, J.; Cañedo, L. M.; Fernández Puentes, J. L.; Silva Elipe, M. V. *J. Antibiot. (Tokyo)* **1997**, *50*, 738–741.
- (84) Marcucci, E.; Bayó-Puxan, N.; Tulla-Puche, J.; Spengler, J.; Albericio, F. *J. Comb. Chem.* **2008**, *10*, 69–78.
- (85) Caroen, J.; Van Der Eycken, J. *Tetrahedron* **2009**, *50*, 41–44.



# **Biological evaluation**

---

I would like to thank Xavier Vila (IRB Barcelona) for performing the antibacterial activity assay with compounds from the RZ1-RZ12 library. This work was carried out at the *Centre de Diagnòstic Biomèdic, Hospital Clínic*, in Barcelona, under the supervision of Dr. Jordi Vila.

I would also like to thank Dr. Anna Lundin and Dr. Edward Trybala, from the Department of Chemical and Biological Engineering at Chalmers University of Technology in Göteborg, Sweden, for performing the antiviral activity assays.

I am very grateful to Noelia Camacho and Dr. Lluís Ribas (IRB Barcelona) for their kind support with the antibacterial activity assays with peptides Z1-Z12 and the antiplasmodial activity assays.

I also gratefully acknowledge Dr. Miguel Moreno (IRB Barcelona) for his guidance in the stability assays, the hemocompatibility test and in liposomes preparation, and helpful discussion regarding the biological assays presented in this chapter.

The optimized experimental conditions for the MTT assays determined and explained in this chapter were applied for the biological evaluation of a postsynthetically modified Trp-based diketopiperazine, giving place to the following publication:

Preciado, S.; Mendive-Tapia, L.; Torres-García, C.; **Zamudio-Vázquez, R.**; Soto-Cerrato, V.; Pérez-Tomás, R.; Albericio, F.; Nicolás, E.; Lavilla, R. *Med. Chem. Commun.* **2013**, 4, 1171-1174.

## INTRODUCTION

### Quinoxaline: one moiety with multiple targets

Compounds containing the quinoxaline moiety are found in a number of natural products as validated clinical candidates and drugs on the market.<sup>1</sup> Quinoxalines, also called benzopyrazines, are 1,4-diazine derivatives, systematically numbered according to Figure 24. This heterocyclic moiety is made of a ring complex containing a benzene ring and a pyrazine ring. Compared to the structurally related carbocycle naphthalene, the presence of nitrogen atoms gives the heterocycle different physicochemical properties: an unsubstituted quinoxaline has lower resonance energy<sup>2</sup> and different polarity than naphthalene or the aza-analogue quinoline.<sup>3</sup> In terms of biological properties, the quinoxaline core shows a different behaviour than the carbocycle due to its lipophilicity and polar surface area.

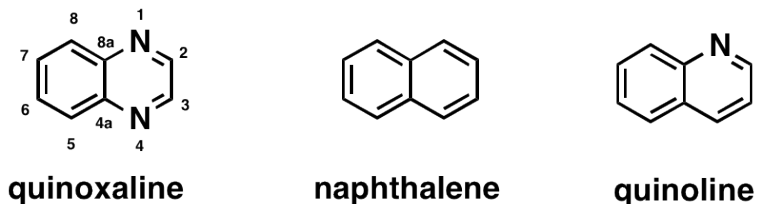


**Figure 24.** Chemical structures of quinoxaline and two analogues.

In recent years, the quinoxaline scaffold has received much attention as a potential therapeutic entity.<sup>4</sup> Some examples of commercial products containing quinoxaline derivatives are Carbadox (a veterinary antibacterial agent), Varenicline (smoking addiction treatment agent) and Brimonidine (ocular hypertension treatment agent) (Figure 25).

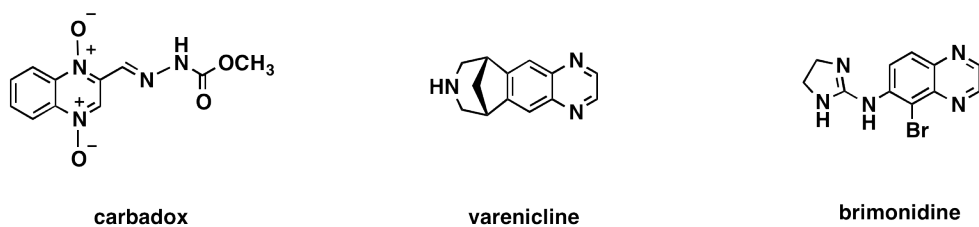
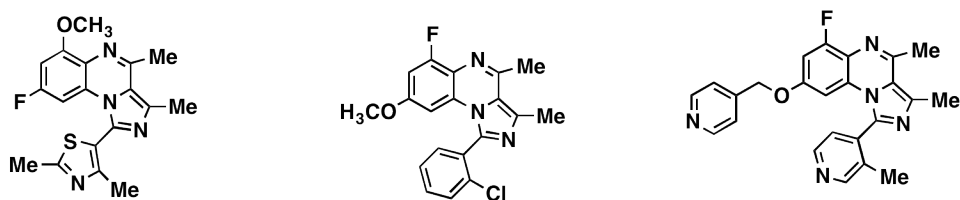


**Figure 25.** Quinoxalines currently used in therapy.

Quinoxalines are moieties of great interest in medicinal chemistry due to their capacity to interact with several biological targets.<sup>5</sup> Many *in vitro* studies have been performed with this interesting scaffold. It has been described the potential of quinoxalines as anti-inflammatory agents,<sup>6</sup> and its inhibition of some kinases, such as PDGFR kinase,<sup>7</sup> tyrosine kinase,<sup>8</sup> human protein kinase CK2<sup>9</sup> and Janus kinase,<sup>10</sup> suggests that this versatile heterocycle could be used for the treatment of various diseases, from allergies to cancer. Moreover, structurally different

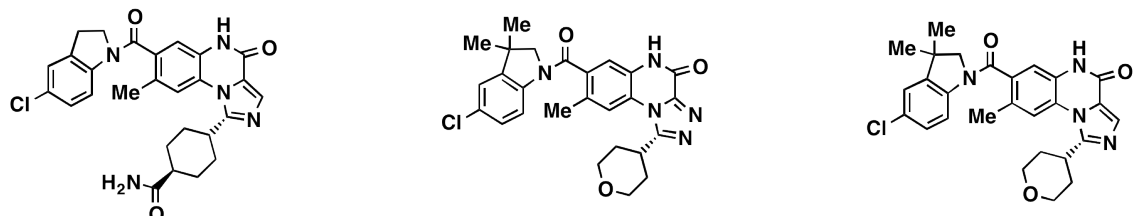
quinoxalines with basic lateral chains have been described as agonists of  $\alpha$ 2-adrenergic receptors (currently used for lowering intraocular pressure),<sup>11</sup> transglutaminase 2<sup>12</sup> and adenosine A receptors modulators.<sup>13</sup>

In terms of treatment for central nervous system (CNS) diseases such as bipolar disorder and schizophrenia, some imidazo[1,5 $\alpha$ ]quinoxalines (Figure 26) were found to be potential drugs due to their inhibition of the cyclic nucleotide phosphodiesterases (PDEs), particularly isozyme PDE10.<sup>14</sup> This class of enzyme is able of inactivating the intracellular messengers cAMP and cGMP.<sup>15</sup> Other additional pathologies related to alterations in phosphorylations and protein-protein interactions of cAMP and cGMP in which these quinoxaline compounds could be potential treatments are depression and dementia.



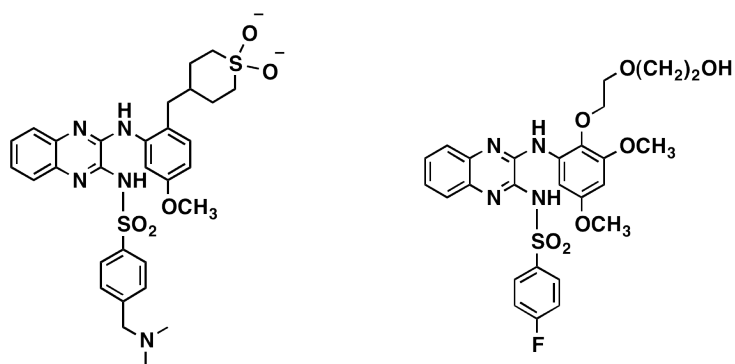
**Figure 26.** Quinoxaline compounds that inhibit PDE10.

Other quinoxalines structurally related to these compounds (Figure 27) have been described as *in vitro* and *in vivo* PDE-9 inhibitors and potential drugs for diseases of the urinary system.<sup>16</sup>



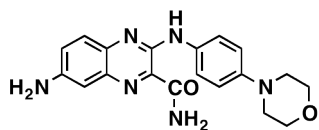
**Figure 27.** Quinoxaline compounds that inhibit PDE9.

Phosphatidylinositol 3-kinases (PI3Ks) are another family of enzymes found to be inhibited by quinoxaline-containing molecules.<sup>17</sup> PI3Ks play decisive roles in breast cancer proliferation and chronic inflammatory diseases due to their capacity to phosphorylate the 3-hydroxyl group of inositol in response to extracellular stimuli, regulating cellular activation, proliferation and migration.<sup>18</sup> Beyond the inhibitors, a series of 2-phenylamino-3-arylsulfonylamino-quinoxalines (Figure 28) tested in cellular assays showed inhibition of the PI3K-induced lipid phosphorylation. In addition, some of these 2,3-disubstituted quinoxalines displayed antitumoral activity as well.<sup>19</sup> Moreover, other structurally related quinoxalines showed high binding affinity and selectivity for the human PI3K isoforms  $\alpha$ ,  $\beta$ ,  $\gamma$ , and  $\delta$ .<sup>20</sup>



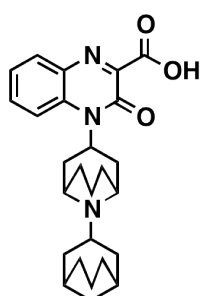
**Figure 28.** Quinoxaline compounds that inhibit PI3Ks.

Quinoxalines are inhibitors of other kinases, which are interesting targets in medicinal chemistry.<sup>21</sup> A great number of kinases are involved in the transmission of signals and control of complex processes within the cells. One of the most relevant kinases is the group of Raf-kinases (RafKs),<sup>22</sup> a family of three serine/threonine specific protein kinases that play an important role in tumorigenesis due to their participation in the mitogen-activated protein kinase (MAPK) cascade.<sup>23</sup> A series of 2,3-disubstituted pyrazines containing carbamoylquinoxalines have been described as inhibitors of the protein kinases Syk, GSK-3 and JAK-3.<sup>24,25</sup> Syk, spleen tyrosine kinase, is activated by transforming viruses such as Epstein Barr virus, mouse mammary tumour virus or bovine leukaemia virus, and the caused abnormalities in Syk functions are implicated in haematopoietic malignancies.<sup>26,27</sup> GSK-3, glycogen synthase kinase 3, is a key enzyme in multiple-cell processes such as inflammation and cancer.<sup>28</sup> JAK, Janus kinase, is a family of intracellular tyrosine kinases whose multiple functions involve the initial response to major cytokine receptor families and they are implicated in myeloproliferative disorders and functions in the lymphoid system.<sup>29</sup> Accordingly, these protein-kinases inhibitor quinoxalines (Figure 29) could be used in the treatment of immune disorders, inflammatory diseases and cancer.

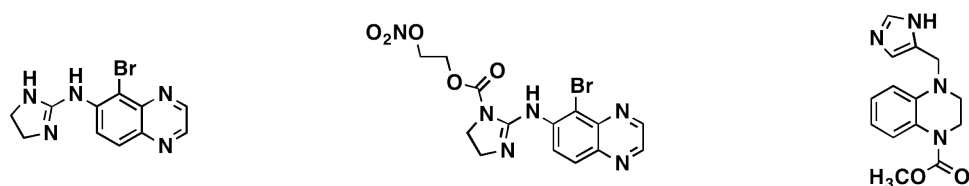


**Figure 29.** Example of a 2-carbamoylquinoxaline that inhibits protein kinases.

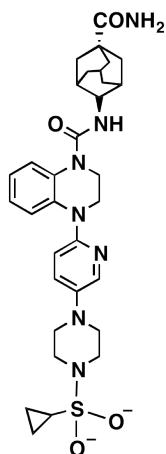
Another reason for the potential use of quinoxalines as antiinflammatory agents is their ability to modulate the histamine-H4 receptor and to inhibit leukocyte recruitment.<sup>30</sup> Additionally, quinoxalines with a piperidine-like scaffold substitution (Figure 30) are able to modulate the opioid receptor like-1 (ORL-1), thus these compounds could be used in pain treatment.<sup>31</sup>

**Figure 30.** Quinoxaline ORL-1 receptor binder.

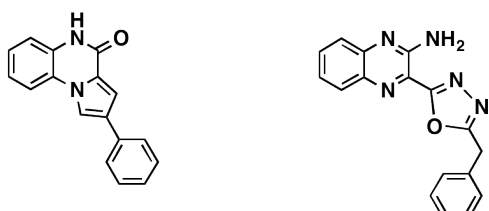
One quinoxaline compound that is currently in the market as an opthalmic solution used in intraocular pressure disorders is the 5-bromo-6-(2-imidazolin-2-ylamino)quinoxaline tartrate. This is an  $\alpha_2$ -adrenergic receptor ( $\alpha$ 2AR) agonist,<sup>32</sup> just as its structurally related compound that bears a nitrooxy-moiety,<sup>33</sup> some 1,2,3,4-tetrahydroquinoxalines, 3,4-dihydro-1,4-benzoxazines and 3,4-dihydro-1,4-benzothiazines,<sup>34</sup> that could be used to treat glaucoma, depression, anxiety and schizophrenia (Figure 31).

**Figure 31.** Quinoxaline 2-adrenergic receptor agonists.

Another tetrahydroquinoxaline was found to inhibit the enzyme 11 $\beta$ -hydroxysteroid dehydrogenase type 1 (11b-HSD1), which catalyses the interconversion between cortisol and cortisone and has been associated with metabolic disorders such as obesity and insulin resistance.<sup>35</sup> Thus, this molecule (Figure 32) could be a potential drug for treating obesity, diabetes or hypertension.<sup>36</sup>

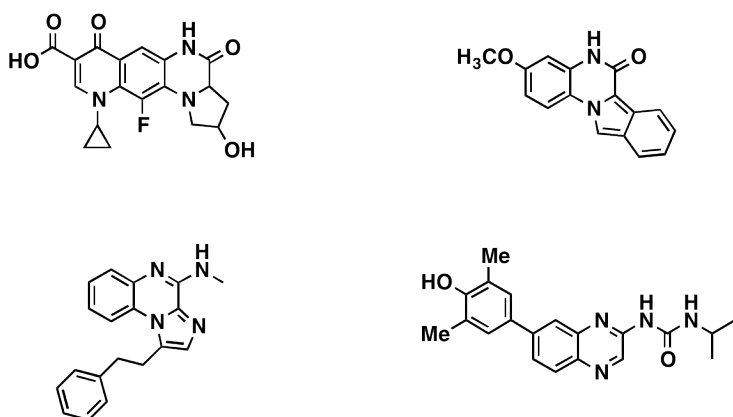
**Figure 32.** A potent tetrahydroquinoxaline 11b-HSD1 inhibitor.

Furthermore, some pyrrolo[1,2-*a*]quinoxalines and related analogues<sup>37,38</sup> (Figure 33) have been described as selective and highly potent adenosine A<sub>3</sub> receptor antagonists, and potential drugs for Alzheimer's and Parkinson's diseases. A<sub>3</sub> adenosine receptors are expressed on the surface of most immune cell types.<sup>39</sup> Thereby, they have been shown to be involved in immune-related diseases, in which quinoxaline antagonists may be promising drugs.



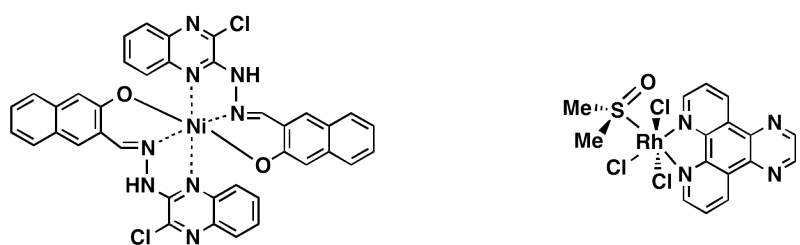
**Figure 33.** Quinoxaline adenosine A receptor modulators.

Pyridoquinoxalines are potent *in vitro* anticancer and antibacterial agents,<sup>40</sup> and new heterocyclic arrangements around the quinoxaline moiety have conferred the same compounds antiviral activity as well.<sup>41</sup> Other compounds with *in vitro* antitumoral activities are isoindoloquinoxalines<sup>42</sup> and imidazoquinoxalines.<sup>43</sup> Moreover, a series of ureas containing the quinoxaline moiety have been described not only as antitumor compounds, but also as metastasis inhibitors<sup>44</sup> (see Figure 34).

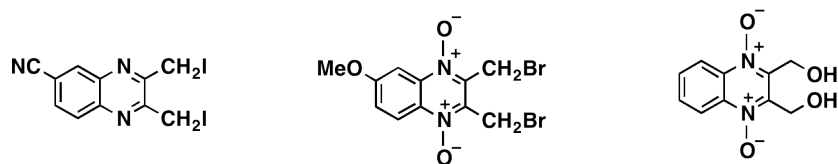


**Figure 34.** Quinoxaline antitumor compounds.

Furthermore, some quinoxalines have been coordinated with different metals such as copper(II), nickel(II), rhodium(III) or iridium(III) to obtain new antineoplastic drugs (Figure 35). In some cases, excellent *in vitro* activity against a number of cancer cell lines has been obtained.<sup>45</sup>

**Figure 35.** Metal coordinated quinoxaline antineoplastic drugs.

Regarding the antibacterial activity of quinoxalines, 2,3-bis(dihalomethyl)quinoxaline and its 1,4-di-*N*-oxides<sup>46</sup> (Figure 36) are used as antibacterial compounds and microbicide agents for medical devices.

**Figure 36.** Quinoxalines with antibacterial activity.

Quinoxaline derivatives have been also described as potential drugs for treatment of various other diseases, such as gastrointestinal disorders, due to their binding to metabotropic glutamate 1 receptor,<sup>47</sup> and atherosclerosis, due to their capability to modify the lipid levels in plasma.<sup>48</sup> Some other derivatives are inhibitors of the Hedgehog signalling pathway, involved in the pathophysiology of cancer.<sup>49</sup> Other quinoxalines are neutrophil elastase inhibitors and may be useful for pulmonary fibrosis, pulmonary emphysema and rheumatoid arthritis treatment.<sup>50</sup> It has also been described that quinoxalines can modulate somatostatin receptor 5,<sup>51</sup> involved in diabetes mellitus, or suppress melanin-concentrating hormone 1 receptor, involved in obesity.<sup>52</sup> Moreover, some quinoxaline derivatives act as apolipoprotein A-I enhancing agents and may be used in the treatment of arteriosclerotic diseases and dyslipidemia.<sup>53</sup> Finally, other quinoxalines were described as modulators of liver nuclear X receptors, essential in cholesterol and bile acid metabolism.<sup>54</sup>

Based on all these biological activities described in the literature for quinoxaline-containing compounds, it was decided to evaluate not only the anticancer activity of the synthesized molecules described in the first chapter of the present thesis, but also their antibacterial, antiviral and antiplasmodial activities were assayed.

## RESULTS AND DISCUSSION

### Antitumoral activity evaluation

The main objective of the herein presented PhD project was not only the design and synthesis of simplified analogues of the natural bisintercalator triostin A, but also to obtain a compound with better antiproliferative activity than the parent compound. For this reason, the synthesized peptides (see chapter 1) were evaluated for their antitumoral activity using the MTT assay.

The MTT (3-[4,5-dimethylthiazol-2-yl]-2,5 diphenyl tetrazolium bromide) assay is a colorimetric assay based on the conversion of MTT into formazan crystals by NAD(P)H-dependent cellular oxidoreductase enzymes in living cells.<sup>55</sup> These enzymes are capable of reducing the tetrazolium dye to its insoluble formazan, which has a purple color and can be solubilized for homogenous measurement to determine mitochondrial activity. Since for most cell populations the total mitochondrial activity is related to the number of viable cells, this assay is broadly used to measure the *in vitro* cytotoxic effects of drugs on cell lines or primary patient cells. The principle of the MTT assay is that for most viable cells mitochondrial activity is constant and thereby an increase or decrease in the number of viable cells is linearly related to mitochondrial activity. Thus, any increase or decrease in viable cell number can be detected by measuring formazan concentration reflected in optical density (OD) using a plate reader.

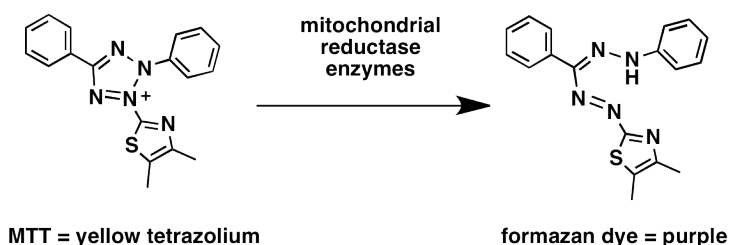


**Figure 37.** Reduction of tetrazolium salt MTT to formazan by mitochondrial reductase

The general purpose of the MTT assay is to measure viable cells in relatively high throughput (96-well plates) without the need for elaborate cell counting. For drug sensitivity measurements the OD values of wells with cells incubated with drugs are compared to the OD of wells with cells not exposed to drugs. For dividing cells the decrease in cell number reflects cell growth inhibition and the drug sensitivity is then usually specified as the concentration of the drug that is required to achieve 50% growth inhibition as compared to the growth of the untreated control (50% inhibitory concentration, IC<sub>50</sub>). For primary (nondividing) cells, drug sensitivity is measured as enhanced cell kill of treated cells as compared to the loss of cells already commonly seen in untreated cells (50% lethal concentration, LC<sub>50</sub>).<sup>56</sup> Tetrazolium dye assays can also be used to measure cytotoxicity (loss of viable cells) or cytostatic activity (shift from proliferative to resting

status) of potential medicinal agents and toxic materials. MTT assays are usually done in the dark since the MTT reagent is sensitive to light.

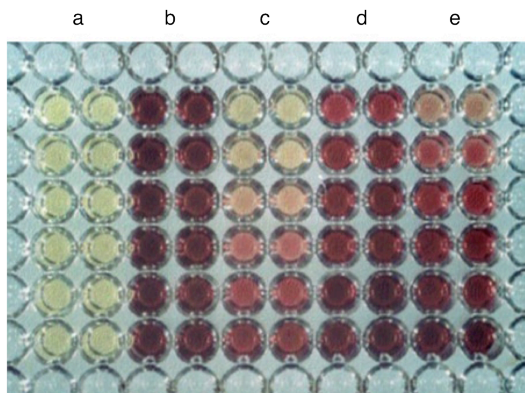


**Figure 38.** A 96-well plate after formazan crystals are dissolved in DMSO. (a) Blanks control wells, (b) untreated cell control wells, (c) cell line with drug C with a dose-response curve from 100% cell death to no response on cell growth, (d) cell line with drug D with a dose-response curve showing no growth inhibition, (e) cell line with drug E with a dose-response curve with dose-dependent modest growth inhibition at high drug concentrations. Outer wells are not used because of possible evaporation.

In order to set up the MTT assay for cells and/or drugs that have not been tested before, several considerations are of crucial importance and vary between cell lines, assay conditions (volume, concentration) and the duration of the assay:

- Detection limits of the assay (minimum and maximum detectable cells)
- Lineal absorbance ratio relative to the number of cells
- Initial cells number and assay lenght (the cells must be in exponential fase when the measurement takes place)
- Concentration of the tested drugs
- Length of exposure to the drug
- Suitable controls and blanks

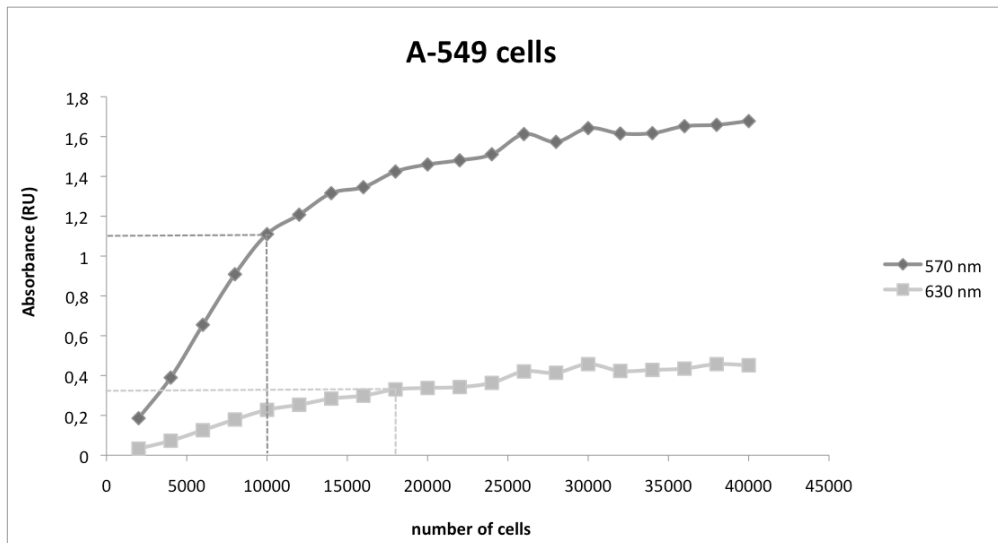
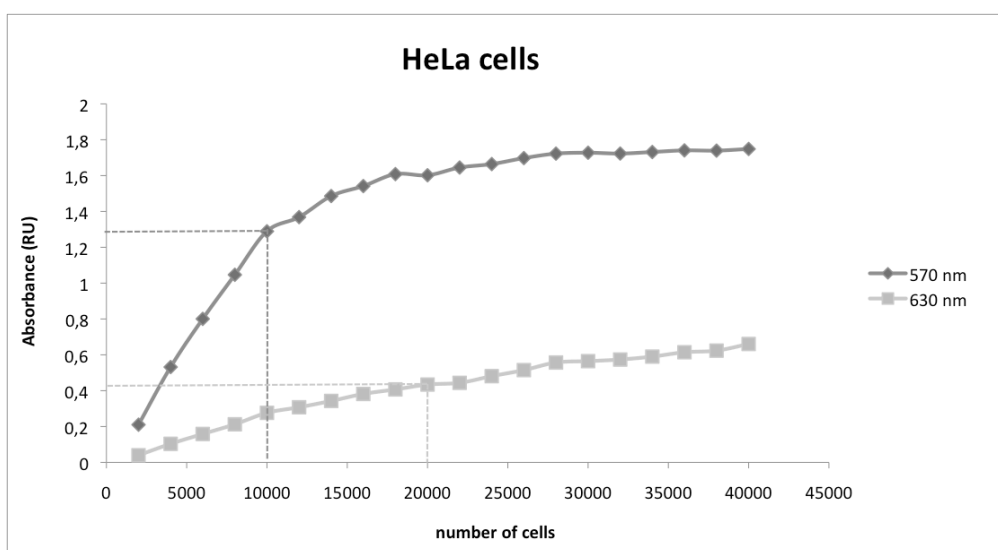
Thus, preliminar determinations of the detection limits of the assay, the lenght of the exponential phase of the cell lines tested and their doubling times were carried out. The four human cancer cell lines that were used for all these experiments were: cervical adenocarcinoma HeLa cells, lung carcinoma A-549 cells, breast adenocarcinoma SK-BR-3 cells, and colon adenocarcinoma HT-29 cells.

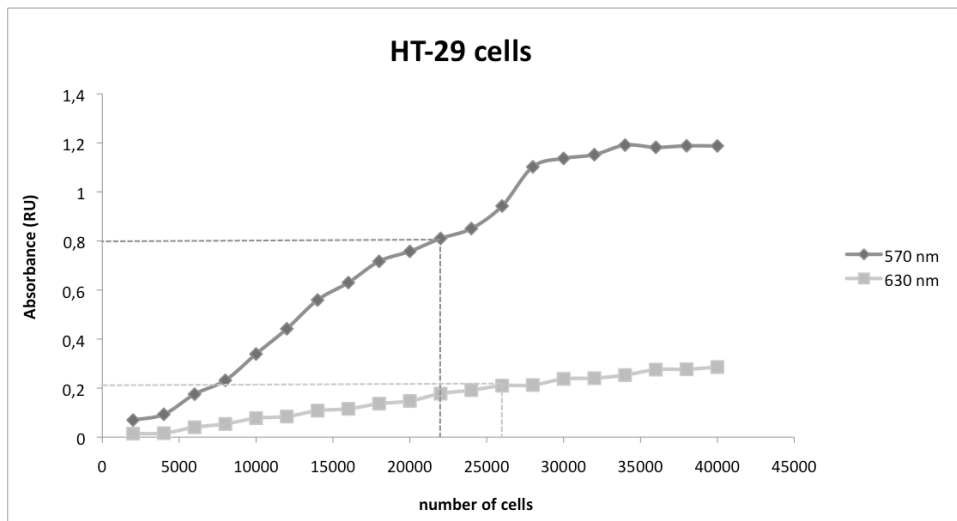
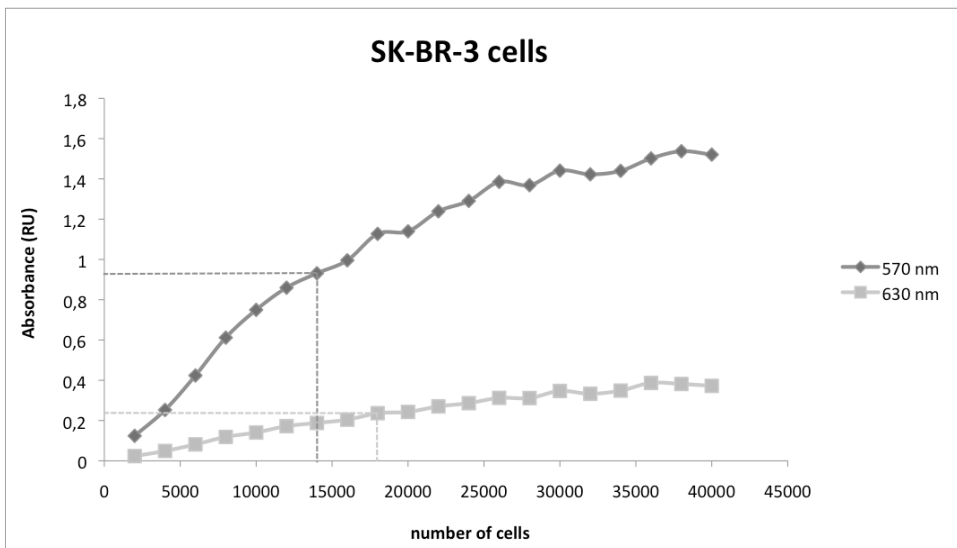
### Preliminary studies to determine the best conditions for the MTT assay

#### Detection limits

To determine the linearity of viable cells number with absorbance level, several cell concentrations were plated and let to attach to the plate surface for 8 hours (before replication happens). Then, MTT was added to each well (1 mg/mL final concentration) and incubated for 4 additional hours. The reduced formazone dye was dissolved in DMSO and measured at 570 and 630 nm.

After representation of the results, the linearity of the measurements at both wavelengths was correlated with the number of cells seeded in the well:





The linearity of viable cell number per well (96-well plate) with absorbance level for the four human cell lines chosen to be used in the cytotoxicity assays are shown in Table 4:

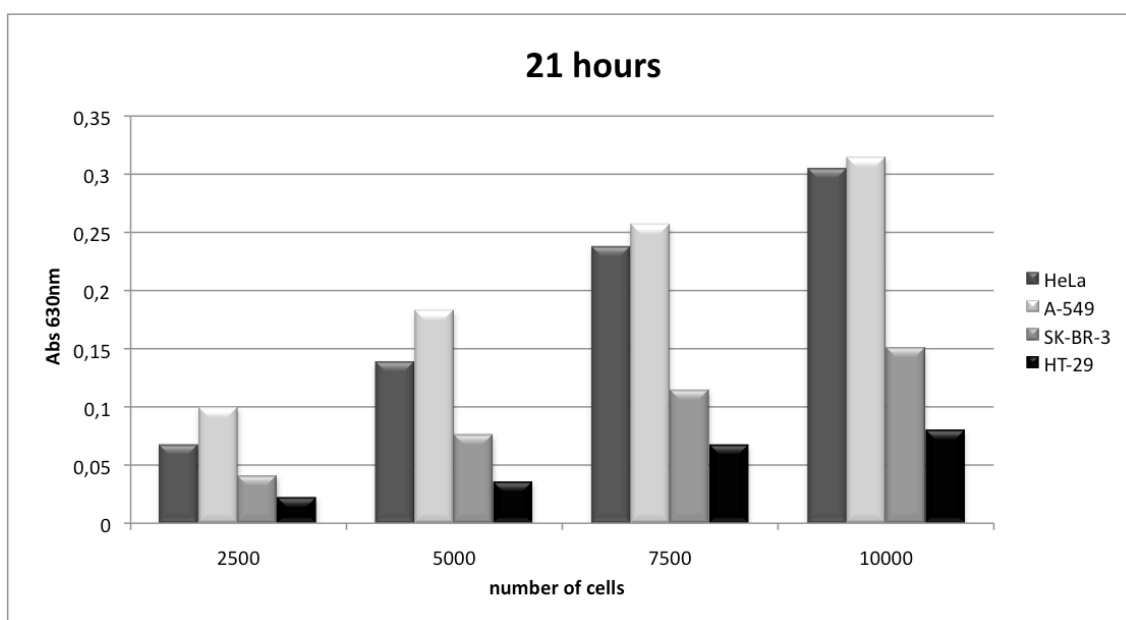
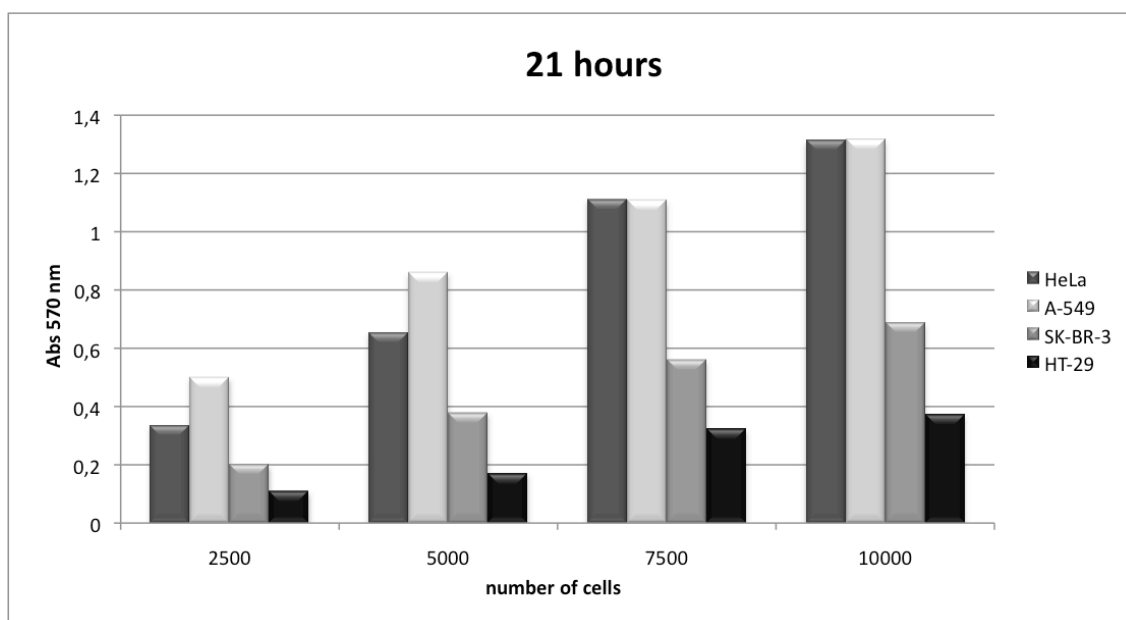
|        | <b>HeLa</b>  | <b>A-549</b> | <b>SK-BR-3</b> | <b>HT-29</b> |
|--------|--------------|--------------|----------------|--------------|
| 570 nm | 10,000 cells | 10,000 cells | 14,000 cells   | 22,000 cells |
| 630 nm | 20,000 cells | 18,000 cells | 18,000 cells   | 26,000 cells |

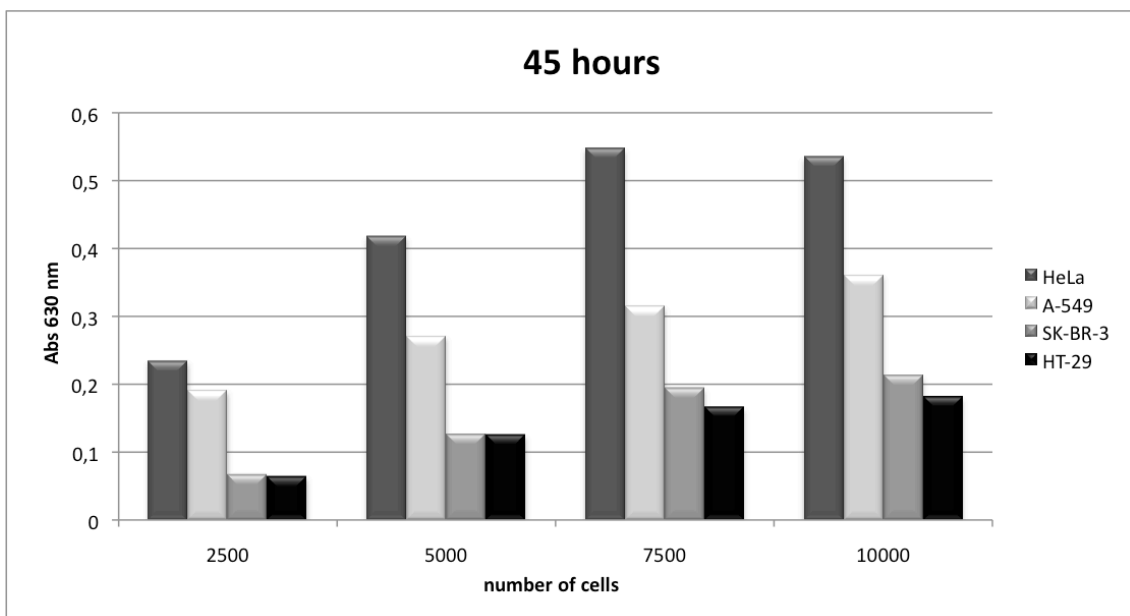
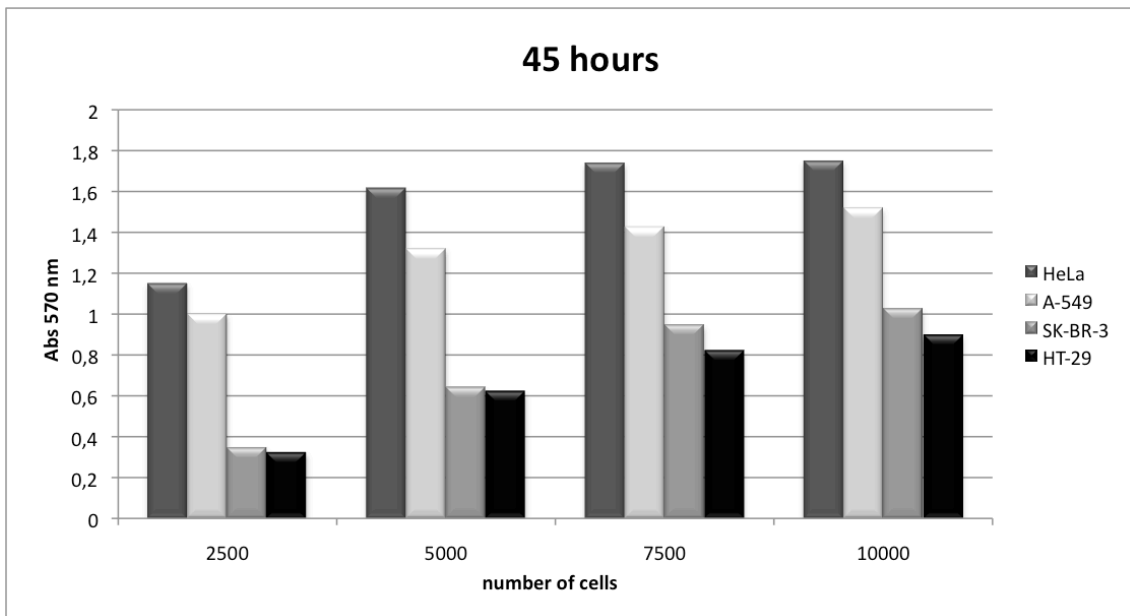
**Table 4.** Detection limits for the four cell lines tested.

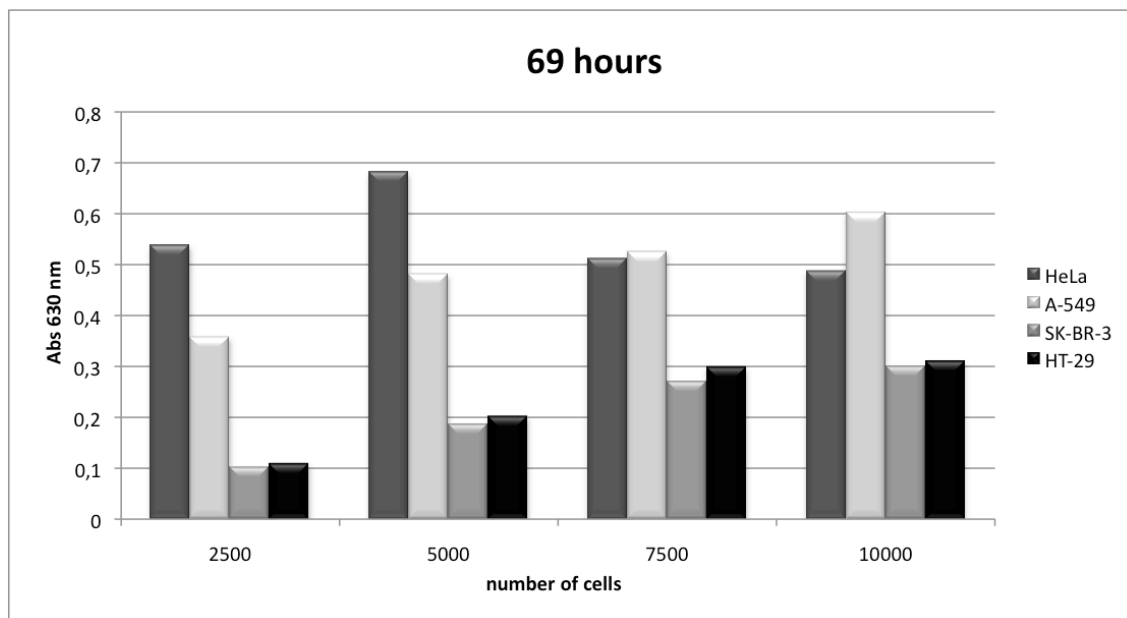
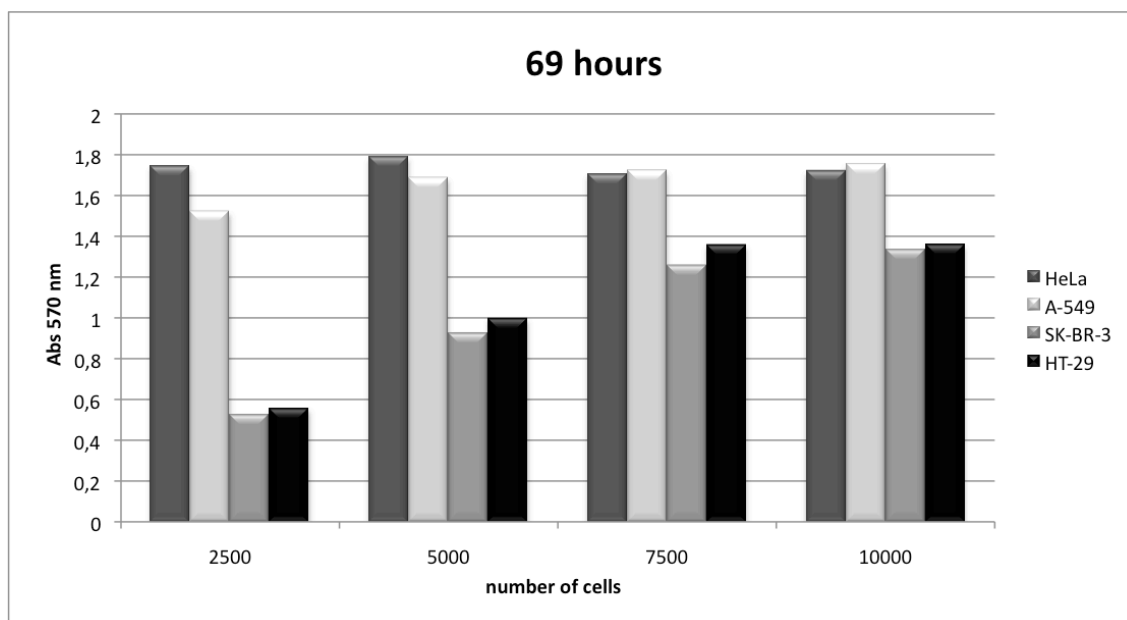
### Exponential growth phase

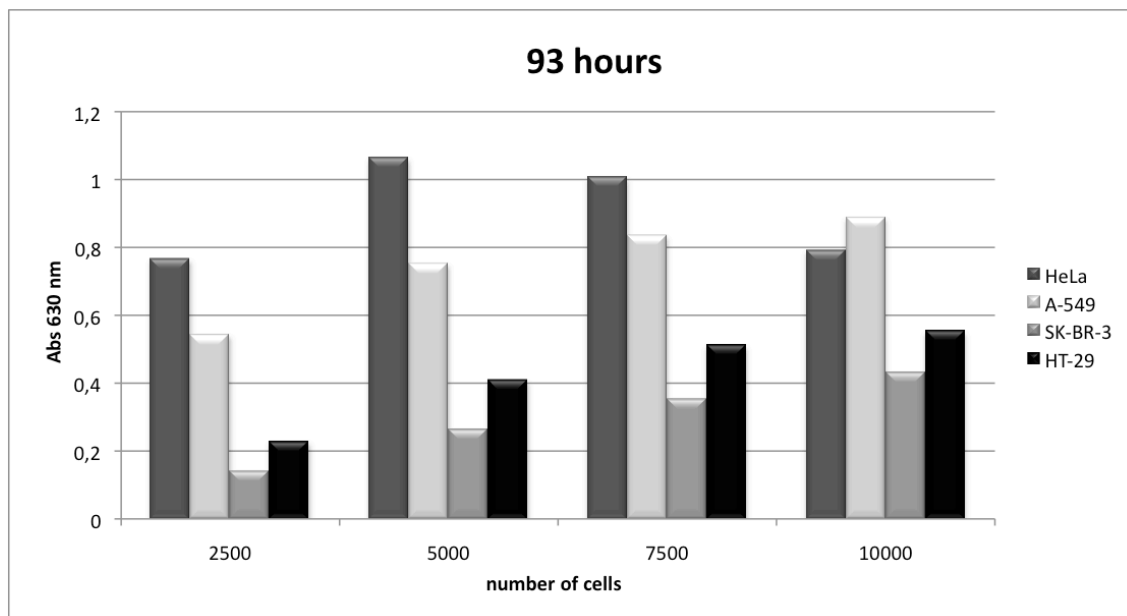
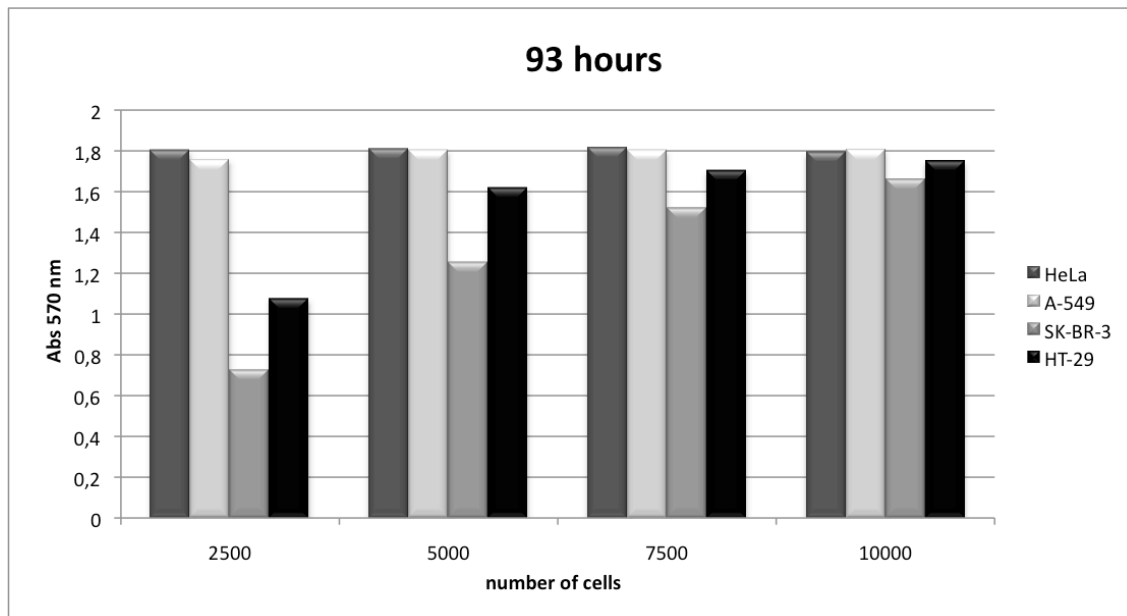
The optimal cell concentration to be plated is dependent on the basic level of mitochondrial activity and the rate of proliferation. In order to establish this, several concentrations of cells were plated in seven plates, and measured daily to determine the growth curve of the cell line to prevent overgrowth, which would influence the experiment.

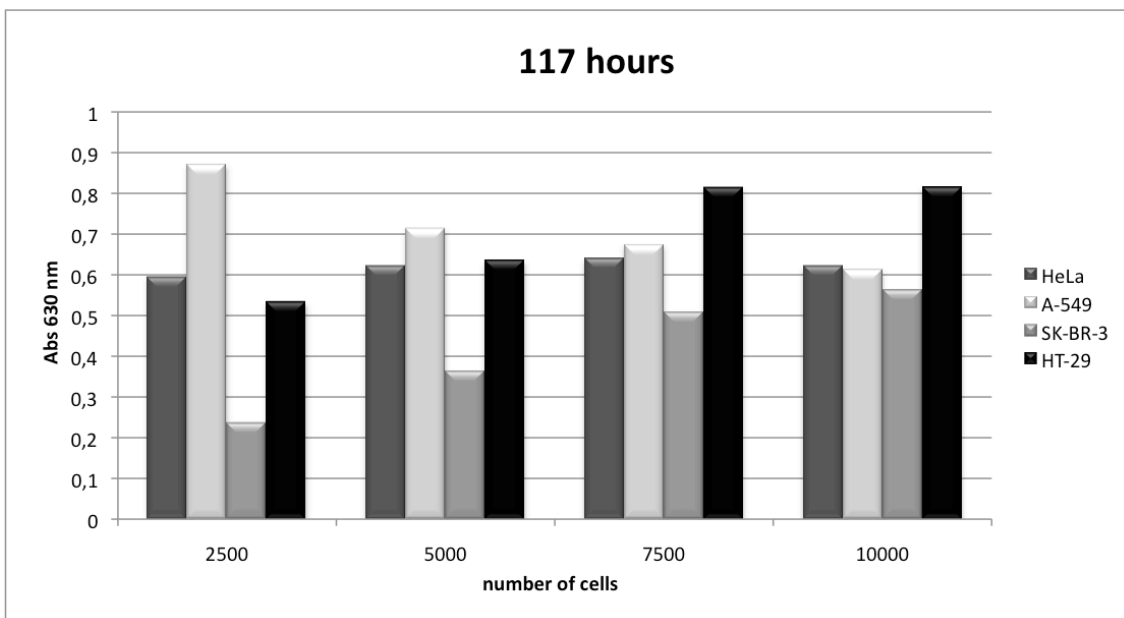
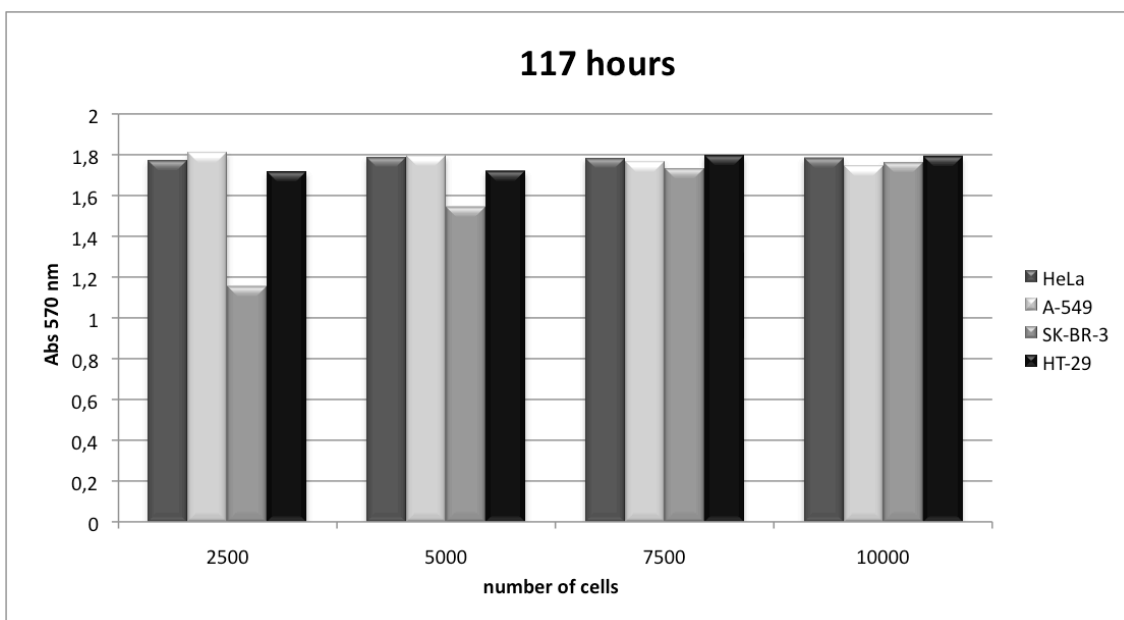
The daily measures (at 570 and 630 nm) for the four cell lines tested are depicted in the following graphs:

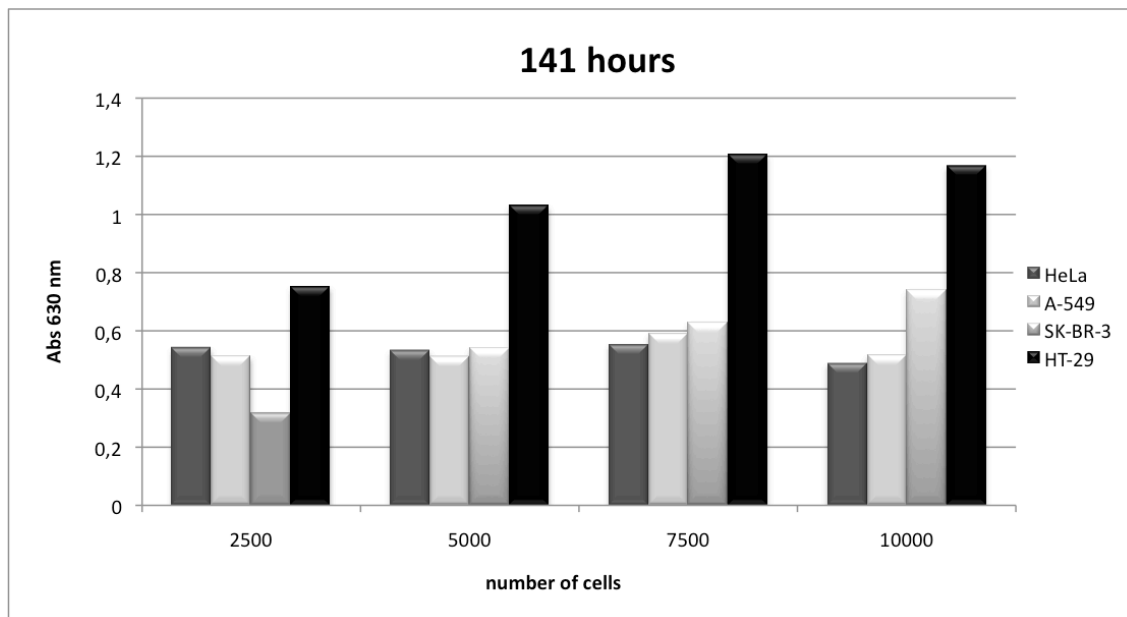
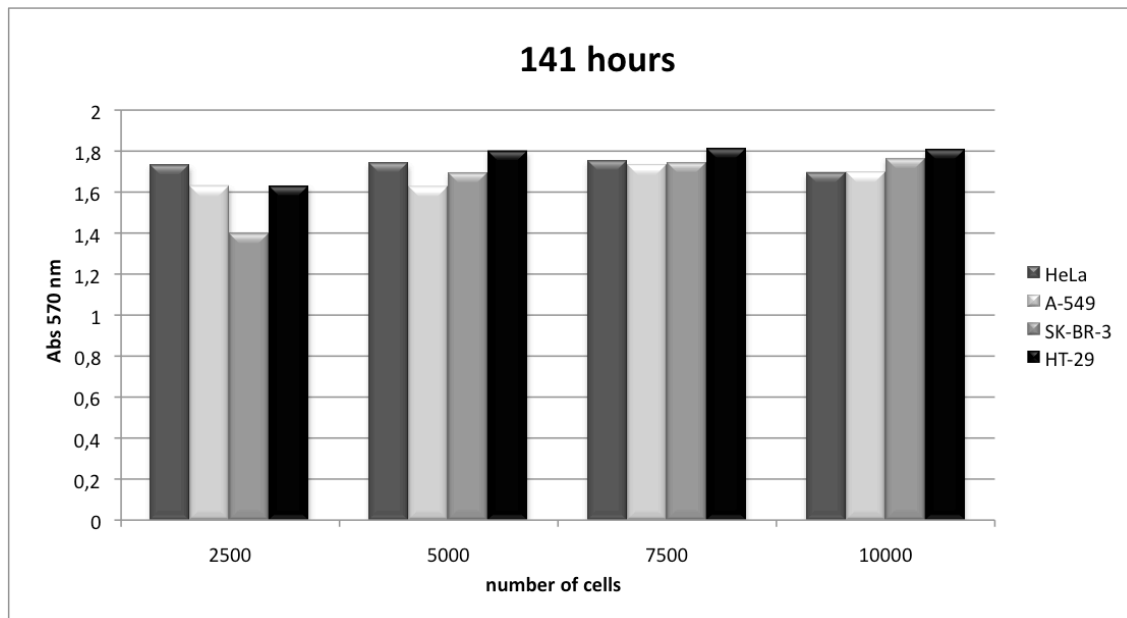


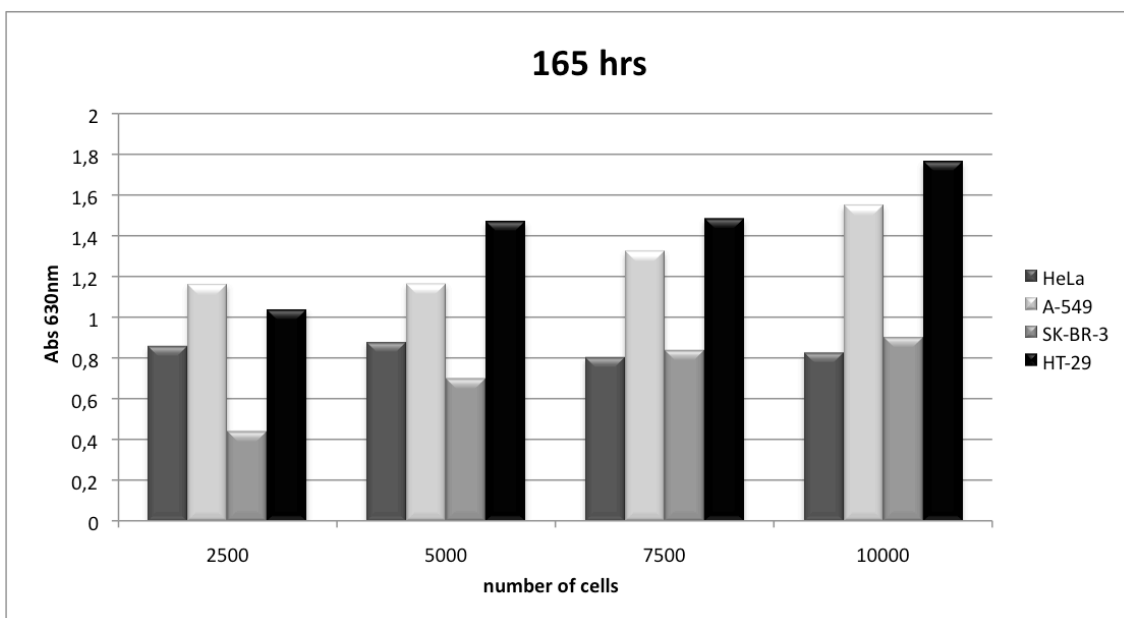
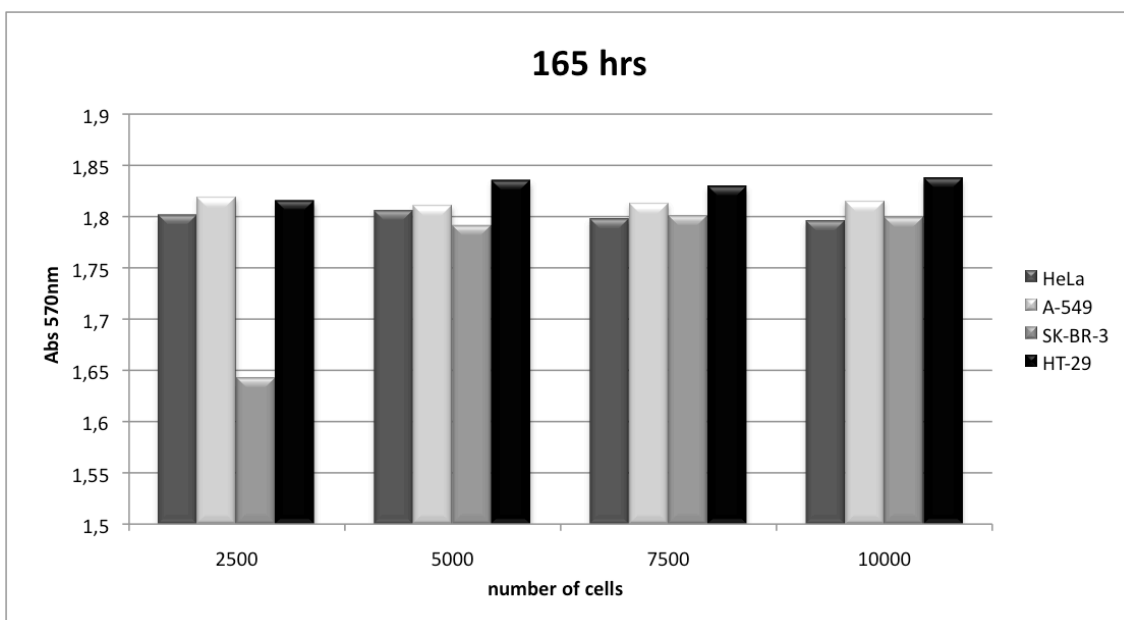






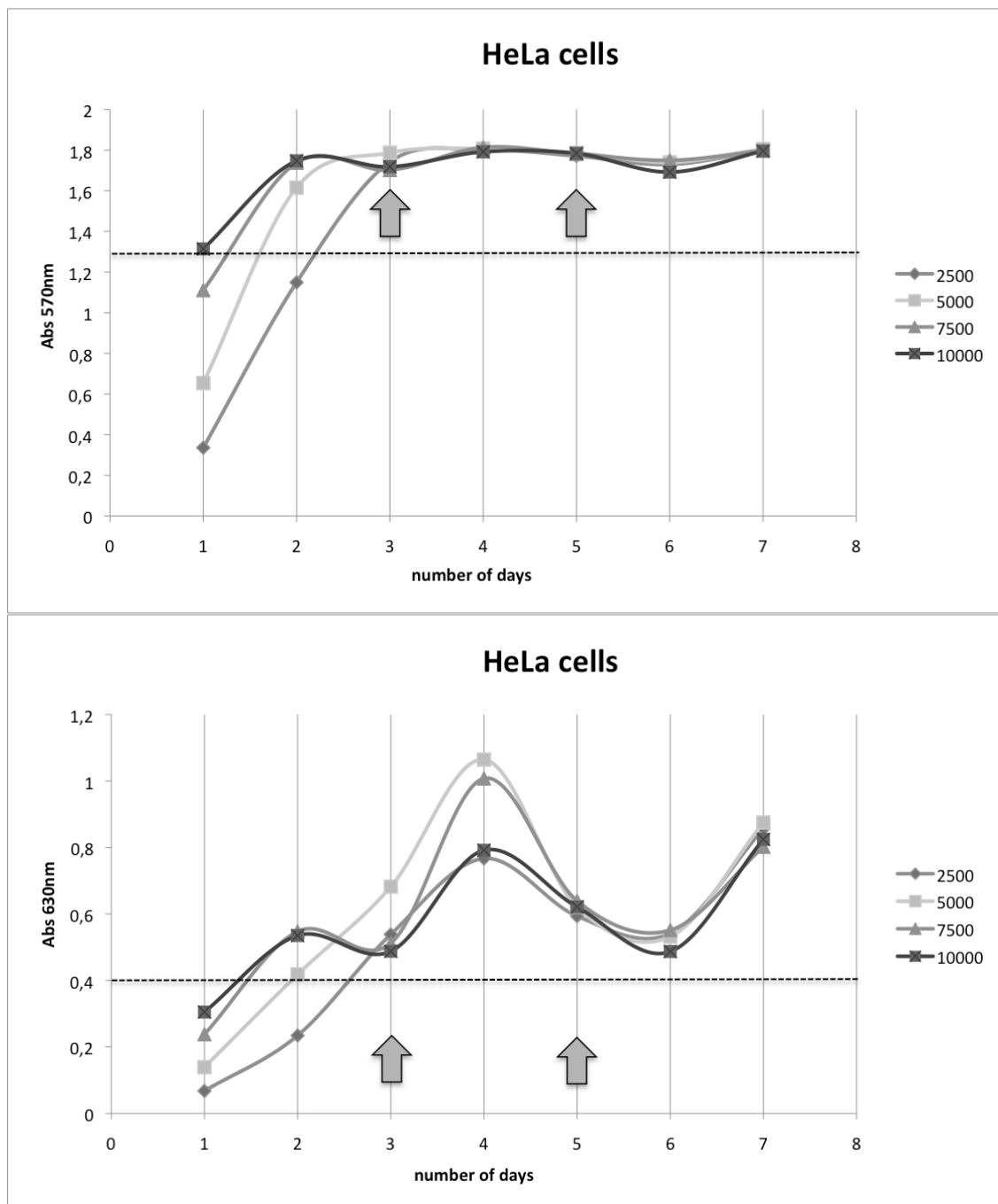




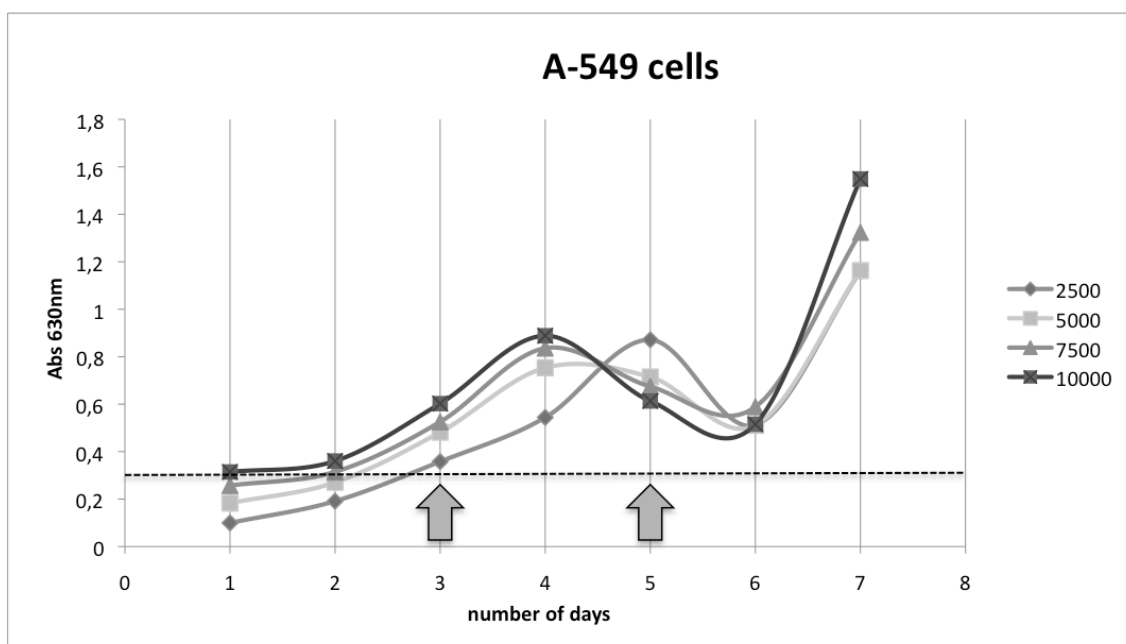
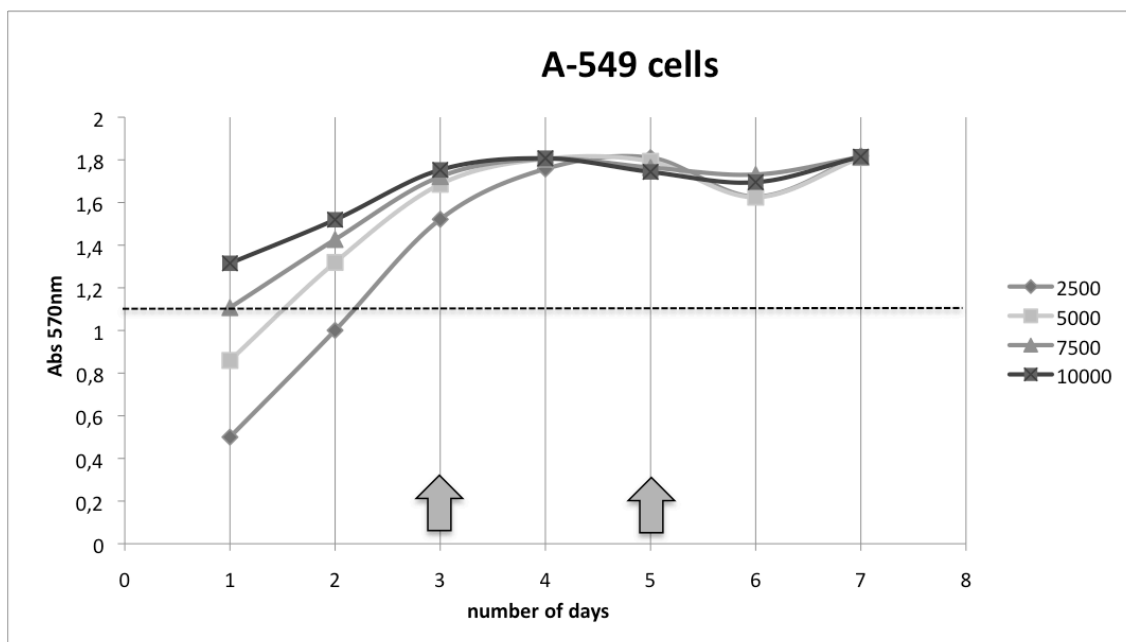


By constructing a growth curve, the logarithmic cell phase is determined (at which the cells duplicate). At a certain time point the cell growth will plateau due to exhaustion of the medium, contact inhibition, and exceeding of the maximal OD value that can accurately be measured.

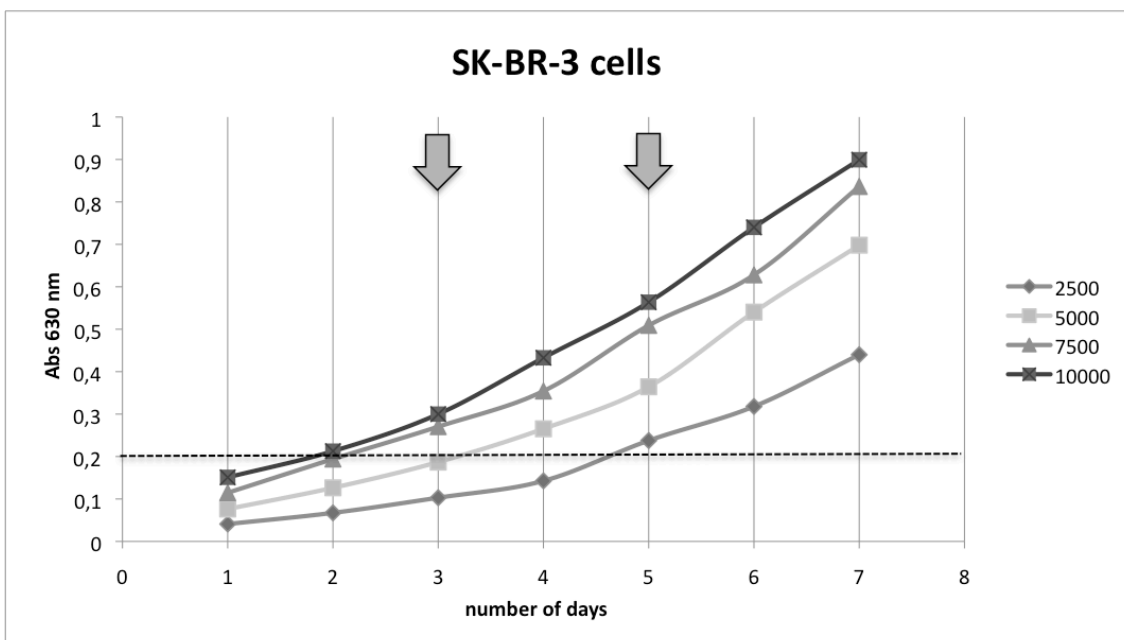
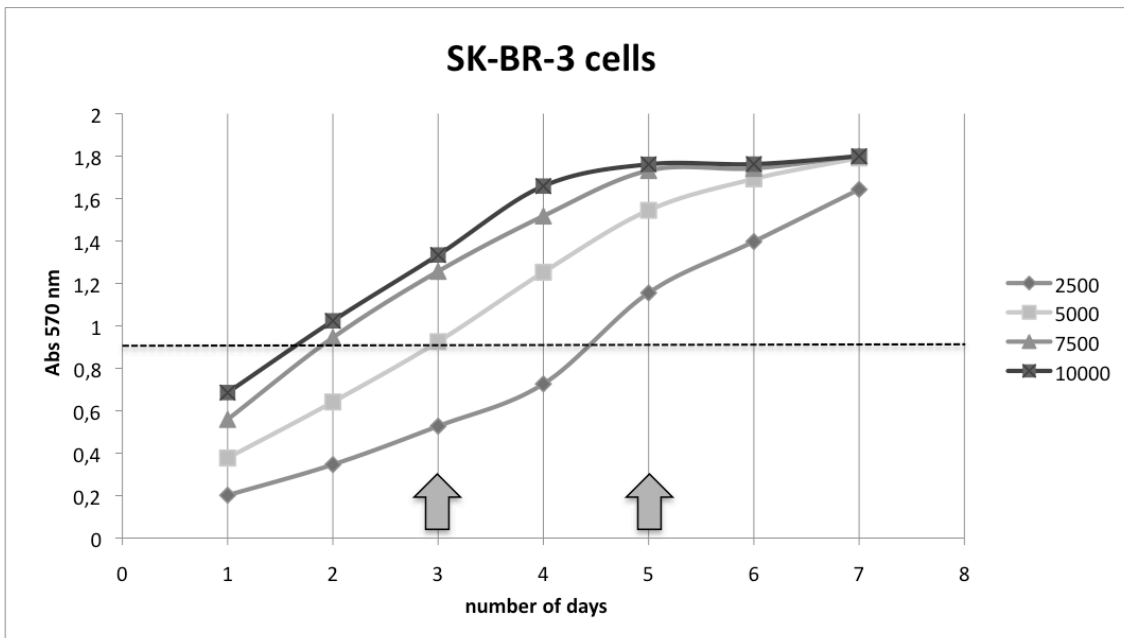
The following graphs are the obtained growth curves of the four different concentrations of cells that were plated. The dashed lines mark the detection limit assay calculated for each cell line at both reading wavelengths. The gray arrows depict the days in which change of media was done to maintain the cell culture.



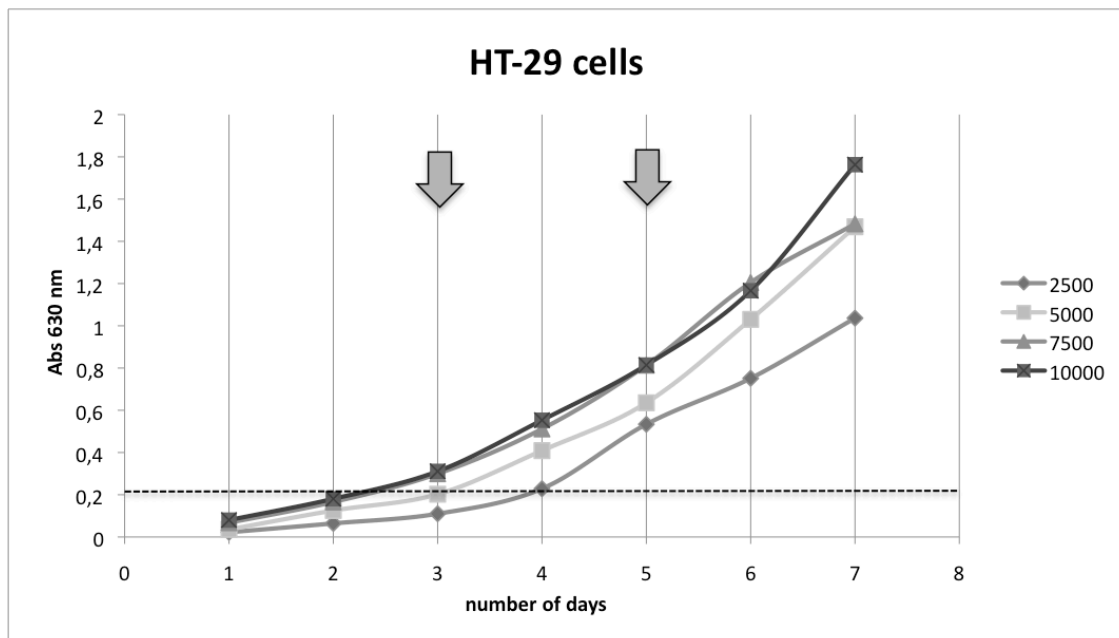
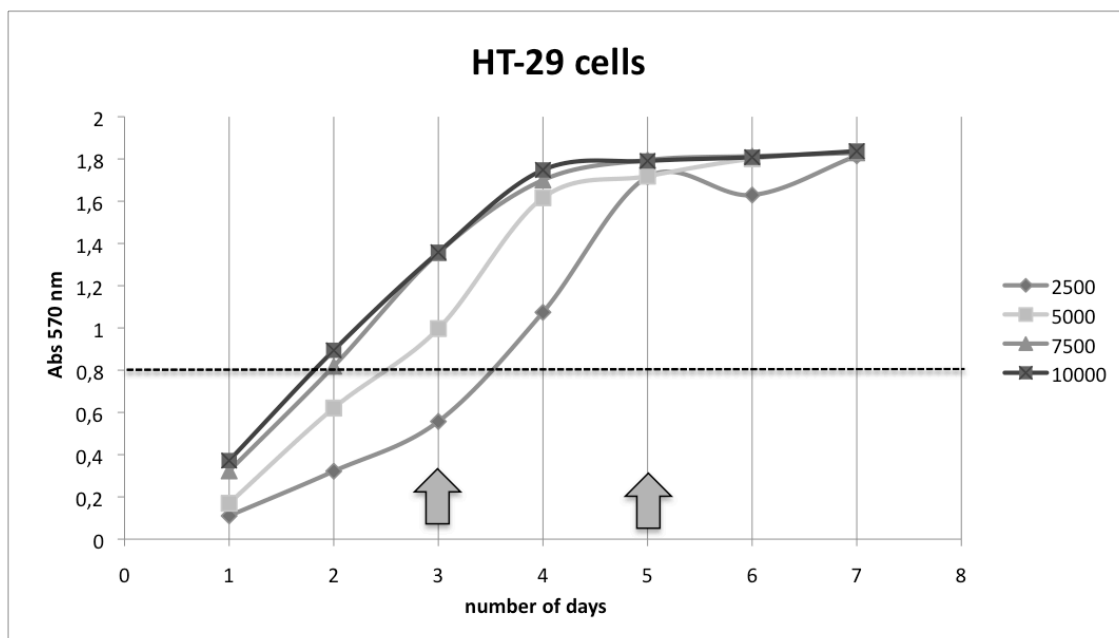
Exponential growth phase = between 20 h and 90 h after plating.



Exponential growth phase = between 20 h and 90 h after plating.



Exponential growth phase = between 20 h and 165 h after plating.



Exponential growth phase = between 20 h and 165 h after plating.

It can be observed that some cell lines, such as HeLa and A-549, are more sensitive to the suction process involved in media change besides being done very carefully. This problem is especially evident with very confluent cultures, so seeding less cells per well helps to overcome this issue.

Since the most optimal concentration of plating is when cells have almost no lag phase and the assay should not proceed after the log phase, the following conditions are the ones found to be the optimal for the cytotoxicity assays:

|                      | <b>Cells plated per well<br/>(96-well plate)</b> | <b>Hours for attachment to<br/>the plate</b> | <b>Maximum of hours after<br/>plating to do the MTT<br/>assay</b> |
|----------------------|--|--|---|
| <b>HeLa cells</b>    | 2500 cells                                       | 12 hours                                     | 45 hours  |
| <b>A-549 cells</b>   | 2500 cells                                       | 12 hours                                     | 45 hours  |
| <b>SK-BR-3 cells</b> | 5000 cells                                       | 12 hours                                     | 69 hours  |
| <b>HT-29 cells</b>   | 5000 cells                                       | 12 hours                                     | 69 hours  |

**Table 5.** Optimal conditions for the MTT assays for the different cell lines tested.

#### Doubling time

To decide the length of exposure to the drug, the doubling time of the cell line that is being used must be calculated, since the study of the effect of the compound on the cell growth requires a minimum of 1 or 2 doubling times of exposure.

Cell line doubling times were determined by daily counting of cells from seven independent cultures and found to amount to 17 h for HeLa, 30 h for A-549, 35 h for SK-BR-3 and 23 h for HT-29.

The equation applied to calculate these doubling times was:

$$ND = \log_{10} \left( \frac{N}{N_0} \right) \cdot 3.33$$

Where:

$ND$  = number of cell replications

$N$  = number of cells counted after growth period

$N_0$  = number of cells plated

The calculated doubling times were the minimum time of exposure to the compounds used in the MTT assays for each cell line.

**Preliminari chemosensitivity test using only one concentration of compound**

To evaluate the potential cytotoxic activity of the synthesized library of compounds RZ1-RZ12 (Figure 39), cells were exposed to 50  $\mu$ M of each compound, following quantitation of the surviving cells by MTT assays. The synthesized triostin A was used as positive control. The results of this initial screening with the four different cell lines are illustrated in Figures 40, 41, 42, and 43.

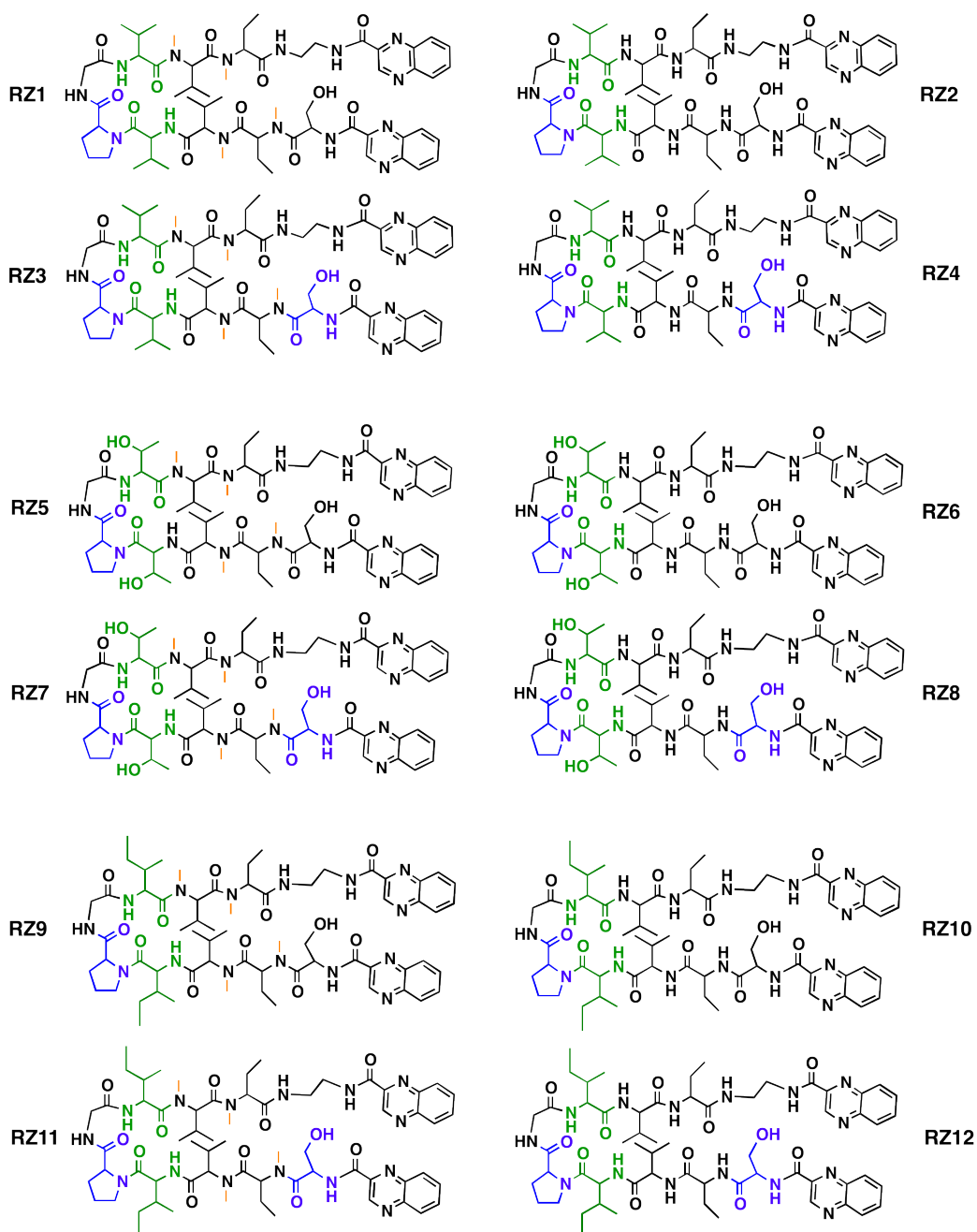


**Figure 39.** Chemical structures of the RZ1-RZ12 library. For identification purposes D-amino acids are shown in blue and N-methylation in orange. The  $\beta$ -branched amino acids (valine, threonine or isoleucine) next to the  $\beta$ -loop that define the four residue  $\beta$ -turn are shown in green.

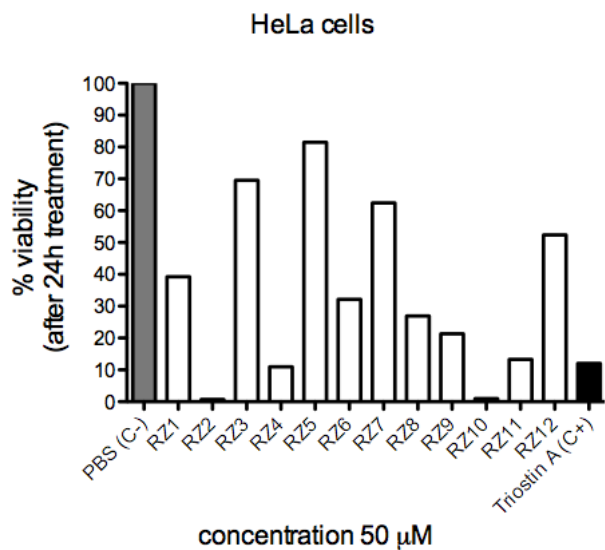


**Figure 40.** Initial screening on HeLa cells of the RZ1-RZ12 library.

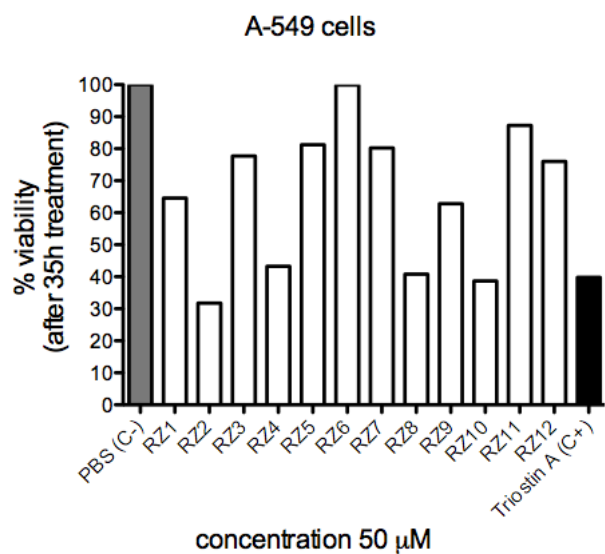


**Figure 41.** Initial screening on A-549 cells of the RZ1-RZ12 library.

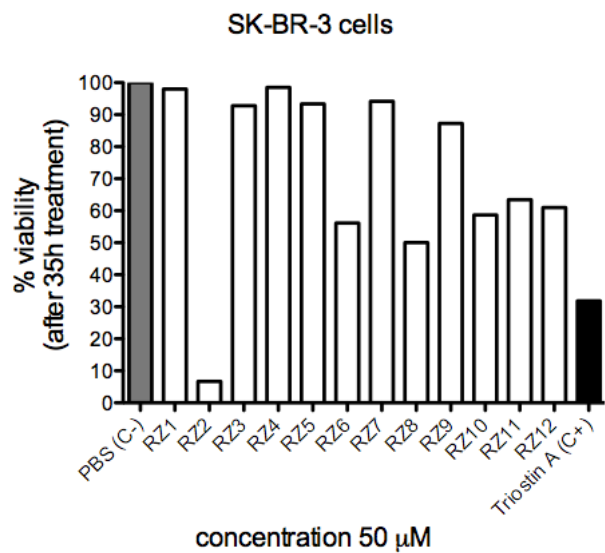


**Figure 42.** Initial screening on SK-BR-3 cells of the RZ1-RZ12 library.

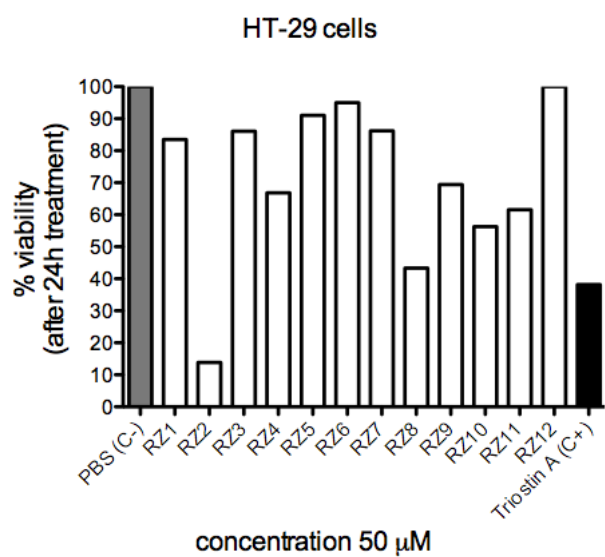


**Figure 43.** Initial screening on HT-29 cells of the RZ1-RZ12 library.

### ***IC<sub>50</sub> values for the library RZ1-RZ12 against tumor cells***

After corroborating through the aforementioned initial screening that the RZ1-RZ12 library displayed cytotoxicity against the four human cancer cell lines tested, IC<sub>50</sub> values were calculated from dose-response relationships following quantitation of the surviving cells exposed to the individual compounds *in vitro* at different concentrations. Exposure lengths to the compounds were the same as in the initial screening.

Based on the fact that some of the synthesized compounds displayed better antitumor activity in the initial screening than triostin A, another positive control was included in for the IC<sub>50</sub> values determination.

Doxorubicin is a DNA intercalator currently used in cancer chemotherapy. It is commonly used in the treatment of hematological malignancies, many types of carcinoma and soft tissue sarcomas. Its chemical structure is illustrated in Figure 44.

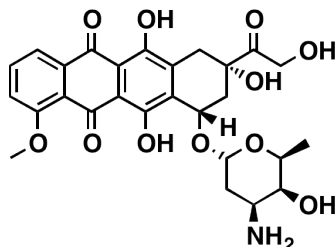


**Figure 44.** Chemical structure of doxorubicin.

The calculated half maximal inhibitory concentrations (IC<sub>50</sub>) for the RZ1-RZ12 library are displayed in Table 6:

| Compound    | IC <sub>50</sub> , $\mu\text{M}$ |               |                   |                |
|-------------|----------------------------------|---------------|-------------------|----------------|
|             | Cervix<br>HeLa                   | Lung<br>A-549 | Breast<br>SK-BR-3 | Colon<br>HT-29 |
| RZ1         | 42.2                             | 51.2          | 96.7              | 88.4           |
| RZ2         | <b>2.7</b>                       | <b>11.9</b>   | <b>5.4</b>        | <b>6.8</b>     |
| RZ3         | 93.8                             | 65.8          | 98.1              | 72.3           |
| RZ4         | 30.9                             | 34.9          | >100              | 75.0           |
| RZ5         | >100                             | 70.7          | 84.6              | 84.8           |
| RZ6         | 45.6                             | 84.5          | 55.3              | 83.1           |
| RZ7         | 84.5                             | 72.8          | >100              | 90.7           |
| RZ8         | 37.1                             | 23.4          | 44.5              | 39.8           |
| RZ9         | 50.9                             | 60.9          | 90.6              | 84.4           |
| RZ10        | 14.1                             | 26.8          | 62.1              | 53.8           |
| RZ11        | 24.3                             | 96.3          | 78.9              | 64.7           |
| RZ12        | 55.4                             | 82.2          | 71.6              | >100           |
| Triostin A  | 18.8                             | 23.5          | 23.1              | 24.7           |
| Doxorubicin | 5.4                              | 0.6           | 0.5               | 8.9            |

**Table 6.** Cytotoxic activity of the RZ1-RZ12 library against several human cancer cell lines.

The most active compound was RZ2 (Figure 45), with low micromolar cytotoxic activities against the four cell lines tested, being in all cases more active than the natural parent compound triostin A, and with better cytotoxic activity than doxorubicin against HeLa and SK-BR-3 cells.

Normalized dose-response curves to compare the cytotoxic activity of this synthetic compound against the two positive controls that were employed in these experiments are given in Figures 46, 47, 48, and 49.

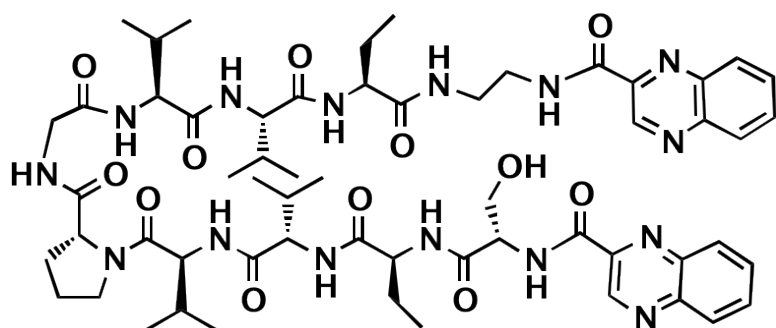


**Figure 45.** Chemical structure of compound RZ2.

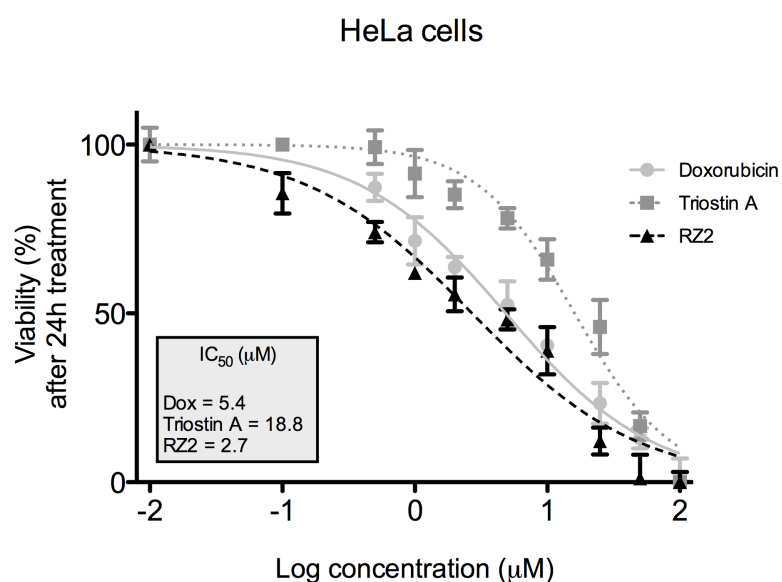


**Figure 46.** Comparative MTT viability measurements of HeLa cells after incubation with compound RZ2 and positive controls (normalized data).

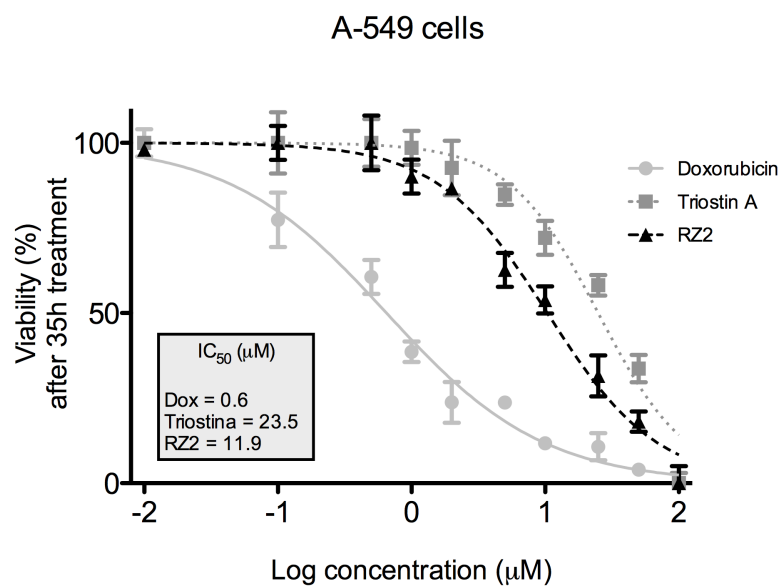


**Figure 47.** Comparative MTT viability measurements of A-549 cells after incubation with compound RZ2 and positive controls (normalized data).

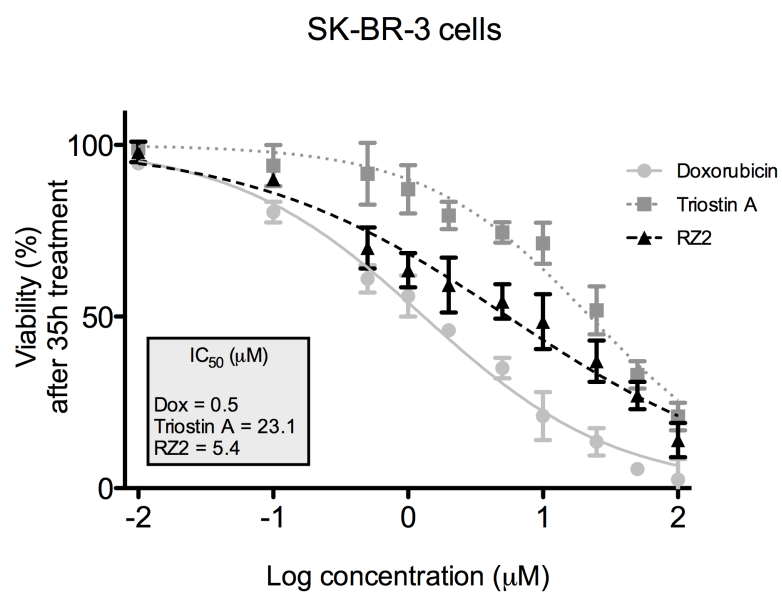


**Figure 48.** Comparative MTT viability measurements of SK-BR-3 cells after incubation with compound RZ2 and positive controls (normalized data).

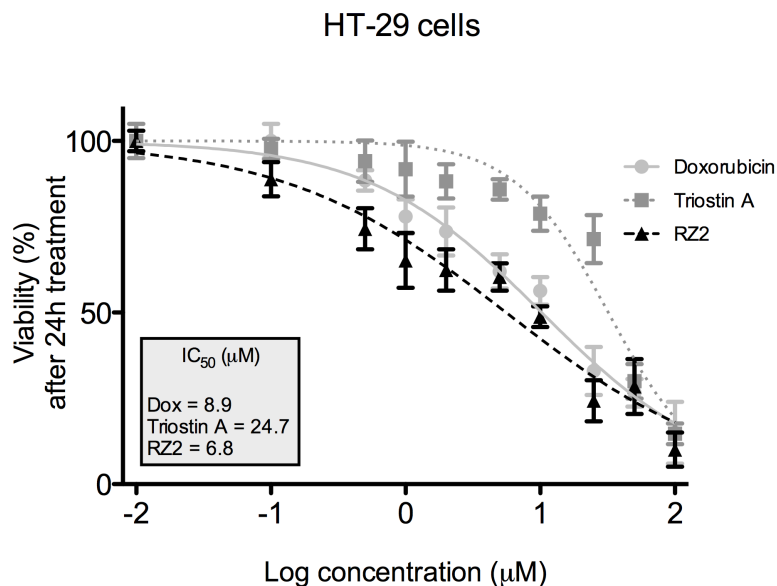


**Figure 49.** Comparative MTT viability measurements of HT-29 cells after incubation with compound RZ2 and positive controls (normalized data).

#### ***IC<sub>50</sub> value for most active compound, RZ2, against non-tumor cells***

To evaluate if compound RZ2 displays any selectivity for its cytotoxic activity between tumor and non-tumor cells, endothelial cells were exposed *in vitro* to this compound and doxorubicin and their  $IC_{50}$  values were calculated from dose-response relationship, following quantitation by the MTT assay. The results are shown in Figure 50.

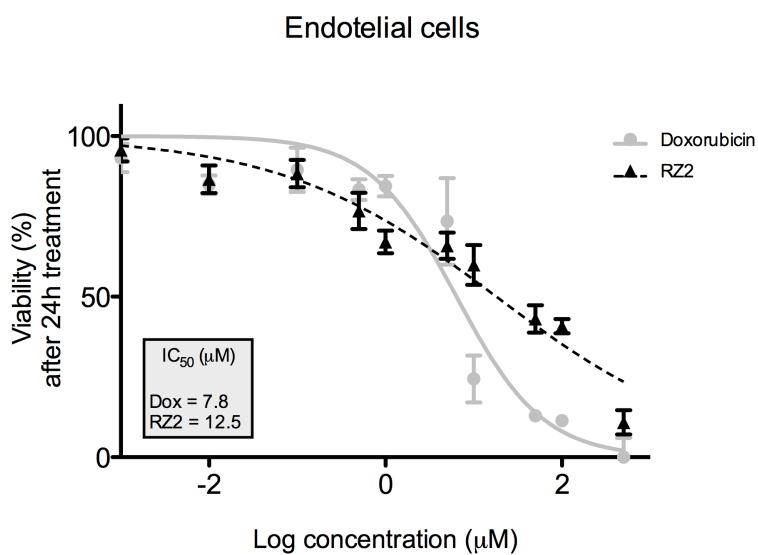


**Figure 50.** Comparative MTT viability measurements of non-tumor cells after incubation with compound RZ2 and doxorubicin (normalized data).

Unfortunately, these results demonstrate that compound RZ2 displays a non-selective cytotoxicity, as most of the antitumor drugs like doxorubicin do. However, non-selectivity was expected taking into account that, at least in design, RZ2 is supposed to be a bisintercalator, so that the only fact that would make this compound be more "selective" towards tumor cells is their faster replication when compared to most of non-tumor cells.

### ***Cytotoxic activity of peptides Z1-Z12***

In order to evaluate the role that the peptide scaffold itself of compounds RZ1-RZ12 may play in the cytotoxic activity, it was decided to evaluate the antitumor activity of peptides Z1-Z12.

The twelve peptides (50 µM and 100 µM) were incubated with the four human cancer cell lines used for the cytotoxic evaluation of compounds RZ1-RZ12 under exactly the same conditions, but no cytotoxicity was observed for none of the peptides.

This finding reveals that the quinoxaline moieties are the ones that confer the cytotoxic activity to compounds RZ1-RZ12. However, the fact that different IC<sub>50</sub> values were obtained for all the library indicates that the peptide scaffold plays a secondary role in the cytotoxicity displayed by the molecule, probably due to affinity in recognition towards the target within the cell or conferring the required orientation to the quinoxaline moieties to interact with their target.

### ***Cytotoxic activity of compounds RZV***

To further evaluate the role of the peptide scaffold and in an efford to obtain cytotoxic compounds in the nanomolar range, some modifications to the peptide scaffold of compound RZ2 were designed based on the chemical structures of the natural bisintercalators triostin A<sup>57</sup> and thiocoraline.<sup>58</sup> The obtained compounds were designated as RZV13, RZV14 and RZV15 (see Figure 51) and evaluated for their antitumor activity using the four cell lines HeLa, A-549, SK-BR-3 and HT-29.

A single dose screen (100 µM) was performed under the optimized conditions determined for each cell line. No cytotoxic activity was observed for compounds RZV.

These results corroborate the important role played by the peptide scaffold of the designed simplified triostin A analogues to allow the quinoxalines to perform their cytotoxic activity. It seems that the peptide confers to both quinoxaline moieties certain position that allow them to interact with their target, since little modifications to the peptide scaffold greatly modify the biological activity of the compounds.

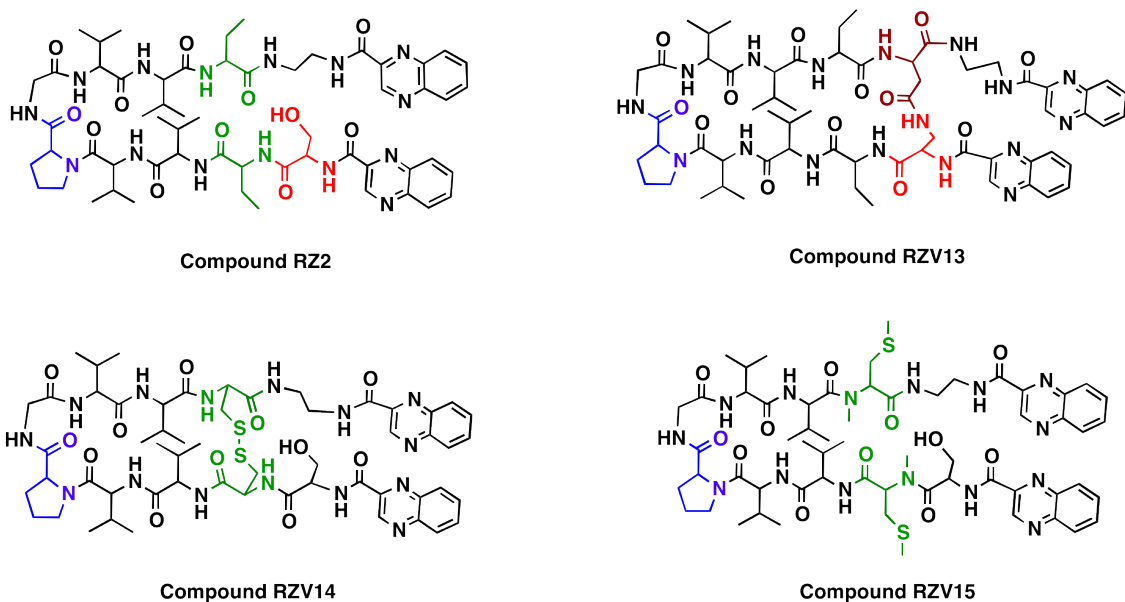


**Figure 51.** Chemical structure of compounds RZV. For identification purposes D-amino acids are shown in blue. Substitutions of the Abu residues from compound RZ2 are highlighted in green. Substitution of the Ser residue is highlighted in red. The additional residue that was not present in the chemical structure of RZ2 is displayed in brown.

#### **Cytotoxic activity of the fluorescent versions of compound RZ2**

Three different fluorescent versions of the most active compound, RZ2, were synthesized by attachment of a carboxyfluorescein moiety for future internalization assays (Figure 52). However, as it has been observed in the previously described cytotoxicity determinations, any slight modification in the chemical structure of the active molecule may decrease or render null biological activity. Thus, after the synthesis of any fluorescent version of a compound and before its use in further biological experiments, it is imperative to conduct the same tests under the same conditions used for the non-fluorescent compound in order to compare their biological activities and elucidate if the fluorescent version keeps the same or similar activity.

In order to determine the antitumor activity of the three fluorescent analogues of compound RZ2, dose-response curves were obtained by assessing cell proliferation at different compounds dilutions and used for calculation of IC<sub>50</sub> values. Cell growth was quantified using the MTT assay on HeLa cells, given the fact that this cell line is the most sensitive to treatment with compound RZ2 and would be the cells used for further biological tests.

As shown in Table 7, the three fluorescent versions displayed cytotoxic activity, but the more active compound was RZ2CF, which bears two quinoxaline moieties, just as the original compound RZ2. The two other compounds were less cytotoxic, pointing out that removal of one quinoxaline renders less potent antitumor analogues.

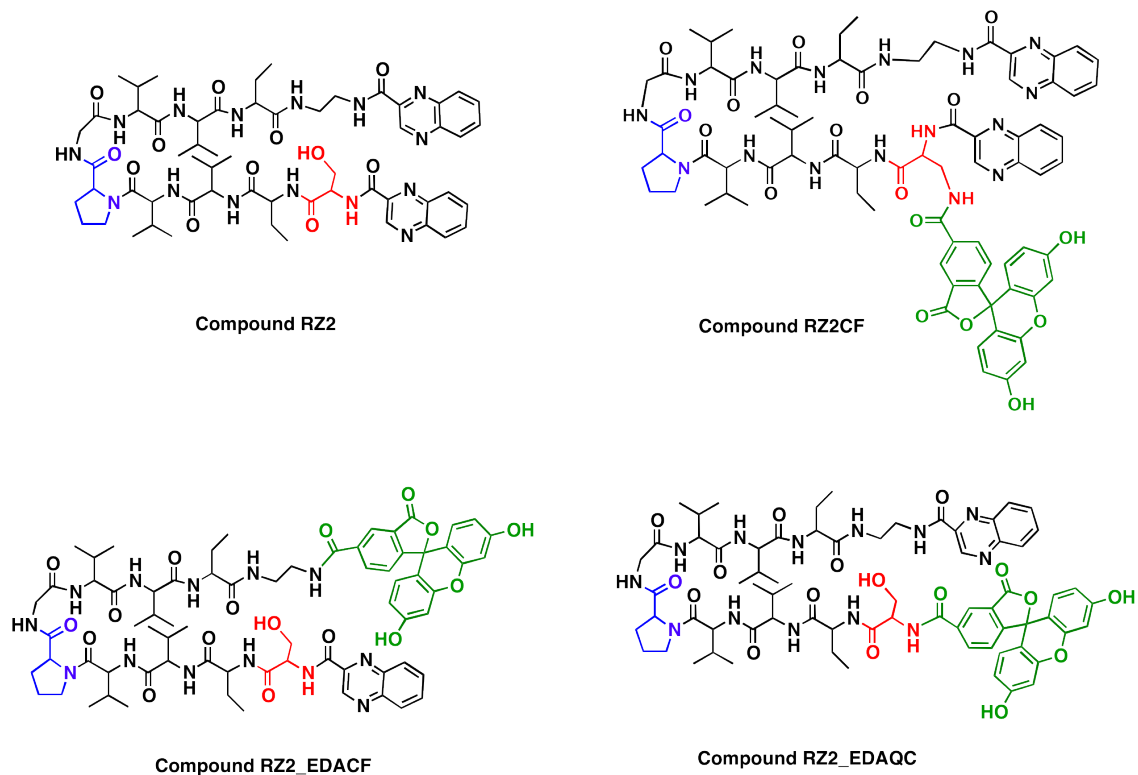


**Figure 52.** Fluorescent synthesized versions of compound RZ2. For identification purposes D-amino acids are shown in blue and CF moieties in green. The Ser residue from RZ2 that is substituted by Dap in RZ2CF is highlighted in red.

|                        | Compound<br>RZ2CF  | Compound<br>RZ2_EDACF | Compound<br>RZ2_EDAQC |
|------------------------|--------------------|-----------------------|-----------------------|
| $\text{IC}_{50}$ value | 10.7 $\mu\text{M}$ | 56.7 $\mu\text{M}$    | 70.5 $\mu\text{M}$    |

**Table 7.** Cytotoxic activity of RZ2 fluorescent analogues against HeLa cells.

Based on these results, it was decided to use the compound RZ2CF for the internalization assays since its biological activity is the closest to the one displayed by the compound RZ2.

#### **Stability assays of compound RZ2**

The compound RZ2 was selected as the best candidate of all the synthesized analogues due to its potent antitumor activity against the four human cancer cell lines tested. However, it is well known that *N*-methylations make peptides more stable towards proteolytic cleavage and enzymatic degradation,<sup>59,60</sup> and the fact that RZ2 has only one D-amino acid and no *N*-methylations could make this quinoxaline-containing peptide unstable under biological conditions.

*In vivo* stability of peptides in blood is modeled well by *in vitro* stability in serum or plasma, where the predominant degradation mechanism is exopeptidase-catalyzed cleavage.<sup>61</sup> Thus, the stability of RZ2 in human serum was studied.

Results in Figure 53 display the course of degradation of compound RZ2 up to 48 h. A little percentage of degradation is observed from 24h, with the maximum degradation (30%) in presence of serum at 48h.

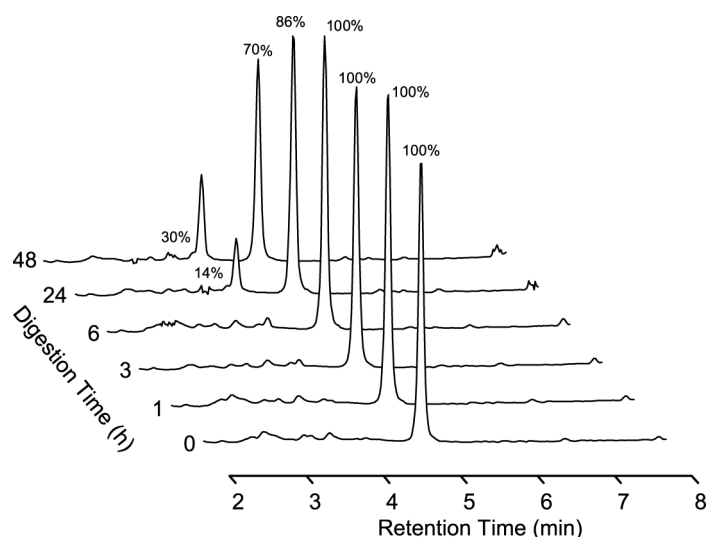


**Figure 53.** HPLC time study of RZ2 digestion mediated by human serum.

Furthermore, the compound's stability in presence of two overexpressed tumor proteases, MMP2 and cathepsin B, was also studied. These enzymes could cleave the peptidic scaffold provoking compound's inactivation. MMP-2 is located on the cellular surface of several cancers and tumor microvascular endothelial cells,<sup>62</sup> and cathepsin B is thought to be overexpressed at the extra and intra-cellular levels, being located mainly in the endo/lysosomal compartments.<sup>63</sup>

Results in Figures 54 and 55 display the course of degradation of compound RZ2 in the presence of both proteases.

It is worth highlighting that the half-life of the compound in presence of serum proteases, cathepsin B or MMP-2 is more than 48 h. These findings represent a major advantage of our antineoplastic molecule over other peptidic compounds that are easily degraded under physiological conditions in short times. These stability assays data indicate that the peptide could be somewhat advantageous in terms of proteolytic stability *in vivo*.

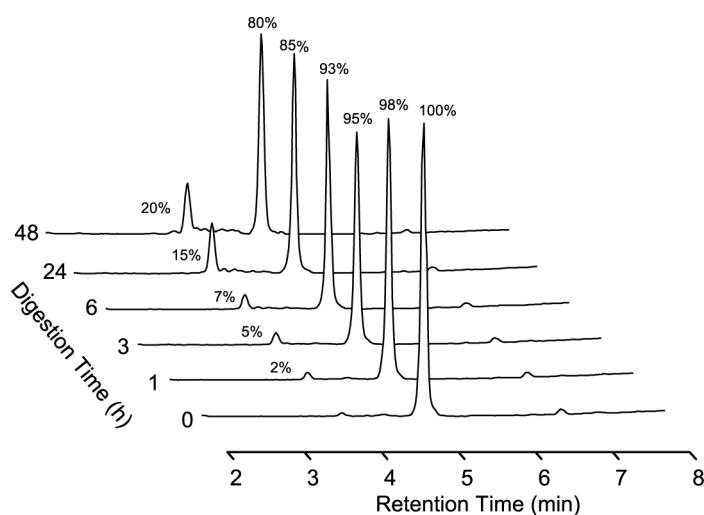


**Figure 54.** HPLC time study of RZ2 digestion mediated by cathepsin B.

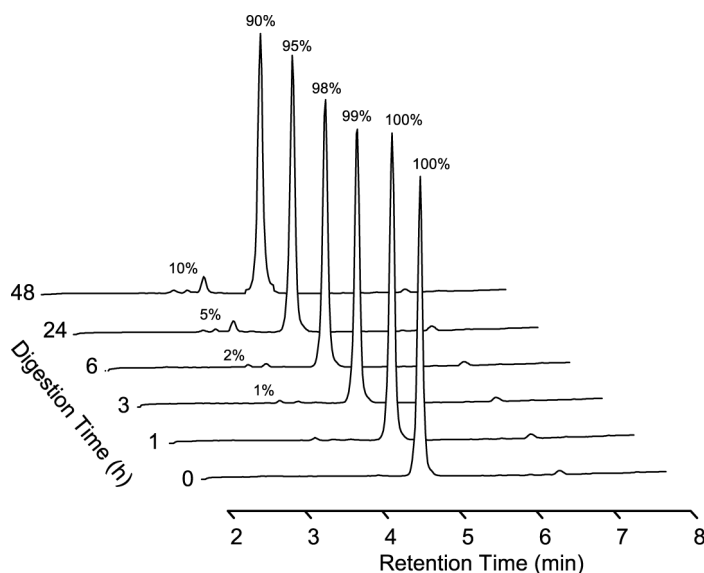


**Figure 55.** HPLC time study of RZ2 digestion mediated by MMP-2.

### ***Enhancing RZ2 cytotoxicity through a liposomal formulation***

Liposomes are synthetic lipid bilayer-enclosed structures up to several hundred nanometers in diameter that can improve the delivery of bioactive molecules. They function as microreservoirs for sustained release<sup>64,65</sup> and represent ideal drug delivery systems, as the microvasculature in tumors is typically discontinuous, having pore sizes (100-780 nm) large enough for liposomes to move from the blood compartment into the extravascular space surrounding the tumor cells.<sup>66</sup> The primary role of liposomal formulations is to extravasate within the site of tumor growth as a result of the EPR effect to provide locally concentrated drug delivery.

Moreover, liposomes have also been used to enhance the cell-uptake of hydrophobic compounds.<sup>67</sup> In this sense, cholesterol is a common constituent of liposomal formulations due to its ability to modulate membrane permeability and biological stability.

Since compound RZ2 showed low solubility in aqueous environments, a drug delivery system based on the authorized liposomal formulation of doxorubicin<sup>68</sup> was prepared. For this, egg phosphatidylcholine (EPC) and cholesterol (Chol) (5:1 molar ratio) were used so as to entrap RZ2 inside small unilamellar vesicles (SUV's) (Figure 56).

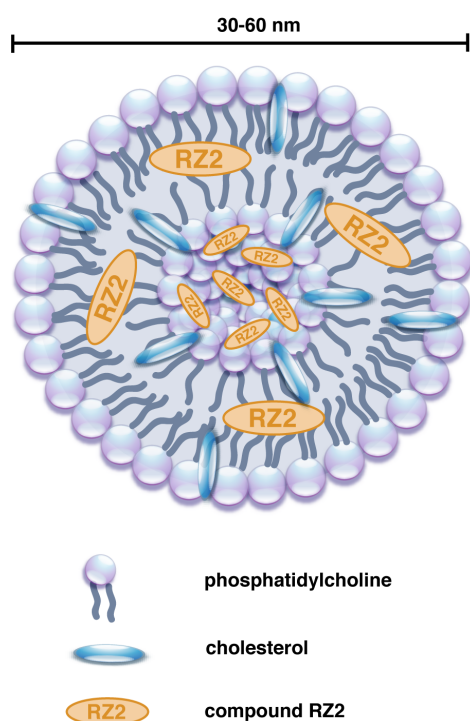


**Figure 56.** Liposomal formulation of compound RZ2.

Next, HeLa cells viability was evaluated after 24 h treatment with RZ2 alone or entrapped into SUVs and equivalent IC<sub>50</sub> values were obtained (IC<sub>50</sub> = 2.2 µM). However, the solubility of the molecule was significantly improved.

As shown in Figure 57, even though compound RZ2 displays a low micromolar IC<sub>50</sub> value, its low solubility impedes the reaching of tumor-cells' viability below 30%, even if employing very high concentrations of the cytotoxic compound. On the other hand, the liposomal formulation notoriously enhances the cells' uptake of compound RZ2, thus allowing the cytotoxic agent to be distributed in a more even manner so that its biological activity is achieved in the expected sigmoidal dose-response way characteristic of all soluble drugs, where 100% cytotoxicity is reached at very high concentrations.

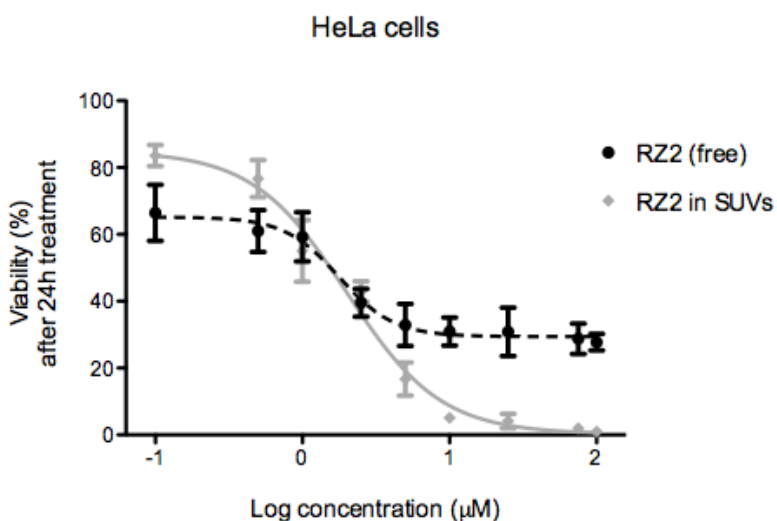


**Figure 57.** MTT viability measurements of HeLa cells after incubation with compound RZ2 alone or entrapped in SUVs (non-normalized data).

### Antibacterial activity evaluation

Quinoxalines are organic heterocycle compounds that have been used as base of synthesis of bioactive derivatives.<sup>69–71</sup> Several research groups have reported their potential as chemotherapeutic molecules due to their antibacterial activity.<sup>72,73</sup> Additionally, the synthesized compounds during the present PhD project are simplified analogues of the so-called "quinoxaline antibiotic" triostin A, which shows activity against Gram-positive bacteria<sup>74</sup> due to the DNA binding of its 2-quinoxalinecarboxylic acid moieties, inducing inhibition of RNA synthesis.<sup>75</sup>

So, it was decided to test some of the members of the RZ1-RZ12 library for their antibacterial activity against four different microorganisms:

- *Escherichia coli* (Gram-negative, rod-shaped facultative anaerobic bacterium)
- *Acinetobacter baumannii* (Gram-negative coccobacillus aerobic bacterium)
- *Pseudomonas aeruginosa* (Gram-negative coccobacillus aerobic bacterium)
- *Staphylococcus aureus* (Gram-positive coccal facultative anaerobic bacterium)

The tested compounds were RZ2, RZ5, RZ7, and RZ8.

Minimum inhibitory concentrations (MICs) were determined by the microdilution method as described by the Clinical and Laboratory Standards Institute.<sup>76</sup>

Briefly, isolated colonies of each type or microorganism were selected from primary agar plates and a suspension of bacteria of appropriate concentration in Mueller-Hinton broth was tested against varying concentrations of the selected compounds in serial two-fold dilutions.

Unfortunately, none of the tested compounds showed any antibacterial activity, with MICs over 256 mg/L.

Additionally, the antibacterial activity of the peptide library Z1-Z12 was also tested against *E. coli*, but as shown in Figure 58, no growth inhibition was observed with either of the peptides.

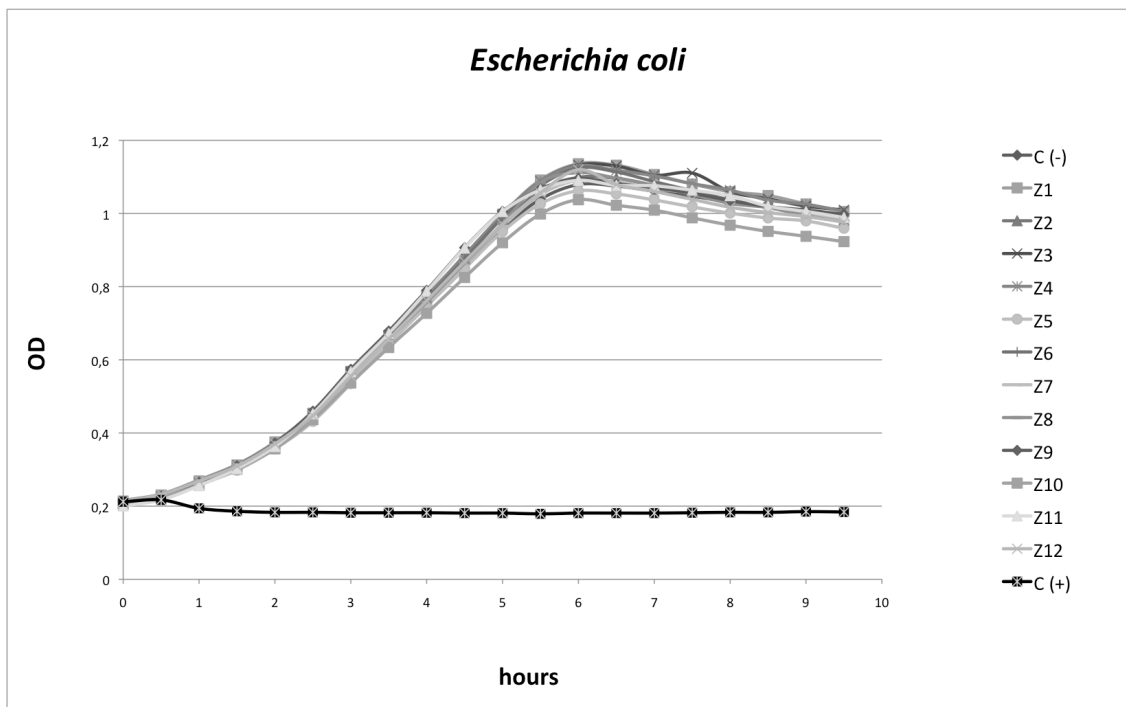


Figure 58. Effect of the peptide library Z1-Z12 on the growth of *E. coli*.

### Antiviral activity evaluation

In recent years, some indoloquinoxalines and benzoindoloquinoxalines have been reported as antivirals and interferon inducers.<sup>77,78</sup> Also, some hydrazinylquinoxalinones were reported as inhibitors of the Epstein-Barr virus early antigen (EBV-EA) activation.<sup>79</sup>

So, it was decided to explore the potential antiviral activity of the most active compounds from the antitumor activity assays, i.e. compounds RZ2 and RZ8. They were evaluated on human coronavirus (HCoV) strain 229E and on respiratory syncytial virus (RSV) strain A2. The cell culture models used to study the effect of the compounds were MRC-5 lung fibroblasts cells for HCoV and HEp2, human laryngeal epidermoid carcinoma cells for RSV.

As displayed in Figure 59 neither compound RZ2 nor RZ8 had any inhibitory capacity on HCoV or RSV in the concentration range tested (0.025-25  $\mu$ M).

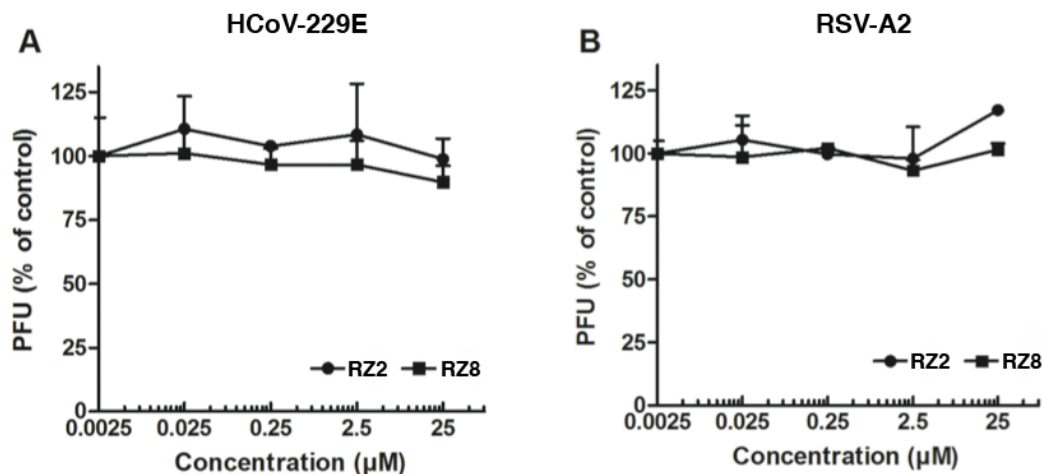


**Figure 59.** Antiviral activity of compounds RZ2 and RZ8.

### Antiplasmodial activity evaluation

Regarding the antiparasitic activity of quinoxaline-containing compounds, several scientific publications have reported that some quinoxaline derivatives are biologically active against *Trypanosoma cruzi*,<sup>80</sup> *Leishmania infantum*, *Leishmania amazonensis*, and *Plasmodium falciparum*.<sup>81</sup>

So, it was decided to test the antiplasmodial activity of compounds RZ2, RZ5, RZ7, and RZ8 at a single concentration of 20  $\mu$ M each, at two different time-points as to evaluate their effect on trophozoites and schizont.

As shown in Figure 60, compounds RZ5, RZ7 and RZ8 are slightly toxic to *Plasmodium falciparum*, however, RZ2 is very active against the parasite at the tested concentration of 20  $\mu$ M. It is worth to highlight that RZ2 is the most active compound against tumor cancer cell lines, and the same was observed for *P. falciparum* inhibition, somewhat confirming the great potential of this newly synthesized compound not only as antitumor drug, but also as antiparasitic molecule.

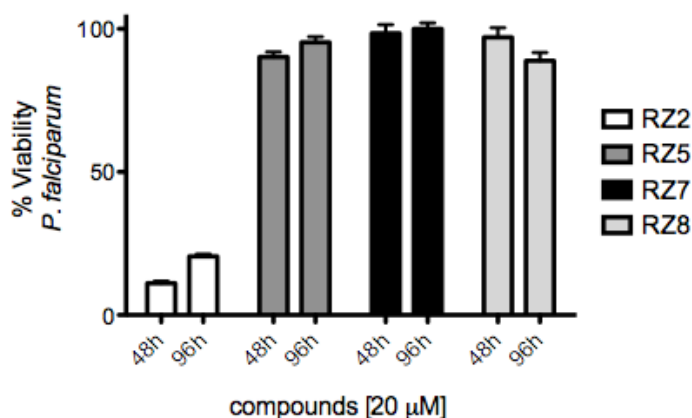


**Figure 60.** Antiplasmodial activity of some compounds from the RZ1-RZ12 library.

#### Hemocompatibility of compound RZ2

In order to predict the hemocompatibility of our hit compound, its capacity to cause red blood cells hemolysis was characterized. Melittin, a cytotoxic peptide from honeybee venom that lyses human erythrocytes, was used as positive control.<sup>82</sup>

The results clearly show that at concentrations up to 100  $\mu$ M RZ2 was not hemolytic *ex vivo* (Figure 61), pointing out the great potential of this compound in antiplasmodial treatment without nocive effects on human red blood cells.

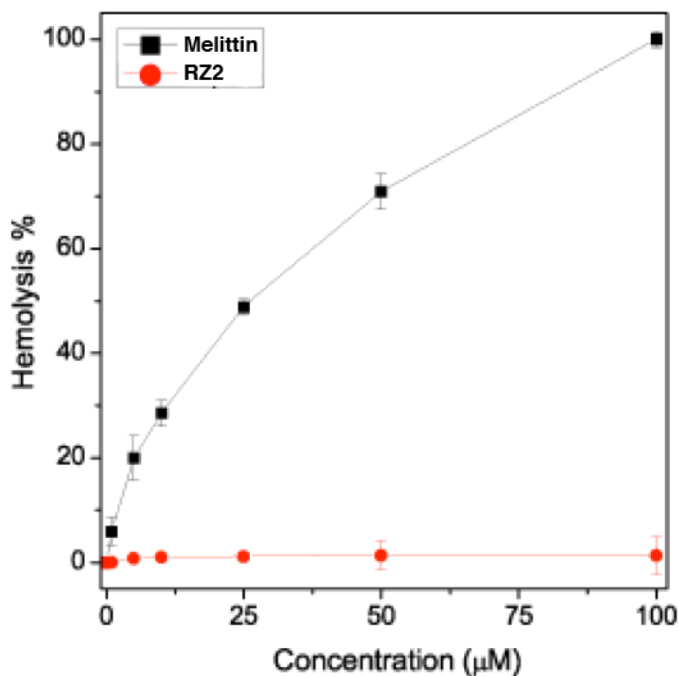


**Figure 61.** Hemolysis assay of compound RZ2.

## MATERIALS AND METHODS

### Antitumoral activity assays

#### ***Cells and cell culture (tumor cell lines)***

Cell culture media and FBS were obtained from Life Technologies Corporation (California, USA) and Thiazolyl Blue Tetrazolium Bromide (MTT) from Sigma-Aldrich (St. Louis, USA). The four human cell lines were obtained from the American Type Culture Collection (ATCC). The HeLa cervical adenocarcinoma cells were grown in DMEM, A-549 lung carcinoma cells in F-12K Medium and SK-BR-3 breast adenocarcinoma and HT-29 colon adenocarcinoma cells in McCoy's 5a Medium Modified, all of them supplemented with 10% fetal bovine serum (FBS), 2 mM L-glutamine and antibiotics. Cells were sub-cultured twice a week and maintained at 37 °C in a humidified atmosphere containing 5% CO<sub>2</sub>. For sub-culturing, cells were detached from culture flasks by incubation with 0.25% trypsin-EDTA 3 min (at 37 °C, 5% CO<sub>2</sub>). Trypsinated cells were centrifuged at 1000 rpm for 10 min at room temperature and gently resuspended in 5 mL of fresh medium preheated at 37 °C. Cellular density was determined in a Neubauer counting plate and the appropriate volume of cells was placed into a fresh culture flask or a 96-well plate. After 12 h incubation, cells were completely attached to the surface.

#### ***Cells and cell culture (brain endothelial primary cells)***

Prior to cells plating, culture flasks were coated with collagen type IV and fibronectin by adding 6 mL of collagen (10 µg/ mL in H<sub>2</sub>O 0.1% v/v acetic acid) for at least 2 h at room temperature, followed by 3 washes with PBS and addition of 5 mL fibronectin (10 µg/mL in PBS) for at least 30 min. Coated flask should be aspirated and used immediately.

Human brain endothelial cells (ScienCell Research laboratories) were maintained in DMEM (4500 mg/L glucose) containing 10% heat inactivated fetal calf serum, 2 mM glutamine, 25 mM HEPES, 5 mL of MEM non-essential amino acids, 50 U/mL penicillin, and 0.05 g/mL streptomycin, and incubated at 37 °C and 5% CO<sub>2</sub>. Culture medium was changed every other day. Trypsinization of cells was done with 0.25% trypsin-EDTA during 5 min at room temperature. Cellular density was determined in a Neubauer counting plate and the appropriate volume of cells was placed into a freshly coated culture flask or a 96-well plate. After 20 h incubation, cells were completely attached to the surface.

### ***Cell growth inhibition assays***

Normally growing cells were plated into 96-well plates and incubated for 24 h at 37 °C to allow attachment to the plate surface. The number of cells plated per well was determined in the

preliminary studies done to determine the best conditions for the MTT assay for each cell line tested. Samples were then added in different concentrations dissolved in a DMSO-PBS vehicle (less than 1% in culture medium). Drugs were run in triplicate or greater and control wells contained appropriate percentages of vehicle. After 24 h or 35 h exposure (as previously determined), the antitumor effect was measured using a solution of MTT, which is bioreduced by viable cells into formazan. The formed crystals were solubilized using DMSO and the amount of formazan was measured by reading the absorbance at 570 nm and 630 nm. The absorbance of wells containing only the MTT reagent (the plate blank) was subtracted from all wells.

The IC<sub>50</sub> values were determined by dose response curve analysis and statistical analysis using GraphPad Prism software version 5.0a.

### ***Stability assays***

For human serum degradation, RZ2 was incubated directly with the serum. For cathepsin B cleavages, 3 µL of a dilution (1/10) of enzyme stock solution ( $\geq$  2000 units/mg) was added to the activation buffer (30 mM DTT, 15 mM EDTA). After 15 min at RT, reaction buffer (1 mM EDTA, 25 mM acetate buffer pH 5.0) and RZ2 solution were added to previously activated cathepsin B solution. For MMP-2 cleavages, 2 µL of enzyme solution (25 mg/mL) was added directly to the reaction buffer (10 mM CaCl<sub>2</sub>, 100mM NaCl, 50 mM Tris pH 7.5), and RZ2 was then added. For the three digestions, the final peptide concentration was 40 µM, except for the human serum that was 100 µM, and the final solution was incubated at 37 °C. Aliquots from cathepsin B and MMP-2 samples were removed at several time points and were immediately frozen in liquid nitrogen and stored. Each sample was defrosted individually, and the compound was rapidly analyzed quantitatively by RP-HPLC. For human serum samples, an aliquot of 50 µL was mixed with 250 µL of cold ethanol, after 30 min of centrifugation (13,000 rpm) the supernatant was evaporated and, finally, each dry sample was re-dissolved with 5 µL of DMSO and, afterwards, 95 µL of water were added. In the end, the samples were analyzed by RP-HPLC.

### ***RZ2 entrapment in liposomes***

Aliquots containing the appropriate amount of lipid (EPC/Chol at a molar ratio of 5:1) in chloroform/methanol (1:1, v/v) and compound RZ2 in DMSO were placed in a test tube, the solvents were removed by evaporation under a stream of O<sub>2</sub>-free nitrogen, and finally, traces of solvents were eliminated under vacuum in the dark for more than 3 h. The lipid-RZ2 film was resuspended in PBS buffer and incubated either at 25 °C with intermittent vortexing for 30 min to hydrate the sample and obtain multilamellar vesicles (MLV). Afterwards, the sample was frozen and thawed five times to ensure complete homogenization and maximization of RZ2/lipid contacts with occasional vortexing. Small unilamellar vesicles (SUV) were prepared from MLVs

using a Branson 250 sonifier (40W) equipped with a titanium microtip until the suspension became transparent. Every 30 s, the sample was cooled for 90 s in ice to prevent overheating of the solution. Finally, a PD-10 column was used to separate non-entrapped peptide from peptide-loaded SUVs.

### **Antibacterial activity assays**

#### ***Turbidity standard for inoculum preparation***

To standardize the inoculum density for the susceptibility test, a BaSO<sub>4</sub> turbidity standard equivalent to a 0.5 McFarland standard should be prepared by adding a 0.5 mL aliquot of 0.048 mol/L BaCl<sub>2</sub> (1.175% w/v BaCl<sub>2</sub>•2H<sub>2</sub>O) to 99.5 mL of 0.18 mol/L (0.36 N) H<sub>2</sub>SO<sub>4</sub> (1% v/v) with constant stirring to maintain a suspension. The correct density of the turbidity standard is verified by measuring absorbance using a spectrophotometer with a 1-cm light path and matched cuvettes. The absorbance at 625 nm should be 0.08 to 0.13 for the 0.5 McFarland standard.

The barium sulfate suspension is transferred in 4 to 6 mL aliquots into screw-cap tubes of the same size as those used for standardizing the bacterial inoculum. The sealed tubes are stored in the dark at room temperature. The barium sulfate standards should be replaced or their densities verified monthly.

#### ***Broth microdilution method***

This method is called “microdilution,” because it involves the use of small volumes of broth dispensed in sterile, plastic microdilution trays that have round or conical bottom wells. Each well should contain 0.1 mL of broth. The most convenient method of preparing microdilution trays is by use of a dispensing device and antimicrobial dilutions made in at least 10 mL of broth. These dilutions are used to dispense 0.1 ( $\pm 0.02$ ) mL into each of the 96 wells of a standard tray. If the inoculum is to be added by pipette, the antimicrobial solutions are prepared at twice the desired final concentration, and the wells filled with 0.05 mL instead of 0.1 mL. Each tray should include a growth control well and a sterility (uninoculated) well.

A standardized inoculum is prepared using either the direct colony suspension or growth method. Within 15 minutes of preparation, the adjusted inoculum suspension is diluted in broth so that, after inoculation, each well contains approximately  $5 \times 10^4$  CFU/mL. A purity check of the inoculum suspension is performed by subculturing an aliquot onto a nonselective agar plate for simultaneous incubation. To prevent drying, the tray is sealed with a tight-fitting plastic cover before incubating.

The amount of growth in the wells containing the antibiotic with the amount of growth in the growth-control wells is compared. For a test to be considered valid, acceptable growth ( $\geq 2$  mm button or definite turbidity) must occur in the growth-control well.

### **Antiviral activity assays**

#### ***Cells and viruses***

Human laryngeal epidermoid carcinoma (HEp-2) and lung fibroblasts (MRC-5) cells (obtained from the ATCC) were grown in Dulbecco's modified Eagle's medium (DMEM) supplemented with 8% fetal calf serum (FCS), 60  $\mu\text{g}/\text{mL}$  of penicillin and 100  $\mu\text{g}/\text{mL}$  of streptomycin. The cells were seeded the day prior to the experiments to be used at ~70% confluence. A laboratory strain A2 of RSV was purchased from ATCC (VR-1540). This preparation of A2 strain was reported to be free from adenovirus contamination.<sup>83</sup> The strain 229E of HCoV was also purchased from ATCC (VR740).

The virus stocks were prepared in HEp-2 and MRC-5 cells respectively, and stored at -80 °C in the presence of 25% sucrose.<sup>84</sup>

#### ***Viral plaque assay***

HEp-2 and MRC-5 cells growing in cluster 12-well plates were washed and 0.4 mL of DMEM-FA containing the test compounds at a final concentration range of 0.025-25  $\mu\text{M}$  were added. Subsequently ~100 PFU of RSV A2 strain or ~100 PFU of HCoV strain 229E in 100  $\mu\text{L}$  of DMEM-FA were added and the cells were incubated for 2-3 h at 37 °C in a humidified 5% CO<sub>2</sub> atmosphere. The medium was then collected and 1.5 mL of 1% methylcellulose solution in DMEM-FA supplemented with respective concentrations of test compounds was added. After 3 days of incubation the cells were stained with 0.25% crystal violet in water solution of 16% ethanol, 1% formaldehyde, and 1% acetic acid and the viral plaques counted.

### **Antiplasmodial activity assays**

#### ***Treatment of blood***

Human blood group B, collected in citrate-phosphate-dextrose (CPD) buffer, was provided by the *Banc de Sang i Teixits* at the *Hospital Vall d'Hebron* in Barcelona ([www.bancsang.net/ca](http://www.bancsang.net/ca)). 10 mL of full blood was collected in 50 mL centrifuge tubes, spun for 5 min at 1200  $\text{g}$ , and plasma and buffy coat were removed. The resulting RBC pellet was resuspended in 40 mL of washing medium containing 10.4 g/L RPMI-1640 (Invitrogen), 25 mM HEPES, 100  $\mu\text{M}$  hypoxanthine, 12.5  $\mu\text{g}/\text{mL}$  gentamicin, and 23.8 mM sodium bicarbonate, pH 7.2. After

centrifugation at 1200 g for 10 min the supernatant was discarded, and after another washing step in 15 mL tubes, the RBC pellet was taken up in one volume of Roswell Park Memorial Institute (RPMI) complete medium (washing medium supplemented with 0.5% Albumax, 0.2% glucose, 25 µg/mL gentamicin, 50 µg/mL hypoxanthine, and 2 mM glutamine), stored at 4 °C and used within 10 days (washed RBCs).

#### ***Plasmodium falciparum* cell culture**

Cultures of *P. falciparum* were grown *in vitro* in group B human RBCs using previously described conditions.<sup>85</sup> Briefly, parasites (thawed from glycerol stocks) were cultured at 37 °C in Petri dishes containing RBCs in RPMI complete medium under a gas mixture of 92% N<sub>2</sub>, 5% CO<sub>2</sub>, and 3% O<sub>2</sub>. Synchronized cultures were obtained by 5% sorbitol lysis,<sup>86</sup> and the medium was changed every 2 days maintaining 3% hematocrit.

For culture maintenance, parasitemias were kept below 5% late forms by dilution with washed RBCs.

#### ***Plasmodium falciparum* growth inhibition assays**

Parasitemia was adjusted to 1.5% with more than 90% of parasites at ring stage after sorbitol synchronization. 200 µL of this *Plasmodium* culture was plated in 96-well plates and incubated in the presence of the compounds for 48 and 96 h in the conditions described above. Parasitemia was determined by fluorescence-assisted cell sorting (FACS).

For FACS analysis, several nucleic acid dyes had been assayed and Syto 11 was found to be the best stain for the discrimination of parasitized from non-parasitized RBCs. Each sample was diluted at 1:100 in PBS and Syto 11 (0.5 mM in DMSO) was added to a final concentration of 0.5 µM. Samples were analyzed using an FC500 flow cytometer (Coulter Corporation, Miami, Florida), set up with the standard configuration. Excitation of the sample was done using a standard 488 nm air-cooled argon-ion laser at 15 mW power. Forward scatter and side scatter were used to gate the RBC population. Syto 11 green fluorescence was collected in a logarithmic scale with a 550 dichroic long filter and a 525 band pass filter. The single-cell population was selected on a forward-side scatter scattergram, and the fluorescence from this population was analyzed. Parasitemia was expressed as the number of parasitized cells per 100 erythrocytes.

***Red blood cells lysis assay***

Human blood was collected in 10 mL EDTA Vacutainer tubes. A small aliquot was assessed for evidence of hemolysis by centrifugation at 800 g for 10 min, and non-hemolyzed samples were carried forward into the assay. Red blood cells (RBCs) were washed three times in PBS pH 7.4 by centrifuging at 800 g for 10 min and resuspending in the same buffer to yield a 10x dilution. RBCs were then diluted in appropriate pH buffer to yield approximately  $\pm 15 \times 10^7$  cells/100  $\mu\text{L}$  PBS in Costar 3797 round-bottom 96-well plates for the lysis assay. The micro titer plate was covered with a low evaporation lid and incubated in a 37 °C warm room for 1 h to induce hemolysis. Negative controls were PBS, while positive controls were 1% v/v solution of Triton X-100 (100% lysis). The plate was then centrifuged at 800 g for 10 min and 80  $\mu\text{L}$  of supernatants were transferred to a Costar 3632 clear bottom 96-well plate. Hemoglobin's absorbance was read at 560 nm using the ELx800 absorbance microplate reader. The results were expressed as percentage of hemoglobin released relative to the positive control (Triton X-100).

## REFERENCES

- (1) Welsch, M. E.; Snyder, S. A.; Stockwell, B. R. *Curr. Opin. Chem. Biol.* **2010**, *14*, 347–361.
- (2) Bird, C. W. *Tetrahedron* **1992**, *48*, 335–340.
- (3) Lumbroso, H.; Curé, J.; Konakahara, T.; Takagi, Y. *J. Mol. Struct.* **1980**, *68*, 293–305.
- (4) Carta, A.; Corona, P.; Loriga, M. *Curr. Med. Chem.* **2005**, *12*, 2259–2272.
- (5) Asif, H.; Diwakar, M. *J. Pharm. Res.* **2011**, *4*, 924.
- (6) Guirado, A.; López Sánchez, J. I.; Ruiz-Alcaraz, A. J.; Bautista, D.; Gálvez, J. *Eur. J. Med. Chem.* **2012**, *54*, 87–94.
- (7) Gazit, A.; Yee, K.; Uecker, A.; Böhmer, F. D.; Sjöblom, T.; Ostman, A.; Waltenberger, J.; Golomb, G.; Banai, S.; Heinrich, M. C.; Levitzki, A. *Bioorg. Med. Chem.* **2003**, *11*, 2007–2018.
- (8) Galal, S. A.; Abdelsamie, A. S.; Soliman, S. M.; Mortier, J.; Wolber, G.; Ali, M. M.; Tokuda, H.; Suzuki, N.; Lida, A.; Ramadan, R. A.; El Diwani, H. I. *Eur. J. Med. Chem.* **2013**, *69*, 115–124.
- (9) Guillou, J.; Le Borgne, M.; Rimbault, C.; Moreau, S.; Savrimoutou, S.; Pinaud, N.; Baratin, S.; Marchivie, M.; Roche, S.; Bollack, A.; Pecci, A.; Alvarez, L.; Desplat, V.; Jose, J. *Eur. J. Med. Chem.* **2013**, *65*, 205–222.
- (10) Baffert, F.; Régnier, C. H.; De Pover, A.; Pissot-Soldermann, C.; Tavares, G. A.; Blasco, F.; Brueggen, J.; Chène, P.; Drueckes, P.; Erdmann, D.; Furet, P.; Gerspacher, M.; Lang, M.; Ledieu, D.; Nolan, L.; Ruetz, S.; Trappe, J.; Vangrevelinghe, E.; Wartmann, M.; Wyder, L.; Hofmann, F.; Radimerski, T. *Mol. Cancer Ther.* **2010**, *9*, 1945–1955.
- (11) Loftus, D. J.; Stolk, J. M.; U'Prichard, D. C. *Life Sci.* **1984**, *35*, 61–69.
- (12) Lee, S.-H.; Kim, N.; Kim, S.-J.; Song, J.; Gong, Y.-D.; Kim, S.-Y. *J. Cancer Res. Clin. Oncol.* **2013**, *139*, 1279–1294.
- (13) Sharma, B. K.; Singh, P. *J. Enzyme Inhib. Med. Chem.* **2007**, *22*, 165–169.
- (14) Högen, N.; Stange, H.; Schindler, R.; Lankau, H.-J.; Grunwald, C.; Langen, B.; Egerland, U.; Tremmel, P.; Pangalos, M. N.; Marquis, K. L.; Hage, T.; Harrison, B. L.; Malamas, M. S.; Brandon, N. J.; Kronbach, T. *J. Med. Chem.* **2010**, *53*, 4399–4411.
- (15) Keravis, T.; Lugnier, C. *Br. J. Pharmacol.* **2012**, *165*, 1288–1305.
- (16) Kaizawa, H.; Sugita, M.; Yamamoto, H.; Kamijo, K.; Tsuchiya, K.; Seo, R.; Yamamoto, S. Quinoxaline compound. WO/2012/033101, March 16, 2012.
- (17) Nishimura, N.; Siegmund, A.; Liu, L.; Yang, K.; Bryan, M. C.; Andrews, K. L.; Bo, Y.; Booker, S. K.; Caenepeel, S.; Freeman, D.; Liao, H.; McCarter, J.; Mullady, E. L.; San Miguel, T.; Subramanian, R.; Tamayo, N.; Wang, L.; Whittington, D. A.; Zalameda, L.; Zhang, N.; Hughes, P. E.; Norman, M. H. *J. Med. Chem.* **2011**, *54*, 4735–4751.
- (18) Miller, T. W.; Rexer, B. N.; Garrett, J. T.; Arteaga, C. L. *Breast cancer Res.* **2011**, *13*, 224.
- (19) Yongzhou, H.; Peng, W.; Lei, Z.; Liu, X.; Liu, T.; Yang, B.; He, Q. Substituted quinoxalinamine compounds, and preparation method and application thereof. CN 102250022, December 16, 2011.
- (20) Allen, D. R.; Buckley, G. M.; Bürli, R.; Davenport, R. J.; Kinsella, N.; Lock, C. J.; Lowe, C.; Mack, S. R.; Pitt, W. R.; Ratcliffe, A. J.; Richard, M. D.; Sabin, V. M.; Sharpe, A.; Tait, L. J.; Warrelow, G. J.; Williams, S. C. Quinoxaline and quinoline derivatives as kinase inhibitors. WO2009081105, July 03, 2009.
- (21) Mielcke, T. R.; Mascarello, A.; Filippi-Chiela, E.; Zanin, R. F.; Lenz, G.; Leal, P. C.; Chiaradia, L. D.; Chirardia, L. D.; Yunes, R. A.; Nunes, R. J.; Battastini, A. M. O.; Morrone, F. B.; Campos, M. M. *Eur. J. Med. Chem.* **2012**, *48*, 255–264.

- (22) Osborne, J. K.; Zaganjor, E.; Cobb, M. H. *Cell Res.* **2012**, *22*, 14–22.
- (23) Santarpia, L.; Lippman, S. M.; El-Naggar, A. K. *Expert Opin. Ther. Targets* **2012**, *16*, 103–119.
- (24) Ramurthy, S.; Costales, A.; Jansen, J. M.; Levine, B.; Renhowe, P. A.; Shafer, C. M.; Subramanian, S. *Bioorg. Med. Chem. Lett.* **2012**, *22*, 1678–1681.
- (25) Bemis, G. W.; Duffy, J. P. Quinoxalines useful as inhibitors of protein kinases. WO2005056547, June 24, 2005.
- (26) Efremov, D. G.; Laurenti, L. *Expert Opin. Investig. Drugs* **2011**, *20*, 623–636.
- (27) Pamuk, O. N.; Tsokos, G. C. *Arthritis Res. Ther.* **2010**, *12*, 222.
- (28) Amar, S.; Belmaker, R. H.; Agam, G. *Curr. Pharm. Des.* **2011**, *17*, 2264–2277.
- (29) Wu, W.; Sun, X.-H. *Acta Biochim. Biophys. Sin. (Shanghai)* **2012**, *44*, 187–196.
- (30) Smits, R. A.; Lim, H. D.; Hanzer, A.; Zuiderveld, O. P.; Guaita, E.; Adami, M.; Coruzzi, G.; Leurs, R.; de Esch, I. J. P. *J. Med. Chem.* **2008**, *51*, 2457–2467.
- (31) Fioravanti, B.; Vanderah, T. W. *Curr. Top. Med. Chem.* **2008**, *8*, 1442–1451.
- (32) Olejnik, O.; Kerslake, E. D. S. Compositions containing alpha-2-adrenergic agonist components. US6673337B2, January 06, 2004.
- (33) Benedini, F.; Impagnatiello, F.; Biondi, S.; Ongini, E.; Chong, W. K. M. Derivatives of alpha2-adrenergic receptor agonist. US2008318965A1, December 25, 2008.
- (34) McCormick, K. D.; Boyce, C. W.; Shih, N.-Y.; Aslanian, R. G.; Fevrier, S.; Mangiaracina, P.; De Lera Ruiz, M.; Yu, Y.; Zheng, J.; Huang, C.-Y.; Liang, B.; Liu, R.-Q.; Liu, R.; Guis, Z. L. 3,4-dihydro-1,4-benzoxazine, 3,4-dihydro-1,4-benzothiazine and 1,2,3,4-tetrahydro-quinoxaline derivatives as alpha2c adrenoreceptor agonists. WO2008100463A1, August 21, 2008.
- (35) Gathercole, L. L.; Lavery, G. G.; Morgan, S. A.; Cooper, M. S.; Sinclair, A. J.; Tomlinson, J. W.; Stewart, P. M. *Endocr. Rev.* **2013**, *34*, 525–555.
- (36) Braun, A.; Mougenot, Patrick Namane, C.; Nicolai, E.; Pacquet, Francois Philippo, Christophe Venier, O.; Crespin, O.; Pascal, C.; Aletru, M.; Gussregen, S. Substituted quinoxalines, their preparation and their therapeutical use as 11 $\beta$ HSD1 modulators. US7947834B2, 2011.
- (37) Liu, C.-H.; Wang, B.; Li, W.-Z.; Yun, L.-H.; Liu, Y.; Su, R.-B.; Li, J.; Liu, H. *Bioorg. Med. Chem.* **2004**, *12*, 4701–4707.
- (38) Gardan, S.; Mayer, S.; Schann, S. Pyrrolo[1,2-a]quinoxaline derivatives as Adenosine A3 receptor modulators and uses thereof. EP1798233A1, June 20, 2007.
- (39) Koscsó, B.; Csóka, B.; Pacher, P.; Haskó, G. *Expert Opin. Investig. Drugs* **2011**, *20*, 757–768.
- (40) Qaisi, A. M. A.; Al Hiari, Y. M. A.; Zahra, J. A. Y.; El Abadelah, M. M. M.; Hussuneh, M. R. A. Quinoline and pyridoquinoxaline derivatives useful as anticancer and/or antibacterial agents. GB2442951A, April 23, 2008.
- (41) Boese, R.; El-Abadelah, M. M.; Zahra, J. A. Y. Indolo[2,3-b]-, Indeno[1,2-b]- and Indeno[2,1-b]pyrido[2,3-f] quinoxaline-3-carboxylic acids and esters, processes for their preparation and their use as antiviral, antibiotic and antitumor agents. EP2128160 A1, December 02, 2009.
- (42) Diana, P.; Martorana, A.; Barraja, P.; Montalbano, A.; Dattolo, G.; Cirrincione, G.; Dall'acqua, F.; Salvador, A.; Vedaldi, D.; Basso, G.; Viola, G. *J. Med. Chem.* **2008**, *51*, 2387–2399.
- (43) Khier, S.; Gattaccea, F.; El Messaoudi, S.; Lafaille, F.; Deleuze-Masquéfa, C.; Bompard, J.; Cooper, J.-F.; Solassol, I.; Pinguet, F.; Bonnet, P.-A.; Bressolle, F. M. M. *Drug Metab. Dispos.* **2010**, *38*, 1836–1847.

- (44) Gerlach, M.; Seipelt, I.; Günther, E.; Schuster, T.; Polymeropoulos, E.; Czech, M.; Claus, E. Quinoxaline derivatives and their use for treating benign and malignant tumour disorders. WO2010115719A1, October 14, 2010.
- (45) Bieda, R.; Ott, I.; Dobroschke, M.; Prokop, A.; Gust, R.; Sheldrick, W. S. *J. Inorg. Biochem.* **2009**, *103*, 698–708.
- (46) Ishikawa, H.; Sugiyama, T.; Yokoyama, A. *Chem. Pharm. Bull. (Tokyo)*. **2013**, *61*, 438–44.
- (47) Madden, D. R.; Thiran, S.; Zimmermann, H.; Romm, J.; Jayaraman, V. *J. Biol. Chem.* **2001**, *276*, 37821–37826.
- (48) Cartigny, D.; Berhal, F.; Nagano, T.; Phansavath, P.; Ayad, T.; Genêt, J.-P.; Ohshima, T.; Mashima, K.; Ratovelomanana-Vidal, V. *J. Org. Chem.* **2012**, *77*, 4544–4556.
- (49) Robarge, K. D.; Brunton, S. A.; Castanedo, G. M.; Cui, Y.; Dina, M. S.; Goldsmith, R.; Gould, S. E.; Guichert, O.; Gunzner, J. L.; Halladay, J.; Jia, W.; Khojasteh, C.; Koehler, M. F. T.; Kotkow, K.; La, H.; Lalonde, R. L.; Lau, K.; Lee, L.; Marshall, D.; Marsters, J. C.; Murray, L. J.; Qian, C.; Rubin, L. L.; Salphati, L.; Stanley, M. S.; Stibbard, J. H. A.; Sutherlin, D. P.; Ubbayaker, S.; Wang, S.; Wong, S.; Xie, M. *Bioorg. Med. Chem. Lett.* **2009**, *19*, 5576–5581.
- (50) Bladh, H.; Larsson, J. Quinoxaline derivatives as neutrophil elastase inhibitors and their use. WO2005021512A1, March 10, 2005.
- (51) Bleicher, K.; Christ, A. D.; Martin, R. E.; Mohr, P. 1-(1-Benzylpiperidin-4-yl)benzimidazole-5-carboxylic acid derivatives for the treatment of diabetes mellitus. WO2008122510A1, 2009.
- (52) Gong, Y.-D.; Jeon, M. K.; Lee, T. H.; Hwang, S. H.; Yoo, S. E. Quinoxaline derivatives and pharmaceutically acceptable salt thereof having mch1r inhibitory activity, process for preparation and use thereof for treating obesity. KR20090090792A, 2009.
- (53) Ishizuka, N.; Sakai, K.; Hayashi, K. New utilities of tricyclic compounds. EP2168576A2, March 31, 2010.
- (54) Hu, B.; Unwalla, R. J.; Goljer, I.; Jetter, J. W.; Quinet, E. M.; Berrodin, T. J.; Basso, M. D.; Feingold, I. B.; Nilsson, A. G.; Wilhelmsson, A.; Evans, M. J.; Wrobel, J. E. *J. Med. Chem.* **2010**, *53*, 3296–3304.
- (55) Mosmann, T. *J. Immunol. Methods* **1983**, *65*, 55–63.
- (56) Van Meerloo, J.; Kaspers, G. J. L.; Cloos, J. In *Methods in molecular biology*; Cree, I. A., Ed.; 2008; Vol. 731, pp. 237–245.
- (57) Shoji, J. I.; Katagiri, K. *J. Antibiot. (Tokyo)*. **1961**, *14*, 335–339.
- (58) Pérez Baz, J.; Cañedo, L. M.; Fernández Puentes, J. L.; Silva Elipe, M. V. *J. Antibiot. (Tokyo)*. **1997**, *50*, 738–741.
- (59) Yoshino, H.; Nakazawa, T.; Arakawa, Y.; Kaneko, T.; Tsuchiya, Y.; Matsunaga, M.; Araki, S.; Ikeda, M.; Yamatsu, K.; Tachibana, S. *J. Med. Chem.* **1990**, *33*, 206–212.
- (60) Tulla-Puche, J.; Marcucci, E.; Prats-Alfonso, E.; Bayó-Puxan, N.; Albericio, F. *J. Med. Chem.* **2009**, *52*, 834–839.
- (61) Powell, M. F.; Stewart, T.; Otvos, L.; Urge, L.; Gaeta, F. C.; Sette, A.; Arrhenius, T.; Thomson, D.; Soda, K.; Colon, S. M. *Pharm. Res.* **1993**, *10*, 1268–1273.
- (62) Talvensaari-Mattila, A.; Pääkkö, P.; Turpeenniemi-Hujanen, T. *Br. J. Cancer* **2003**, *89*, 1270–1275.
- (63) Brix, K.; Dunkhorst, A.; Mayer, K.; Jordans, S. *Biochimie* **2008**, *90*, 194–207.
- (64) Storm, G.; Wilms, H. P.; Crommelin, D. J. *Biotherapy* **1991**, *3*, 25–42.
- (65) Maurer, N.; Fenske, D. B.; Cullis, P. R. *Expert Opin. Biol. Ther.* **2001**, *1*, 923–947.
- (66) Hobbs, S. K.; Monsky, W. L.; Yuan, F.; Roberts, W. G.; Griffith, L.; Torchilin, V. P.; Jain, R. K. *Proc. Natl. Acad. Sci. U. S. A.* **1998**, *95*, 4607–4612.
- (67) Bhardwaj, U.; Burgess, D. J. *Int. J. Pharm.* **2010**, *388*, 181–189.

- (68) Abraham, S. A.; Waterhouse, D. N.; Mayer, L. D.; Cullis, P. R.; Madden, T. D.; Bally, M. B. *Methods Enzymol.* **2005**, *391*, 71–97.
- (69) Zanetti, S.; Sechi, L. A.; Molicotti, P.; Cannas, S.; Bua, A.; Deriu, A.; Carta, A.; Paglietti, G. *Int. J. Antimicrob. Agents* **2005**, *25*, 179–181.
- (70) Carta, A.; Paglietti, G.; Rahbar Nikookar, M. E.; Sanna, P.; Sechi, L.; Zanetti, S. *Eur. J. Med. Chem.* **2002**, *37*, 355–366.
- (71) Sanna, P.; Carta, A.; Loriga, M.; Zanetti, S.; Sechi, L. *Farmaco* **1999**, *54*, 169–177.
- (72) Parhi, A. K.; Zhang, Y.; Saionz, K. W.; Pradhan, P.; Kaul, M.; Trivedi, K.; Pilch, D. S.; LaVoie, E. J. *Bioorg. Med. Chem. Lett.* **2013**, *23*, 4968–4974.
- (73) Vieira, M.; Pinheiro, C.; Fernandes, R.; Noronha, J. P.; Prudêncio, C. *Microbiol. Res.* **2013**, <http://dx.doi.org/10.1016/j.micres.2013.06.015>.
- (74) Matsuura, S. *J. Antibiot. (Tokyo)* **1965**, *18*, 43–46.
- (75) Lee, J. S.; Waring, M. J. *Biochem. J.* **1978**, *173*, 115–128.
- (76) CLSI. Performance standards for antimicrobial susceptibility testing, 2008, Seventeenth informational supplement. Document M10.
- (77) Shibinskaya, M. O.; Karpenko, A. S.; Lyakhov, S. A.; Andronati, S. A.; Zholobak, N. M.; Spivak, N. Y.; Samochina, N. A.; Shafran, L. M.; Zubritsky, M. J.; Galat, V. F. *Eur. J. Med. Chem.* **2011**, *46*, 794–798.
- (78) Shibinskaya, M. O.; Lyakhov, S. a; Mazepa, A. V; Andronati, S. a; Turov, A. V; Zholobak, N. M.; Spivak, N. Y. *Eur. J. Med. Chem.* **2010**, *45*, 1237–1243.
- (79) Galal, S. a; Abdelsamie, A. S.; Soliman, S. M.; Mortier, J.; Wolber, G.; Ali, M. M.; Tokuda, H.; Suzuki, N.; Lida, A.; Ramadan, R. A.; El Diwani, H. I. *Eur. J. Med. Chem.* **2013**, *69C*, 115–124.
- (80) Torres, E.; Moreno-Viguri, E.; Galiano, S.; Devarapally, G.; Crawford, P. W.; Azqueta, A.; Arbilla, L.; Varela, J.; Birriel, E.; Di Maio, R.; Cerecetto, H.; González, M.; Aldana, I.; Monge, A.; Pérez-Silanes, S. *Eur. J. Med. Chem.* **2013**, *66*, 324–334.
- (81) Barea, C.; Pabón, A.; Pérez-Silanes, S.; Galiano, S.; Gonzalez, G.; Monge, A.; Deharo, E.; Aldana, I. *Molecules* **2013**, *18*, 4718–4727.
- (82) DeGrado, W. F.; Musso, G. F.; Lieber, M.; Kaiser, E. T.; Kézdy, F. J. *Biophys. J.* **1982**, *37*, 329–338.
- (83) Cameron, R.; Buck, C.; Merrill, D.; Lutnick, A. *Virus Res.* **2003**, *92*, 151–156.
- (84) Gupta, C. K.; Leszczynski, J.; Gupta, R. K.; Siber, G. R. *Vaccine* **1996**, *14*, 1417–1420.
- (85) Cranmer, S. L.; Magowan, C.; Liang, J.; Coppel, R. L.; Cooke, B. M. *Trans. R. Soc. Trop. Med. Hyg.* **1997**, *91*, 363–365.
- (86) Lambros, C.; Vanderberg, J. P. *J. Parasitol.* **1979**, *65*, 418–420.



# **Insights into the mode of action**

---

I would like to thank Dr. Axel Bidón Chanal and Dr. F. Javier Luque, from the *Departament de Fisicoquímica and Institut de Biomedicina (IBUB), Facultat de Farmàcia, Universitat de Barcelona*, for performing the molecular simulations.

I also gratefully acknowledge Dr. Saška Ivanova (IRB Barcelona) for her kind guidance in all the apoptosis and autophagy related experiments.

Work on DNA-binding presented in this chapter was carried out in the Centre for Biological Sciences of the University of Southampton, in Southampton, UK. The PhD candidate spent five months in the United Kingdom as an EMBO short-term fellowship awardee, investigating the sequence specific interaction of ligands with DNA.

Some of the results derived from this internship originated the following publication:

**Zamudio-Vázquez, R.; Albericio, F.; Tulla-Puche, J.; Fox, K. R. *ACS Med. Chem. Lett.* **2013**.**

DOI: 10.1021/ml400323x

## INTRODUCTION

### Cell death mechanisms

The Nomenclature Committee on Cell Death (NCCD) defines different cell death types according to morphological criteria and suggests discrimination between dying as a process and death as an end point. Moreover, it is recommended to take into account that several mechanisms can lead to cell death, but not all of them are necessarily present when this occurs.

The following morphological and/or molecular criteria are met when cell death happens:

- The cell has entirely lost the integrity of the plasma membrane
- The cell and its nucleus have undergone complete fragmentation into "apoptotic bodies"
- *In vivo*, the fragmented cell has been engulfed by an adjacent cell

On the other hand, "dying cells" are in the process of cell death, characterized by reversible processes such as:

- Massive caspase activation
- Loss of the mitochondrial transmembrane potential ( $\Delta\psi_m$ )
- Permeabilization of the outer mitochondrial membrane
- Exposure of phosphatidylserine residues on the plasma membrane

Cell death has been categorized into at least three mechanisms: necrosis, apoptosis and autophagy (Figure 62). Paradoxically, autophagy is a process that also allows cells to escape cell death.<sup>1</sup>

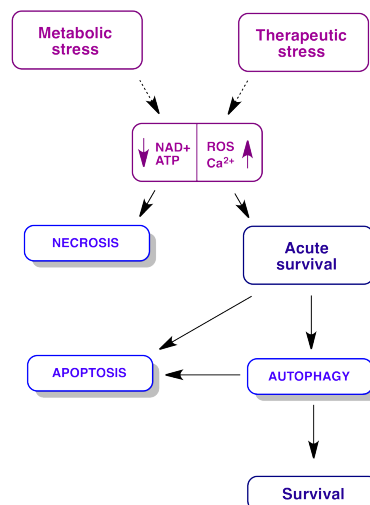


**Figure 62.** The relationship between necrosis, apoptosis and autophagy.

Necrosis is an irreversible inflammatory form of cell death, in which the plasma membrane suffers total disruption leading to the spillage of the intracellular content into the surroundings thus activating the host immune system as a damage response.<sup>2</sup> Because of this, necrosis has been considered an unprogrammed mechanism. However, increasing evidence suggests that there are specific regulators that lead this death pathway.<sup>3,4</sup>

Several studies have identified some regulators of death receptor-induced necrotic cell death: the receptor-interacting protein kinase 1 (RIPK1) and the tumor necrosis factor (TNF) receptor-associated factor 2 (TRAF2).<sup>5,6</sup> Activation of RIPK1 leads to its translocation to the inner mitochondrial membrane, resulting in ATP depletion and the accumulation of ROS.<sup>7</sup> High intracellular calcium concentrations and ROS lead to membrane permeabilization and irreversible necrotic cell death.<sup>8</sup>

"Oncosis" is the term that defines cell death morphology with mechanical rupture of the plasma membrane, cytoplasmic swelling, dilation of cytoplasmic organelles, as well as moderate chromatin condensation (see Figure 63). This morphological appearance is that of necrosis, as well as partial apoptosis evolving into necrosis.<sup>9</sup>



**Figure 63.** Example of necrotic cells after treatment with TFE.

Apoptosis is an inherently controlled and continual phenomenon throughout the life of organisms where it plays a vital role in development, physiology and homeostasis under both physiological and pathological conditions, and can be initiated or inhibited by a variety of environmental stimuli.<sup>10</sup> The apoptotic pathway is triggered when damage within the cell caused by radiation, toxins or external environmental stressors can no longer be repaired. This death signal then involves widespread proteolysis by caspases, nucleosomal fragmentation by endonucleases, and cell surface tagging for phagocyte engulfment.<sup>11</sup>

Apoptosis is regulated by many molecules, such as the pro- and anti-apoptotic proteins, and consists of two pathways, the extrinsic and the intrinsic pathway. Although the two of them act independently at the beginning, they converge during the activation of the caspase cascade.<sup>12</sup>

Proteins such as Bcl-2, Bcl-extra long (Bcl-xL) and myeloid cell leukaemia-1 (Mcl-1) act in an anti-apoptotic manner.<sup>13</sup> On the contrary, proteins such as Bax and BH3-homologous agonist killer (Bak) act in a pro-apoptotic manner forming pores in the outer mitochondrial membrane, thus allowing other pro-apoptotic proteins to enter the cytosol and activate effector caspases.<sup>14</sup> Other pro-apoptotic proteins that also belong to the Bcl-2 family include BH3-interacting domain death agonist (Bid), Bcl-2 interacting mediator (Bim), Bcl-2 interacting killer (Bik), Bcl-2 modifying factor, Harakiri, Noxa and p53-upregulated modulator of apoptosis (Puma).<sup>15</sup>

Another key protein in the apoptotic death pathway is p53, a tumour suppressor and transcription factor induced by cellular stress. It regulates cell growth, differentiation, transformation, DNA synthesis and repair, and apoptosis. As a transcription factor, it is able to enhance the expression of molecules involved in both the extrinsic and intrinsic apoptotic pathways, but it is also able to suppress the expression of proapoptotic molecules when regulating prosurvival pathways.<sup>16</sup>

Apoptosis is the result of a shifted balance towards the pro-apoptotic molecules that leads to activation of the caspase cascade.<sup>17</sup> These proteinases are divided into three groups:

- 1)** Inflammatory caspases: caspase-1, caspase-4 and caspase-5
- 2)** Initiator caspases: caspase-2, caspase-8, caspase-9 and caspase-10
- 3)** Executioners: caspase-3, caspase-6 and caspase-7

All of them exist within the cell as inactive precursors that are activated by cleavage by other members of the caspase family or by autocatalytic cleavage resulting in cellular death.<sup>18</sup>

The apoptotic extrinsic pathway is triggered by binding of ligands to their respective death receptors, followed by the assembly of the death-inducing signalling complex (FasL, Fas receptor, FADD and procaspase-8). Procaspsases -8 and -10 are cleaved, followed by cleavage of executioner procaspsases.<sup>19</sup>

The intrinsic pathway, also known as the mitochondrial pathway, is caused by the presence of unfolded proteins, genomic stress or metabolic stress. It starts with the permeabilization of the outer mitochondrial membrane and further release of pro- and anti-apoptotic proteins into the cytosol, such as the pro-apoptotic protein cytochrome *c*. This triggers the assembly of the apoptosome, which activates caspase-9, leading to caspase-3 activation followed by cell death.<sup>19,20</sup> However, this pathway can also be activated by caspase-8, followed by release of cytochrome *c* from the mitochondria and procaspase-3 cleavage, resulting in cell death.

One of the hallmarks of cancer cells is their ability to evade apoptosis. This can occur by an increase in antiapoptotic molecules or by a decrease or defective function in proapoptotic

proteins.<sup>21</sup> As the catalogue of genetic and epigenetic defects that can suppress apoptosis in most cancers is expanding, understanding the significance of the alternative stress fates, autophagy and necrosis, has become increasingly important.<sup>22</sup>

Autophagy (*self-eating*) is a tightly regulated catabolic process of self-degradation of cytoplasmic components sequestered in double-membrane autophagosomes that fuse with lysosomes or vacuoles for breakdown by resident hydrolases.<sup>23</sup> It is stimulated by nutrient or growth factor deprivation, hypoxia, reactive oxygen species (ROS), DNA damage, protein aggregates, damaged organelles, or intracellular pathogens.<sup>24</sup> To date, three major types of autophagy have been described: macroautophagy, microautophagy, and chaperone-mediated autophagy. Whereas macroautophagy uses the intermediate organelle "autophagosome" that fuses with the lysosome to become an autolysosome, in microautophagy the lysosome itself engulfs small cytoplasmic components by inward invagination of its membrane and in chaperone-mediated autophagy unfolded proteins are directly delivered into the lysosome through a multimeric translocation complex.<sup>25</sup> Herein we refer to macroautophagy simply as "autophagy".

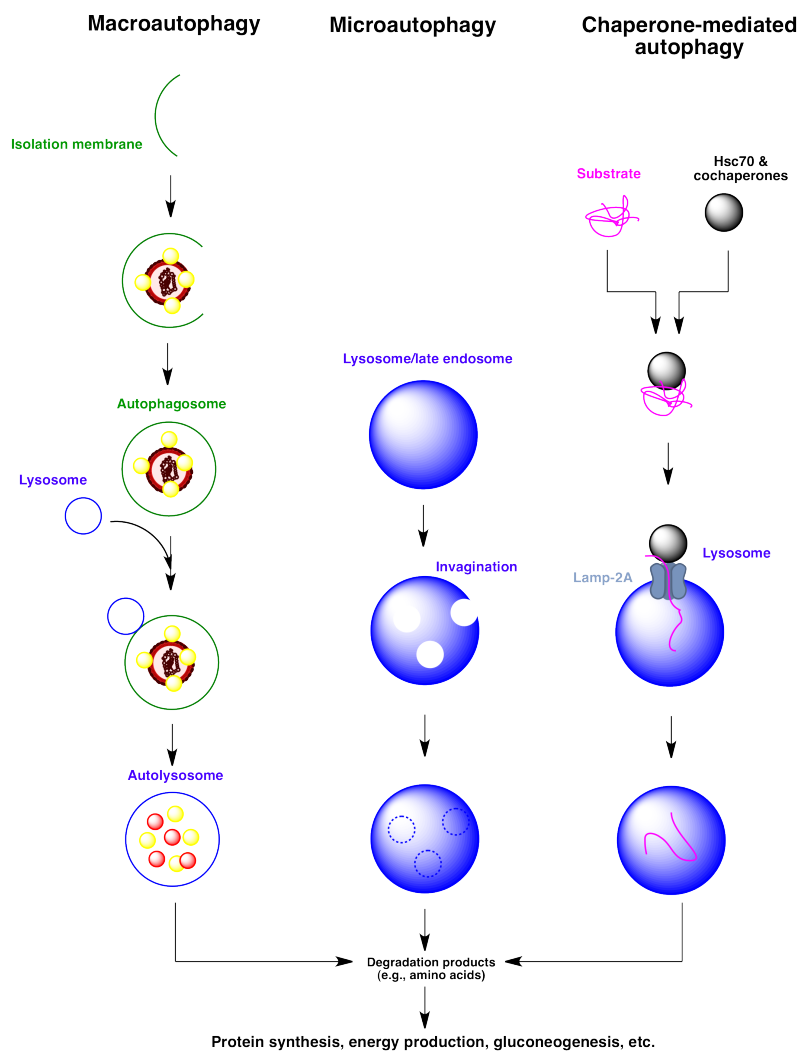


**Figure 64.** Different types of autophagy.

Autophagy has been observed in cancer cells undergoing metabolic and therapeutic stresses, and it is a reversible damage response unlike apoptosis and necrosis.<sup>22</sup> Autophagy promotes cell survival and, in most cases, protects cells against stressful situations by serving as an intracellular mechanism by which cells dispose of damaged organelles and proteins and recycle macromolecules as source of energy or as building blocks for the synthesis of new metabolites.<sup>26–28</sup> This process is under the control of tumor suppressors and oncogenes: the former ones have a stimulatory effect whereas the latter ones down-regulate it.<sup>29</sup> However, the role of autophagy in tumors is complex and ranges from tumor suppressive role to a role in adapting to the environment. Nowadays, combining autophagy-inducing therapies with autophagy inhibitors is currently being tested in several malignancies.

## RESULTS AND DISCUSSION

### DNA-binding assays

The natural antibiotics echinomycin and triostin A bind to GC-rich DNA sequences with micromolar dissociation constants<sup>30,31</sup> and are highly selective for the CpG dinucleotide.<sup>32,33</sup> This sequence selectivity has been demonstrated with several high-resolution structures of these bisintercalators bound to short oligonucleotides due to the formation of hydrogen bonds between the alanine carbonyls and the 2-amino groups of the guanines.<sup>34–37</sup> On the other hand, the synthetic analogue TANDEM,<sup>38</sup> which lacks the four *N*-methyl groups that triostin A bears, binds to AT-rich DNA sequences, with selectivity towards the dinucleotide TpA.<sup>39</sup> This difference in sequence binding arises because removal of the *N*-methyl groups enables the formation of intramolecular hydrogen bonds between the alanine carbonyls and the valine NH groups, as shown by several NMR studies.<sup>40</sup> Another triostin A derivative that resulted AT-selective is an analogue containing *N*-methylcysteine and valine.<sup>41</sup> Both of these synthetic molecules bind with lower affinities than the natural compound, though they display highly cooperative interactions depending on the flanking sequences, with higher affinity to ATAT and not to TTAA.<sup>42–44</sup> It has been also shown that the cross bridge, present in triostin A, does not affect the sequence selectivity, but its removal renders a dramatic decrease in affinity.<sup>45</sup>

It is important to highlight that the quinoxaline chromophores alone do not bind to DNA, as observed with derivatives lacking these intercalating groups.<sup>38</sup> Moreover, replacing the quinoxaline moieties of echinomycin with quinolines increases the affinity for AT-rich DNA sequences.<sup>46,47</sup> Furthermore, other natural bisintercalators with different intercalating moieties than quinoxalines, such as luzopeptins and thiocoraline, bind to DNA with higher affinity but reduced sequence selectivity.<sup>48,49</sup>

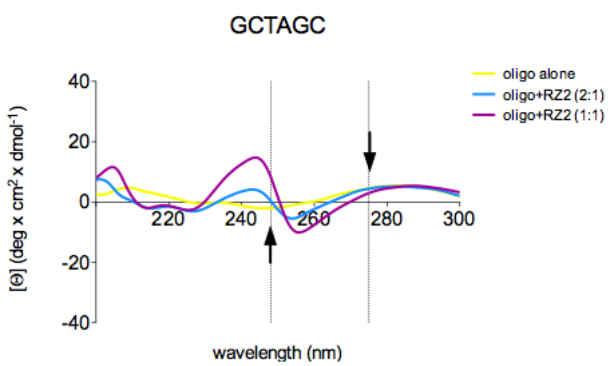
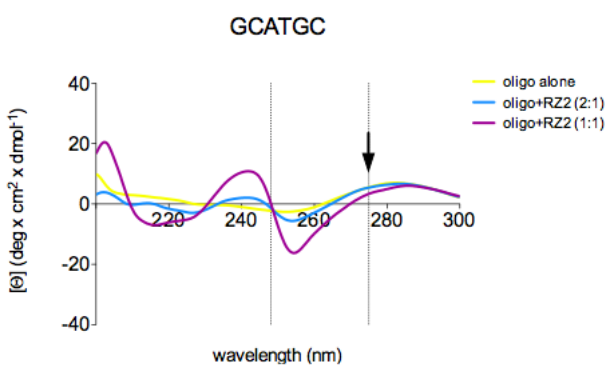
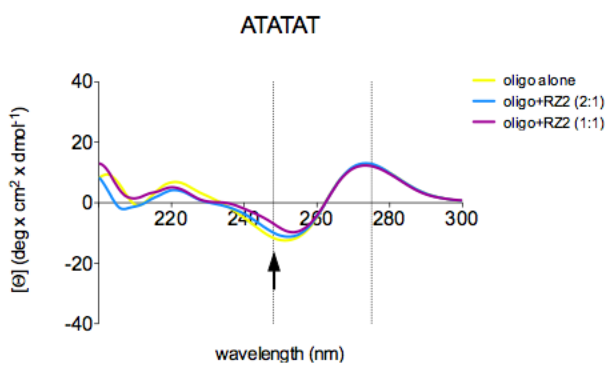
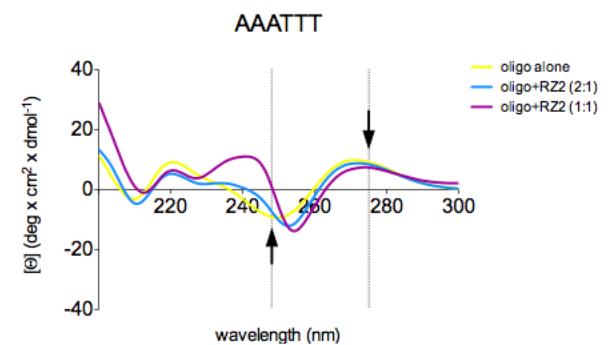
Since the synthesized molecules during this PhD project are simplified analogues of the natural bisintercalator triostin A (see Chapter 1), we expected them to display their cytotoxic activity through bisintercalation as well. To corroborate this, some DNA-binding assays were performed, where the most active compound from the RZ1-RZ12 library, i.e. RZ2, was assayed.

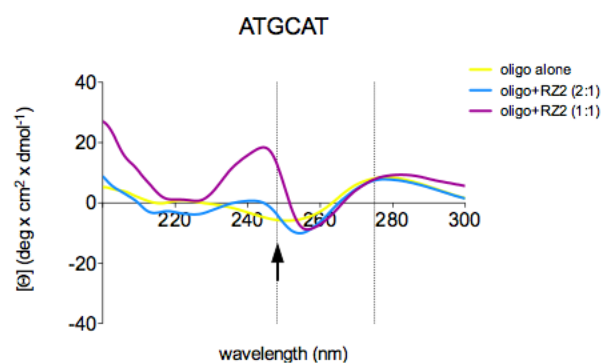
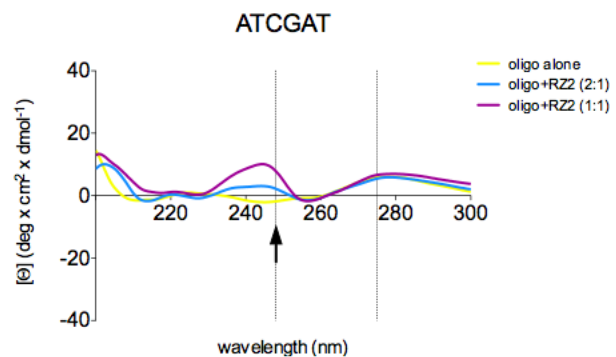
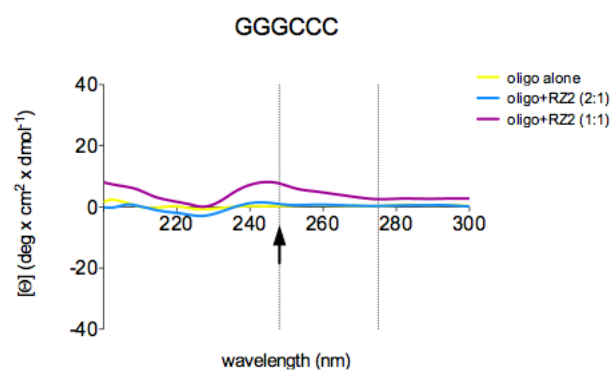
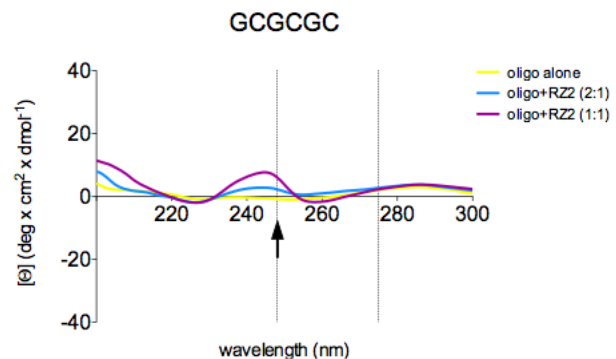
### ***Circular dichroism spectroscopy***

Circular dichroism (CD) is a very sensitive, powerful technique for diagnosing changes in DNA morphology during drug-DNA interactions, as the positive band due to base stacking (275 nm) and the negative band due to right-handed helicity (248 nm) are quite sensitive to the mode of DNA interaction with small molecules.<sup>50,51</sup> The change in CD signal of DNA observed on interaction with a compound may often be assigned to the corresponding change in DNA structure. Thus, simple groove binding and electrostatic interaction of small molecules show little or no perturbation on the base-stacking and helicity bands, while intercalation decreases the intensity of the positive band while the negative band undergoes a reduction.<sup>52</sup>

Therefore, CD experiments were performed to study DNA binding properties of compound RZ2, the most active compound against human cancer cells of the synthesized library. For this experiment, several short DNA oligonucleotides were designed so as to evaluate the possible binding selectivity of this compound for CpG steps, as triostin A does, or TpA steps, as in the case of TANDEM.

Figure 65 displays CD spectra of the designed DNA oligos treated with compound RZ2 with the ratio of 0.5 and 1 ([DNA]/[RZ2]). In some cases, the positive band (~275 nm) of the DNA oligos decreases in intensity with the addition of the compound, while in the majority of the experiments the negative band (~247 nm) undergoes a reduction. However, none of these changes in intensity are very significant, even when using the same concentration of compound and oligonucleotide, suggesting that the compound causes just a slight perturbation to DNA. These results are not conclusive to state that compound RZ2 is a DNA binder.





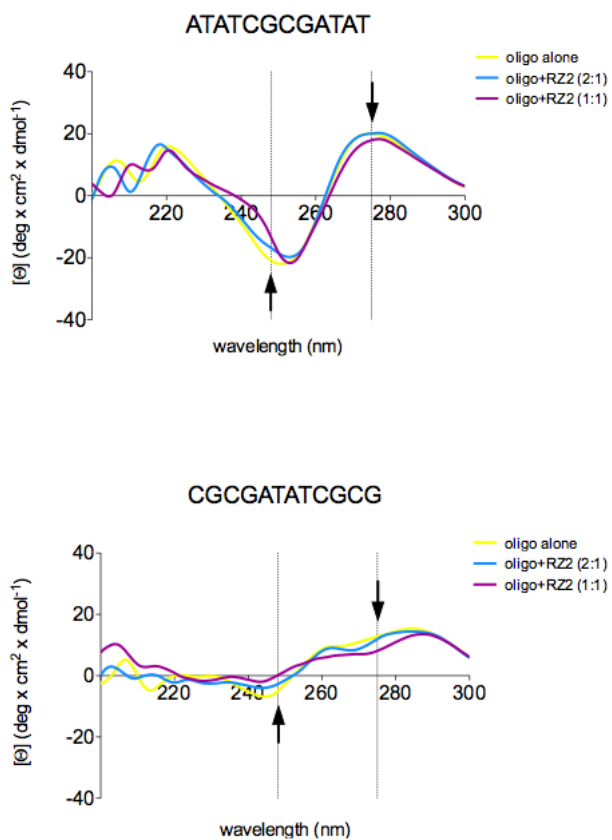


**Figure 65.** CD spectra of the designed oligonucleotides in alone and their interaction with compound RZ2. All the spectra were recorded in 10 mM potassium phosphate buffer (pH 7.5) at room temperature.

#### **Band shift experiment**

The *tyrT* plasmid is derived from the promoter of the tyrosine tRNA gene and its sequence is shown in Figure 66.

#### ***tyrT***

5'-AATTCCGGTTACCTTAATCCGTTACGGATGAAAATTACGCAACCAGTTCTTTTT  
 3'-----GGCCAATGGAAATTAGGCAATGCCTACTTTAATGCGTTGGTCAAGAAAAAA  
 CTCTCCTAACACTTACAGCGGGCGGTCAATTGATATGAAGCGCCCCGCTTCC-3'  
 GAGAAGGATTGTGAAATGTCGCCGCGCAGTAAACTATACTTCGCGGGCGAAGGGCTC-5'

**Figure 66.** Sequence of the *tyrT* DNA fragment used in the band shift experiment.

A native gel was run using this plasmid DNA in the presence of three concentrations of the synthetic analogue RZ2 as well as the bisintercalator echinomycin as positive control (Figure 67). A clear band shift was observed with the natural compound, whereas compound RZ2 showed no appreciable binding to DNA under the conditions used for this experiment.



**Figure 67.** Band shift experiment with compound RZ2. Echinomycin was used as positive control.

The same experiment was carried out testing some other of the synthesized compounds but, again, no DNA binding was observed (Figure 68). The same negative result was obtained with the 2-quinoxalinecarboxylic acid alone, corroborating that these entities are not able to intercalate by themselves into the genetic material.

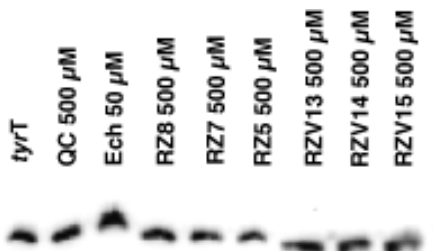


**Figure 68.** Band shift experiment with some of the synthesized compounds and QC. Echinomycin was used as positive control

### **DNase I footprinting**

Footprinting was first used in 1978 for studying the interaction between proteins and DNA.<sup>53</sup> This was then adapted as a method for identifying the sequence-specific interaction of small molecules with DNA.<sup>54,55</sup> This method can be employed to estimate the binding strength and the association and dissociation rate constants for slow binding reactions. After its development, it has been successfully used to study the sequence specificity of many ligands, such as echinomycin<sup>33</sup> and triostin A,<sup>39</sup> as well as their synthetic analogues.<sup>43</sup> Footprinting is one of the

most powerful techniques for the study of ligand-DNA interactions and it is currently being used for assessing the sequence selectivity of novel ligands.

Footprinting is a protection assay designed to elucidate the sequence-specific binding sites for a ligand on double-stranded DNA. The ligand under study protects the target DNA from digestion by a cleavage agent, such as DNase I or hydroxyl radicals. The main principle of the method is illustrated in Figure 69.



**Figure 69.** Schematic representation of the footprinting experiment. The DNA fragment is labelled by radioactivity means (green star) at one end of one strand and digested with DNase I under conditions of single-hit kinetics. A DNA ligand (in orange) protects from cleavage at its binding site and this is evident as a footprint when the products of digestion are resolved on a denaturing polyacrylamide gel.

The DNA substrate for the reaction is usually between 50 and 200 base pairs long and is radiolabelled at one end of one strand. This substrate is cleaved by a chemical or enzymatic agent in the presence of a DNA-binding agent, and the regions to which the ligand is bound are protected from digestion, creating a gap or "footprint" in the ladder of cleavage products when these are resolved on denaturing polyacrylamide gels. This reaction requires that each DNA molecule is only cleaved once (i.e. single-hit kinetics). By running control and ligand-treated digestion alongside suitable markers, the exact binding sites for the ligand can be easily determined.

The ideal cleavage agent should produce an even distribution of cleavage products and be quick, cheap and easy to use. A number of enzymatic and chemical cleavage agents have been used for footprinting studies including micrococcal nuclease, methidiumpropyl-EDTA·Fe(II) (MPE), DNase II, copper phenanthroline, uranyl photocleavage, and hydroxyl radicals. However, DNase I is the most commonly used, due to its low cost and ease of use, but it generates an uneven ladder of cleavage products, as the efficiency of the enzyme is affected by the global and local DNA structure.<sup>56,57</sup>

DNase I is a monomeric glycoprotein with a molecular weight of about 30 kDa. It is a double-strand-specific endonuclease that requires the presence of divalent cations to cleave the phosphodiester backbone.<sup>58</sup> Optimal cleavage of the O3'-P bond is obtained using calcium or magnesium, and the reaction is easily stopped by chelating these ions with EDTA.

AT rich sequences are poor substrates for this enzyme since the minor groove is too narrow for the insertion of the exposed peptide loop by which DNase I binds to the groove and the phosphate backbone.<sup>59,60</sup> GC rich regions are too rigid and therefore poor substrates as well.

DNase I binds to about 10 base pairs of the DNA duplex. As a result, the size of the drug's binding sites may be overestimated. Since the enzyme binds across the width of the minor groove, which runs at an angle relative to the helix axis, the enzyme can approach closer to the 5'-side of the ligand binding site than the 3'-side. As a result, footprints are often staggered by 2-3 base pairs across the two strands, relative to the actual binding site. Although hydroxyl radical footprints are more accurate than those with DNase I,<sup>61,62</sup> it was decided to use the latest since it is less time consuming, faster, and it is not sensitive to the presence of DMSO —needed to dissolve the tested hydrophobic compounds— as free radicals are.

The success of this technique depends on using an appropriate DNA substrate, since the binding preferred sequence of a highly selective ligand may not be present in the chosen fragment. Natural DNA fragments with a random distribution of available sequences may not be best suited for testing all possible binding sites of a ligand with unknown properties. As the selectivity of the ligand increases there is a greater chance that its preferred sequence may not be included in the fragment. In addition, the binding of simple ligands may be affected by the neighbouring base pairs. If some properties of the ligand-binding site are already known, then it may be easier to design a synthetic oligonucleotide to use as a template. A ligand with unknown binding properties might first be tested on a natural fragment to obtain a general idea of its sequence preference, followed by the use of a synthetic template containing the putative binding site(s).

A common procedure is to clone a designed sequence into a polylinker site of pUC vectors and further isolate it within a restriction fragment to be used as a footprinting substrate. Recently, a set of templates particularly useful for ligands with small recognition sites has been created (Figure 70). MS1 and MS2 are DNA fragments that contain all the 136 possible tetranucleotide sequences, but cloned in opposite orientations so as to facilitate visualization of the binding sites that are located at opposite ends of the fragments.<sup>42</sup> HexA and HexB are a series of fragments that together contain all the 64 possible symmetrical hexanucleotide sequences.<sup>44</sup>

**MS1** 5'-CCTAGGTATCGCCGTTATGTCACCGGCTAAAGGTTGACGTGATCAGCATCGCGTAGTCCAATTGAGGGCAAGATAGGACCATATC  
GTTAACCCGCACCTCTCAATACATTGACGGGCCACCCAGACAAAACAGTAGAGTCGGAGCTACGCCCTAGG- 3'

**MS2** 5'-GGATCCGATTGAGGCTGAGATGACAAAACAGACCCCCACGGACGTACTTACATAACTCTCACGCCCTAATTGCTATACCAAGGATAGA  
ACGGGAGCTAACCTTGATCGCGCTACGACTAGTGCAGTTGAAATCGGCCATGTGATTGCCGATATGGATCC- 3'

**HexA** 5'-GGATCCGGGATATCGATATGGGCCAAATTAGCTATAGATCTAGAATTCCGGACCGCGGTTAACGTTACCGTACCGCTAGGCTG  
CAGCTGCGCATGCTAGCGCTTAAGTACTAGTGCACGTGGCATGGATCC- 3'

**HexB** 5'-GGATCCATGCATTAATTGAAATGGATCATGACGTCGACATGTACATATGTATACCGCGTACCGTACGGCTTAAAGCTT  
CAATTGCCGGCTAATTAGGGCCCTCGAGCTCGCATGGCCGGATCC- 3'

**Figure 70.** Sequences of the "universal" footprinting substrates. The fragments were each labeled at the 3'-end and only the labeled strand is shown.

These "universal" footprinting substrates were used for studying the sequence selectivity of the compounds described and illustrated in the first chapter of the present thesis. This work was carried out by the PhD candidate in a 5-month internship in the laboratory of Prof. Keith Fox.

Radioactivity was the method of choice for labelling the DNA substrates, since it allows the detection of attomolar concentrations of DNA in an efficient way. All substrates were labelled at the 3'-end by filling in the sticky-ends with  $[\alpha\text{-}^{32}\text{P}]$ dATP using a reverse transcriptase.

Some examples of a DNase I footprinting gels are illustrated in Figures 71 and 72. In these experiments, the known bisintercalators echinomycin, triostin A, TANDEM and the monointercalator doxorubicin were used in different concentrations as positive controls to compare the outcome with compounds RZ2, RZ8 and the 2-quinoxalinecarboxylic acid alone (QC).

In all these gels the bisintercalator controls gave clear footprints that correspond to the sequences to which they have already been reported as selective. In the case of doxorubicin, long non-selective gaps are observed, demonstrating the high DNA-binding affinity exerted by this compound without any sequence selectivity at all.

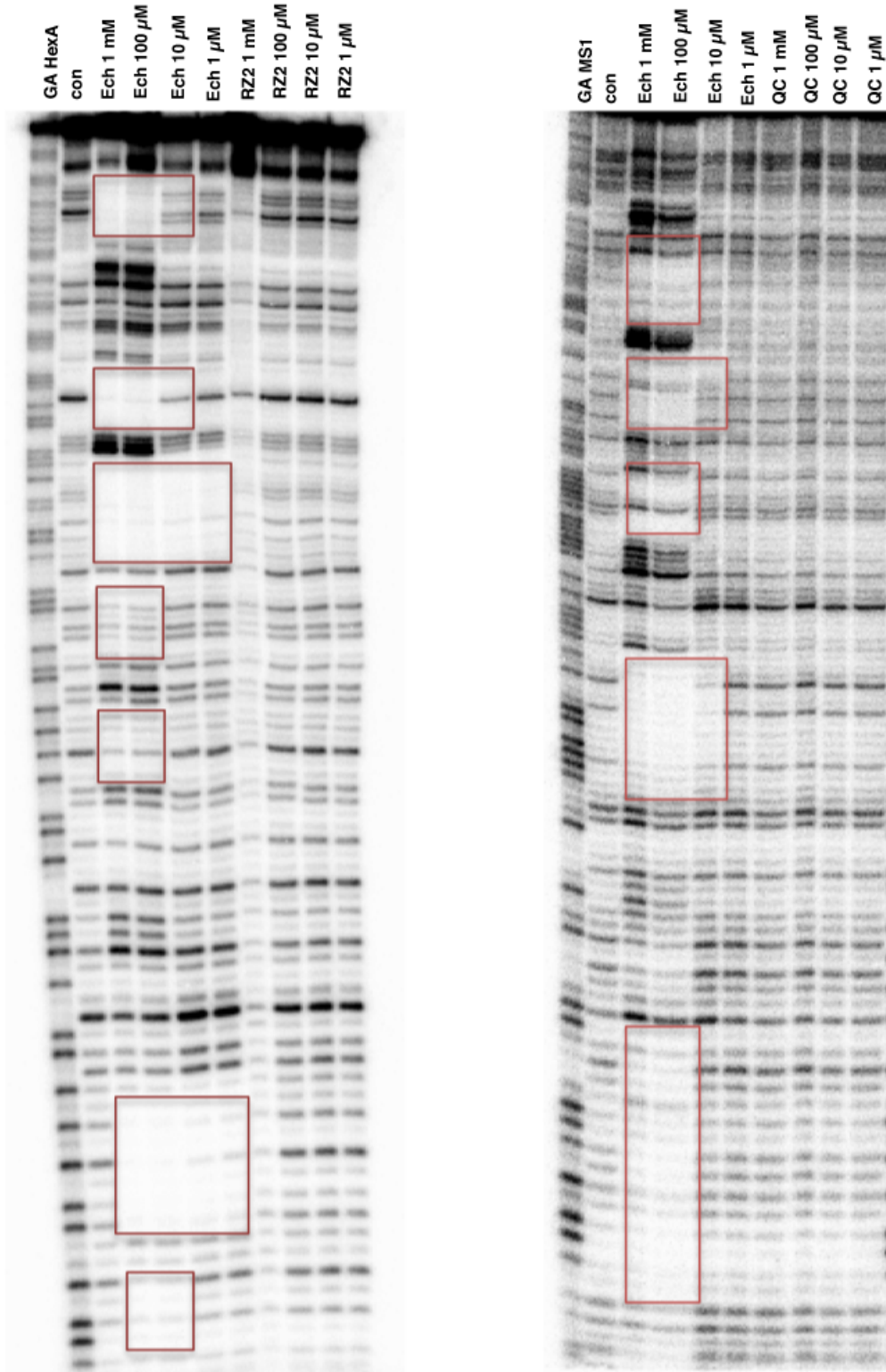


**Figure 71.** DNase I digestion of HexA and MS1 in the presence of echinomycin, RZ2 and QC. Track labeled GA is a marker lane specific for purines; con is a control showing digestion of the DNA in the absence of added ligand; echinomycin is the positive control; RZ2 and QC are the tested compounds. Footprints are indicated in red.

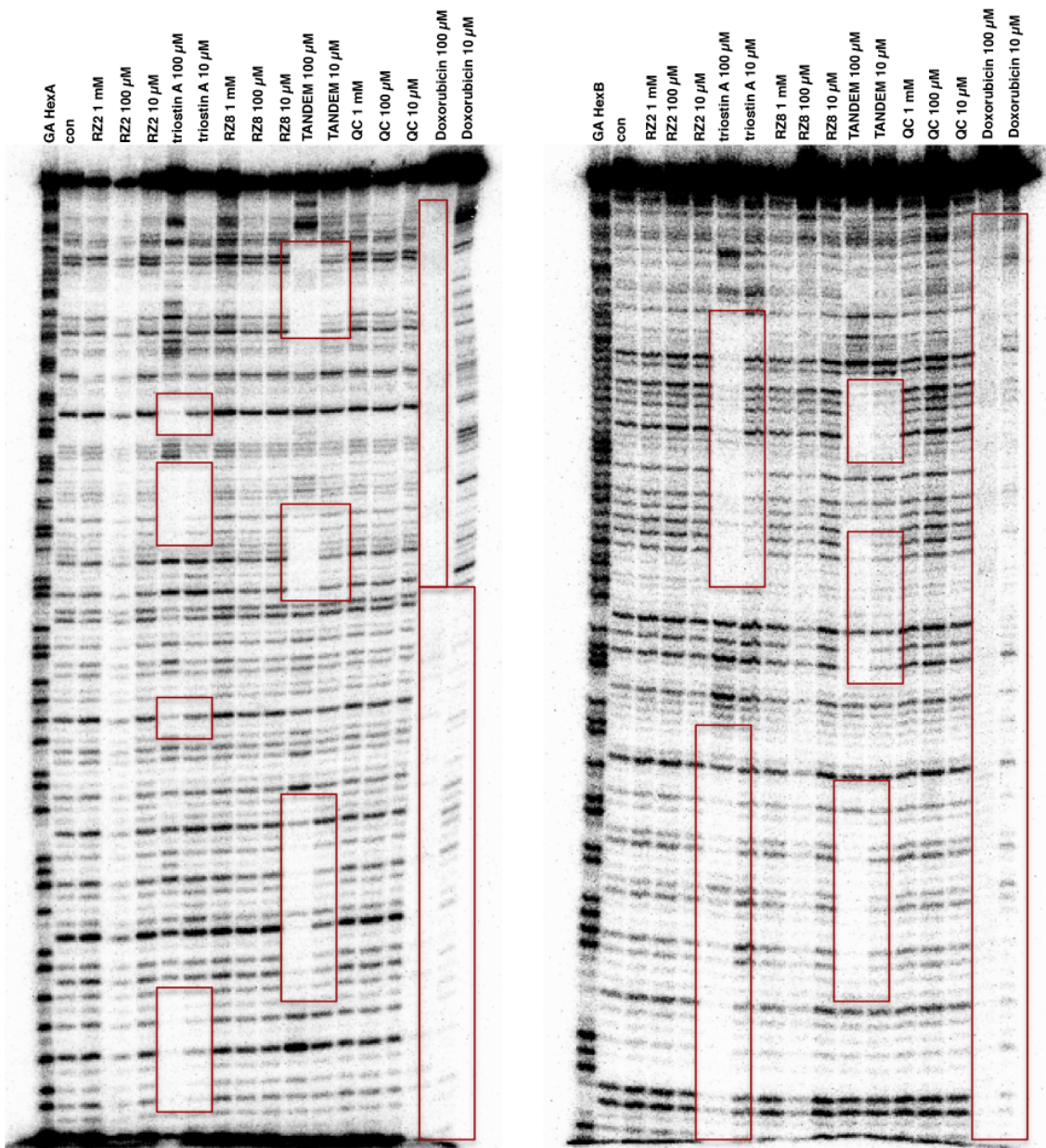


**Figure 72.** DNase I digestion of HexA and HexB in the presence of different compounds. Track labeled GA is a marker lane specific for purines; con is a control showing digestion of the DNA in the absence of added ligand; triostin A, TANDEM and doxorubicin are the positive controls; RZ2, RZ8 and QC are the tested compounds. Footprints are indicated in red.

DNase I footprinting experiments were performed with the four "universal" footprinting fragments. Clear footprints with the positive controls were obtained even at low drug concentrations, whereas the hit compound RZ2 did not produce any footprint at all, as observed in Figure 73.

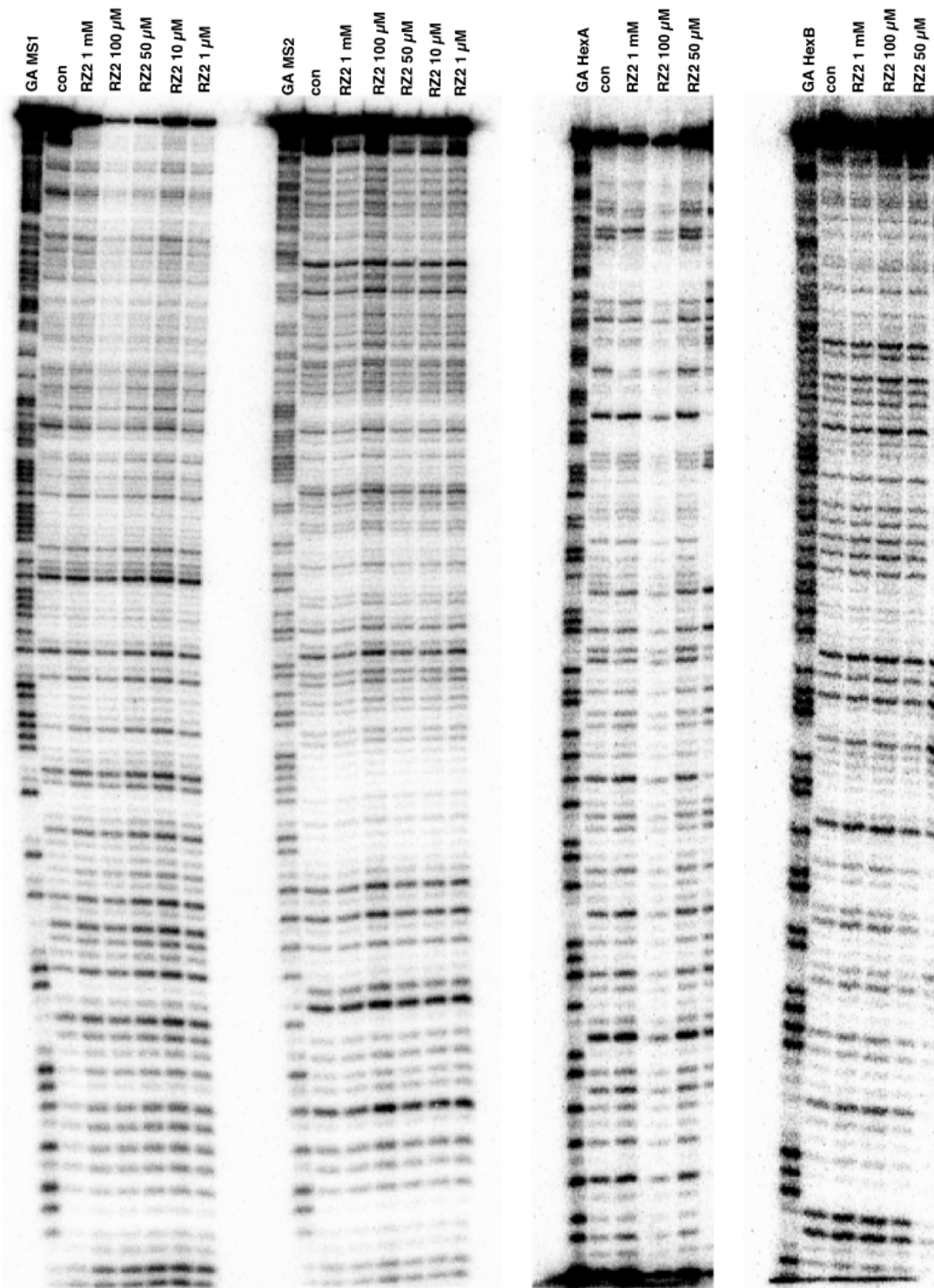


**Figure 73.** DNase I footprinting gels of compound RZ2 using all the universal substrates.

The same results were observed for all the synthetic compounds tested, as shown in Figure 74.

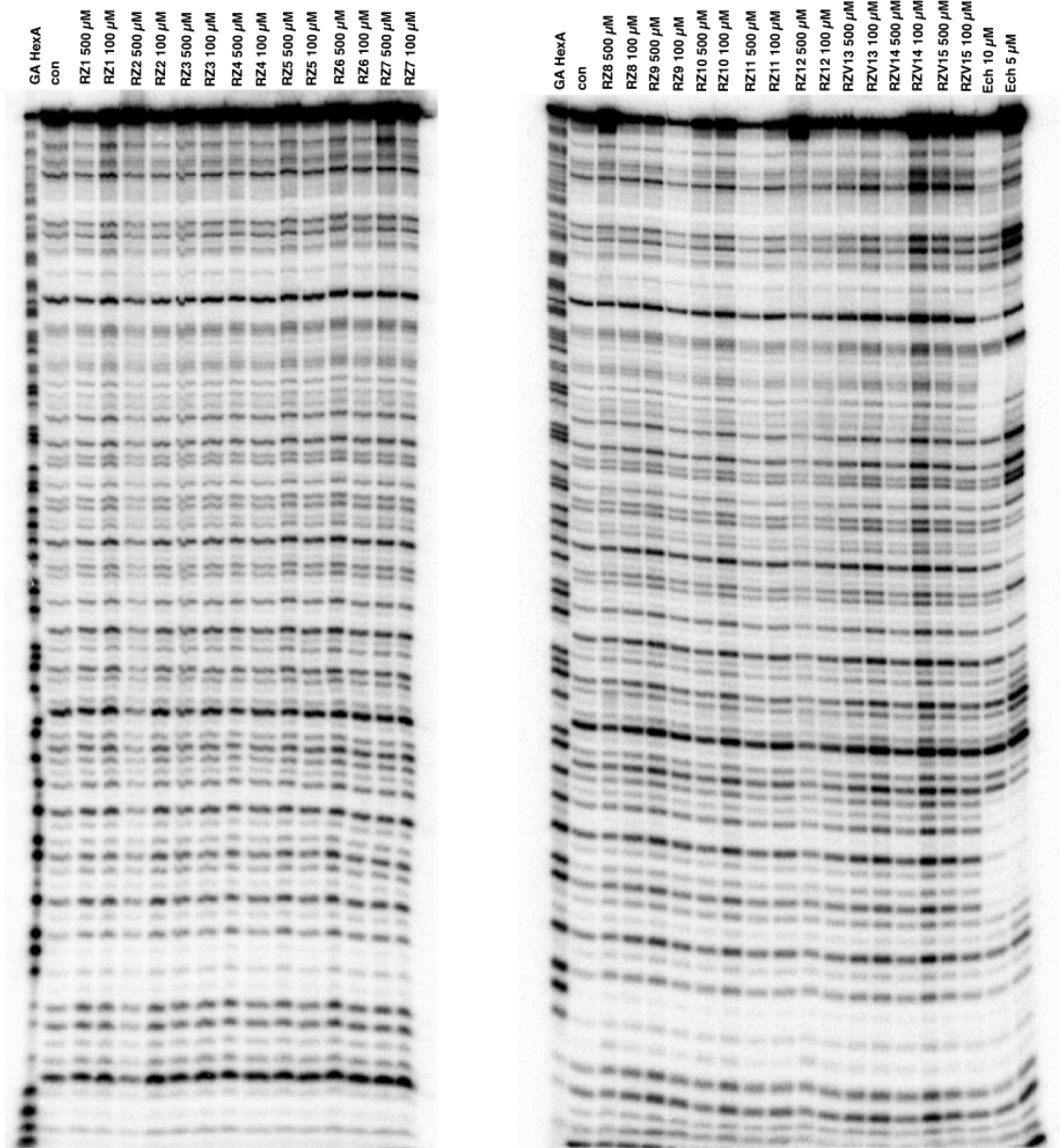


**Figure 74.** DNase I digestion of HexA in the presence of all the synthesized compounds. Echinomycin was used as positive control and it is the only compound that produced footprints.

The footprinting substrates employed in these experiments can quickly give an indication of the preferred binding site for most small molecules. Unfortunately, the fact that no footprints were obtained with the synthesized compounds of this project clearly indicates that these molecules are not DNA-binders.

### Molecular dynamics simulations

In order to understand the reasons that govern the fact that the synthesized analogues do not bisintercalate into the DNA as it was hypothesized in the design of this project, a conformational study of the most cytotoxic compound, RZ2, was carried out by means of molecular dynamics simulations.

5 independent simulations of 1.15  $\mu$ s each at 298 °K were run, starting with a completely unfolded structure of the peptide immersed in an octahedral box of water (5867 water molecules). The conformational preferences for the 12 residues starting from the completely unfolded peptide along these 5 independent molecular dynamics simulations are depicted in Figure 75.

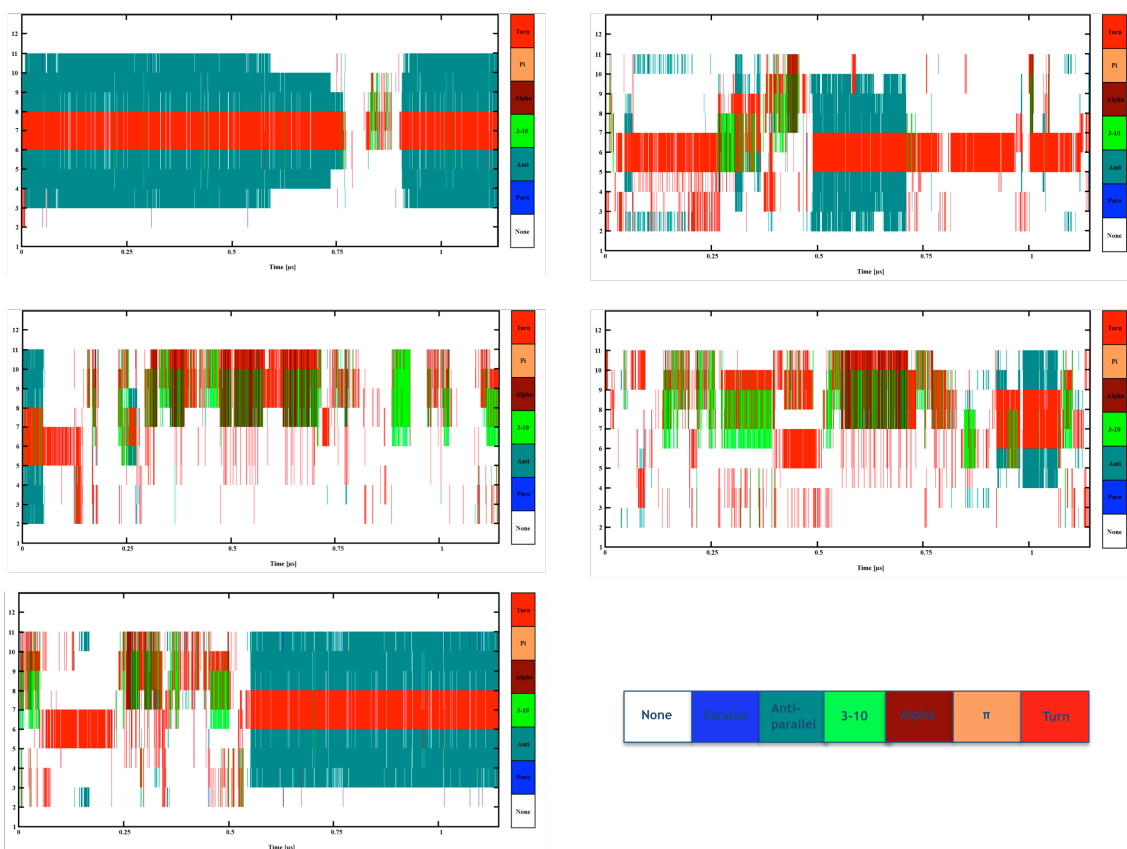


**Figure 75.** Five independent molecular dynamics simulations for compound RZ2.

The results suggest that the preferred conformation of the compound in an aqueous environment is the antiparallel  $\beta$ -sheet, with a  $\beta$ -turn formed between the D-Pro and the Gly residues. The analysis of the data (Figure 76) corroborates that the probability of occurrence of this conformation is much higher than any other possible, and the resulted most populated conformers of compound RZ2 are illustrated in Figure 77.

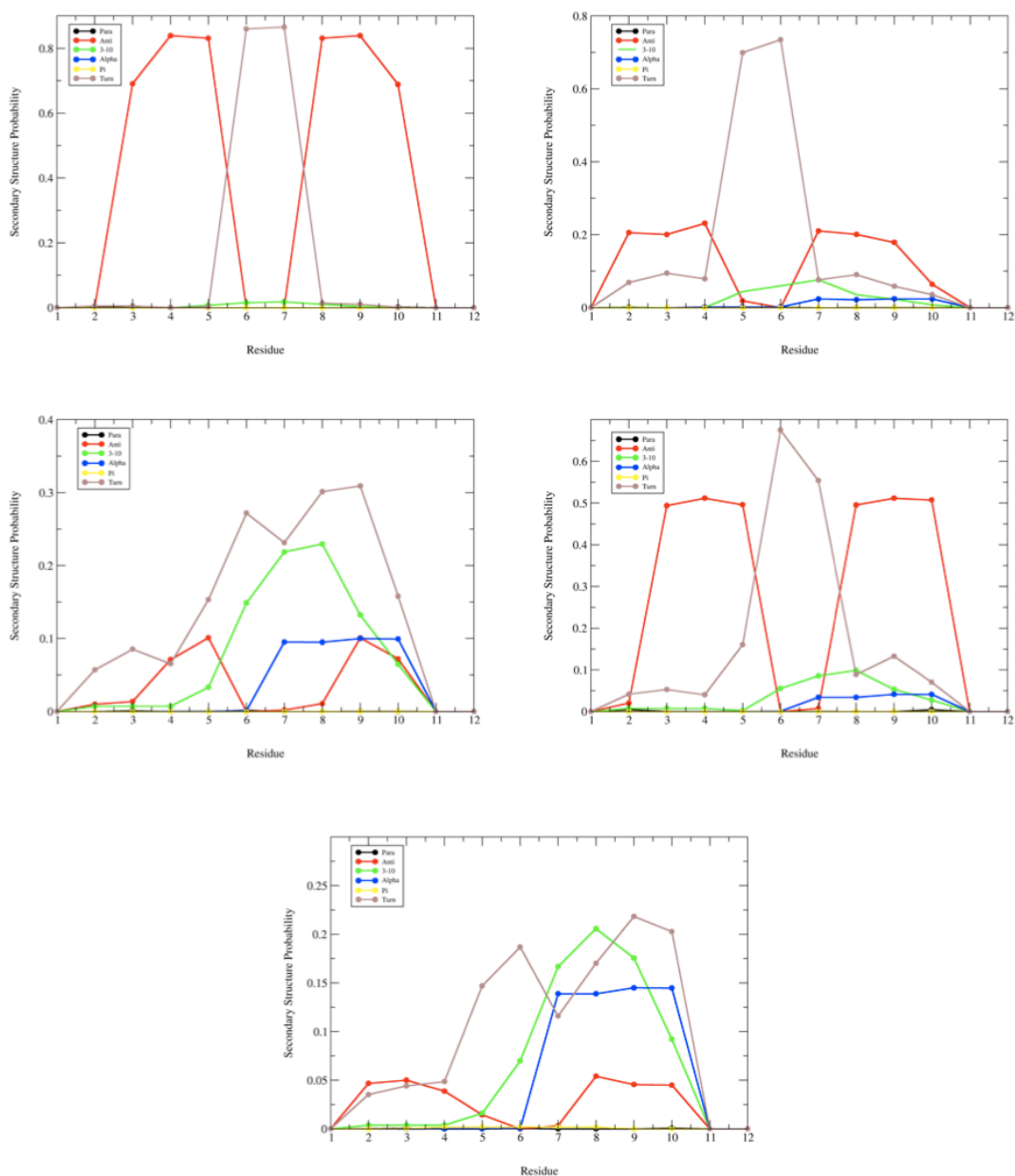
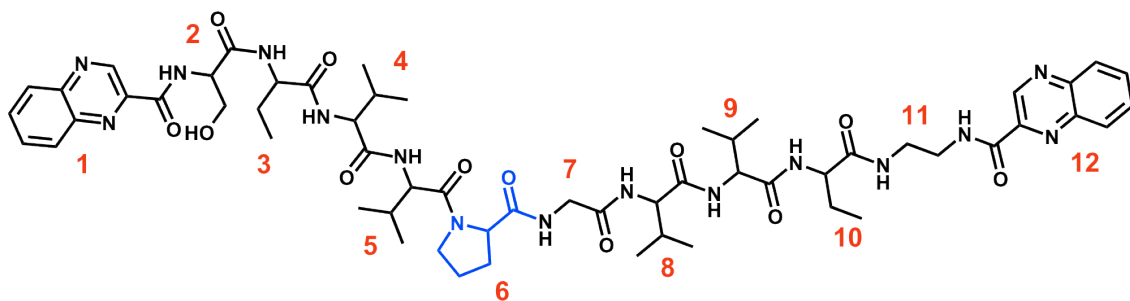


**Figure 76.** Probability per residue to adopt certain conformation. The parallel β-sheet appears in black, the antiparallel β-sheet in red, the 3-10 helix in green, the alpha helix in blue, the π turn in yellow and the β-turn in pink.

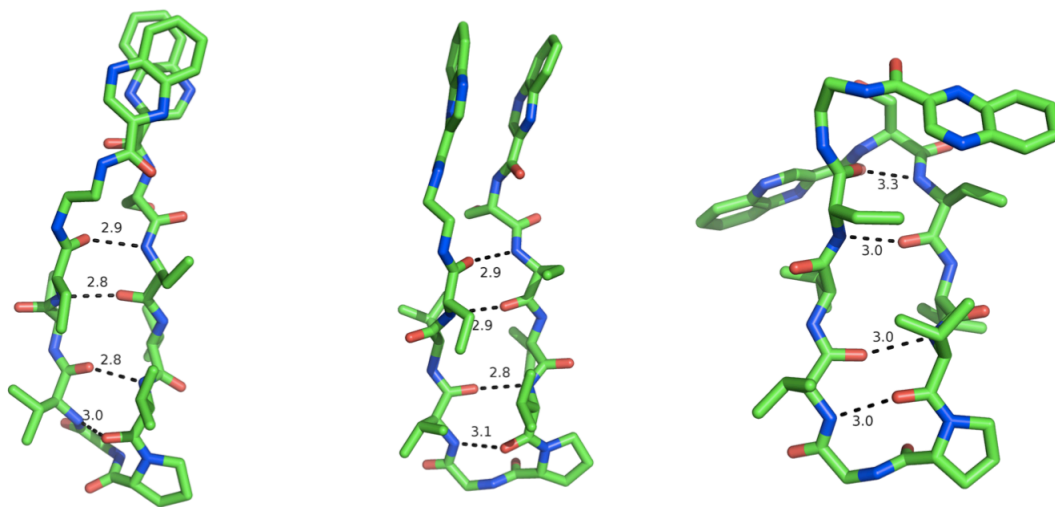


**Figure 77.** Most populated conformers of compound RZ2.

Additionally, Replica Exchange Simulations with a total temperature range from 298.93 °K to 310.41 °K converge again to an antiparallel  $\beta$ -sheet within 220 ns of REMD simulation (Figures 78 and 79).

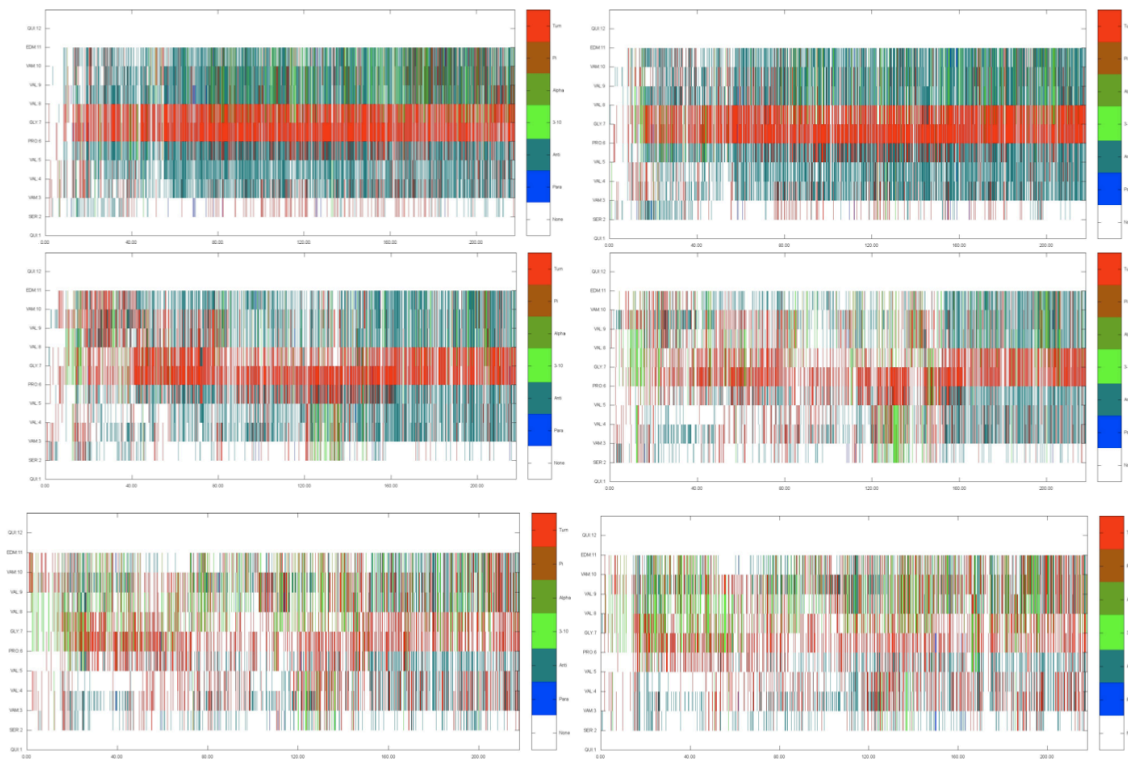


**Figure 78.** Replica Exchange Molecular Dynamics simulations of RZ2 with 44 replicas.

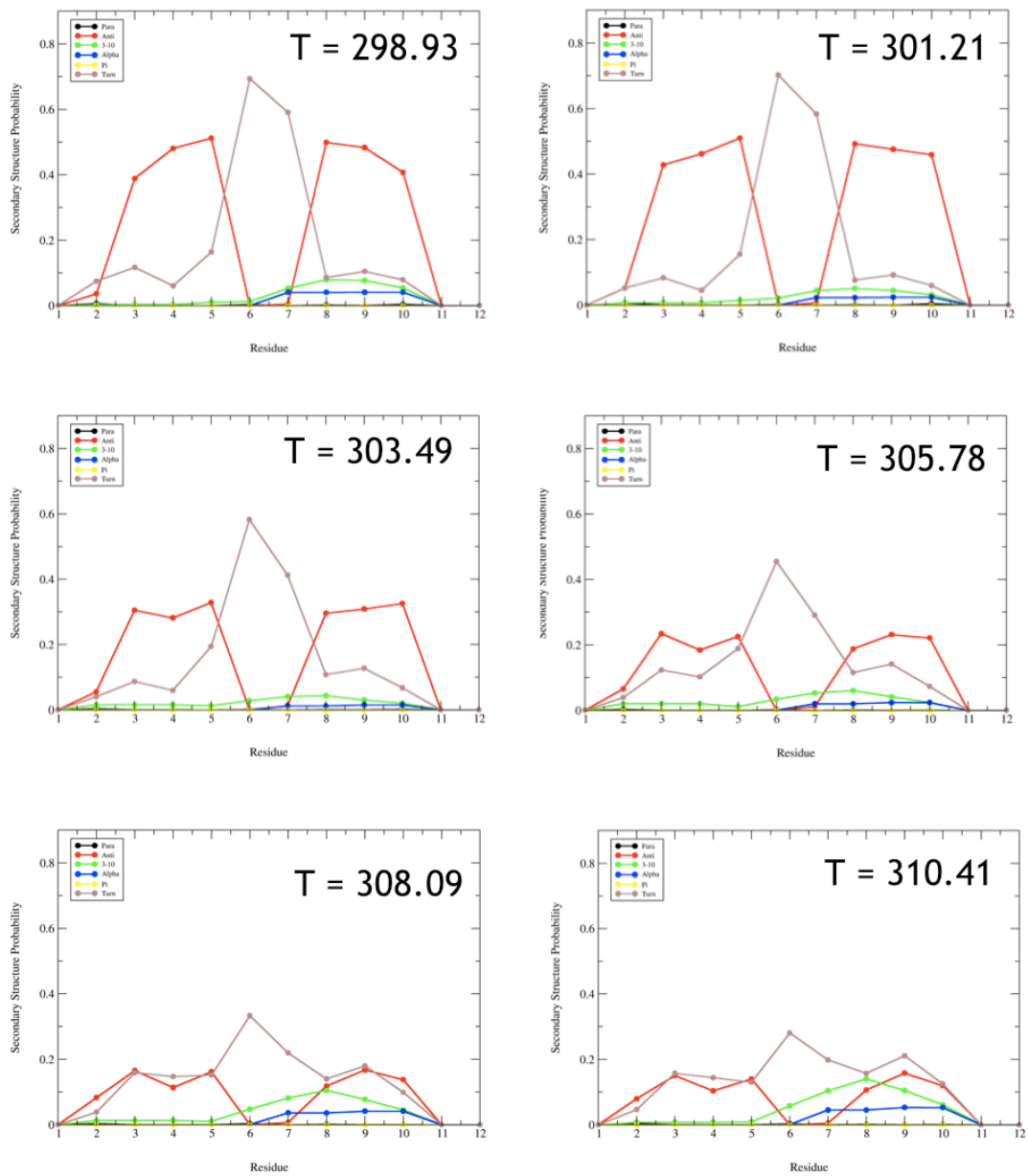


**Figure 79.** Probability per residue to adopt certain conformation at different temperatures. The parallel  $\beta$ -sheet appears in black, the antiparallel  $\beta$ -sheet in red, the 3-10 helix in green, the alpha helix in red, the  $\pi$  turn in yellow and the  $\beta$ -turn in pink.

As expected, the antiparallel  $\beta$ -sheet is the most populated conformer at 298.93 °K. Increasing the temperature makes other possible conformers more accessible and, as a consequence, the total amount of antiparallel  $\beta$ -sheet conformer is diminished. What is really meaningful is that the amount of that conformer is increased in all the temperatures as the simulation time is increased. However, in all the simulations the distance between the centres of the two quinoxaline-rings remains around 4 Å, showing a clear preference of the quinoxaline rings to stack together (Figure 80).

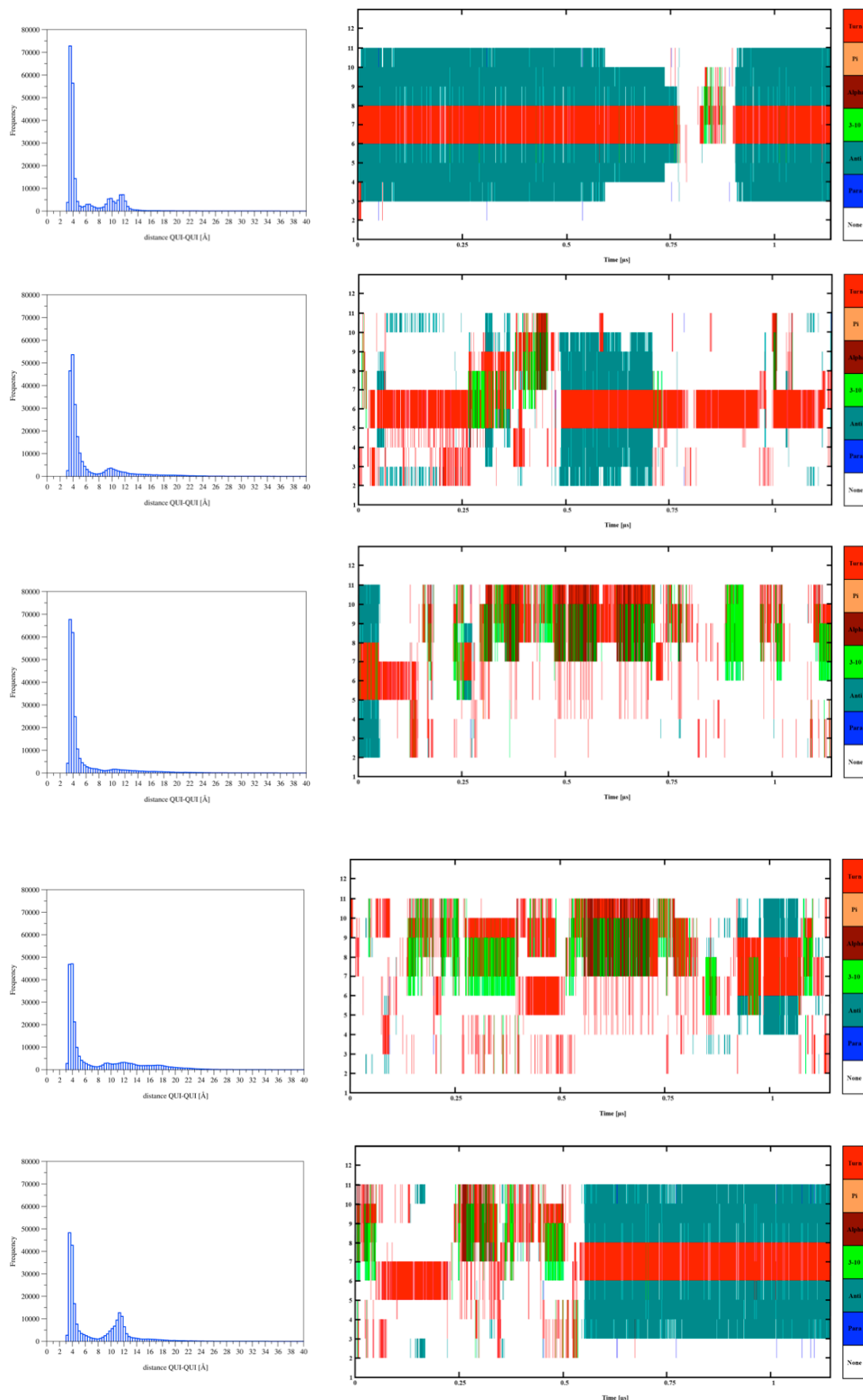


**Figure 80.** Distance distribution between the quinoxalines for each simulation.

Formation of the  $\pi$ - $\pi$  stacking interaction between rings happens at the beginning of all the simulations starting from the unfolded state of the peptide and drives the conformational evolution. So, this very high proximity of the heterocycles would explain RZ2's impossibility to bisintercalate into the DNA. Besides the fact that the compound does adopt the predicted antiparallel  $\beta$ -sheet conformation, the 4 Å separation between the chromophores is too little distance compared to the 10.5 Å between the quinoxalines in triostin A, which seems to be the ideal distance to allow the sandwiching of two DNA base pairs.

Additional simulations were run for other compounds from the RZ1-RZ12 library, in order to investigate if the same conformation and separation between the intercalating moieties is exhibited by the other analogues. In these experiments, 4 simulations were run, where the first one started from the completely unfolded state and the others taking as the starting point one of the 3 most populated conformers (REP0, REP3 and REP4) of the original peptide in the antiparallel  $\beta$ -sheet conformation.

The other three tested compounds exhibited a similar antiparallel  $\beta$ -sheet conformation than compound RZ2 with a very close proximity of the quinoxalines, explaining the fact that none of the compounds resulted a DNA-bisintercalator (Figures 81-86).

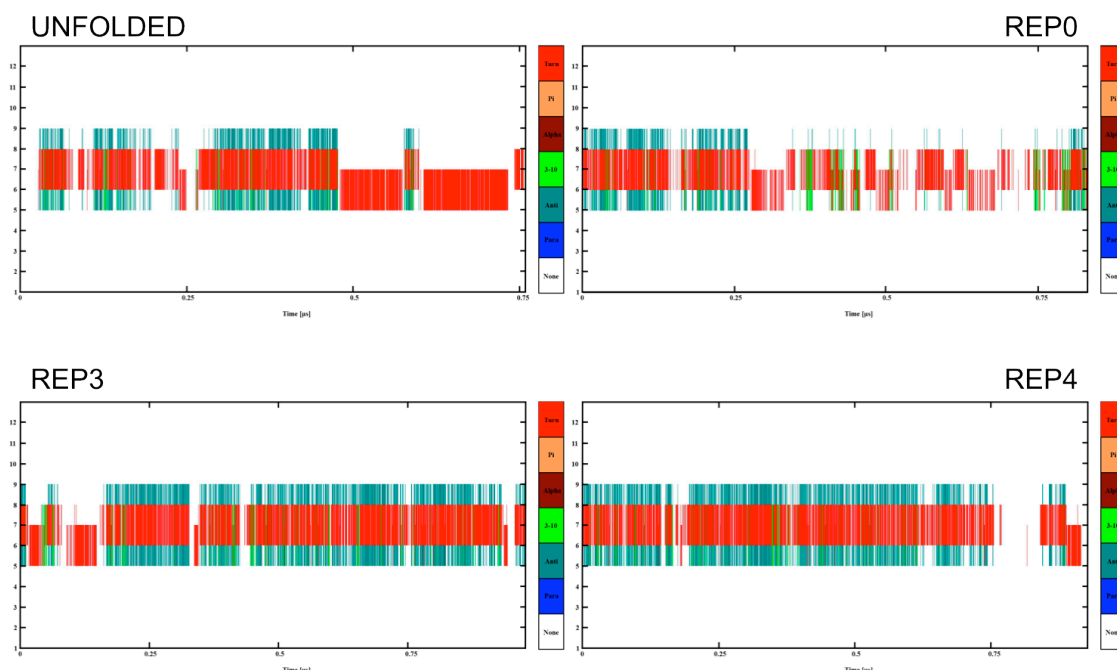


**Figure 81.** Molecular dynamics simulations for compound RZ1.

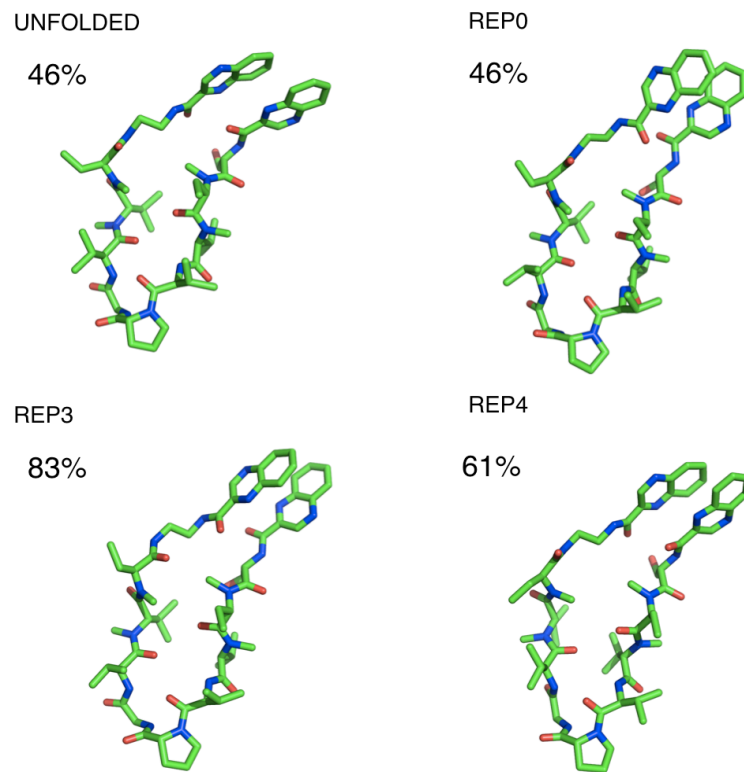


**Figure 82.** Most populated conformation for RZ1 in each simulation and its population percentage.

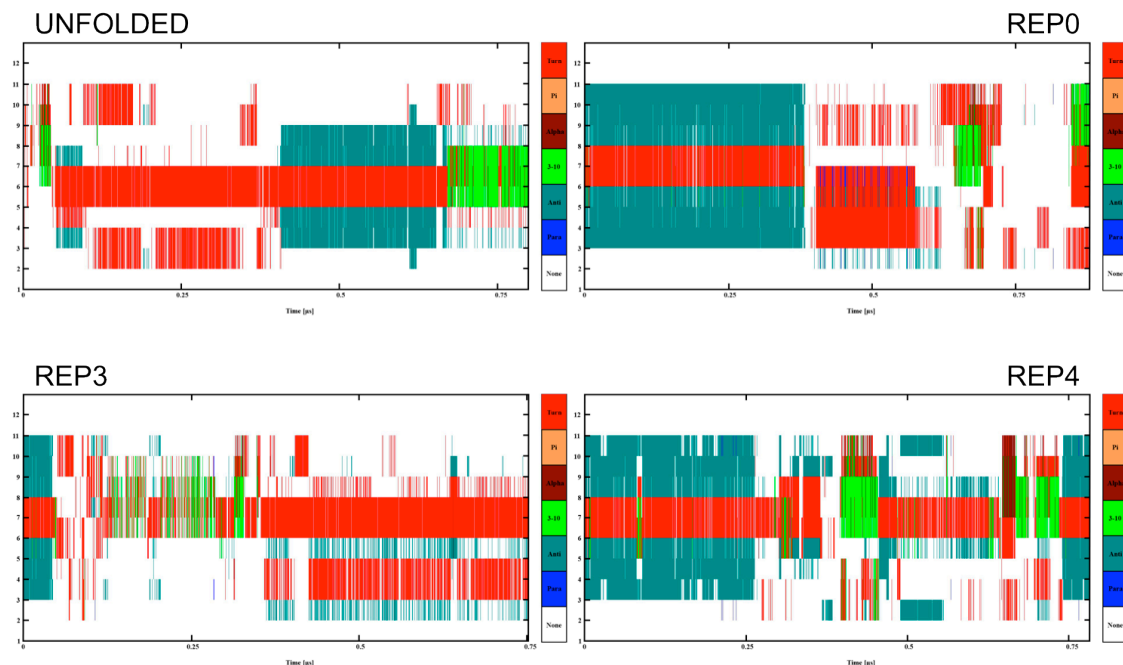


**Figure 83.** Molecular dynamics simulations for compound RZ6.

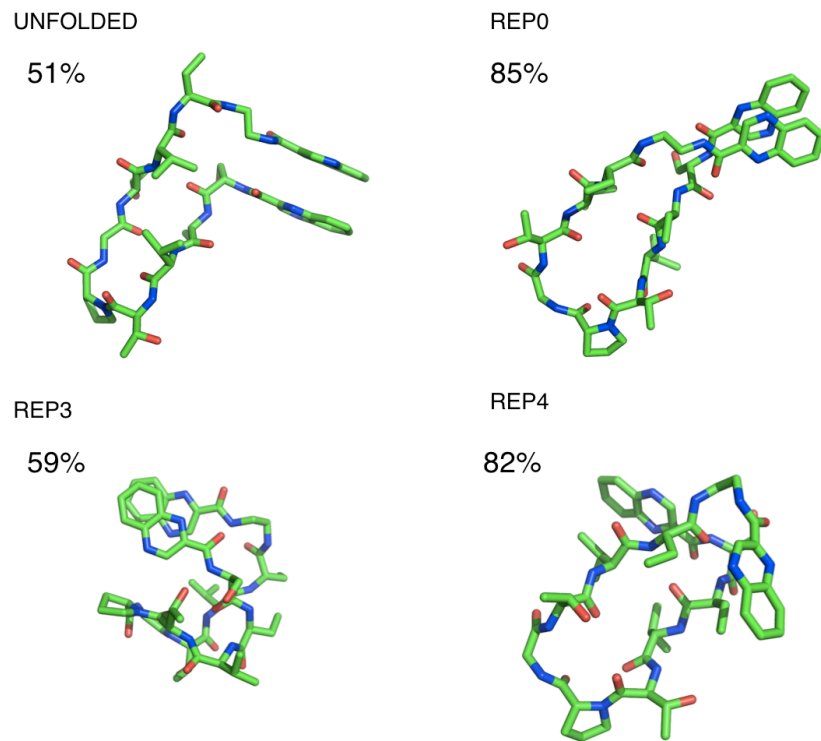


**Figure 84.** Most populated conformation for RZ6 in each simulation and its population percentage.

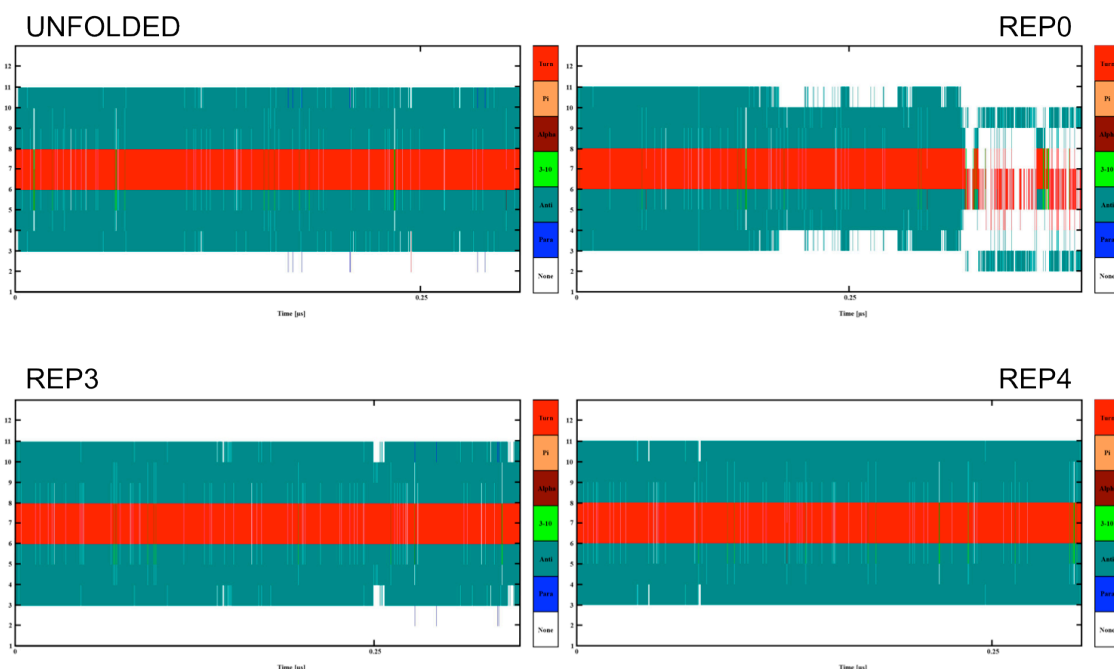


**Figure 85.** Molecular dynamics simulations for compound RZ10.

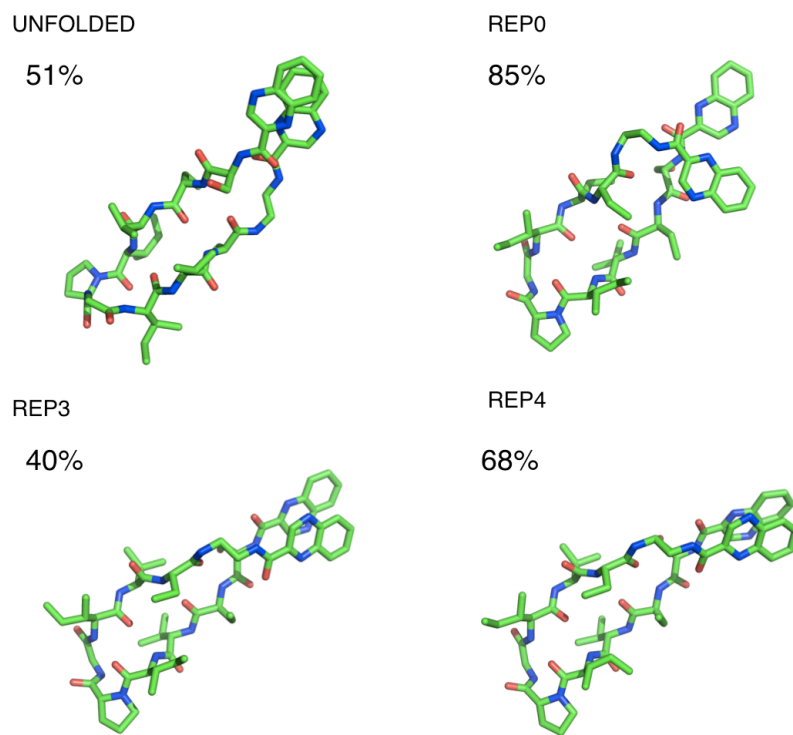


**Figure 86.** Most populated conformation for RZ10 in each simulation and its population percentages.

### Topoisomerase inhibition assay

Topoisomerases are nuclear enzymes with an essential role in DNA replication and transcription, as well as in chromosome structure, by altering the topological state of DNA. All cells have two major forms of topoisomerases: type I and type II. The former ones make single-stranded cuts in DNA and are further subdivided into type IA (homologous to *E. coli* topoisomerase I) and type IB (homologous to human topoisomerase I). Type II topoisomerases cut and pass double stranded DNA.<sup>63–66</sup>

Eukaryotic topoisomerases can only relax DNA, and their role is critical for decatenation of interlocked DNA, since semiconservative DNA replication results in catenated sister chromatids.<sup>67,68</sup> These enzymes are important targets for many chemotherapeutic agents and antibiotics, such as the broad-spectrum quinolones antibiotics.<sup>69</sup> Additionally, some anticancer agents address eukaryotic topoisomerases. These agents, such as camptothecin and topotecan (topoisomerase I drugs), doxorubicin and etoposide (topoisomerase II drugs), form a drug-enzyme-DNA complex, preventing the subsequent DNA-resealing step normally catalyzed by

topoisomerases. Thus, the target topoisomerase is converted into a DNA-damaging agent, giving these drugs the denomination of "topoisomerase poisons".<sup>70,71</sup>

After the negative results obtained for DNA-binding with the RZ1-RZ12 library, some assays were performed to assess their possible ability to inhibit both forms of DNA topoisomerase *in vitro*. The most active compound against the human cancer cell lines tested, RZ2, was assayed.

#### **Topoisomerase I activity assay**

This *in vitro* assay is based on topoisomerase I relaxation of supercoiled DNA, which has different electrophoretic mobility than relaxed DNA.

Most plasmid DNAs isolated from natural sources are negatively supercoiled and can be used to assay topoisomerase I activity. In this experiment, supercoiled plasmid pBR322 was used as supplied in the assay kit.

Human topoisomerase I was supplied at a concentration of 10 U/ $\mu$ L in dilution buffer, which was also used to dilute the enzyme's concentration to 1 U/ $\mu$ L. First, a test using different concentrations of enzyme was carried out to determine the optimal working concentration to achieve total DNA relaxation. As shown in Figure 87, all the tested concentrations caused the expected relaxation of the supercoiled plasmid, so it was decided to assay 1 U of topoisomerase I for relaxing 0.5  $\mu$ g of supercoiled pBR322 when incubated in assay buffer in a total reaction volume of 20  $\mu$ L for 30 minutes.

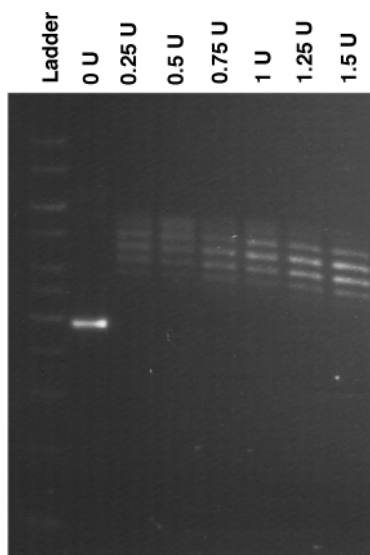


**Figure 87.** Optimization for the topoisomerase I assay.

For the assay with compound RZ2, a range of the compound concentrations was tested. The agent under examination was added before the enzyme for studying inhibition of relaxation catalyzed by topoisomerase I. Since compound RZ2 was dissolved in DMSO, solvent controls were evaluated as well.

As shown in Figure 88, the quinoxaline-containing peptide did not inhibit the activity of human topoisomerase I, since relaxed topoisomers are evident in all the lanes.

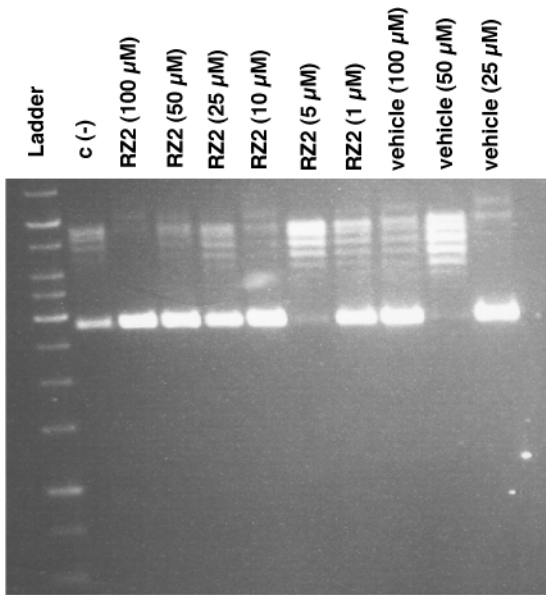


**Figure 88.** Topoisomerase I relaxation assay with compound RZ2. C(-) indicates the presence of enzyme without addition of any compound.

### **Topoisomerase II activity assay**

This *in vitro* assay is based on topoisomerase II decatenation of double-stranded DNA.

Like topoisomerase I, topoisomerase II catalyzes relaxation of supercoiled DNA. However, topoisomerase II is unique in its ability to catalyze the decatenation of intact double stranded DNA, a property that allows the enzyme to separate replicated DNA molecules at mitosis.

This assay utilizes kinetoplast DNA (kDNA), which forms a network of interlocked circles,<sup>72</sup> as supplied in the assay kit.

The relaxation by topoisomerase II requires ATP and a divalent cation. The enzyme decatenates the interlocked circles of the kDNA and the free circles migrate as a band on the gel. However, catenated circles are unable to enter on agarose gels.

Human topoisomerase II was supplied at a concentration of 2 U/ $\mu$ L in dilution buffer, which was also used to dilute the enzyme's concentration to 1 U/ $\mu$ L. First, a test using different

concentrations of enzyme was carried out to determine the optimal working concentration to achieve total DNA decatenation. As shown in Figure 89, the lower tested concentrations were better, since very high concentrations catalyze the catenation of circular DNA. A reasonable concentration for the assay was, again, 1 U for 100 ng of kDNA when incubated in 1x assay buffer plus 1 mM ATP in a total reaction volume of 20  $\mu$ L for 30 minutes.

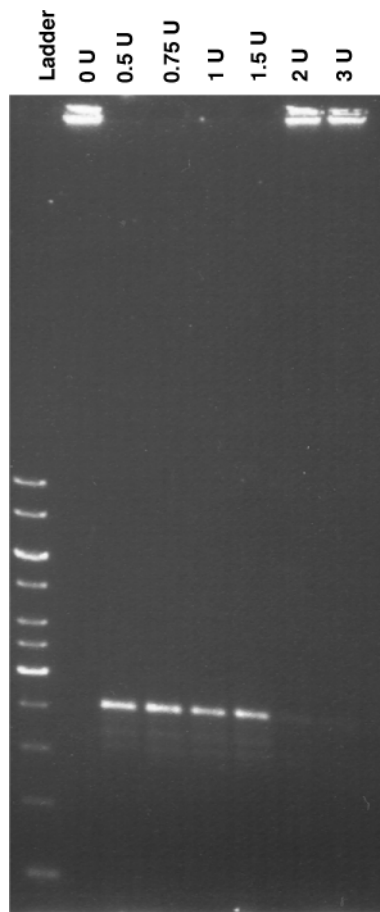


**Figure 89.** Optimization for the topoisomerase II assay.

For the assay with compound RZ2, a range of the compound concentrations was tested. The agent under examination was added before the enzyme for studying inhibition of the enzyme. Since compound RZ2 was dissolved in DMSO, solvent controls were evaluated as well.

As shown in Figure 90, the quinoxaline-containing peptide did not inhibit the activity of human topoisomerase II, since decatenated products are observed in all the lanes.

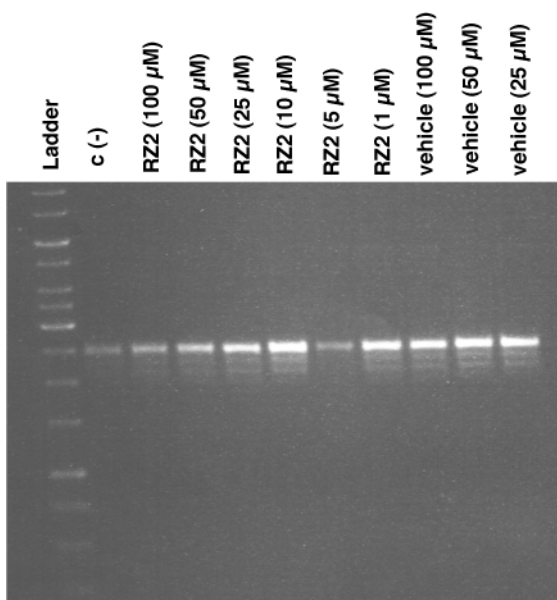


**Figure 90.** Topoisomerase II decatetralin assay with compound RZ2. C(-) indicates the presence of enzyme without addition of any compound.

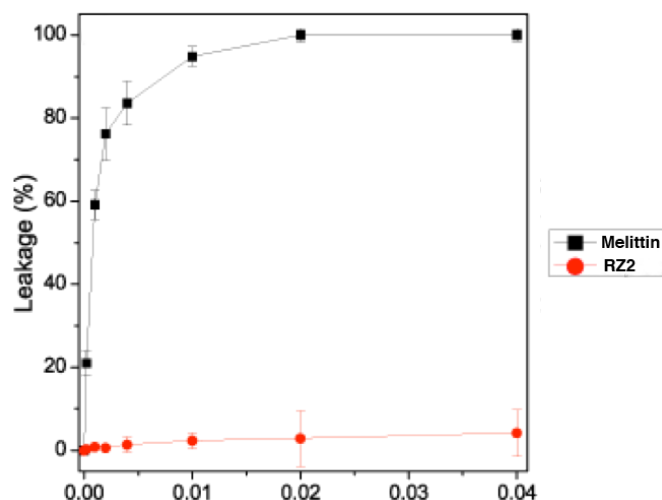
### Studies on the mechanism of cell death

On the basis of the aforementioned results, it was demonstrated that RZ2 is not a DNA-binder and that it is not a topoisomerase poison. Thus, its mechanism of action is different from that of bisintercalators such as triostin A, TANDEM, echinomycin and thiocoraline. Thus, some experiments on the mechanism of cell death were carried out to get insights into the mode of action by which this quinoxaline-containing peptide displays its antitumor activity.

#### **Does RZ2 cause necrosis to cancer cells?**

Necrosis is an inflammatory form of cell death, in which the plasma membrane suffers total disruption leading to the spillage of the intracellular content. Thus, the capacity to perturb the bilayer of liposomes, which mimics cell surfaces, was studied for compound RZ2. Leakage of intraliposomal CF was assayed by treating probe-loaded liposomes (final lipid concentration, 0.125 mM) with different amounts of RZ2. The effects were compared with the well-known necrotic effect of melittin.<sup>73</sup>

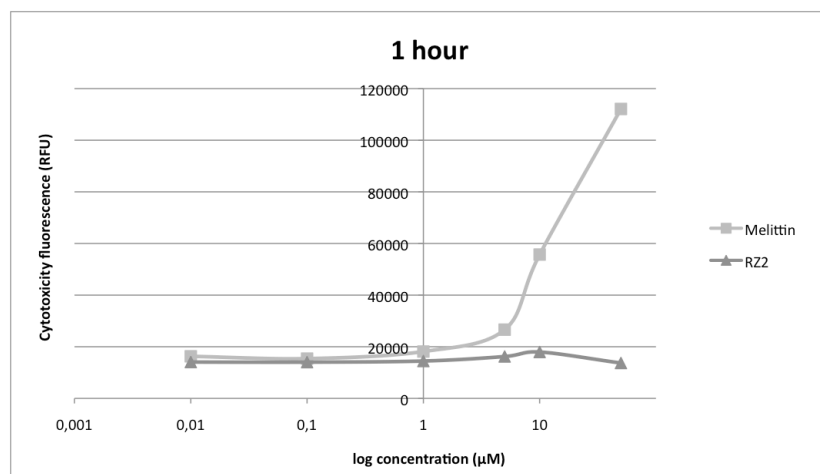
Dye leakage results in Figure 91 show the incapacity of the compound to permeabilize the bilayer in comparison to the high effect of melittin.

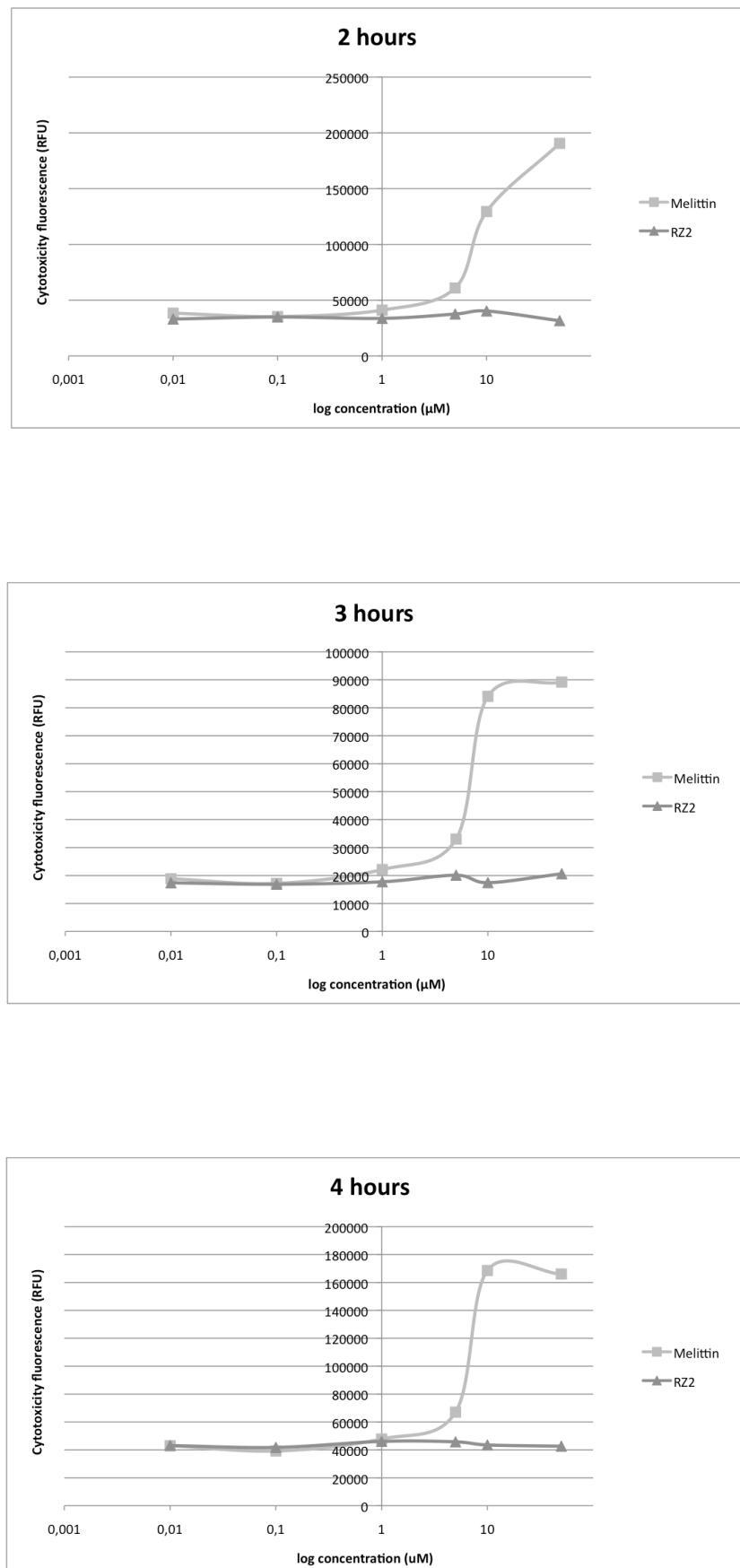


**Figure 91.** Effect on membrane rupture of LUVs containing CF. The ordinate shows the compound/lipid (EPC/Chol 5:1) ratio (mol:mol). Data are expressed as the mean  $\pm$  SE ( $n=3$ ).

Another assay was carried out using a fluorogenic cell-impermeant peptide substrate (bis-alanylalanyl-phenylalanyl-rhodamine 110; bis-AAF-R110) to measure dead-cell protease activity, which is released from cells that have lost membrane integrity. Because bis-AAF-R110 is not cell-permeant, viable cells do not generate any signal from this substrate.

Figure 92 illustrates the necrotic effect of compound RZ2 and melittin on HeLa cells at different concentrations and times of exposure. Whereas the positive control causes evident plasma membrane permeabilization at a concentration between 1 and 5  $\mu$ M, the quinoxaline-containing molecule does not generate significant fluorescent signal, indicating that RZ2 does kill cancer cells through necrosis.





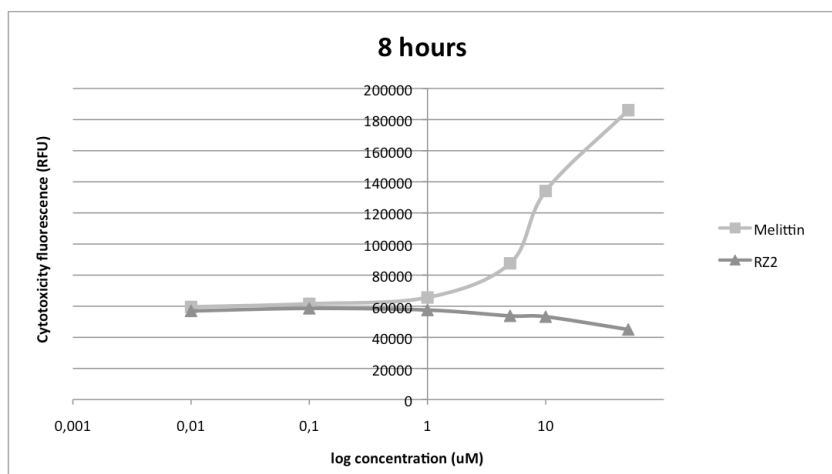


Figure 92. Necrotic effect of RZ2 and melittin on HeLa cells.

### Does RZ2 cause apoptosis to cancer cells?

Apoptosis is distinguishable from necrosis by characteristic biochemical and morphological changes, including the shrinkage of the cytoplasm and the collapse of the cytoskeleton, condensation of the nuclear chromatin resulting in DNA fragmentation and blebbing of the plasma membrane that leads to the formation of apoptotic bodies.<sup>12</sup> Because no single parameter defines apoptosis, a combination of different measurements for reliable detection of apoptosis was used.

In apoptotic cells, phosphatidyl serine (PS) is translocated from the plasma membrane and it is exposed to the external cellular environment. Annexin V, a  $\text{Ca}^{2+}$ -dependent phospholipid-binding protein, has a high affinity for PS and it helps to identify apoptotic cells when labeled with a fluorophore by binding to the exposed PS on the membrane.<sup>74</sup> On the other hand, cells with plasma membrane permeabilization (dead cells) are permeant to propidium iodide (PI), which is internalized and binds to the nucleic acids in the cell.<sup>75</sup> PI permeability assays coupled to annexin V labeling in HeLa cells showed increased PI/annexin V labeling in response to RZ2 in a time-dependant manner (Figure 93).

RZ2-specific induction of apoptosis was confirmed by an increase in annexin V-positive cells in response to the compound over time (Figure 94A) and by an increase in the sub-G<sub>1</sub> DNA fragmentation from 1% of the total cell population to 27% after 72 h of exposure (Figure 94B).

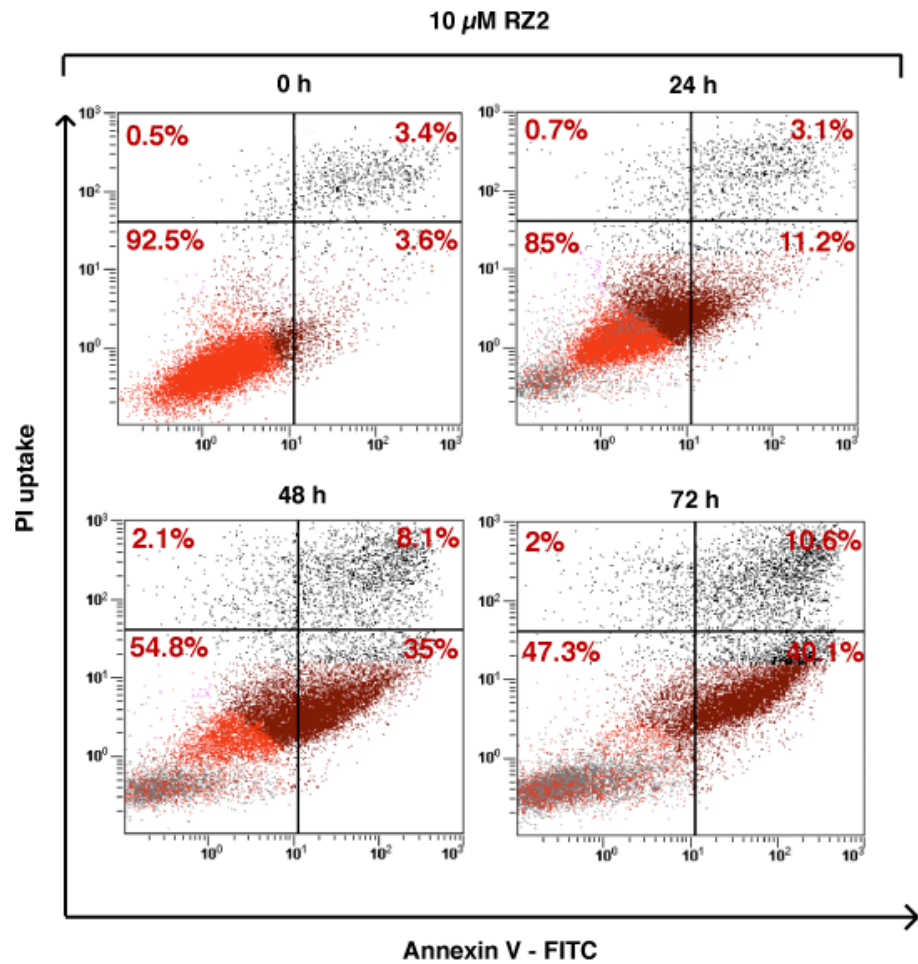


**Figure 93.** Flow cytometry results of the effect of RZ2 on apoptosis and necrosis in HeLa cells. Total events are 10,000. The percentage of cells that are single, double positive or double negative for annexin V and PI are indicated in each grid. The upper left grid represents the number of PI single positive cells. The lower right grid represents the number of annexin V single positive cells. The upper right grid represents the number of cells positive for both PI and annexin V. The lower left grid denotes the viable population.

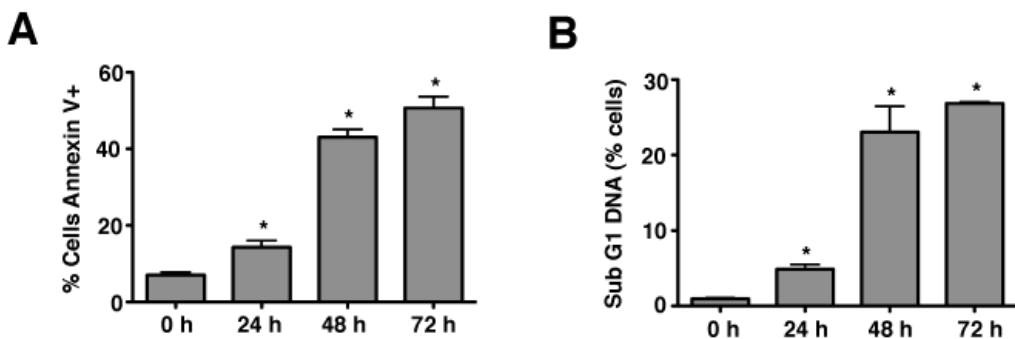


**Figure 94.** Annexin V+ HeLa cells and subG<sub>1</sub> fragmentation after RZ2 treatment. (A) HeLa cells were incubated for 0 h (control), 24 h, 48 h and 72 h with 10  $\mu$ M RZ2 and stained for annexin V/PI. Data are mean $\pm$ s.e.m. (n=3). \*Significantly different from control ( $P<0.05$ ). (B) Flow cytometry analysis of the subG<sub>1</sub> DNA fragmentation in ethanol-fixed HeLa cells after incubation with 10  $\mu$ M RZ2 for 0 h (control), 24 h, 48 h and 72 h. Data are given as mean $\pm$ s.e.m. (n=3). \*Significantly different from control ( $P<0.05$ ).

Further examination of the morphological changes in respond to RZ2 treatment was assessed by fluorescence staining. HeLa cells were stained with the fluorescent dye Hoechst 33528 and visualized. The nuclear fragmentation of apoptotic cells after 48 h of treatment with RZ2 was evident under the microscope (Figure 95), where the condensed chromatin areas are well distinguishable from the evenly distributed fluorescence occurring in control nuclei. Pyknosis and karyorrhexis were evident after 48 h and 72 h, but the nuclei subjected to 24 h treatment with RZ2 were intact, round and homogeneous. This observation, together with the low increase in annexin V-positive cells and the only 5% sub-G<sub>1</sub> DNA fragmentation result of 24 h exposure to RZ2, suggests that activation of apoptosis does not occur after 24 h of treatment.

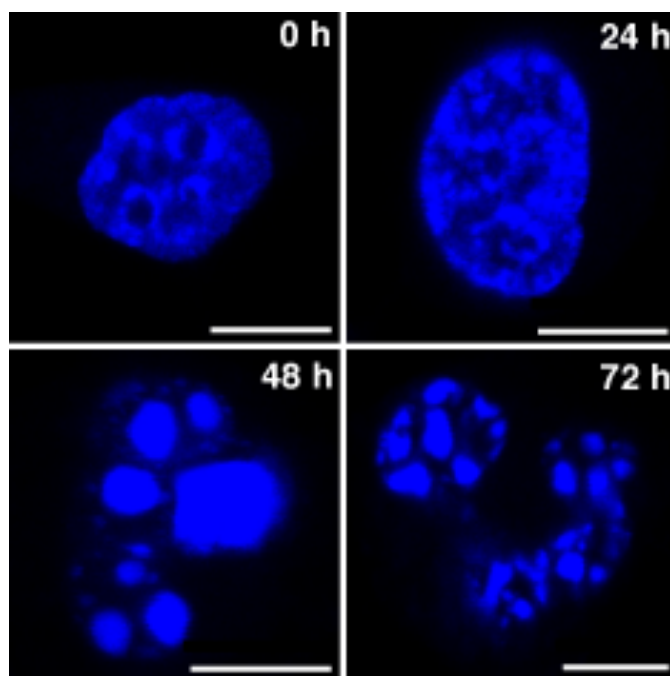


**Figure 95.** Morphological analysis of nuclear fragmentation of HeLa cells treated with RZ2. Pictures were taken using a Leica SP2 confocal microscope after incubation with 10  $\mu$ M RZ2 for 0 h (control), 24 h, 48 h and 72 h. Scale bars = 10  $\mu$ m.

The active forms of caspases 3 and 7 in apoptotic living cells show specificity for cleavage at the C-terminus of the aspartate residue of the sequence DEVD (Asp-Glu-Val-Asp).<sup>76</sup> Detection of DEVD hydrolysis is a reliable method for monitoring apoptosis induction events and caspases 3/7 activity over time in living cells.<sup>77</sup> Thus, the fluorogenic substrate Ac-DEVD-AFC was used as an indicator of the active form of effector caspases, which are the ones that trigger the apoptotic process. For this, HeLa cells were treated with two concentrations of RZ2 (10  $\mu$ M and 25  $\mu$ M) (Figure 96).

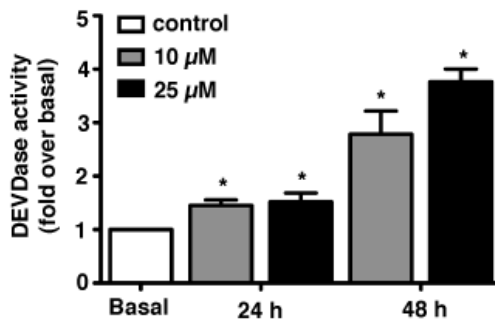


**Figure 96.** Caspase activity detected by measurement of DEVD-AFC substrate processing. HeLa cells were treated with 10  $\mu$ M and 25  $\mu$ M RZ2 for 24 h and 48 h. Data are mean $\pm$ s.e.m. (n=3). \*Significantly different from control (P<0.05).

Significant increase in DEVDase activity was not observed after 24 h with none of the two concentrations, but after 48 h there was a nearly 3-fold increase with 10  $\mu$ M RZ2 and a 4-fold increase with the concentration of 25  $\mu$ M.

HeLa cells showed increase in active (cleaved) caspase 3 levels as well as cleaved poly(ADP-ribose) polymerase (PARP), another marker of cells undergoing apoptosis (Figure 97). However, these increases were not significant at 24 h, opposite to the cells treated with RZ2 for 48 h.

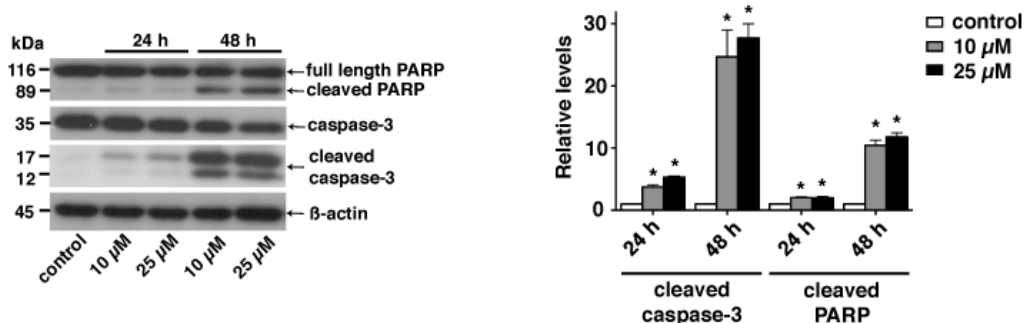


**Figure 97.** Total cleaved caspase 3 and PARP levels detected by western blot. HeLa cells were treated with 10  $\mu$ M and 25  $\mu$ M RZ2 for 24 h and 48 h. Non-treated cells were used as control.  $\beta$ -actin was used for loading normalization. Data are mean $\pm$ s.e.m. (n=3). \*Significantly different from control (P<0.05).

All these observations confirm that HeLa cells die as a result of apoptosis when exposed to RZ2, but this death pathway is not activated from the beginning of the treatment.

### Does RZ2 cause a cell-cycle arrest?

To gain insights into the mechanism by which RZ2 antiproliferative effect is achieved, its effect on cell cycle distribution was investigated by flow cytometry. Non-synchronized HeLa cells cultures treated with 10  $\mu$ M RZ2 resulted in the accumulation of S phase, from 26% to 47% after 72 h in a time-dependant manner, with concomitant decrease in percentage of cells in G<sub>1</sub> phase. Cells treated for 24 hours started accumulating in G<sub>2</sub> phase from 20% to 35%. However, by 48 h a decrease was observed and by 72 h cells in G<sub>2</sub> phase were 23% (Figure 98).

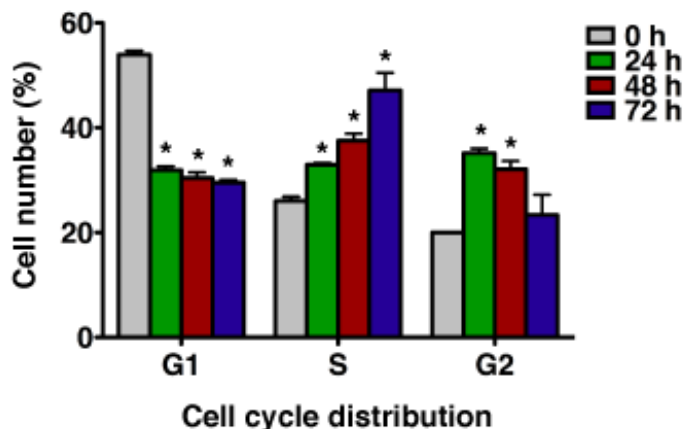


**Figure 98.** Cell cycle distribution of HeLa cells treated with RZ2. HeLa cells treated with 10  $\mu$ M RZ2 for 0 h (control), 24 h, 48 h and 72 h are expressed as the percentage of cells in the indicated phases of the cell cycle. Data are mean $\pm$ s.e.m. (n=3). \*Significantly different from control (P<0.05).

Regulation of cell growth is mainly controlled through cell cycle control mechanisms. Progression of eukaryotic cells through the cell cycle is orchestrated by the sequential activation and inactivation of cyclin-dependent kinases (CDKs). p21 is a potent cyclin-dependent kinase inhibitor, and thus functions as a regulator of cell cycle progression<sup>78</sup> and plays an essential role in growth arrest. It has been reported that p21 not only affects the G<sub>1</sub>-S and G<sub>2</sub>-M transitions<sup>79</sup> but its overexpression leads S-phase arrest.<sup>80</sup> Since RZ2 alters cell cycle progression provoking an S phase arrest in HeLa cells, the expression levels of p21 were assessed by western blot analysis.

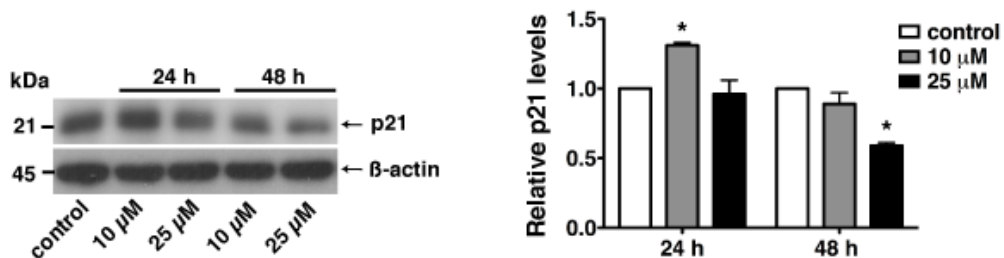


**Figure 99.** Expression of p21 measured by western blot. HeLa cells were treated with 10  $\mu$ M and 25  $\mu$ M RZ2 for 24 h and 48 h. Densitometric quantification of p21 levels are relative to control, non-treated cells.  $\beta$ -actin was used for loading normalization. Data are mean $\pm$ s.e.m. (n=3). \*Significantly different from control (P<0.05).

As shown in Figure 99, p21 expression increased slightly (1.3 fold) after 24 h treatment with 10  $\mu$ M RZ2 but decreased after 48 h treatment to almost the basal level (0.96 fold). When HeLa cells were treated with 25  $\mu$ M RZ2 for 24 h a subtle decrease in p21 expression (0.89 fold) was followed by a more significant decrease (0.59 fold) after 48 h of treatment.

Based on these observations and that increases in p53 protein levels and its phosphorylated form at Ser-15 were not observed, it is postulated that RZ2 causes apoptosis through a p53-independent mechanism and that the S arrest in HeLa cells is not induced by activation of the p21 gene transcription. So, the next question to be answered was: what happens in the first 24 hours of RZ2 treatment within the cell?

***Does RZ2 trigger autophagy?***

Autophagy is a degradation pathway responsible for the disposal of damaged organelles and the clearance of aggregation-prone proteins.<sup>81</sup> It plays an important role in physiological responses such as starvation, where nonselective degradation enables cells to survive by energy production and macromolecule synthesis from the degradation products.

Microtubule-associated protein 1A/1B-light chain 3 (LC3) is a soluble protein, whose cytosolic form (LC3-I) is conjugated to phosphatidylethanolamine to form LC3-phosphatidylethanolamine conjugate (LC3-II) and recruited to autophagosomal membranes. Thus, lysosomal turnover of the autophagosomal marker LC3-II reflects starvation-induced autophagic activity, so detection of LC3 by immunoblotting appears to be the best marker at the present for monitoring autophagy.<sup>82</sup>

In addition, it has been reported that p62, also known as Sequestosome-1, directly interacts with LC3<sup>83</sup> and is a selective substrate for autophagy. There is also evidence that p62 acts as cargo receptor for selective autophagy of various ubiquitinated substrates.<sup>84</sup>

Thus, the role of autophagy in RZ2-induced human cancer cell death was studied. HeLa cells were treated with RZ2 for 24 h and 48 h, and autophagy was assayed by immunodetection of p62 and LC3bII.

As shown in Figure 100, LC3-II significantly increases after 24 h of treatment with either 10 or 25  $\mu$ M RZ2, indicating induction of autophagosomes formation. However, p62 was also increased (Figure 100), suggesting a blockage in later steps of autophagy after LC3 activation (lipidation to LC3-II). Noteworthy is the fact that p62 and LC3-II expression levels after 48 h decay in concordance to the activation of the apoptotic pathway (caspase 3 activation and PARP cleavage).

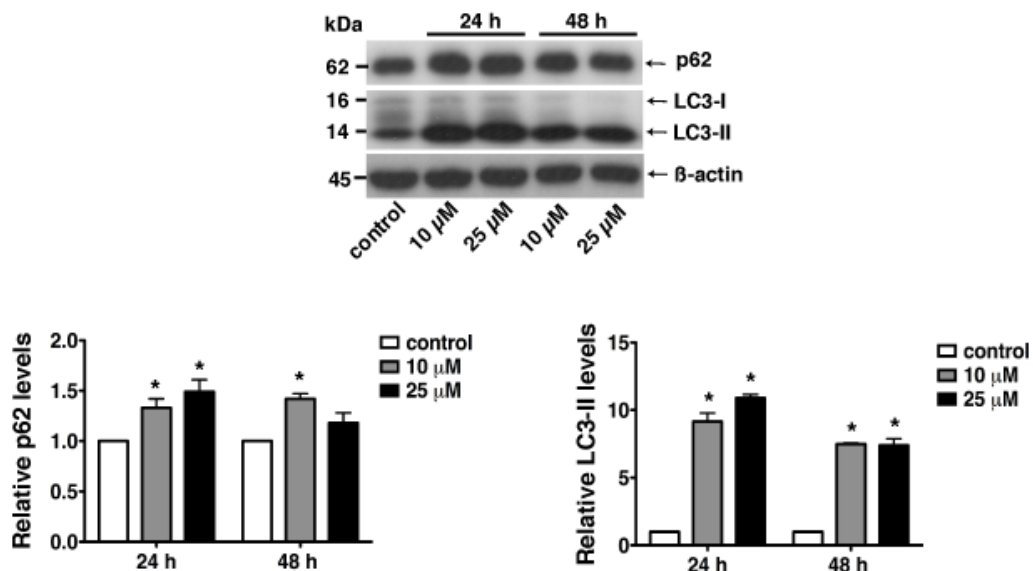


**Figure 100.** Expression of p62 and LC3-II measured by western blot. HeLa cells were treated with 10  $\mu$ M and 25  $\mu$ M RZ2 for 24 h and 48 h. The expression of p62 and LC3-II was measured by western blot. Densitometric quantification of p62 levels are relative to control, non-treated cells.  $\beta$ -actin was used for loading normalization. Data are mean $\pm$ s.e.m. ( $n=3$ ). (A, right panel) Densitometric quantification of LC3-II levels (relative to control, non-treated cells). Data are mean $\pm$ s.e.m. ( $n=3$ ). \*Significantly different from control ( $P<0.05$ ).

Autophagy may be a survival tactic when apoptosis is not an effective option, such as in cell starvation, but it may be a prominent pathway to death when autophagy progresses too far without rescue of the cell. It is thought that RZ2 causes such a big stress to the cells that they cannot rescue themselves by autophagy in the first 24 h of treatment, so cells death occurs after this time.

#### RZ2 is internalized into the cell in acidic compartments

In order to visualize if RZ2 is internalized into the cytosol, HeLa cells were incubated with a high concentration (50  $\mu$ M) of its more active fluorescent version, RZ2CF, for 24 h and images were acquired with an inverted spinning disk microscope every 15 minutes.

No accumulation of the compound was evident neither on the membrane nor into the cytoplasm in the first 8 h of treatment. Afterwards, some intense fluorescence was observed into small spherical granules within the cells. However, the presence of RZ2CF inside the cells was not unarguably evident until a significant increase of fluorescent vesicles was observed when the cytoskeleton of the apoptotic cells collapsed.

Since absorption and fluorescence properties of CF are strongly pH dependent, the absorption spectra of RZ2CF at different pH values was evaluated. As shown in Figure 101, the absorbance of compound RZ2CF at pH values similar to the ones in lysosomes (pH 4.5-5), late endosomes (pH 5-6), and early endosomes (6-7) is lower than its absorbance at extracellular and cytosolic pH (7.5). Hence, RZ2CF cannot be seen into the cells while it is into acidic

compartments, until a dramatic change in their pH as a result of the apoptotic process enhances the fluorescence intensity of CF.

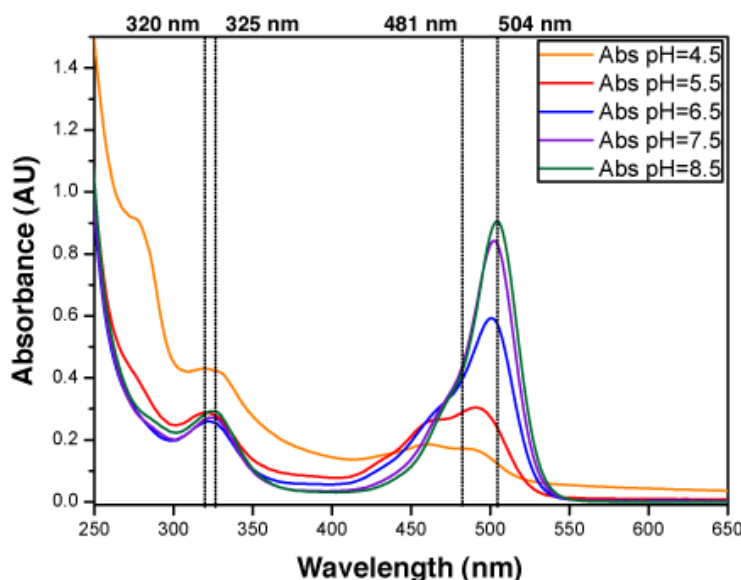


**Figure 101.** Absorption spectra of RZ2CF at different pH values.

To investigate if compound RZ2 promotes the formation of acidic compartments, HeLa cells were treated with 10 and 25  $\mu$ M RZ2 for 24 h and incubated with Lysotracker Green for the last 20 min before flow cytometry analysis.

As shown in Figure 102, lysotracker staining was significantly enhanced by a 1.8 fold-change with 10  $\mu$ M RZ2 and by a 2 fold-change with 25  $\mu$ M RZ2 when compared to control (untreated) cells. These results corroborate that RZ2 affects the endosomal/lysosomal system promoting the formation of acidic compartments within the cell.

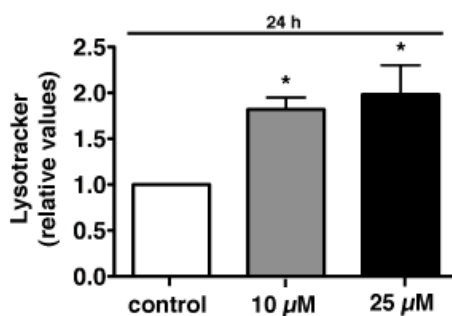


**Figure 102.** Acidic compartments of HeLa cells treated with RZ2. Acidic compartments of HeLa cells treated with 10  $\mu$ M and 25  $\mu$ M RZ2 for 24 h were stained with Lysotracker Green and analyzed by flow cytometry. Data are given as mean $\pm$ s.e.m. ( $n=3$ ). \*Significantly different from control ( $P<0.05$ ).

To examine collocalization of the compound with acidic compartments, HeLa cells were treated with 25  $\mu$ M RZ2CF for 24 h and live-cell confocal microscopy was performed using Lysotracker red. Cells' nuclei were stained with Hoechst 33342 (blue). As shown in Figure 103, fluorescence in the green channel due to RZ2CF collocalizes with most of the compartments stained with Lysotracker, suggesting that the site of cytotoxic actions of RZ2 is likely lysosomes.

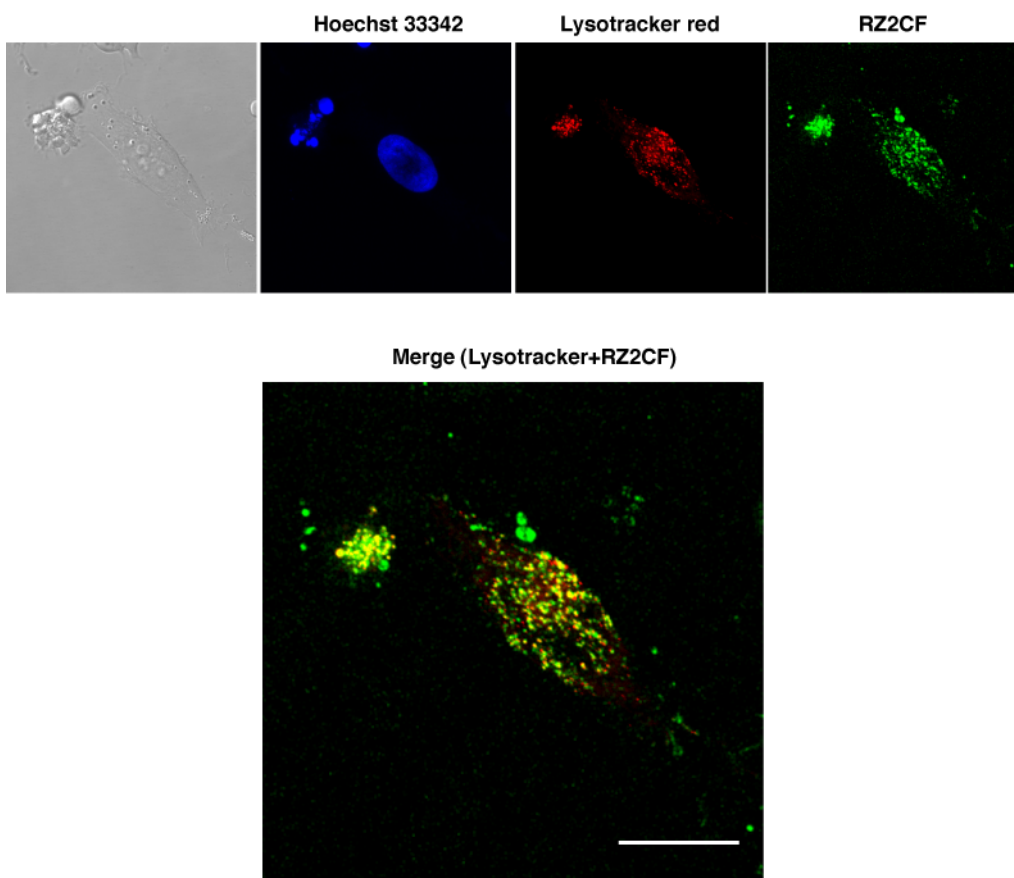


**Figure 103.** Confocal laser scanning microscopy of HeLa cells after 24 h incubation with 25  $\mu$ M RZ2CF. Green fluorescence is due to the 5-carboxyfluorescein labeled RZ2 compound. Scale bar = 20  $\mu$ m.

Since RZ2 accumulates in acidic compartments, it is plausible that RZ2 blocks the formation of autophagolysosomes. To test this hypothesis, Bafilomycin A<sub>1</sub> was used, since it is a specific inhibitor of the vacuolar type H(+)-ATPase (V-ATPase) that inhibits the acidification of organelles containing this enzyme, such as endosomes and lysosomes,<sup>85</sup> thus blocking the turnover of autophagosomes.

As shown in Figure 104, the presence of 100 nM bafilomycin A<sub>1</sub> led to a further increase in LC3-II expression levels compared to those of RZ2 alone. Thus, RZ2 induces the formation of autophagosomes without blocking their fusion with lysosomes. Moreover, based on the increase of p62, the fact that RZ2 is not degraded by cathepsin B, and the observation of a significant accumulation of RZ2CF in acidic compartments leading to cell death, it is postulated

that RZ2 blocks the autophagic response inhibiting protein degradation due to its excessive accumulation in the endosomal/lysosomal system.

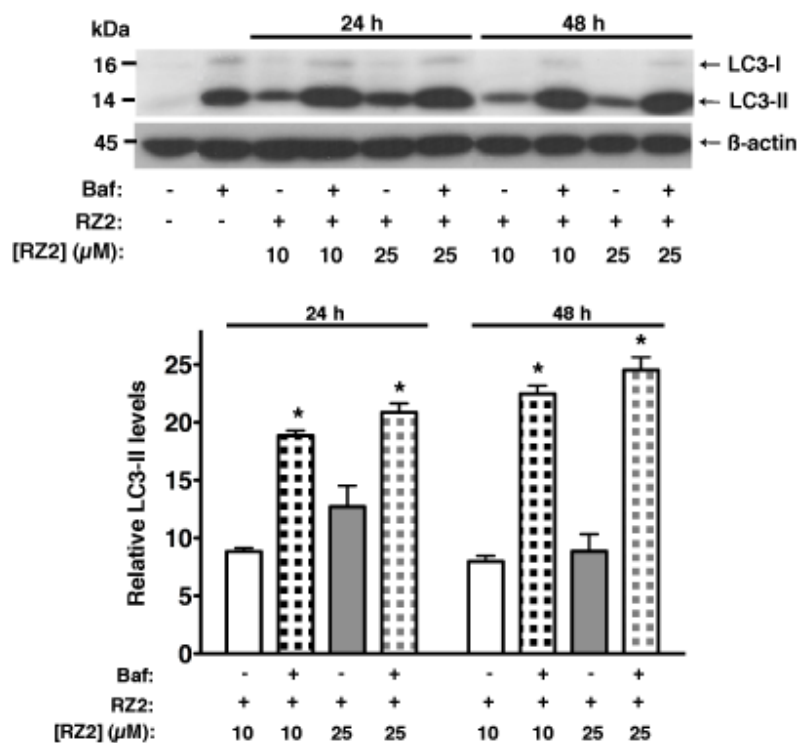


**Figure 104.** LC3-II expression measured by western blot in the presence or absence of Baf. HeLa cells were treated with 10 µM and 25 µM RZ2 for 24 h and 48 h, in the presence or absence of 100 nM Bafilomycin A<sub>1</sub> (Baf) for 16 h. LC3-II expression was measured by western blot. Densitometric quantification of LC3-II levels is relative to control, non-treated cells. β-actin was used for loading normalization. Data are mean±s.e.m. (n=3). \*Significantly different from compound RZ2 treated without Baf (P<0.05).

### Gene expression microarray

Microarrays are the most frequently used technology for genome-wide expression profiling, which holds great promises for elucidating the mode of action of drugs.<sup>86</sup> Within the cell, drugs pass through and affect a plethora of metabolic pathways, thus genomic microarray technology offers a solution to genotype the variations involved.<sup>87</sup>

In order to further evaluate the mode of action of RZ2, the changes in gene expression before the apoptotic pathway activation were studied. For this, global perturbations in genome-wide RNA expression in HeLa cells treated with a low concentration (5 µM) of RZ2 for 24 h were measured by gene expression microarray. The whole list of genes in the array (ranked by mean foldchange against vehicle treated cells, from most upregulated to most downregulated) was analyzed against Human GO Biological Process and KEGG databases in order to detect overrepresented genesets. A Gene Set Enrichment Analysis (GSEA) was employed due to its capability of assessing the group behaviour of a set of genes.<sup>88</sup>

Figure 105 shows that two of the biological processes found to be enriched are the response to starvation and the defense response. Furthermore, the p53 signaling pathway as well as the positive regulation of caspase activity are depleted, which corroborates the previous observations where RZ2 triggers a p53-independent death pathway that starts with autophagosomes induction further followed by autophagy blockade and caspase activation leading to apoptosis only after 24 h of treatment.

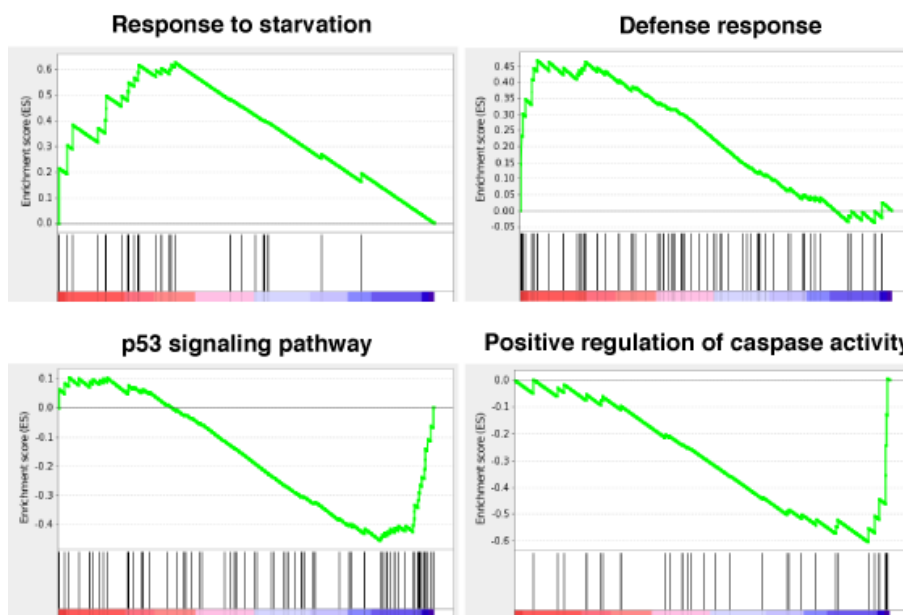


**Figure 105.** GSEA plots for the effects in response to RZ2 treatment to HeLa cells. Enrichment effects (upper) and suppression effects (lower) in response to 5  $\mu$ M RZ2 treatment to HeLa cells for 24 h.

Analyzing all the gene sets significantly enriched at nominal  $p$  value  $<1\%$  it was observed that many metabolic pathways were upregulated, specially those of amino acids metabolism, suggesting that RZ2 induces metabolic stress in HeLa cells predominantly through accumulation in acidic compartments (see Table 8).

Typically, a combination of metabolic stresses rather than loss of a single nutrient occurs.<sup>1</sup> Amino acid deficiency can activate autophagy to mitigate damage and provide nutrients for short-term survival<sup>89</sup> but despite this effort to relieve stress, autophagy induction can lead to apoptosis rather than protection from cell death.

## Enriched biological processes

Analyzed against Human GO Biological Process database

| NAME   | SIZE | ES         | NES        | NOM p-val    | FDR q-val    | FWER p-val |
|--|------|------------|------------|--------------|--------------|------------|
| NEGATIVE REGULATION OF VIRAL GENOME REPLICATION                        | 31   | 0.78148    | 23.377.488 | 0.0          | 0.0          | 0.0        |
| TYPE I INTERFERON-MEDIATED SIGNALING PATHWAY                           | 63   | 0.6223165  | 21.376.133 | 0.0          | 0.0013449127 | 0.003      |
| GLUCONEOGENESIS  | 43   | 0.6545361  | 20.812.266 | 0.0          | 0.0017658928 | 0.006      |
| GLUCOSE METABOLIC PROCESS  | 100  | 0.5201211  | 19.662.635 | 0.0          | 0.015336841  | 0.069      |
| TRICARBOXYLIC ACID CYCLE   | 28   | 0.6652144  | 19.528.044 | 0.0          | 0.015737018  | 0.089      |
| GLYCOGEN CATABOLIC PROCESS   | 17   | 0.7423281  | 19.227.481 | 0.0          | 0.020900121  | 0.138      |
| HEART MORPHOGENESIS  | 33   | 0.6222864  | 18.866.948 | 0.0021141649 | 0.03054183   | 0.23       |
| CHOLESTEROL BIOSYNTHETIC PROCESS                                       | 31   | 0.6195491  | 18.463.035 | 0.0          | 0.050183658  | 0.403      |
| DETECTION OF CHEMICAL STIMULUS INVOLVED IN SENSORY PERCEPTION OF SMELL | 35   | 0.59830683 | 1.845.602  | 0.004338395  | 0.045365784  | 0.407      |
| RESPONSE TO STARVATION   | 26   | 0.62742585 | 18.224.932 | 0.0          | 0.05745298   | 0.499      |
| CHOLESTEROL METABOLIC PROCESS  | 64   | 0.5222403  | 18.058.045 | 0.0021929825 | 0.06435228   | 0.566      |
| NUCLEOSOME DISASSEMBLY   | 15   | 0.70671594 | 17.638.073 | 0.0022522523 | 0.09996373   | 0.753      |
| 2-OXOGLUTARATE METABOLIC PROCESS                                       | 15   | 0.6950013  | 17.544.839 | 0.006342495  | 0.103279024  | 0.789      |
| DEFENSE RESPONSE TO GRAM-POSITIVE BACTERIUM                            | 35   | 0.57379705 | 17.334.262 | 0.0          | 0.120651476  | 0.855      |
| DEFENSE RESPONSE TO VIRUS  | 134  | 0.44864517 | 17.256.721 | 0.0          | 0.12224841   | 0.882      |
| REGULATION OF LONG-TERM NEURONAL SYNAPTIC PLASTICITY                   | 17   | 0.6614782  | 16.878.102 | 0.008264462  | 0.17050302   | 0.954      |
| GLYCOLYSIS   | 44   | 0.52585274 | 16.848.214 | 0.004524887  | 0.16583481   | 0.958      |
| RESPONSE TO INTERFERON-GAMMA   | 18   | 0.6420967  | 16.800.141 | 0.00814664   | 0.16316774   | 0.96       |
| RESPONSE TO VIRUS  | 111  | 0.44196787 | 16.724.387 | 0.0          | 0.1669617    | 0.971      |
| TRNA AMINOACYLATION FOR PROTEIN TRANSLATION                            | 41   | 0.5206481  | 16.553.028 | 0.008583691  | 0.18781683   | 0.989      |
| MESODERM DEVELOPMENT   | 29   | 0.5585808  | 16.388.875 | 0.014861995  | 0.20903493   | 0.997      |
| DEFENSE RESPONSE   | 62   | 0.46768925 | 16.212.648 | 0.0065075923 | 0.23426242   | 1.0        |
| HEXOSE TRANSPORT   | 40   | 0.5199293  | 16.208.147 | 0.00856531   | 0.22479299   | 1.0        |
| GLUCOSE TRANSPORT  | 57   | 0.48236126 | 16.195.284 | 0.0022123894 | 0.21754394   | 1.0        |
| CELLULAR RESPONSE TO CAMP  | 24   | 0.5690456  | 16.113.114 | 0.010706638  | 0.22602929   | 1.0        |

Analyzed against KEGG database

| NAME  | SIZE | ES         | NES        | NOM p-val    | FDR q-val   | FWER p-val |
|---|------|------------|------------|--------------|-------------|------------|
| ANTIGEN PROCESSING AND PRESENTATION         | 67   | 0.56711996 | 19.694.042 | 0.0          | 0.008319669 | 0.007      |
| CITRATE CYCLE (TCA CYCLE)                   | 30   | 0.6613612  | 1.887.204  | 0.0          | 0.016198507 | 0.027      |
| ARGININE AND PROLINE METABOLISM             | 53   | 0.5263432  | 17.498.868 | 0.0021978023 | 0.06352819  | 0.15       |
| ALANINE, ASPARTATE AND GLUTAMATE METABOLISM | 32   | 0.5861432  | 17.467.111 | 0.002118644  | 0.04911635  | 0.155      |
| PENTOSE PHOSPHATE PATHWAY                   | 27   | 0.6031213  | 17.422.475 | 0.0          | 0.04110694  | 0.162      |
| BUTANOATE METABOLISM                        | 30   | 0.58920115 | 17.397.012 | 0.008403362  | 0.035617013 | 0.168      |
| CYSTEINE AND METHIONINE METABOLISM          | 36   | 0.552814   | 16.946.765 | 0.0061601643 | 0.05180359  | 0.261      |
| GLYCINE, SERINE AND THREONINE METABOLISM    | 32   | 0.56515574 | 16.854.066 | 0.004385965  | 0.049957566 | 0.284      |
| PYRUVATE METABOLISM                         | 40   | 0.5274333  | 16.726.722 | 0.0066666667 | 0.050190784 | 0.317      |
| RNA TRANSPORT                               | 147  | 0.4243381  | 1.667.155  | 0.0          | 0.048890114 | 0.34       |
| STAPHYLOCOCCUS AUREUS INFECTION             | 50   | 0.5078036  | 16.595.896 | 0.0043668123 | 0.04789632  | 0.362      |
| DNA REPLICATION                             | 36   | 0.52958566 | 16.502.188 | 0.0          | 0.049027342 | 0.389      |
| FC EPSILON RI SIGNALING PATHWAY             | 76   | 0.46568626 | 16.477.689 | 0.0          | 0.046987664 | 0.404      |
| MATURITY ONSET DIABETES OF THE YOUNG        | 24   | 0.5807541  | 16.430.821 | 0.0121951215 | 0.045871757 | 0.422      |
| PPAR SIGNALING PATHWAY                      | 69   | 0.47274315 | 16.372.145 | 0.0022371365 | 0.044800457 | 0.433      |
| STEROID BIOSYNTHESIS                        | 19   | 0.6150128  | 16.327.245 | 0.018518519  | 0.044979498 | 0.452      |
| STARCH AND SUCROSE METABOLISM               | 41   | 0.5027506  | 16.081.402 | 0.012631579  | 0.05354015  | 0.533      |
| MISMATCH REPAIR                             | 23   | 0.56066436 | 15.932.007 | 0.0186722    | 0.0580496   | 0.577      |
| GRAFT-VERSUS-HOST DISEASE                   | 36   | 0.50296897 | 15.616.245 | 0.018306635  | 0.07396781  | 0.673      |
| AMINOACYL-TRNA BIOSYNTHESIS                 | 41   | 0.48372048 | 15.290.956 | 0.023255814  | 0.092925616 | 0.77       |

|   |    |            |            |             |            |       |
|---|----|------------|------------|-------------|------------|-------|
| CARBOHYDRATE DIGESTION AND ABSORPTION   | 40 | 0.4856828  | 15.251.759 | 0.023157895 | 0.09149643 | 0.777 |
| ALLOGRAFT REJECTION                     | 35 | 0.48605764 | 15.161.515 | 0.036585364 | 0.09465729 | 0.804 |
| GLYOXYLATE AND DICARBOXYLATE METABOLISM | 18 | 0.581714   | 15.144.846 | 0.03837953  | 0.09232531 | 0.81  |
| FAT DIGESTION AND ABSORPTION            | 44 | 0.46393788 | 14.797.084 | 0.018292682 | 0.11710185 | 0.896 |
| TYPE I DIABETES MELLITUS                | 40 | 0.47028983 | 14.718.544 | 0.019693654 | 0.11942241 | 0.919 |

## Depleted biological processes

Analyzed against Human GO Biological Process database

| NAME   | SIZE | ES          | NES         | NOM p-val    | FDR q-val    | FWER p-val |
|--|------|-------------|-------------|--------------|--------------|------------|
| POSITIVE REGULATION OF SMOOTH MUSCLE CELL PROLIFERATION          | 40   | -0.68550247 | -21.012.874 | 0.0          | 0.0032914614 | 0.003      |
| ACTIN FILAMENT BUNDLE ASSEMBLY                                   | 23   | -0.72596234 | -1.975.864  | 0.0          | 0.033468474  | 0.058      |
| OSTEOBLAST DIFFERENTIATION                                       | 55   | -0.6077046  | -19.740.663 | 0.0          | 0.022681424  | 0.059      |
| POSITIVE REGULATION OF CELL DEATH                                | 17   | -0.7698962  | -19.417.777 | 0.0          | 0.03348752   | 0.115      |
| NEGATIVE REGULATION OF CANONICAL WNT RECEPTOR SIGNALING PATHWAY  | 75   | -0.5531178  | -19.010.564 | 0.0          | 0.050461974  | 0.202      |
| NEURON FATE COMMITMENT   | 18   | -0.72952    | -18.940.889 | 0.0          | 0.048924215  | 0.228      |
| POSITIVE REGULATION OF FIBROBLAST PROLIFERATION                  | 39   | -0.60197735 | -18.527.478 | 0.0          | 0.077671245  | 0.385      |
| POSITIVE REGULATION OF CELL MIGRATION                            | 107  | -0.5081286  | -18.291.582 | 0.0          | 0.09294567   | 0.489      |
| CELLULAR RESPONSE TO LIPOPOLYSACCHARIDE                          | 64   | -0.5428616  | -18.166.375 | 0.001754386  | 0.09708997   | 0.546      |
| POSITIVE REGULATION OF COLLAGEN BIOSYNTHETIC PROCESS             | 16   | -0.72859824 | -18.145.195 | 0.0          | 0.08963202   | 0.554      |
| RESPONSE TO NICOTINE   | 20   | -0.69304776 | -18.109.995 | 0.0018450185 | 0.08463673   | 0.571      |
| NEGATIVE REGULATION OF BMP SIGNALING PATHWAY                     | 32   | -0.6188053  | -18.027.955 | 0.0018484289 | 0.08784394   | 0.609      |
| RESPONSE TO WOUNDING   | 52   | -0.5552653  | -18.022.307 | 0.0          | 0.08151701   | 0.611      |
| ACTIVATION OF MAPKK ACTIVITY                                     | 46   | -0.5567821  | -17.886.662 | 0.0037950664 | 0.08847992   | 0.673      |
| POSITIVE REGULATION OF ANGIOGENESIS                              | 82   | -0.50954443 | -17.815.975 | 0.0          | 0.090419225  | 0.704      |
| KERATINOCYTE DIFFERENTIATION                                     | 52   | -0.54526466 | -17.757.224 | 0.0018796993 | 0.09097363   | 0.73       |
| WOUND HEALING  | 61   | -0.5415706  | -17.729.709 | 0.001776199  | 0.088597     | 0.744      |
| RESPONSE TO PROGESTERONE STIMULUS                                | 24   | -0.6415636  | -17.707.795 | 0.003992016  | 0.08631312   | 0.752      |
| POSITIVE REGULATION OF ENDOTHELIAL CELL MIGRATION                | 29   | -0.6099705  | -17.676.376 | 0.005791506  | 0.08513202   | 0.771      |
| CELLULAR RESPONSE TO TUMOR NECROSIS FACTOR                       | 39   | -0.5662046  | -17.267.431 | 0.0035906644 | 0.1311437    | 0.908      |
| ANGIOGENESIS   | 200  | -0.43098354 | -17.253.217 | 0.0          | 0.12686282   | 0.911      |
| CELLULAR RESPONSE TO TRANSFORMING GROWTH FACTOR BETA STIMULUS    | 31   | -0.58403707 | -17.245.928 | 0.0018691589 | 0.1223194    | 0.911      |
| NEGATIVE REGULATION OF NEURON PROJECTION DEVELOPMENT             | 24   | -0.6207839  | -17.238.826 | 0.003868472  | 0.11788281   | 0.913      |
| POSITIVE REGULATION OF TYROSINE PHOSPHORYLATION OF STAT3 PROTEIN | 25   | -0.61646545 | -17.23.497  | 0.011811024  | 0.113749705  | 0.914      |
| POSITIVE REGULATION OF CASPASE ACTIVITY                          | 30   | -0.60460305 | -17.232.732 | 0.0058139535 | 0.109419934  | 0.914      |

Analyzed against KEGG database

| NAME   | SIZE | ES          | NES         | NOM p-val    | FDR q-val  | FWER p-val |
|--|------|-------------|-------------|--------------|------------|------------|
| HYPERTROPHIC CARDIOMYOPATHY (HCM)                      | 83   | -0.4805204  | -17.229.849 | 0.0          | 0.22669855 | 0.237      |
| FOCAL ADHESION   | 198  | -0.42973024 | -16.892.631 | 0.0          | 0.16908604 | 0.328      |
| ECM-RECEPTOR INTERACTION                               | 83   | -0.46843156 | -16.544.653 | 0.0          | 0.16659679 | 0.45       |
| DILATED CARDIOMYOPATHY                                 | 90   | -0.46640205 | -16.402.359 | 0.0034904014 | 0.14379661 | 0.505      |
| REGULATION OF ACTIN CYTOSKELETON                       | 209  | -0.40250874 | -16.015.072 | 0.0          | 0.16906388 | 0.634      |
| P53 SIGNALING PATHWAY                                  | 68   | -0.45710045 | -15.446.469 | 0.005628518  | 0.23524497 | 0.829      |
| PATHOGENIC ESCHERICHIA COLI INFECTION                  | 54   | -0.47557902 | -15.445.068 | 0.015789473  | 0.20189527 | 0.83       |
| AFRICAN TRYpanosomiasis                                | 33   | -0.5121842  | -15.140.245 | 0.0295858    | 0.22667436 | 0.903      |
| NICOTINATE AND NICOTINAMIDE METABOLISM                 | 24   | -0.5284027  | -14.682.057 | 0.06417112   | 0.2944122  | 0.966      |
| ARRHYTHMOGENIC RIGHT VENTRICULAR CARDIOMYOPATHY (ARVC) | 74   | -0.41809237 | -14.397.104 | 0.032846715  | 0.33283636 | 0.983      |
| MAPK SIGNALING PATHWAY                                 | 266  | -0.35635197 | -14.314.214 | 0.0032733225 | 0.32307726 | 0.984      |
| ERBB SIGNALING PATHWAY                                 | 86   | -0.40528017 | -14.128.402 | 0.035460994  | 0.33730334 | 0.993      |
| VASCULAR SMOOTH MUSCLE CONTRACTION                     | 113  | -0.3815718  | -14.037.989 | 0.018771332  | 0.33122876 | 0.996      |

|  |     |             |             |              |            |       |
|--|-----|-------------|-------------|--------------|------------|-------|
| CYTOKINE-CYTOKINE RECEPTOR INTERACTION       | 251 | -0.34622884 | -13.995.738 | 0.0049586776 | 0.31694412 | 0.996 |
| METABOLISM OF XENOBIOTICS BY CYTOCHROME P450 | 60  | -0.41922906 | -13.972.542 | 0.03314917   | 0.30057806 | 0.996 |
| CIRCADIAN RHYTHM - MAMMAL                    | 21  | -0.52086455 | -1.391.138  | 0.07453416   | 0.29437596 | 0.997 |
| SHIGELLOSIS                                  | 59  | -0.41932362 | -13.802.059 | 0.06010929   | 0.29975033 | 0.999 |
| MALARIA                                      | 49  | -0.43517372 | -13.716.549 | 0.05950096   | 0.30014303 | 0.999 |
| UBIQUITIN MEDiated PROTEOLYSIS               | 135 | -0.35590848 | -13.628.969 | 0.03130435   | 0.30144557 | 0.999 |
| TGF-BETA SIGNALING PATHWAY                   | 84  | -0.38812914 | -13.611.718 | 0.06137184   | 0.2906321  | 1.0   |
| NEUROTROPHIN SIGNALING PATHWAY               | 126 | -0.36456087 | -13.510.429 | 0.035149384  | 0.2982771  | 1.0   |
| RHEUMATOID ARTHRITIS                         | 86  | -0.38484907 | -13.427.604 | 0.07102804   | 0.30108902 | 1.0   |
| DRUG METABOLISM - CYTOCHROME P450            | 60  | -0.39869827 | -13.383.447 | 0.069518715  | 0.29627332 | 1.0   |
| DORSO-VENTRAL AXIS FORMATION                 | 24  | -0.48580304 | -13.218.433 | 0.120792076  | 0.31575605 | 1.0   |
| GAP JUNCTION                                 | 90  | -0.36182046 | -12.875.705 | 0.074600354  | 0.3795134  | 1.0   |

**Table 8.** List of the biological processes found to be enriched or depleted. Size describes the number of genes in the gene set after filtering out those genes not in the expression dataset. ES is the Enrichment Score for the gene set; that is, the degree to which this gene set is overrepresented at the top or bottom of the ranked list of genes in the expression dataset. NES is the Normalized Enrichment Score; that is, the enrichment score for the gene set after it has been normalized across analyzed gene sets. NOM p-val is the Nominal p value; that is, the statistical significance of the enrichment score. The nominal p value is not adjusted for gene set size or multiple hypothesis testing; therefore, it is of limited use in comparing gene sets. FDR q-val is the False Discovery Rate; that is, the estimated probability that the normalized enrichment score represents a false positive finding. FWER p-val is the FamilyWise-Error Rate; that is, a more conservatively estimated probability that the normalized enrichment score represents a false positive finding.

### Effects of RZ2 on mitochondria

Since mitochondria regulate cellular metabolism and determine whether cell death happens as a result of its membrane permeabilization,<sup>90</sup> the effect of RZ2 on mitochondrial membrane potential and superoxide mitochondrial levels was investigated using tetramethylrhodamine ethyl ester (TMRE) and MitoSOX red dye, respectively.

Mitochondria possess function-related membrane potentials. The dissipation of the inner mitochondrial transmembrane potential ( $\Delta\psi_m$ ) marks the point-of-no-return during the apoptotic program.<sup>91</sup> Mitochondrial depolarization is associated with outer mitochondrial membrane permeability which is induced by many physiological effectors.<sup>92</sup>

TMRE is a cellular permeant, positively-charged, dye that accumulates in active mitochondria due to their relative negative charge and is extensively used for labeling and measuring the membrane potential of mitochondria in living cells. Depolarized or inactive mitochondria have decreased membrane potential and fail to sequester TMRE. Mitochondrial transmembrane potential was examined by uptake of TMRE through flow cytometry.

As shown in Figure 106, HeLa cells treated with 10  $\mu$ M RZ2 retained less TMRE than untreated cells (0.71 fold) and cells treated with 25  $\mu$ M RZ2 showed even less retention (0.65 fold). Moreover, mitochondria's membrane depolarization was also assessed and, as it is shown in

Figure 106, 19.8% mitochondria are depolarized after 24 h when treated with 10  $\mu$ M RZ2, and 30% when treated with 25  $\mu$ M RZ2.

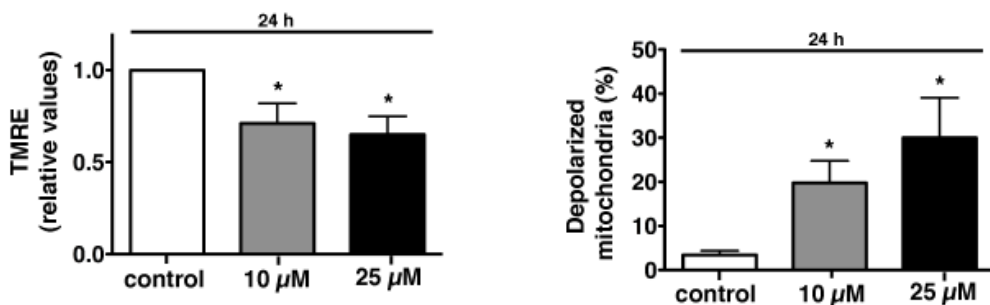


**Figure 106.** Active and depolarized mitochondria after RZ2 treatment in HeLa cells. HeLa cells were treated with 10  $\mu$ M and 25  $\mu$ M RZ2 for 24 h, stained with TMRE and analyzed by flow cytometry to assess the active mitochondria and percentage of cells with completely depolarized mitochondria. Data are given as mean $\pm$ s.e.m. (n=3). \*Significantly different from control (P<0.05).

Mitochondrial superoxide is generated as a byproduct of oxidative phosphorylation and is the predominant reactive oxygen species (ROS) in mitochondria. In order to examine ROS levels in HeLa cells either exposed to RZ2 or not, MitoSOX, a fluorophore for the specific detection of superoxide in the mitochondria of living cells, was used. MitoSOX red fluorogenic dye is live-cell permeant and is rapidly and selectively targeted to mitochondria and it is oxidized by superoxide but not by other ROS generating systems.

As shown in Figure 107, there is a hyperproduction of superoxide anions (1.44 fold) with 10  $\mu$ M RZ2, and even higher levels (1.82 fold) with 25  $\mu$ M RZ2.

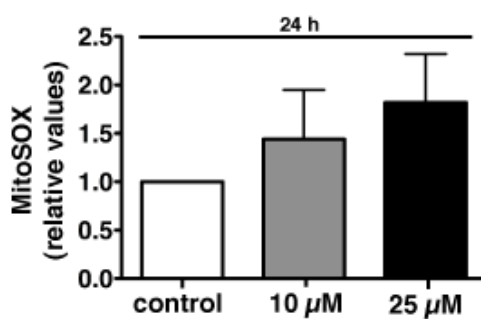


**Figure 107.** Superoxide mitochondrial production after treatment with RZ2. HeLa cells were treated with 10  $\mu$ M and 25  $\mu$ M RZ2 for 24 h and analyzed by flow cytometry after addition of MitoSOX.

Starvation induced autophagy is associated with increased oxidative stress because of an increase of ROS levels in the cell and cytochrome c release is mostly associated with a permanent loss of  $\Delta\psi_m$ , which triggers the assembly of caspase 3 activation complex. So it is pondered that after 24 h of exposure to RZ2, the cytoprotective efforts of autophagy in HeLa

cells are disrupted due to the malfunction in the lysosomal machinery caused by the accumulation of RZ2 in acidic compartments, leading to a decrease in  $\Delta\psi_m$ , as well as an increase in mitochondrial superoxide production, and cell death starts along with caspases activation.

## MATERIALS AND METHODS

### Circular dichroism (CD)

Circular dichroism spectra were recorded with a Jasco 810 UV-Vis spectropolarimeter, with a CDF 426S/426L peltier. The spectra were obtained in a wavelength range of 190 to 250 nm, with a time response of 4s, a scan speed of 10 nm/min, and a step resolution of 0.1 nm. All CD spectroscopic studies were carried out with a continuous flow of nitrogen purging the polarimeter, and the measurements were performed at room temperature with 0.5 cm pathway cells. The CD spectra were run from 320-220 nm and the buffer background was automatically subtracted. The CD spectrum of the oligos alone (100 µM) was recorded as control experiment. Each spectrum was the average of three accumulations.

The choice of buffer in CD measurements is critical, since they have to be as "transparent" as possible. Most of the structural information of interest is found in the lower UV range, where the high absorbance of some buffers can mask the CD signals. 10 mM potassium phosphate was the buffer of choice for these experiments. To achieve a pH 7.5, the proper ratios of the mono and dibasic forms of potassium phosphate were prepared, without using HCl to adjust the pH since chloride ions interfere with CD in the lower UV.

Experimental ellipticity values were transformed to molar ellipticity per residue ( $[\theta]_{MR}$ ) according to the equation:

$$[\theta]_{MR} = \frac{\theta}{C \cdot l \cdot n}$$

Where:

- $\theta$  Ellipticity
- $[\theta]_{MR}$  Molar ellipticity per residue (mdeg·cm<sup>2</sup>·dmol<sup>-1</sup>)
- $C$  Concentration (M)
- $l$  Path length (cm)
- $n$  Number of residues

DNA oligonucleotides were purchased from Biomers (Ulm, Germany).

### Band shift experiment

3'-end radiolabeled *tyrT* fragment (1.5 µL) was mixed with different concentrations of the tested compounds (dissolved in 10 mM Tris-HCl, pH 7.5, containing 10 mM NaCl) and controls and left to equilibrate for 30 minutes at room temperature. A native 6% polyacrylamide gel was run at 400 V for about 45 minutes. The gel was then fixed in 10% (v/v) acetic acid, transferred to

Whatman 3MM paper, and dried under vacuum at 80°C. Dried gel was exposed to a Kodak Phosphor storage screen, which was scanned using a Molecular Dynamics Storm 860 phosphorimager.

### **DNase I footprinting**

#### ***Chemicals and enzymes***

Oligonucleotides were synthesized by Oswel DNA Service (Southampton, UK) on a 40-nmol scale or kindly provided by Tom Brown (School of Chemistry, University of Southampton). All enzymes were purchased from New England Biolabs (Hitchin, UK). Sequagel (19:1 acrylamide:bisacrylamide solution containing 8 M urea) was purchased from National Diagnostics (Hull, UK). DNase I was purchased from Sigma-Aldrich (Poole, UK) and stored at -20°C at a concentration of 7200 units/mL in 20 mM NaCl containing 1mM MgCl<sub>2</sub>. [α-<sup>32</sup>P]dATP was purchased at a concentration of 3000 Ci/mmol (Perkin Elmer, MA, USA).

The compounds were stored at -20°C at a concentration of 5 mM in dimethyl sulfoxide and diluted to working concentrations immediately before use.

#### ***Buffers***

- Sterile 2YT medium for bacterial culture: 16 g tryptone, 10 g yeast extract and 5 g NaCl per 1 L H<sub>2</sub>O.
- For eluting DNA from gel slices (TE1 buffer): 10 mM Tris-HCl, pH 7.5, containing 10 mM EDTA.
- For labeled-DNA resuspension after gel purification (TE2 buffer): 10 mM Tris-HCl, pH 7.5, containing 0.1 mM EDTA.
- For drug solutions: 10 mM Tris-HCl, pH 7.5, containing 10 mM NaCl.
- DNase I solution: 20 mM NaCl, 2 mM MgCl<sub>2</sub>, 2 mM MnCl<sub>2</sub>.
- Loading dye for non-denaturing gels: 20% Ficoll, 10 mM EDTA, 0.1% bromophenol blue.
- DNase I stop solution: formamide containing 10 mM EDTA, 0.1% bromophenol blue and 1 mM NaOH.
- Electrophoresis buffer (10x stock): 108 g Tris, 55 g boric acid and 9.4 g EDTA in 1 L H<sub>2</sub>O.

All salts were purchased from Sigma-Aldrich (molecular biology grade).

### ***Cloning the footprinting template***

#### MS1 and MS2

Fragments are prepared by PCR using one full length synthetic strand (purchased from Oswel DNA service). This contains four extra bases at each end to permit subsequent restriction enzyme cleavage prior to cloning. A short oligonucleotide is annealed to the 17 bases at the 3'-end and the sequence is made fully double stranded by extension with *Taq* DNA polymerase.

The amplified DNA is cut with *Bam*HI (the sequence GGATCC should be included toward the 5'-end of the primers). Before doing this it is important to remove the thermostable polymerase from the PCR reaction, or this will simply fill in the stick-ends that have been generated to facilitate the cloning.

These PCR products are purified on 2% agarose gels. This is then ligated into *Bam*Hicut pUC18 and cloned into *Escherichia coli* TG2 and white colonies are selected from agar plates containing ampicillin, 5-bromo-4-chloro-3-indoyl-β-D-galactopyranoside (X-Gal) and isopropyl β-D-1-thiogalactopyranoside (IPTG). The sequence of the clones must be confirmed by sequencing.

It is often desirable to obtain each sequence cloned in both orientations, so that binding sites close to the ends of the fragment can be easily resolved using one or other clone. This is important for obtaining high resolution data for the entire sequence, as bands at the top of a footprinting gel are often too close together for proper analysis. Bands that are close to the top of the gel in one orientation will be near the bottom in the opposite orientation. MS1 and MS2 are the same sequence but in both orientations. One may be fortunate and obtain both orientations while screening the positive clones; if not the orientation can be changed by simply cutting the purified plasmid with *Bam*HI and re-ligating the mixture.

#### HexA and HexB

Because footprinting fragments that have been cloned into pUC polylinker sites often are isolated by cleaving with *Eco*RI/*Pst*I or *Hind*III/*Sac*I, the insert HexA contains the sites for *Eco*RI (GAATTC) and *Pst*I (CTGCAG) but not *Hind*III (AAGCTT) and *Sac*I (GAGCTC), whereas HexB contains the sites for *Hind*III and *Sac*I but not *Eco*RI and *Pst*I. For each sequence, the upper strand was synthesized with an extra 20 bases at each end for simple PCR amplification and to facilitate subsequent cleavage with *Bam*HI. A 20-mer oligonucleotide was annealed to the 3'-end of this sequence and extended with *Taq* DNA polymerase to prepare the full double-

stranded sequence. This product was isolated by gel electrophoresis, cut with *Bam*HI, and cloned into the *Bam*HI site of pUC19. Successful clones were isolated as white colonies from agar plates supplemented with carbenicillin, X-Gal and IPTG.

Clones with these sequences in the reverse orientation (HexA-reverse and HexB-reverse) were obtained by cutting the forward clones with *Bam*HI and religating the mixture. These reverse clones were obtained as light blue colonies from X-Gal/ IPTG-containing plates (these inserts are multiples of 3 base pairs, and the insertion does not completely inactivate the LacZ gene; both of the forward clones contain in-frame stop codons and, therefore, result in white colonies.)

### **Plasmid preparation**

The Qiagen minipreps commercial kit for plasmid preparation was used.

The plasmid DNA is extracted from a 5 mL culture according to the manufacturer's instructions and this is eluted into 50 µL of elution buffer. This can be stored at -20 °C for future use, though it is recommended to use it immediately for efficient labelling.

### **3'-labelling**

The entire 50 µL plasmid stock prepared from a 5 ml culture is radiolabelled. This is first digested with two restriction enzymes to release the fragment. These enzymes are chosen from those cutting at opposite ends of the polylinker fragment (*Hind*III-*Sac*I for MS1, MS2 and HexA and *Eco*RI-*Pst*I for HexB). *Hind*III and *Eco*RI have a 5'-overhang containing a T, suitable for filling with a polymerase using [ $\alpha$ -<sup>32</sup>P]dATP. If both restriction enzymes produce similar sticky ends, then the second restriction digest must be performed after the labelling reaction and after the polymerase inactivation, so as to avoid labeling both ends of the fragment. It is convenient to use a buffer that is compatible with both restriction enzymes as well as reverse transcriptase, so as to avoid the need for changes of buffer during the process.

After restriction digestion at 37 °C for 1 h, 1 µL of [ $\alpha$ -<sup>32</sup>P]dATP is added together with 0.5 µL AMV reverse transcriptase (Sigma) and incubated for 1 h at 37 °C. The radiolabelled fragment is then separated from the remainder of the plasmid on a non-denaturing polyacrylamide gel. Twenty microlitres of 20% Ficoll solution containing 10 mM EDTA and 0.1% bromophenol blue is added to the radiolabelled mixture and the sample is applied to a 5-8% non-denaturing polyacrylamide gel. The gel (40 cm long, 0.3 mm thick) is run at 800 V in 1x TBE running buffer for about 2 h, until the bromophenol blue has run most of the way down the gel. The glass plates are separated and the gel covered with Saran wrap. The position of the labeled DNA fragment is established by short (1 min) exposure to an X-ray film. The relevant band is then cut from the gel with a sharp razor blade. The radiolabeled DNA is eluted inserting the gel slice on

top of a small plug of glass wool inserted at the bottom of a P1000 pipette tip and covered with 300 µL of TE1 buffer. The top of the tip is sealed with parafilm, placed in an open Eppendorf tube and gently agitated overnight at room temperature.

The eluted DNA is finally precipitated by adding at least three volumes of ethanol, mixing by inversion and left of dry ice for at least 10 min. The sample is spun at 14,000 g for 10 min to collect the DNA, and the supernatant is removed in 200 µL aliquots. Each aliquot has to be checked against a hand-held Geiger counter to confirm that it does not contain any radioactivity.

The precipitate is washed with 200 µL of 70% ethanol and spun again for 1 min. The supernatant is removed and the samples dried under vacuum. The radiolabeled DNA is dissolved in an TE2 buffer at a concentration of approximately 10 counts per second/µL on a hand-held Geiger counter. For footprinting experiments, it is generally not necessary to know the exact concentration of the DNA template, so long as it is lower than the ligand concentration.

With fresh plasmid and [ $\alpha$ -<sup>32</sup>P]dATP this process typically generates about 150 µL of radiolabelled footprinting fragment.

### ***GA track marker***

A GA marker track shows the location of purines within the target DNA sequence, thereby allowing identification of the sequences of the footprinting sites. This has often been achieved using Maxam-Gilbert chemical sequencing reactions with dimethylsulphate (specific for G) or formic acid (for G + A) followed by cleavage with hot piperidine.

This procedure is laborious and time consuming. Instead, GA track markers were prepared using a much simpler empirical method for generating purine (G+A) marker lanes, which are freshly prepared for each footprintin experiment. 1.5 µL labelled DNA are mixed with 20 µL sterile water and 4 µL DNase I stop solution (10 mM EDTA, 1 mM NaOH, 0.1% bromophenol blue, 80% formamide). The sample is then incubated at 100 °C for about 40 min with the microcentrifuge tube cap open to allow evaporation.

### ***DNase I footprinting experiment***

Radiolabeled DNA dissolved in TE2 (1.5 µL) was mixed with various concentrations (2x the desired concentration) of the tested compounds (dissolved in 10 mM Tris-HCl, pH 7.5, containing 10 mM NaCl). The mixture was left to equilibrate overnight at room temperature, before adding 2 µL DNase I (approximately 0.01 units/mL) dissolved in 20 mM NaCl, containing 2 mM MgCl<sub>2</sub> and 2 mM MnCl<sub>2</sub>. The digestion was stopped after 1 min by adding 4 µL of

formamide containing 10 mM EDTA, 1 mM NaOH, and 0.1% (w/v) bromophenol blue. The digestion products were boiled for 3 min and then crash cooled on ice, immediately before loading onto denaturing 8% polyacryl amide gels containing 8 M urea (0.3 mm thick, 40 cm long gels), which were run hot at 1500 V for about 2 h. Gels were prepared and run in 1x TBE buffer and preheated by running for 30 min before loading the samples.

Gels were fun until the bromophenol blue reached the bottom of the gel, then the glass plates were separated and the gel immersed in 2 L of 10% (v/v) acetic acid for at least 10 min. This fixes the DNA in the gel and removes a large amount of the urea before drying. Next, the gel is removed from the acid and most of the liquid is drained off. A sheet of Whatman 3MM paper is layed onthe the wet gel and then peeled this back, transferring the gel onto the filter paper. This is coved with Saran wrap, and dried at 80 °C for 1 h on a gel dryer.

Dried gels were exposed to a Kodak Phosphor storage screen overnight, which was scanned using a Molecular Dynamics STORM 860 phosphorimager (GE Healthcare) at a pixel size of 100  $\mu\text{m}$ .

### **Topoisomerase I inhibition assay**

#### **Materials**

- 10x topoisomerase I reaction buffer (20 mM Tris-HCl pH 7.5, 200 mM NaCl, 0.25 mM EDTA, 5 % glycerol, 50  $\mu\text{g}/\text{mL}$  albumin)
- Substrate: plasmid pBR322
- Purified human topoisomerase I
- Topoisomerase dilution buffer (10 mM Tris-HCl pH 7.5, 1 mM DTT, 1 mM EDTA, 100 mM NaCl, 50% (v/v) glycerol, 100  $\mu\text{g}/\text{mL}$  albumin)

All of them supplied in the Human Topoisomerase I Assay Kit (Inspiralis, Norwich UK).

#### **Relaxation assay**

2  $\mu\text{L}$  of 10x topoisomerase I reaction buffer and 0.5  $\mu\text{g}$  of supercoiled pBR322 are added to each of a series of 1.5 mL microcentrifuge tubes on ice. Then, a range of concentrations of compound RZ2 in DMSO is added and the volumes are adjusted with distilled water so that the final reaction volume in each tube is 20  $\mu\text{L}$ . Next, 1 U of topoisomerase I is added to the tubes, which are incubated for 30 min at 37 °C.

5 µL of 5x loading dye are added to each tube and the contents are loaded on a 1% agarose gel. This is run 2 to 3 hours at 5 V/cm, stained with ethidium bromide, destained briefly with water and photographed with a UV transilluminator.

### **Topoisomerase II inhibition assay**

#### **Materials**

- 10x topoisomerase II reaction buffer (50 mM Tris-HCl pH 7.5, 125 mM NaCl, 10 mM MgCl<sub>2</sub>, 5 mM DTT, 100 µg/mL albumin)
- 30x ATP stock (30 mM ATP)
- Substrate: kDNA
- Purified human topoisomerase II
- Topoisomerase II dilution buffer (50 mM Tris-HCl pH 7.5, 100 mM NaCl, 1 mM DTT, 0.5 mM EDTA, 50% (v/v) glycerol, 50 µg/mL albumin)

All of them supplied in the Human Topo II Decatenation Assay Kit (Inspiralis, Norwich UK).

#### **Decatenation assay**

2 µL of 10x topoisomerase II reaction buffer and 100 ng kinetoplast DNA are added to each of a series of 1.5 mL microcentrifuge tubes. Then, 0.7 µL of (30x) ATP are added, followed by a range of concentrations of compound RZ2 in DMSO. Next, the volumes are adjusted with distilled water so that the final reaction volume in each tube is 20 µL and 1 U of human topoisomerase is added to the tubes, which are incubated for 30 min at 37 °C. Reactions are stopped by the addition of an equal volume chloroform/isoamyl alcohol (24:1 v/v) and another volume of 2x stop dye (40% sucrose, 1 mM EDTA, 100 mM Tris-HCl pH 7.5, 0.5 µg/mL bromophenol blue).

The contents of each tube are loaded on a 1% agarose gel and run for 2-3 hours at 5 V/cm. The gel is then stained with ethidium bromide, destained briefly with water, and photographed with a UV transilluminator.

#### **Leakage measurement**

Aliquots containing the appropriate amount of lipid in chloroform/methanol (1:1, v/v) were placed in a test tube, the solvents were removed by evaporation under a stream of O<sub>2</sub>-free nitrogen, and finally traces of solvents were eliminated under vacuum in the dark for more than 3 h. After that, 1 mL of buffer containing 10 mM HEPES, 100 mM NaCl, 0.1 mM EDTA, pH 7.4 buffer and

CF at a concentration of 40mM was added, and multilamellar vesicles were obtained. Large unilamellar vesicles (LUVs) with a mean diameter of 200 nm were prepared from multilamellar vesicles by the LiposoFast device from Avestin, Inc., using polycarbonate filters with a pore size of 0.2  $\mu$ m (Nuclepore Corp., Cambridge, CA, USA). Breakdown of the vesicle membrane leads to content leakage, i.e., CF fluorescence. Non-encapsulated CF was separated from the vesicle suspension through a Sephadex G-25 filtration column eluted with buffer containing 10 mM HEPES, 150 mM NaCl, and 0.1 mM EDTA, pH 7.4. Leakage of intraliposomal CF was assayed by treating the probe-loaded liposomes (final lipid concentration, 0.125 mM) with the appropriate amount of RZ2 or melittin in Costar 3797 round-bottom 96-well plates, each well containing a final volume of 100  $\mu$ L. The micro titer plate was incubated at 37 °C for 1 h to induce dye leakage. Leakage was measured at various compound-to-lipid ratios. Changes in fluorescence intensity were recorded using the FL600 fluorescence microplate reader with excitation and emission wavelengths set at 492 and 517 nm, respectively. One hundred percent release was achieved by adding Triton X-100 to a final concentration of 1% v/v to the microtiter plates. Fluorescence measurements were made initially with probe-loaded liposomes, afterwards by adding RZ2 solution and, eventually, adding Triton X-100 to obtain 100% leakage. The results were expressed as percentage of CF released relative to the positive control (Triton X-100).

### **Death-cell protease assay**

#### **Materials**

- Assay buffer
- bis-AAF-R110 substrate (100 nM in DMSO)

As supplied by Promega (Madison, WI, USA).

#### **Protocol**

A 96-well plate is set up containing 5000 HeLa cells in DMEM without phenol red supplemented with 10% fetal bovine serum (FBS), 2 mM L-glutamine and antibiotics. After cells attachment to the plate's surface, the compounds and vehicle controls are added in a final volume of 100  $\mu$ L per well and incubated for different times as specified. Then, 20  $\mu$ L of the bis-AAF-R110 substrate, previously dissolved in the assay buffer, are added to all wells and briefly mix. The mixture is incubated for 30 minutes at 37 °C. Finally, the fluorescence is measured ( $\lambda_{Ex}=485$  nm,  $\lambda_{Em}=520$  nm).

## Cells and cell culture

Cell culture media and FBS were obtained from Life Technologies Corporation (California, USA). HeLa cervical adenocarcinoma cells were obtained from the American Type Culture Collection (ATCC), and were grown in DMEM supplemented with 10% fetal bovine serum (FBS), 2 mM L-glutamine and antibiotics. Cells were sub-cultured twice a week and maintained at 37 °C in a humidified atmosphere containing 5% CO<sub>2</sub>. For sub-culturing, cells were detached from culture flasks by incubation with 0.25% trypsin-EDTA 3 min (at 37 °C, 5% CO<sub>2</sub>). Trypsinated cells were centrifuged at 1000 rpm for 10 min at room temperature and gently resuspended in 5 mL of fresh medium preheated at 37 °C. Cellular density was determined in a Neubauer counting plate and the appropriate volume of cells was placed into a fresh culture flask or plates. After 12 h incubation, cells were completely attached to the surface.

## Western blotting assays

Cells were homogenized in RIPA (150 mM NaCl, 10 mM Tris, pH 7.2, 0.1% SDS, 1% Triton X-100, 1% deoxycholate, 5 mM EDTA, 1 mM NaVO<sub>4</sub>, 5 mM NaF, 1 mM PMSF, and protease inhibitor mixture (Roche)) and centrifuged at 10,000 g for 15 min at 4 °C. Equal amounts of proteins from total homogenates were resolved in 12% acrylamide gels for SDS-PAGE and transferred to Immobilon membranes (Millipore). The membranes were blocked with PBS-Tween 20 (0.05%) containing 3% non-fat dried milk for 1 h and incubated overnight at 4 °C with primary antibodies, followed by incubation with horseradish peroxidase-conjugated goat anti-rabbit or anti-mouse IgG (1:10,000 dilution; Pierce, Rockford, IL, USA). Immunoreactive proteins were visualized using a chemiluminescence substrate (Millipore) and quantitatively analyzed by densitometry using Image J Software (Bethesda, MD, USA). All experiments were performed in at least triplicate. β-actin was used as loading control.

## Antibodies

Antibodies for caspase-3 (1:700), PARP (1:1000), p53 total (1:1000) and p53 Ser15 (1:1000) are from Cell Signaling Technology (Danvers, MA USA), p62 (1:2000) from BD Biosciences (Franklin Lakes, NJ USA), LC3 (1:2000) from MBL International Corporation (Woburn, MA USA), and actin (1:15000) from Sigma (St. Louis, USA).

## Autophagy flux analysis

HeLa cells were incubated in the presence or absence of 100 nM bafilomycin for 4 h. After that time, they were processed for immunodetection of LC3. LC3-II abundance was normalized by β-actin levels.

### **Confocal microscopy**

For live imaging studies, HeLa cells were plated on 8-well Lab-Teck chambered 1.0 borosilicate coverglass system (Nalge Nunc International, Rochester, NY). Cells were placed in a chamber under culture conditions (DMEM at 37 °C and 5% CO<sub>2</sub>), and live cells were visualized using a Leica SP2 Confocal Microscope. To prevent crosstalk, emission signals were recorded sequentially. Images were then processed with ImageJ software (NIH).

### **Nuclear staining with Hoechst 33528**

Cells were seeded into a 8-well Lab-Teck chambered 1.0 borosilicate coverglass system (Nalge Nunc International, Rochester, NY), and Hoechst 33528, a DNA-specific fluorescent dye, was added to each well and incubated with the cells for 10 min at 37 °C before visualization under the microscope.

### **Detection of sub-G<sub>1</sub> hypodiploid cells**

Apoptotic sub-G<sub>1</sub> hypodiploid cells were detected via flow cytometry. Cells were first treated with compound RZ2 for 24 h. Harvested cells were then washed and the supernatant was also collected. 70% ethanol was used to fix the cells. The cells were then incubated with a solution containing 0.1% (v/v) Triton X-100 (Sigma) in PBS with DNase free RNase A (Sigma) (0.2 mg/mL) and PI (Molecular Probes) (20 µg/mL) for 30 min at 37 °C. Flow cytometric analysis was performed using a flow cytometer. The sub-G<sub>1</sub> hypodiploid cells were assessed based on histograms generated by the computer program.

### **Flow cytometric analysis of apoptosis and necrosis**

Extent of apoptosis was measured through Alexa Fluor® 488 annexin V/Dead Cell Apoptosis Kit (Invitrogen, USA) as described by the manufacturer's instructions. Briefly, HeLa cells were harvested at the indicated times after treatment. Culture medium supernatant and PBS washes were retained to ensure that both floating and adherent cells were analyzed. After incubation for 15 min with Alexa Fluor® 488 annexin V and PI working solution, cells were subjected to FACS analysis.

### **Cell apoptosis assays**

DNA fragmentation was determined in HeLa cells previously permeabilized with ethanol and labeled with propidium iodide (PI). The sub-G<sub>1</sub> population was quantified by flow cytometry. DEVDase activity was determined in 30 µg of RIPA total protein cell lysate (without protease

inhibitors). Cleavage of the fluorogenic substrated Ac-DEVD-AFC. Caspase 3 and PARP cleavage were determined in 50 µg RIPA total protein cell lysate of control and treated cells.

### **Flow cytometric analysis of cellular DNA content**

Flow cytometric analysis of cellular DNA content was performed as described in Current Protocols in Cytometry. Both floating and attached cells were collected and poured together in the centrifuge tubes. Cells were washed with phosphate-buffered saline (PBS), re-suspended and fixed in 70% ice-cold ethanol for 4 h at 4°C. Subsequently, they were treated with a IP/Triton X-100/RNase A for 30 min. Finally, cells were analyzed in a Coulter XL flow cytometer. At least 10,000 events per sample were analyzed three times. The percentage of cells in G<sub>0</sub>/G<sub>1</sub> phase, S phase and G<sub>2</sub>/M phase was analyzed using the Multicycle software.

### **Labeling of acidic compartment**

HeLa cells were loaded with 100 nM Lysotracker Green (Molecular Probes, Invitrogen) for the last 20 min of incubation. Cells were then analyzed by flow cytometry.

### **Mitochondrial membrane potential assay (TMRE assay)**

TMRE membrane potential kit from Abcam (Cambridge, MA) was used according to manufacturer's instructions. TMRE was added to the media at 50 nM final concentration and cells were incubated for 20 min at 37 °C, 5% CO<sub>2</sub>. After incubation, cells were trypsinized, centrifuged, and cell pellets were resuspended in 0.4 mL of medium and analyzed by flow cytometry. The excitation/emission fluorescence for TMRE is 549/575 nm.

### **Determination of mitochondrial superoxide**

MitoSOX red mitochondrial superoxide indicator (Invitrogen, San Diego, CA) was used to detect superoxide, as a general measure of cellular oxidative stress in the mitochondria of live cells. The red fluorescence was analyzed by flow cytometry (excitation/emission fluorescence is 510/580 nm).

### **Microarray experiment**

HeLa cells treated with 5 µM RZ2 or just the vehicle for 24 h are washed with PBS and then lysed in 0.35 mL lysis buffer containing β-mercaptoethanol. Isolation steps are done following PureLink® RNA Mini Kit technical manual. The optional step of DNase treatment is performed. RNA quantification is done using a ND-1000 spectrophotometer using the elution buffer as blank. RNA integrity control was done using RNA Nanochips 6000 on Agilent's Bioanalyzer

2100 according to the technical manual. RNA expression profiling was performed following the Pico Profiling method. Briefly, cDNA library preparation and amplification were performed from 25 ng total RNA using WTA2 (Sigma-Aldrich) with 17 cycles of amplification. 8 µg cDNA were subsequently fragmented by DNase I and biotinylated by terminal transferase obtained from GeneChip Mapping 250K Nsp Assay Kit (Affymetrix). Hybridization mixture was prepared according to Affymetrix protocol. Each sample was hybridized to a GeneChip PrimeView Human Gene Expression Array (Affymetrix). Arrays were washed and stained in a Fluidics Station 450 and scanned in a GeneChip Scanner 3000 (both Affymetrix) according to manufacturer's recommendations. CEL files were generated from DAT files using GCOS software (Affymetrix).

### ***Microarray data analysis***

Arrays were processed in Bioconductor,<sup>93</sup> using RMA background correction and summarization. Foldchanges between samples were computed after MA mean and variance normalization using the GAM method. An empirical Bayes partial density model was then used to identify significant differentially expressed genes with a False Discovery Rate (FDR) of 5% and a log<sub>2</sub> foldchange threshold of 3 (8 times up or down regulated). The whole list of genes in the array (ranked by mean foldchange from most upregulated to most downregulated) was analyzed against Human GO Biological Process and KEGG databases in order to detect overrepresented genesets with a GSEA pre-ranked analysis.

Data were deposited in the NCBI GEO repository.

### **Expression of results and statistical methods**

Data are presented as mean±s.e.m. of a number of 3 independent experiments. Data were subjected to analysis of variance, and comparisons between groups were performed using a protected Tukey's t-test. A value of  $p<0.05$  was chosen as the limit of statistical significance.

## REFERENCES

- (1) Degenhardt, K.; Mathew, R.; Beaudoin, B.; Bray, K.; Anderson, D.; Chen, G.; Mukherjee, C.; Shi, Y.; Gélinas, C.; Fan, Y.; Nelson, D. A.; Jin, S.; White, E. *Cancer Cell* **2006**, *10*, 51–64.
- (2) Zeh, H. J.; Lotze, M. T. *J. Immunother.* **2005**, *28*, 1–9.
- (3) Golstein, P.; Kroemer, G. *Trends Biochem. Sci.* **2007**, *32*, 37–43.
- (4) Festjens, N.; Vanden Berghe, T.; Vandenabeele, P. *Biochim. Biophys. Acta* **2006**, *1757*, 1371–1387.
- (5) Chan, F. K.-M.; Shisler, J.; Bixby, J. G.; Felices, M.; Zheng, L.; Appel, M.; Orenstein, J.; Moss, B.; Lenardo, M. J. *J. Biol. Chem.* **2003**, *278*, 51613–51621.
- (6) Lin, Y.; Choksi, S.; Shen, H.-M.; Yang, Q.-F.; Hur, G. M.; Kim, Y. S.; Tran, J. H.; Nedospasov, S. A.; Liu, Z. *J. Biol. Chem.* **2004**, *279*, 10822–10828.
- (7) Temkin, V.; Huang, Q.; Liu, H.; Osada, H.; Pope, R. M. *Mol. Cell. Biol.* **2006**, *26*, 2215–2225.
- (8) El Mahdani, N. E.; Ameyar, M.; Cai, Z.; Colard, O.; Maslia, J.; Chouaib, S. *J. Immunol.* **2000**, *165*, 6756–6761.
- (9) Kroemer, G.; El-Deiry, W. S.; Golstein, P.; Peter, M. E.; Vaux, D.; Vandenabeele, P.; Zhivotovsky, B.; Blagosklonny, M. V.; Malorni, W.; Knight, R. A.; Piacentini, M.; Nagata, S.; Melino, G. *Cell Death Differ.* **2005**, *12*, 1463–1467.
- (10) Kerr, J. F. R.; Wyllie, A. H.; Currie, A. R. *Br. J. Cancer* **1972**, *26*, 239–257.
- (11) Letai, A. G. *Nat. Rev. Cancer* **2008**, *8*, 121–132.
- (12) Indumathy, S.; Dass, C. R. *J. Pharm. Pharmacol.* **2013**, *65*, 1280–1301.
- (13) Hellwig, C. T.; Passante, E.; Rehm, M. *Curr. Mol. Med.* **2011**, *11*, 31–47.
- (14) Chipuk, J. E.; Green, D. R. *Trends Cell Biol.* **2008**, *18*, 157–64.
- (15) Giam, M.; Huang, D. C. S.; Bouillet, P. *Oncogene* **2008**, *27 Suppl 1*, S128–136.
- (16) Zhao, J.; Lu, Y.; Shen, H.-M. *Cancer Lett.* **2012**, *314*, 8–23.
- (17) Siddiqi, A.; Marciniak, R. *Cancer Biol. Ther.* **2008**, *7*, 740–741.
- (18) Olsson, M.; Zhivotovsky, B. *Cell Death Differ.* **2011**, *18*, 1441–1449.
- (19) Ola, M. S.; Nawaz, M.; Ahsan, H. *Mol. Cell. Biochem.* **2011**, *351*, 41–58.
- (20) Speirs, C. K.; Hwang, M.; Kim, S.; Li, W.; Chang, S.; Varki, V.; Mitchell, L.; Schleicher, S.; Lu, B. *Am. J. Cancer Res.* **2011**, *1*, 43–61.
- (21) Fulda, S.; Debatin, K.-M. *Oncogene* **2006**, *25*, 4798–4811.
- (22) Amaravadi, R. K.; Thompson, C. B. *Clin. cancer Res.* **2007**, *13*, 7271–7279.
- (23) He, C.; Klionsky, D. J. *Annu. Rev. Genet.* **2009**, *43*, 67–93.
- (24) Kroemer, G.; Mariño, G.; Levine, B. *Mol. Cell* **2010**, *40*, 280–293.
- (25) Mizushima, N.; Komatsu, M. *Cell* **2011**, *147*, 728–741.
- (26) Gu, Y.; Wang, C.; Cohen, A. *FEBS Lett.* **2004**, *577*, 357–360.
- (27) Iwata, J.; Ezaki, J.; Komatsu, M.; Yokota, S.; Ueno, T.; Tanida, I.; Chiba, T.; Tanaka, K.; Kominami, E. *Journal Biol. Chem.* **2006**, *281*, 4035–4041.

- (28) Lum, J. J.; Bauer, D. E.; Kong, M.; Harris, M. H.; Li, C.; Lindsten, T.; Thompson, C. B. *Cell* **2005**, *120*, 237–248.
- (29) Lorin, S.; Hamaï, A.; Mehrpour, M.; Codogno, P. *Semin. Cancer Biol.* **2013**, *23*, 361–379.
- (30) Wakelin, L. P. G.; Waring, M. J. *Biochem. J.* **1976**, *157*, 721–740.
- (31) Lee, J. S.; Waring, M. J. *Biochem. J.* **1978**, *173*, 115–128.
- (32) Low, C. M.; Drew, H. R.; Waring, M. J. *Nucleic Acids Res.* **1984**, *12*, 4865–4879.
- (33) Van Dyke, M. M.; Dervan, P. B. *Science (80-)* **1984**, *225*, 1122–1127.
- (34) Gao, X. L.; Patel, D. J. *Q. Rev. Biophys.* **1989**, *22*, 93–138.
- (35) Gilbert, D. E.; Feigon, J. *Biochemistry* **1991**, *30*, 2483–2494.
- (36) Ughetto, G.; Wang, A. H.; Quigley, G. J.; van der Marel, G. A.; van Boom, J. H.; Rich, A. *Nucleic Acids Res.* **1985**, *13*, 2305–2323.
- (37) Wang, A. H.; Ughetto, G.; Quigley, G. J.; Rich, A. *J. Biomol. Struct. Dyn.* **1986**, *4*, 319–342.
- (38) Lee, J. S.; Waring, M. J. *Biochem. J.* **1978**, *173*, 129–144.
- (39) Low, C. M.; Olsen, R. K.; Waring, M. J. *FEBS Lett.* **1984**, *176*, 414–420.
- (40) Viswamitra, M. A.; Kennard, O.; Cruse, W. B.; Egert, E.; Sheldrick, G. M.; Jones, P. G.; Waring, M. J.; Wakelin, L. P.; Olsen, R. K. *Nature* **1981**, *289*, 817–819.
- (41) Lavesa, M.; Olsen, R. K.; Fox, K. R. *Biochem. J.* **1993**, *289*, 605–607.
- (42) Lavesa, M.; Fox, K. R. *Anal. Biochem.* **2001**, *293*, 246–250.
- (43) Low, C. M.; Fox, K. R.; Olsen, R. K.; Waring, M. J. *Nucleic Acids Res.* **1986**, *14*, 2015–2033.
- (44) Hampshire, A. J.; Fox, K. R. *Anal. Biochem.* **2008**, *374*, 298–303.
- (45) Fox, K. R.; Olsen, R. K.; Waring, M. J. *Br. J. Pharmacol.* **1980**, *70*, 25–40.
- (46) Bailly, C.; Echepare, S.; Gago, F.; Waring, M. J. *Anticancer. Drug Des.* **1999**, *14*, 291–303.
- (47) Fox, K. R.; Gauvreau, D.; Goodwin, D. C.; Waring, M. J. *Biochem. J.* **1980**, *191*, 729–742.
- (48) Fox, K. R.; Davies, H.; Adams, G. R.; Portugal, J.; Waring, M. J. *Nucleic Acids Res.* **1988**, *16*, 2489–507.
- (49) Negri, A.; Marco, E.; García-Hernández, V.; Domingo, A.; Llamas-Saiz, A. L.; Porto-Sandá, S.; Riguera, R.; Laine, W.; David-Cordonnier, M.-H.; Bailly, C.; García-Fernández, L. F.; Vaquero, J. J.; Gago, F. *J. Med. Chem.* **2007**, *50*, 3322–3333.
- (50) Pasternack, R. F. *Chirality* **2003**, *15*, 329–332.
- (51) Uma Maheswari, P.; Palaniandavar, M. J. *Inorg. Biochem.* **2004**, *98*, 219–230.
- (52) Nordén, B.; Tjerneld, F. *Biopolymers* **1982**, *21*, 1713–1734.
- (53) Galas, D. J.; Schmitz, A. *Nucleic Acids Res.* **1978**, *5*, 3157–3170.
- (54) Fox, K. R. *Methods Mol. Biol.* **1997**, *90*, 1–22.
- (55) Hampshire, A. J.; Rusling, D. A.; Broughton-Head, V. J.; Fox, K. R. *Methods* **2007**, *42*, 128–140.
- (56) Drew, H. R.; Travers, A. A. *Cell* **1984**, *37*, 491–502.
- (57) Drew, H. R. *J. Mol. Biol.* **1984**, *176*, 535–557.
- (58) Price, P. A. *J. Biol. Chem.* **1975**, *250*, 1981–1986.
- (59) Lahm, A.; Suck, D. *J. Mol. Biol.* **1991**, *222*, 645–667.

- (60) Weston, S. A.; Lahm, A.; Suck, D. *J. Mol. Biol.* **1992**, *226*, 1237–1256.
- (61) Tullius, T. D.; Dombroski, B. A. *Proc. Natl. Acad. Sci. U. S. A.* **1986**, *83*, 5469–5473.
- (62) Tullius, T. D. *Nature* **1988**, *332*, 663–664.
- (63) Pommier, Y.; Pourquier, P.; Fan, Y.; Strumberg, D. *Biochim. Biophys. Acta* **1998**, *1400*, 83–105.
- (64) Wang, J. C. *Q. Rev. Biophys.* **1998**, *31*, 107–144.
- (65) Leppard, J. B.; Champoux, J. J. *Chromosoma* **2005**, *114*, 75–85.
- (66) Schoeffler, A. J.; Berger, J. M. *Q. Rev. Biophys.* **2008**, *41*, 41–101.
- (67) Postow, L.; Crisona, N. J.; Peter, B. J.; Hardy, C. D.; Cozzarelli, N. R. *Proc. Natl. Acad. Sci. U. S. A.* **2001**, *98*, 8219–8226.
- (68) Nitiss, J. L. *Nat. Rev. Cancer* **2009**, *9*, 327–337.
- (69) Drlica, K.; Malik, M. *Curr. Top. Med. Chem.* **2003**, *3*, 249–282.
- (70) Kaufmann, S. H. *Biochim. Biophys. Acta* **1998**, *1400*, 195–211.
- (71) Guano, F.; Pourquier, P.; Tinelli, S.; Binaschi, M.; Bigioni, M.; Animati, F.; Manzini, S.; Zunino, F.; Kohlhagen, G.; Pommier, Y.; Capranico, G. *Mol. Pharmacol.* **1999**, *56*, 77–84.
- (72) Marini, J. C.; Miller, K. G.; Englund, P. T. *J. Biol. Chem.* **1980**, *255*, 4976–4979.
- (73) Ownby, C. L.; Powell, J. R.; Jiang, M. S.; Fletcher, J. E. *Toxicon* **1997**, *35*, 67–80.
- (74) Van Engeland, M.; Nieland, L. J. W.; Ramaekers, F. C. S.; Schutte, B.; Reutelingsperger, C. P. M. *Cytometry* **1998**, *31*, 1–9.
- (75) Honda, O.; Kuroda, M.; Joja, I.; Asaumi, J.; Takeda, Y.; Akaki, S.; Togami, I.; Kanazawa, S.; Kawasaki, S.; Hiraki, Y. *Int. J. Oncol.* **2000**, *16*, 283–288.
- (76) Nicholson, D. W.; Ali, A.; Thornberry, N. A.; Vaillancourt, J. P.; Ding, C. K.; Gallant, M.; Gareau, Y.; Griffin, P. R.; Labelle, M.; Lazebnik, Y. A. *Nature* **1995**, *376*, 37–43.
- (77) Gurtu, V.; Kain, S. R.; Zhang, G. *Anal. Biochem.* **1997**, *251*, 98–102.
- (78) Gartel, A. L.; Tyner, A. L. *Mol. Cancer Ther.* **2002**, *1*, 639–649.
- (79) Niculescu III, A. B.; Chen, X.; Smeets, M.; Hengst, L.; Prives, C.; Reed, S. I. *Mol. Cell. Biol.* **1998**, *18*, 629–643.
- (80) Ogryzko, V. V.; Wong, P.; Howard, B. H. *Mol. Cell. Biol.* **1997**, *17*, 4877–4882.
- (81) Komatsu, M.; Kurokawa, H.; Waguri, S.; Taguchi, K.; Kobayashi, A.; Ichimura, Y.; Sou, Y.-S.; Ueno, I.; Sakamoto, A.; Tong, K. I.; Kim, M.; Nishito, Y.; Iemura, S.; Natsume, T.; Ueno, T.; Kominami, E.; Motohashi, H.; Tanaka, K.; Yamamoto, M. *Nat. Cell Biol.* **2010**, *12*, 213–223.
- (82) Tanida, I.; Ueno, T.; Kominami, E. In *Autophagosome and Phagosome*; Deretic, V., Ed.; Methods in Molecular Biology - Humana Press, 2008; Vol. 445, pp. 77–88.
- (83) Ichimura, Y.; Kumanomidou, T.; Sou, Y.; Mizushima, T.; Ezaki, J.; Ueno, T.; Kominami, E.; Yamane, T.; Tanaka, K.; Komatsu, M. *J. Biol. Chem.* **2008**, *283*, 22847–22857.
- (84) Lamark, T.; Kirkin, V.; Dikic, I.; Johansen, T. *Cell cycle* **2009**, *8*, 1986–1990.
- (85) Klionsky, D. J.; Elazar, Z.; Seglen, P. O.; Rubinsztein, D. C. *Autophagy* **2008**, *4*, 849–850.
- (86) Bilitewski, U. In *Microchip Methods in Diagnostics*; Bilitewski, U., Ed.; Humana Press - Methods in Molecular Biology, 2009; Vol. 509, pp. 1–14.

- (87) Auer, H.; Newsom, D. L.; Kornacker, K. In *Microchip methods in diagnostics*; Bilitewski, U., Ed.; Humana Press - Methods in Molecular Biology, 2009; Vol. 509, pp. 35–46.
- (88) Subramanian, A.; Tamayo, P.; Mootha, V. K.; Mukherjee, S.; Ebert, B. L.; Gillette, M. A.; Paulovich, A.; Pomeroy, S. L.; Golub, T. R.; Lander, E. S.; Mesirov, J. P. *Proc. Natl. Acad. Sci. USA* **2005**, *102*, 15545–15550.
- (89) Nobukuni, T.; Joaquin, M.; Roccio, M.; Dann, S. G.; Kim, S. Y.; Gulati, P.; Byfield, M. P.; Backer, J. M.; Natt, F.; Bos, J. L.; Zwartkruis, F. J. T.; Thomas, G. *Proc. Natl. Acad. Sci. U. S. A.* **2005**, *102*, 14238–14243.
- (90) Loeffler, M.; Kroemer, G. *Exp. Cell Res.* **2000**, *256*, 19–26.
- (91) Zamzami, N.; Marchetti, P.; Castedo, M.; Zanin, C.; Vayssi  re, J. L.; Petit, P. X.; Kroemer, G. *J. Exp. Med.* **1995**, *181*, 1661–1672.
- (92) Kroemer, G.; Reed, J. C. *Nat. Med.* **2000**, *6*, 513–519.
- (93) Gentleman, R. C.; Carey, V. J.; Bates, D. M.; Bolstad, B.; Dettling, M.; Dudoit, S.; Ellis, B.; Gautier, L.; Ge, Y.; Gentry, J.; Hornik, K.; Hothorn, T.; Huber, W.; Iacus, S.; Irizarry, R.; Leisch, F.; Li, C.; Maechler, M.; Rossini, A. J.; Sawitzki, G.; Smith, C.; Smyth, G.; Tierney, L.; Yang, J. Y. H.; Zhang, J. *Genome Biol.* **2004**, *5*, R80.

# **General conclusions**

---

---



## GENERAL CONCLUSIONS

According to estimates from the International Agency for Research on Cancer (IARC), more than 13 million people will dye from cancer by 2030. Moreover, taking into account that it is estimated that 1 out of 3 people will face a cancer diagnosis in their lifetime, cancer is one of the biggest concerns in our society.

Since the discovery of alkylating molecules capable of preventing cellular division, the fight against cancer using chemotherapy has become a common priority shared worldwide by researchers. During the last 70 years, chemists have designed diverse compounds aimed to stop the rapid replication of abnormal cells but, still, the objective of synthesizing a cytotoxic drug capable of a specific effect on malignant cells without toxicity on normal cells has not been reached. Furthermore, the appearance of multidrug resistance in a number of patients under chemotherapy treatment demands more investment and continual research for the development of new antineoplastic therapies.

The main objective of this Doctoral Thesis has been the design and synthesis of novel compounds with antitumoral activity, taking as basis the chemical structure of the natural bisintercalator triostin A.

In the first chapter, the design and synthesis of short peptides defined by a  $\beta$ -hairpin motif with two quinoxaline units covalently attached to both ends were described. The main characteristic of these simplified triostin A analogues is that they display the U-shape exhibited by the majority of the natural bisintercalators when interacting with DNA.

Synthetically challenging peptides bearing consecutive *N*-methyl and  $\beta$ -branched amino acids were obtained after careful selection of a suitable coupling system for the solid-phase synthesis of the peptidic scaffold. The use of COMU–Oxyma–DIEA resulted to be the best option, with a superior coupling efficiency than HATU–HOAt–DIEA, and allowed to perform couplings at 50 °C when required.

At the end, a small library of twelve peptides, fifteen quinoxaline-containing peptides and three fluorescent versions of compound RZ2 were obtained by solid-phase peptide synthesis with the introduction of the heterocycles and side-chains deprotection carried out in solution as final stages. All the compounds were obtained in excellent purities for further biological evaluation. Moreover, the parent compound triostin A was also synthesized using reported procedures developed in our research group to be used as positive control in the *in vitro* assays.

In the second chapter, a detailed study was performed in order to establish the optimal experimental conditions for the cytotoxic evaluation of the synthesized compounds. The exponential growth phase and linear absorbance ratio relative to the number of cells was determined for the four human cancer cell lines tested: HeLa, A-549, SK-BR-3 and HT-29. Based on these results, the initial cells number and assay length was decided.

The most active compound was RZ2, with low micromolar cytotoxic activities against the four cell lines tested, being in all cases more active than the natural parent compound triostin A, and with better cytotoxic activity than the commercial drug doxorubicin against cervical and breast adenocarcinoma cells. This quinoxaline-containing peptide has no *N*-methylations, feature that simplifies its synthesis making it possible to obtain significant amounts of compound. It was also demonstrated that the lack of *N*-methylations does not affect the proteolytic stability of RZ2, finding that its half-life in presence of serum proteases, cathepsin B or MMP-2 is more than 48 hours. Furthermore, a liposomal formulation of this analogue was prepared, using phosphatidylcholine and cholesterol, allowing a notorious enhancement in RZ2 solubility, thus cells uptake of the cytotoxic compound.

Additionally, the cytotoxic activity of the peptide scaffolds of compounds RZ1-RZ12 without the quinoxaline moieties was also assayed. None of the peptides displayed any biological activity, revealing that the heterocycles confer the antitumor activity to the synthesized quinoxaline-containing peptides.

None of the tested compounds exhibited any antibacterial or antiviral activity. However, compound RZ2 resulted biologically active against the parasite *Plasmodium falciparum*. This result, together with the observation that RZ2 is not injurious to human red blood cells, confirms the great potential of this compound not only as antitumor drug, but also as antiparasitic molecule.

In the third chapter, the DNA-binding properties of the most cytotoxic compound, RZ2, were explored. The negative results obtained in circular dichroism, band-shift, and DNase I footprinting experiments clearly indicate that this quinoxaline-containing peptide does not interact with DNA. Thus, our analogues display their biological activity through a different mechanism of action than triostin A. The explanation for this unexpected conclusion was revealed by molecular dynamics simulations. It was observed that the synthesized compound does adopt the predicted antiparallel  $\beta$ -sheet conformation, but the separation between the quinoxaline moieties is too little (4 Å) to allow the sandwiching of two DNA base pairs.

*In vitro* assays with human topoisomerases I and II were also assayed for compound RZ2, but no inhibition was observed, pointing out that the compound is not a topoisomerase poison either.

Experiments on the mechanism of cell death were carried out to get insights into the mode of action by which this quinoxaline-containing peptide displays its antitumor activity. It was observed that RZ2 causes a cell cycle arrest in the S-phase to HeLa cells. It was also demonstrated that this hit molecule is endocytosed into the cells and accumulates in acidic compartments, triggering autophagosome formation. However, RZ2 excess in the endosomal/lysosomal system finally leads to cell apoptosis when the metabolic and oxidative stresses cannot be repaired. Furthermore, since RZ2 is stable under physiological conditions

and in the presence of some proteases, the peptide remains intact in the presence of the tumoral overexpressed cathepsin B, which is located mainly in lysosomes. Therefore, the peptide cannot be hydrolyzed even when engulfed as autophagosomal content via autophagy.

Taken together, our findings report a well-scalable peptidic compound decorated with two quinoxaline units that may be useful for clinical applications in cancer treatment and may contribute to the design of other molecules to investigate and develop antitumor chemotherapeutics.

# **Resumen en español**

---

---



## SÍNTESIS, EVALUACIÓN BIOLÓGICA Y ESTUDIOS SOBRE EL MODO DE ACCIÓN DE PÉPTIDOS UNIDOS A QUINOXALINAS

### Introducción general

El cáncer es un problema de salud mundial que, se estima, afectará a más de 16 millones de personas alrededor del mundo cada año. Entre los distintos métodos existentes para tratar el cáncer, la quimioterapia sigue siendo la elección primordial para la mayoría de los pacientes. Sin embargo, a pesar de los esfuerzos de distintos grupos de investigación desde el descubrimiento de las mostazas nitrogenadas como compuestos alquilantes capaces de detener el crecimiento de las células tumorales, no se ha logrado obtener un compuesto capaz de detener la replicación de células anormales sin afectar a las demás células sanas del cuerpo.

Gracias a la investigación de los distintos receptores celulares sobreexpresados en las células cancerígenas, así como de los péptidos y proteínas relacionadas con la aparición o la resistencia del cáncer, ha emergido una nueva opción de tratamiento basada en dichas biomoléculas. El uso de péptidos como agentes terapéuticos es viable, pues su síntesis y modificación estructural es relativamente fácil, poseen una buena biocompatibilidad, así como facilidad para penetrar en el tejido tumoral dado su pequeño peso molecular. Los péptidos pueden ser la parte funcional de una proteína pero de menor tamaño y su eficacia, selectividad y especificidad de unión es mejor que las de otra molécula pequeña de otra naturaleza; además, generan menor respuesta inmune y toxicidad en el paciente.

Los péptidos presentan una baja biodisponibilidad cuando se suministran por vía oral, además de que normalmente son metabolizados en pocos minutos por las peptidasas presentes en el plasma y en el aparato gastrointestinal. Por ello, por mucho tiempo fueron considerados como una mala opción en el desarrollo de fármacos. Sin embargo, las modificaciones estructurales que permite la química orgánica, como son la incorporación de D-aminoácidos y/o N-metilaciones, han permitido la obtención de péptidos mucho más resistentes a la degradación *in vivo*.

En los últimos años, el uso de péptidos como posibles fármacos ha resurgido y muchos grupos de investigación están enfocados en el diseño y la síntesis de nuevos péptidos con actividad antitumoral. Como resultado, se han aprobado varios péptidos para ser usados en quimioterapia, y muchos otros se encuentran en fases avanzadas de ensayos clínicos, por lo que el futuro de estas biomoléculas como drogas antineoplásicas es alentador.

### Objetivos de la presente tesis

El objetivo general de este trabajo de investigación fue la síntesis de distintos análogos del compuesto triostina A, que es un bisintercalador con propiedades antineoplásicas y antibacterianas. Dichos análogos deberían de ser más fáciles de sintetizar, además de poseer una mejor actividad antitumoral que el compuesto natural.

Para ello, distintos objetivos específicos surgieron a lo largo del desarrollo de la presente tesis:

- Diseño, síntesis y caracterización de una pequeña librería de péptidos unidos a quinoxalinas, con una estructura inspirada en la triostina A (un octadepsipéptido que presenta dos quinoxalinas unidas covalentemente por medio de enlaces amida).
- Desarrollo de una ruta sintética eficiente que permitiese la obtención de secuencias peptídicas ricas en aminoácidos *N*-metilados y  $\beta$ -ramificados.
- Establecimiento de las condiciones experimentales óptimas para la evaluación *in vitro* de las propiedades citotóxicas de los compuestos sintetizados utilizando cuatro líneas celulares inmortalizadas.
- Evaluación biológica de los compuestos más citotóxicos como antibacterianos, antiparasitarios y antivirales.
- Evaluación de las propiedades de unión al ADN de los compuestos sintetizados utilizando distintas metodologías, destacando el ensayo de DNase I *footprinting*.
- Estudio del mecanismo de muerte celular provocado por el compuesto más citotóxico, RZ2.
- Síntesis y corroboración de la citotoxicidad de análogos del compuesto RZ2 unido a carboxifluoresceína, con el fin de realizar estudios de colocalización utilizando microscopía confocal, para determinar el sitio de acción de dicho compuesto.
- Evaluación de las perturbaciones en la expresión de ARN en células tumorales provocadas por el tratamiento con RZ2.
- Análisis del impacto a nivel mitocondrial que genera el compuesto RZ2 en células cancerígenas.

## Capítulo 1: Síntesis Química

La equinomicina fue descubierta en el año 1957 en los cultivos bacterianos de la cepa *Streptomyces echinatus* sp. Se determinó que su estructura química consiste en un depsipeptido cíclico al cual están unidas dos quinoxalinas por medio de enlaces tipo amida (Figura 1), y que éstas le confieren propiedades antibacterianas, así como una fuerte actividad antitumoral.

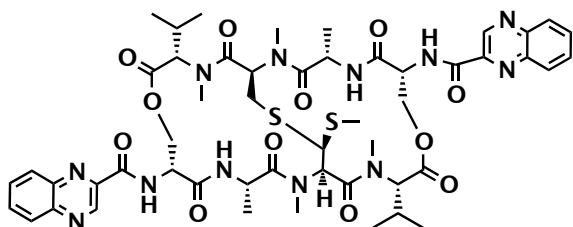


Figura 1. Estructura química de la equinomicina.

Este compuesto entró en estudios de fase clínica I y arrojó resultados muy alentadores en su uso como antineoplásico. Los ensayos clínicos de fase II mostraron una toxicidad tolerable en pacientes en estadíos avanzados de cáncer, pero no hubo evidencias de una respuesta positiva en la regresión de la enfermedad.

En 1974 se demostró que la equinomicina se une al ADN insertando sus quinoxalinas entre un par de pasos del material genético, posicionando la estructura péptidica en el surco menor. De esta manera, el compuesto forma un complejo ADN-ligando que bloquea la progresión de la ARN polimerasa, inhibiendo la transcripción. Este fue el primer reporte de lo que ahora conocemos como "bisintercalador", convirtiendo a la equinomicina en la molécula prototípico que describiría este mecanismo de acción. También se descubrió que este compuesto se une al material genético con una especificidad por las secuencias CpG, y que posee muy poca afinidad de unión a secuencias de ADN ricas en adeninas y timinas.

Al día de hoy, este producto natural se obtiene por un proceso de fermentación de *Streptomyces echinatus*, y está disponible comercialmente. Se ha descrito que dichos estreptomicetos biosintetizan la equinomicina por medio de sintetasas peptídicas no ribosomales, y que hay ocho genes implicados en la biosíntesis de los heterociclos quinoxalínicos. También se descubrió que la triostina A es el precursor biosintético de la equinomicina.

La triostina A también es un octadepsipeptido cíclico antibacteriano que posee dos quinoxalinas en su estructura y cuatro N-metilaciones. A partir del año 1977 se han reportado muchos análogos sintéticos de esta molécula, entre los cuales destaca TANDEM, un análogo con la

misma estructura química que el compuesto natural pero carente de *N*-metilaciones (Figura 2). El resultado más sorprendente de los experimentos relativos a la especificidad de unión de estas dos moléculas a distintas secuencias de ADN es que, mientras la triostina exhibe una afinidad de unión similar a la equinomicina por secuencias CpG, TANDEM se une a las secuencias ATA y TAT. En base a estas observaciones se estipuló que la secuencia peptídica que se posiciona en el surco menor del ADN también determina la especificidad de unión, y que no es un papel que desempeñan de manera única los heterociclos.

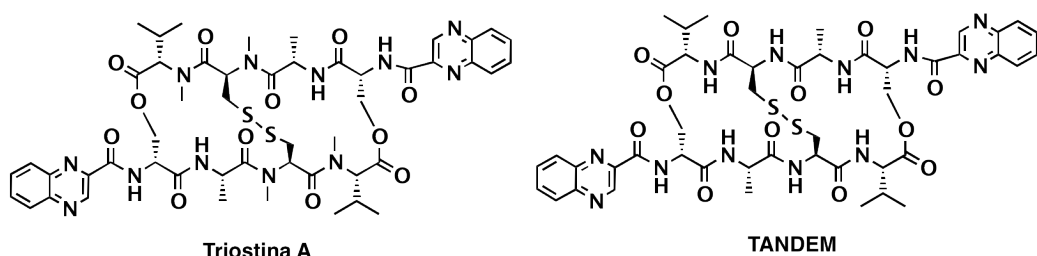


**Figura 2.** Estructuras químicas de la triostina A y su análogo TANDEM

Experimentos de RMN y cristalografía de rayos X han demostrado que la equinomicina, la triostina A y el TANDEM, así como otros bisintercaladores, tienen una forma de U cuando están unidos al ADN, con ambos heterociclos posicionados a ambos extremos de dicha U, de tal manera que el péptido semeja a una pinza que posiciona a un par de bases nitrogenadas en su extremo abierto.

En base a dicha observación se planteó el diseño de una pequeña librería de péptidos análogos a dichos bisintercaladores, pero con una estructura más sencilla con la finalidad de obtener mejores rendimientos y mayores posibilidades de escalado. Todos los péptidos sintetizados se caracterizan por una estructura secundaria de  $\beta$ -lámina antiparalela determinada por un giro  $\beta$  formado por la combinación D-Pro-Gly. También se incluyeron residuos beta ramificados a ambos extremos de dicho giro  $\beta$  con el objetivo de favorecer aún más la forma de  $\beta$  horquilla como producto de las interacciones hidrofóbicas entre las cadenas laterales de los aminoácidos, así como de las interacciones diagonales existentes entre éstas y que promueven la conformación secundaria de  $\beta$ -lámina.

En resumen, la nueva librería de péptidos unidos a quinoxalinas que se diseñó presenta las siguientes características:

- Un giro  $\beta$  promovido por la presencia del dipéptido D-Pro-Gly.
- La presencia de aminoácidos beta ramificados a ambos lados del giro  $\beta$  (treonina, isoleucina y valina).

- La presencia de dos residuos de valina, cada uno unido a los aminoácidos beta ramificados, dado que la valina es parte de la estructura de la triostina A, de la equinomicina y del TANDEM.
- Dos ácidos  $\alpha$ -aminobutíricos que imitan a los residuos de cisteína presentes en dichos compuestos naturales pero que simplifican la estructura peptídica por la ausencia de puentes disulfuro.
- Un residuo de serina que en la mitad de los compuestos sintetizados posee una configuración D como las serinas presentes en la triostina A, pero que en los demás compuestos tiene una configuración L.
- La unión de una molécula de etilendiamina en el extremo C-terminal de los péptidos por medio de un enlace amida, con el objetivo de obtener péptidos con dos extremos N-terminales para una posterior unión del ácido 2-quinoxalincarboxílico en solución.
- La presencia de dos quinoxalinas unidas a ambos extremos N-terminales de los péptidos, por medio de enlaces tipo amida.
- Cuatro residuos N-metilados, dado que la triostina A también los posee. Sin embargo, también se sintetizaron los correspondientes análogos carentes de N-metilaciones para estudiar un posible cambio de afinidad de unión al ADN, tal y como pasa con el compuesto TANDEM.

Las entidades peptídicas fueron sintetizadas en fase sólida, dado que es una técnica versátil y ventajosa que permite una rápida preparación de péptidos utilizando pasos de filtración y lavado de resina para eliminar el exceso de reactivos y otros productos secundarios de reacción.

Como esquema de protección se optó por la estrategia Fmoc/tBu y el soporte polimérico de elección fue la resina 2-clorotritil, que minimiza la formación de diquetopiperazinas al realizar síntesis peptídica con aminoácidos N-metilados consecutivos y permite la conservación del grupo protector *tert*-butilo aún después de la escisión del enlace péptido-resina.

Por otra parte, se comprobó que esta resina permite la N-metilación *in situ*, utilizando las condiciones de reacción descritas por Mitsunobu y posteriormente optimizadas por Kessler, siempre y cuando esta reacción se realice después del primer aminoácido incorporado a la resina. Para la N-metilación del ácido  $\alpha$ -aminobutírico, una vez acoplado a la fase sólida, primero se llevó a cabo la protección de la amina libre utilizando cloruro o-nitrobencensulfónico; la N-metilación bajo condiciones de Mitsunobu incluye el uso de metanol en presencia de trifenilfosfina y DIAD, utilizando THF como disolvente bajo condiciones anhidras. Finalmente, la

desprotección del grupo o-NBS se realiza con mercaptoetanol y DBU usando DMF como disolvente (Figura 3).

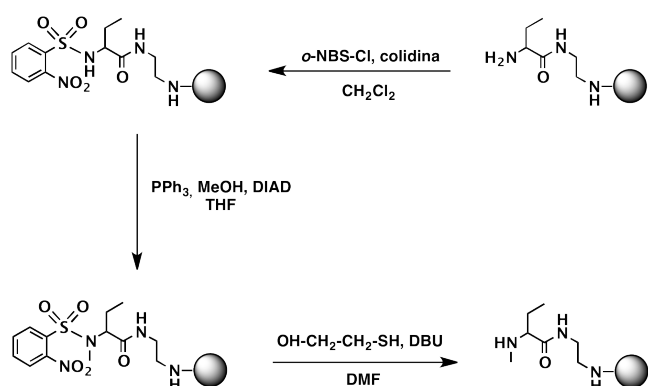


**Figura 3.** Procedimiento para la *N*-metilación selectiva en fase sólida.

Se evaluaron dos sistemas de acoplamiento para la síntesis en fase sólida de los péptidos, con especial atención en el porcentaje de acoplamiento obtenido en el caso de la incorporación de aminoácidos estéricamente impedidos sobre otros de igual naturaleza, o sobre aquellos con aminas alquiladas. La primera opción fue el sistema HATU–HOAt–DIEA, bien conocido por su capacidad para lograr acoplamientos difíciles y por minimizar el riesgo de racemización. Por otra parte, también se usó el sistema de acoplamiento desarrollado en nuestro grupo de investigación: COMU–Oxyma–DIEA. Después de varias pruebas utilizando distintos tiempos de reacción, temperaturas, número de reacoplamientos y uso de microondas, se determinó que el sistema de acoplamiento COMU–Oxyma–DIEA es la mejor opción para acoplamientos donde la formación del enlace amida está impedida por factores estéricos o por la *N*-metilación de la amina libre. Se comprobó también que este sistema es altamente efectivo, inclusive a temperaturas de reacción de hasta 50 °C, necesarias y recomendables en muchas ocasiones para lograr acoplamientos altamente impedidos.

Después de la escisión del enlace péptido-resina utilizando una solución al 20% de ácido trifluoroacético (TFA) en  $\text{CH}_2\text{Cl}_2$ , condiciones que permiten mantener la protección con el grupo *t*Bu de las cadenas laterales, se llevó a cabo la incorporación de las quinoxalinas. Para esta reacción en solución se optó por el uso de una sal de fosfonio debido a su mayor estabilidad en presencia de base: el sistema PyBOP (2.4 eq), HOAt (2.4 eq) y DIEA (hasta pH 8) permitió el acoplamiento de ácido 2-quinoxalincáboxílico (2.4 eq) en ambos extremos *N*-terminales de los péptidos sintetizados. Finalmente, la desprotección total de las cadenas laterales se llevó a cabo en 2 horas usando una solución de TFA– $\text{H}_2\text{O}$  (95:5).

Los doce péptidos unidos a quinoxalinas fueron purificados mediante cromatografía líquida de alta eficacia en fase reversa, obteniendo purezas superiores al 90% en todos los casos (librería

RZ1-RZ12, Figura 4). También se purificaron alícuotas de los doce péptidos sintetizados antes de la incorporación de las quinoxalinas con el fin de utilizarlos en futuros ensayos biológicos.

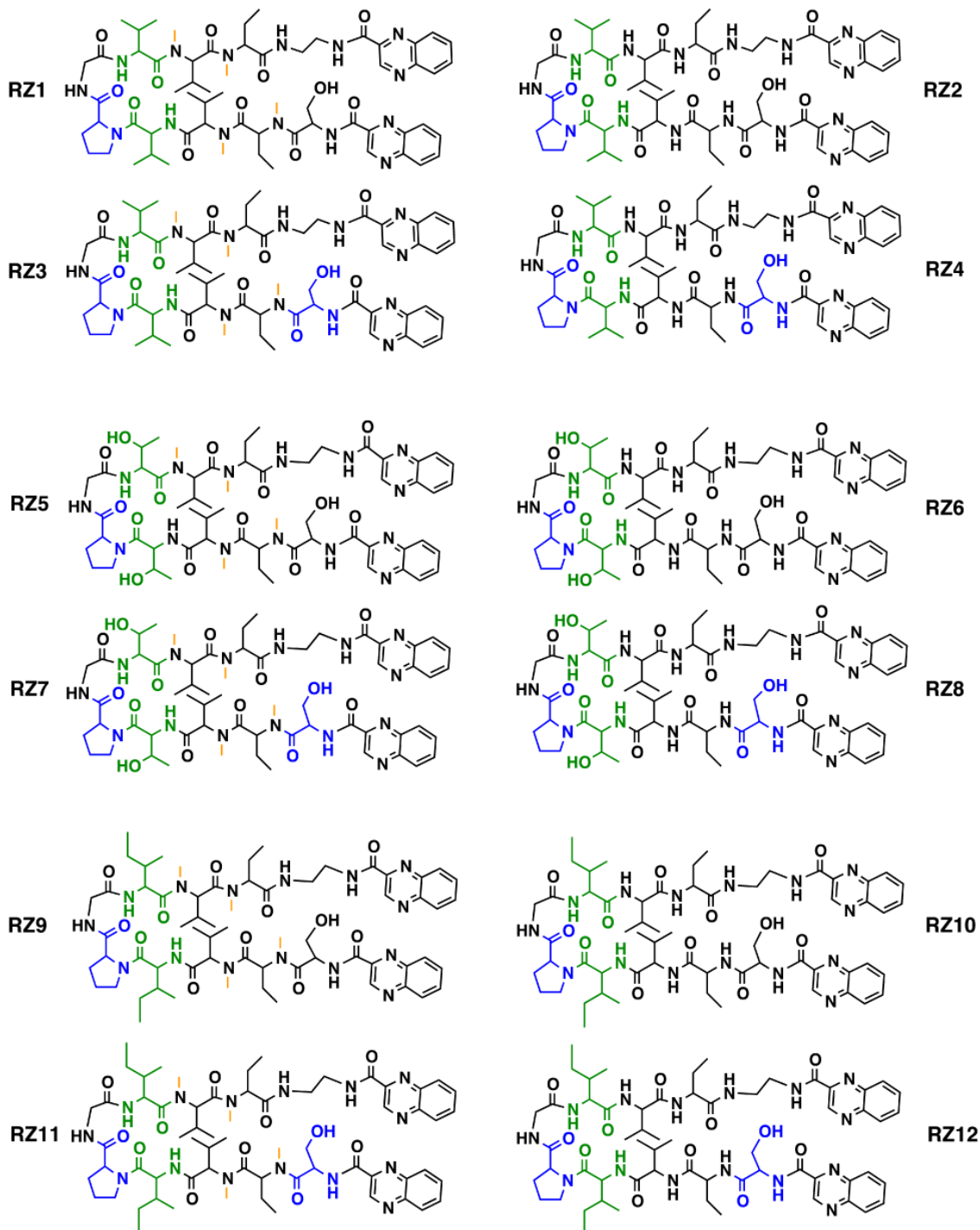


**Figura 4.** Estructuras químicas de la librería RZ1-RZ12. Los D-aminoácidos se muestran en color azul. Las N-metilaciones se han resaltado en color anaranjado. Los aminoácidos β-ramificados (valina, treonina e isoleucina) que definen el giro β junto con el dipéptido D-Pro-Gly aparecen en color verde.

Como se describirá en el capítulo 2, el compuesto que resultó ser más citotóxico frente a las líneas tumorales ensayadas fue RZ2, por lo que se sintetizaron tres distintas versiones

fluorescentes de éste utilizando el fluoróforo 5-carboxifluoresceína. Estos análogos serían utilizados para ensayos de colocalización utilizando microscopía confocal.

También se sintetizaron tres análogos extras basados en la estructura química de RZ2: RZV13, que es una versión cíclica; RZV14, en el cual los ácidos  $\alpha$ -aminobutíricos son sustituidos por cisteínas para la posterior formación de un puente disulfuro, asemejando aún más la estructura de la triostina A; RZV15, en el cual los ácidos  $\alpha$ -aminobutíricos son sustituidos por NMe-Cys(Me), previamente sintetizada en solución.

Finalmente, se realizó la síntesis de los aminoácidos Alloc-NMe-Val-OH y Boc-NMe-Cys(Acm)-OH para su utilización en la síntesis en fase sólida del compuesto natural triostina A, que sería utilizada como control positivo en los ensayos biológicos.

## **Capítulo 2: Actividad Biológica**

En los últimos años se han descrito distintos compuestos que contienen quinoxalinas o derivados de éstas con diversas actividades biológicas interesantes. Inclusive, algunos de estos compuestos se encuentran en ensayos clínicos o ya han recibido aprobación para su comercialización. Tres ejemplos de estos derivados son el Carbadox (un agente antibacteriano usado en veterinaria), la Vareniclina (medicamento para tratar la adicción al tabaco) y la Brimonidina (tratamiento para la hipertensión ocular).

Las quinoxalinas son moléculas de gran interés en la química médica dada su capacidad para interactuar con diversas dianas terapéuticas. Se ha descrito el potencial de éstas como antiinflamatorios, gracias a su capacidad de modulación del receptor H4, y como inhibidores de varias quinasas, por lo que podrían utilizarse para el tratamiento de distintos padecimientos, desde alergias hasta el cáncer.

En términos de posibles tratamientos para enfermedades del sistema nervioso central, se han reportado algunas imidazo[1,5 $\alpha$ ]quinoxalinas que inhiben a la phosphodiesterasa PDE10, por lo que podrían utilizarse para tratar esquizofrenia, bipolaridad, depresión y demencia. Se han reportado otros derivados capaces de inhibir tanto *in vitro* como *in vivo* a la phosphodiesterasa PDE9, por lo que podrían emplearse en el tratamiento de enfermedades del sistema urinario.

Otras quinoxalinas unidas a estructuras semejantes a la piperidina han sido reportadas como posibles fármacos para el tratamiento del dolor.

Cabe también resaltar la actividad antitumoral reportada para muchos compuestos que contienen quinoxalinas. Algunos de ellos son inhibidores de las fosfatidilinositol 3-quinasas, las cuales fungen un papel decisivo en la proliferación del cáncer de pecho, así como en

enfermedades inflamatorias crónicas. Algunos otros compuestos son inhibidores de las quinasas Raf, una familia de tres quinasas implicadas en las mutaciones cancerígenas.

Otros compuestos relacionados con las quinoxalinas han sido descritos como tratamientos potenciales para la obesidad, la diabetes y la hipertensión, así como inhibidores de metástasis y agentes antimicrobianos.

Es por ello que se decidió evaluar no sólo la actividad antitumoral de los compuestos sintetizados, sino que también se realizaron pruebas *in vitro* sobre la posible actividad antibacteriana, antiparasitaria y antiviral de algunos de los compuestos, en especial, del compuesto más citotóxico, RZ2.

Como primer punto de este segundo capítulo de la presente tesis, y en concordancia con el objetivo principal de la misma, se evaluó la actividad antineoplásica de todos los análogos sintetizados. Para ello se utilizó en ensayo colorimétrico de MTT, el cual es ampliamente usado para medir los efectos citotóxicos de nuevos fármacos sobre líneas celulares o cultivos primarios. Este ensayo se basa en la conversión del MTT a cristales de formazano como producto de las enzimas oxidoreductasa presentes en las células vivas. El formazano obtenido posee un color morado intenso y los cristales se solubilizan con DMSO para realizar medidas de absorbancia, relacionadas con la actividad mitocondrial de las células ensayadas. De esta manera, el incremento o la disminución del número de células viables se puede detectar por medio de la medida de absorbancia del formazano disuelto.

Cuando este ensayo se realiza en células inmortalizadas, la disminución en el número celular refleja la inhibición del crecimiento celular que causa el compuesto que está siendo evaluado, con respecto al control celular que no ha sido expuesto al compuesto. En el caso de células de cultivos primarios, la sensibilidad al compuesto evaluado se reporta como el aumento en muerte celular comparado con la pérdida de células que normalmente se observa en este tipo de cultivos. El ensayo de MTT se utiliza para medir tanto la actividad citotóxica como la actividad citostática de compuestos con potencial terapéutico o de productos tóxicos.

A pesar de que este ensayo se utiliza en muchos laboratorios y es una manera fácil de medir la viabilidad celular en placas de 96 pocillos, permitiendo la evaluación de muchos compuestos o varias concentraciones del compuesto en un solo ensayo, las condiciones del ensayo utilizando nuevas líneas celulares y/o nuevos compuestos no pueden ser extrapoladas a partir de otros ensayos, puesto que se podrían obtener resultados erróneos. Es de gran importancia el evaluar cuál es el número mínimo y máximo de células que se pueden detectar con el espectrofotómetro que se utilizará para la medición de absorbancia, así como los límites entre los que se mantiene una relación lineal entre la absorbancia medida y el número de células. En base a estos resultados se puede determinar el número de células que se sembrarán para el

ensayo, así como la duración de éste, dado que las células deben encontrarse en su fase exponencial de crecimiento tanto al momento de adicionar el compuesto a evaluar, como al realizar la medición de absorbancia. Por otra parte, es también importante estudiar el tiempo de duplicación para las líneas celulares que se utilizarán, puesto que este factor determinará el tiempo de exposición al compuesto para la obtención de resultados fidedignos.

En base a los puntos explicados anteriormente, antes de realizar los ensayos de citotoxicidad de los compuestos sintetizados, se realizaron las determinaciones correspondientes a los límites de detección del ensayo, la duración de la fase exponencial de las cuatro líneas tumorales que se utilizarían, así como los tiempos de duplicación de éstas.

Las líneas celulares que se utilizaron para estos experimentos fueron:

- HeLa: células de adenocarcinoma cérvico-uterino
- A-549: células de carcinoma de pulmón
- SK-BR-3: células de adenocarcinoma de seno
- HT-29: células de adenocarcinoma de colon

Para la determinación de la linearidad entre el número de células viables y la absorbancia leída, distintas concentraciones de cada una de las líneas celulares fueron sembradas en los pocillos de la placa, entre un rango de 2,000 células por pocillo hasta 40,000 células por pocillo. Después de transcurridas 8 horas de la siembra y antes de que la replicación celular tuviese lugar se realizó el ensayo de MTT. La graficación de los resultados muestra claramente una relación lineal entre el número de células y la absorbancia en las concentraciones celulares más pequeñas. Sin embargo, conforme aumenta el número de células por pocillo se llega a una saturación en la señal de absorbancia, que es cuando la medición ya no corresponderá con el número real de células viables.

Los límites de detección obtenidos en este estudio se detallan en la Tabla 1. Estos resultados correlacionan el número de células viables por pocillo (en una placa de 96 pocillos) con respecto a la absorbancia obtenida a dos longitudes de onda distintas para las cuatro líneas tumorales ensayadas.

|        | células HeLa | células A-549 | células SK-BR-3 | células HT-29 |
|--------|--------------|---------------|-----------------|---------------|
| 570 nm | 10,000       | 10,000        | 14,000          | 22,000        |
| 630 nm | 20,000       | 18,000        | 18,000          | 26,000        |

**Tabla 1.** Límites de detección para las cuatro líneas celulares ensayadas.

El número de células óptimo a sembrar para la realización del experimento depende del nivel de actividad mitocondrial de cada línea celular, así como de su velocidad de proliferación. Para prevenir una saturación de crecimiento durante la realización del ensayo se tiene que determinar el tiempo que tarda cada línea celular para iniciar su fase exponencial de crecimiento, pues es en este momento cuando se tiene que añadir el compuesto a ensayar, así como el tiempo que le toma a las células sembradas el alcanzar su pico máximo de crecimiento, que es cuando la saturación en confluencia detiene su proliferación.

Para determinar el inicio y duración de la fase exponencial de crecimiento de las líneas celulares, se sembraron siete placas con cuatro concentraciones distintas (2500, 5000, 7500 y 10000 células por pocillo) y se realizaron los siete ensayos de MTT en días consecutivos para llevar un conteo de la viabilidad celular. A aquellas células que permanecieron sembradas durante más de dos días se les realizó un cambio de medio cada tercer día para evitar la muerte celular por falta de nutrientes y la disminución del pH causada por el propio metabolismo de las células.

Después de la recogida y análisis de los datos obtenidos en este segundo estudio, se obtuvieron las correspondientes curvas de crecimiento para las cuatro líneas celulares. De esta manera se pudo calcular la fase logarítmica de crecimiento, así como los días que tarda cada una de las líneas celulares en llegar a los límites de linearidad para el experimento, así como el tiempo en el que su crecimiento se detiene al llegar a un máximo de confluencia.

Las conclusiones de los dos estudios realizados se detallan en la Tabla 2, donde se exponen las mejores condiciones experimentales para la realización de los ensayos de MTT.

| CÉLULAS        | Número de células a sembrar en placa de 96 pocillos | Horas necesarias para una total adhesión a la placa | Número máximo de horas para iniciar el ensayo después de la siembra |
|----------------|---|---|---|
| <b>HeLa</b>    | 2500  | 12  | 45  |
| <b>A-549</b>   | 2500  | 12  | 45  |
| <b>SK-BR-3</b> | 5000  | 12  | 69  |
| <b>HT-29</b>   | 5000  | 12  | 69  |

**Tabla 2.** Condiciones para los ensayos de MTT

También se determinó el tiempo de duplicación de cada línea celular, una vez en etapa de crecimiento exponencial. Este dato es importante puesto que se requiere exponer a las células el tiempo equivalente a 1 o 2 replicaciones celulares para evaluar correctamente el efecto de los compuestos sobre la duplicación de las mismas.

Después de un conteo diario de siete cultivos diferentes, se estableció un tiempo de replicación de 17 horas para las células HeLa, 30 horas para A-549, 35 horas para SK-BR-3 y 23 horas

para HT-29. Por lo tanto, se estableció un tiempo de exposición a los compuestos de 24 horas para las células HeLa y HT-29, y 35 horas para A-549 y SK-BR-3.

Finalmente, y después de los estudios exhaustivos para el establecimiento de las condiciones experimentales para la evaluación *in vitro* de las propiedades citotóxicas de los compuestos sintetizados, los correspondientes ensayos de MTT fueron realizados con distintas concentraciones de los péptidos unidos a quinoxalinas RZ1-RZ12 y los valores de la concentración requerida para inhibir el crecimiento celular en un 50% fueron determinados a partir de las curvas de dosis-respuesta que se obtuvieron.

La triostina A sintetizada se utilizó como control positivo. Sin embargo, algunos compuestos resultaron ser más activos que el compuesto natural, por lo que se agregó un segundo control positivo al experimento: la doxorrubicina.

Los resultados obtenidos se muestran en la Tabla 3:

| Compuesto     | IC <sub>50</sub> , $\mu\text{M}$ |             |            |            |
|---------------|----------------------------------|-------------|------------|------------|
|               | HeLa                             | A-549       | SK-BR-3    | HT-29      |
| RZ1           | 42.2                             | 51.2        | 96.7       | 88.4       |
| <b>RZ2</b>    | <b>2.7</b>                       | <b>11.9</b> | <b>5.4</b> | <b>6.8</b> |
| RZ3           | 93.8                             | 65.8        | 98.1       | 72.3       |
| RZ4           | 30.9                             | 34.9        | >100       | 75.0       |
| RZ5           | >100                             | 70.7        | 84.6       | 84.8       |
| RZ6           | 45.6                             | 84.5        | 55.3       | 83.1       |
| RZ7           | 84.5                             | 72.8        | >100       | 90.7       |
| RZ8           | 37.1                             | 23.4        | 44.5       | 39.8       |
| RZ9           | 50.9                             | 60.9        | 90.6       | 84.4       |
| RZ10          | 14.1                             | 26.8        | 62.1       | 53.8       |
| RZ11          | 24.3                             | 96.3        | 78.9       | 64.7       |
| RZ12          | 55.4                             | 82.2        | 71.6       | >100       |
| Triostina A   | 18.8                             | 23.5        | 23.1       | 24.7       |
| Doxorrubicina | 5.4                              | 0.6         | 0.5        | 8.9        |

**Tabla 3.** Actividades citotóxicas de la librería RZ1-RZ12.

El compuesto más activo resultó ser RZ2, con concentraciones inhibitorias del crecimiento de las cuatro líneas celulares de muy pocos micromoles. Lo más destacable de este dato es que el objetivo principal de la presente Tesis Doctoral se había cumplido: se obtuvo un análogo de la triostina A con una estructura química mucho más sencilla, lo cual facilita el escalado de la síntesis para la obtención de mayor cantidad de producto a un coste económico y temporal mucho menor.

Para evaluar la posibilidad de que el compuesto RZ2 ejerciera su actividad citotóxica sobre las células tumorales de manera selectiva, sin afectar a células normales, también se realizó un ensayo de MTT utilizando células endoteliales humanas. Desafortunadamente se observó el mismo efecto citotóxico en las células sanas, tal y como pasa con la doxorrubicina. Este resultado era de esperar, dado que los bisintercaladores se unen al material genético de todas

las células y la única manera por la que muestran cierta afinidad por las células tumorales es la rápida replicación celular que las caracteriza, lo que exige mayor duplicación de ADN y favorece mayor rango de intercalación de estos compuestos.

También se evaluó la actividad antitumoral de los péptidos Z1-Z12, es decir, las mismas estructuras peptídicas correspondientes a la librería RZ1-RZ12, pero sin las quinoxalinas. Ninguno de los péptidos resultó citotóxico, ni siquiera a las concentraciones más elevadas. Este resultado corrobora la importancia de las entidades quinoxalínicas en la estructura de los compuestos sintetizados, ya que son las responsables de la actividad biológica. Sin embargo, el hecho de que la citotoxicidad de los compuestos varía aunque las diferencias estructurales entre ellos no son muy grandes, sugiere que la entidad peptídica también posee un rol de importancia en la citotoxicidad de los compuestos, probablemente facilitando el reconocimiento entre el compuesto y la diana terapéutica.

A pesar de que los compuestos RZV13, RZV14 y RZV15 fueron sintetizados con la intención de mejorar la actividad antitumoral mostrada por el compuesto RZ2, ninguno de los tres resultó ser citotóxico. De nuevo, este resultado corrobora que las quinoxalinas no son las únicas partes estructurales de los compuestos que determinan la actividad biológica.

También se evaluó la actividad antitumoral de las tres versiones fluorescentes del compuesto RZ2, utilizando sólo la línea tumoral HeLa. Dado que la 5-carboxifluoresceína es una molécula relativamente grande si se compara con el tamaño del péptido, la unión de ésta podría ocasionar un cambio importante en la disposición espacial del compuesto, pudiendo provocar la pérdida de la actividad biológica, por lo que su uso en microscopía confocal no nos daría un resultado comparable a lo que pasaría en el caso de RZ2.

Afortunadamente, las tres versiones sintetizadas resultaron citotóxicas frente a las células empleadas, aunque el compuesto más activo fue RZ2CF, con una actividad muy parecida al compuesto RZ2. Por lo tanto, éste fue el compuesto que se decidió utilizar en los estudios de microscopía.

Dado que el compuesto RZ2 no posee *N*-metilaciones y la D-Pro que forma el giro  $\beta$  es el único D-aminoácido en su estructura, se temía que el péptido fuese tendiente a una rápida degradación enzimática causada por las exopeptidasas en condiciones biológicas.

Se evaluó la estabilidad de RZ2 en suero humano a 1, 3, 6, 24 y 48 horas. Sorprendentemente, sólo un 14% del péptido se degradó a las 24 horas y un 30% a las 48 horas.

Además, se evaluó la estabilidad del mismo compuesto frente a dos proteasas que están sobreexpresadas en células tumorales: la catepsina B y la MMP2. La primera se encuentra tanto a nivel extracelular como intracelular, donde se localiza principalmente en los

compartimentos endosomales y lisosomales. La MMP2 se localiza en la superficie celular de muchas células tumorales y en las células endoteliales características de la microvascularización tumoral. De nuevo, RZ2 resultó ser muy estable a la degradación causada por estas dos enzimas, de tal manera que el compuesto sintetizado parece poseer una estabilidad proteolítica *in vivo* notable y atípica.

El gran inconveniente del compuesto RZ2 es su baja solubilidad en medios acuosos, lo que provoca que, a muy altas concentraciones, se precipite en el medio celular. Esto provoca que las células no estén expuestas a la concentración de compuesto que se agrega en el ensayo de citotoxicidad, dado que el compuesto en suspensión no logra entrar a las células, por lo que no ejerce su efecto con la respuesta esperada. Es por ello, que aunque se aumentara la concentración de compuesto, nunca se llegaba a obtener una inhibición total del crecimiento celular.

Para mejorar la probabilidad de entrada del compuesto en las células se ideó un sistema liposomal que ayudara a solubilizar al compuesto en medios acuosos. Para formar los liposomas, se utilizó fosfatidilcolina y colesterol en un radio molar 5:1, y el compuesto RZ2 se atrapó en vesículas unilamelares pequeñas.

Se evaluó la citotoxicidad de esta formulación liposomal en células de adenocarcinoma cérvico-uterino, y aunque la concentración requerida para un 50% de inhibición del crecimiento celular fue la misma que para el compuesto RZ2 *per se*, se observó una mejora notable en la solubilidad del compuesto. En este experimento se obtuvo la típica curva sigmoidal que presentan los antineoplásicos solubles, en las que se llega a un 0% de crecimiento celular a dosis altas del compuesto.

Algunos de los compuestos de la librería RZ1-RZ12 se evaluaron como posibles agentes antibacterianos en el Hospital Clínico de Barcelona. Para estos experimentos se utilizaron cuatro cepas bacterianas distintas:

- *Escherichia coli*
- *Acinetobacter baumannii*
- *Pseudomonas aeruginosa*
- *Staphylococcus aureus*

Se utilizó el método de microdilución, tal y como fue descrito por el Instituto de Estándares Clínicos y de Laboratorios. Ninguno de los compuestos resultó tener actividad antibacteriana.

También se evaluó la posible actividad antibacteriana de los péptidos Z1-Z12 utilizando *Escherichia coli*, pero ninguno de los péptidos logró inhibir el crecimiento bacteriano.

Los dos compuestos con mayor actividad citotóxica, es decir, RZ2 y RZ8, fueron enviados al departamento de química e ingeniería genética de la Universidad de Tecnología Chalmers (Suecia) para ser evaluados como antivirales. Dichos compuestos se evaluaron frente a dos virus humanos (HCoV y RSV), pero ninguno de los dos provocó alguna inhibición en la proliferación viral.

Como último ensayo biológico se evaluó la posible actividad antiparasitaria de algunos de los compuestos de la librería RZ1-RZ12. Para estos ensayos se utilizó al parásito causante de la malaria, *Plasmodium falciparum*. De nueva cuenta, el compuesto RZ2 resultó activo a concentraciones micromolares cercanas al rango nanomolar.

Con el fin de evaluar la hemocompatibilidad de RZ2, se realizaron estudios de hemólisis de glóbulos rojos humanos *ex vivo* en presencia de este compuesto y usando a la melitina como control positivo. Ni siquiera concentraciones tan altas como 100 µM del péptido unido a quinoxalinas provocó la hemólisis que se observó a muy bajas concentraciones del control. Con este experimento se demuestra que el compuesto RZ2 también podría ser un posible fármaco contra *Plasmodium* y que el tratamiento no afectaría a los glóbulos rojos.

### **Capítulo 3: Estudios sobre el Modo de Acción**

Dado que los compuestos sintetizados como parte de este proyecto son análogos simplificados del bisintercalador triostina A, se esperaba que el mecanismo de acción de las moléculas sintetizadas fuese el mismo que el del producto natural. Por ello, se realizaron distintas pruebas para corroborar la unión de los análogos al ADN.

En primera instancia se realizaron estudios de dicroísmo circular. Esta técnica es muy sensible en la detección de cambios morfológicos del material genético como producto de la interacción con algún ligando. Inclusive, los cambios observados en la banda positiva característica a 275 nm y en la banda negativa a 248 nm puede arrojar algún indicio sobre el tipo de interacción del ligando con el ADN.

Para estos experimentos se mandaron sintetizar 10 oligonucléótidos cortos de 6 o 12 bases y con una secuencia tal que formasen una doble cadena en solución.

El análisis de datos no mostró un cambio significativo en la intensidad de las bandas características antes mencionadas con ninguno de los oligos.

Posteriormente, y como parte de la estancia de investigación en el extranjero relacionada con el proyecto que se presenta en este documento, se realizaron estudios más específicos para evaluar la posible interacción de los compuestos sintetizados con el ADN.

Como experimento preliminar se marcó radioactivamente el plásmido *tyrT*, se incubó con distintas concentraciones del compuesto RZ2 y la equinomicina se usó como control positivo. Se hizo correr un gel en condiciones nativas para analizar el desplazamiento de las bandas, pero el único compuesto que causó un desplazamiento más lento del material genético fue el bisintercalador natural, mientras que las bandas del ADN que se incubó con el compuesto RZ2 migraron de manera normal, sugiriendo que este compuesto no interactúa con el ADN. Los mismos resultados negativos se obtuvieron con otros compuestos de la librería RZ1-RZ12 y con los tres compuestos RZV.

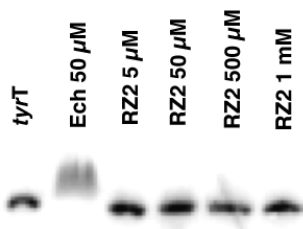


**Figura 5.** Experimento de migración de bandas de ADN. La equinomicina (Ech) se usó como control positivo.

Se evaluó entonces la posible interacción de los compuestos sintetizados utilizando la técnica de DNase I *footprinting*.

Esta técnica fue usada por vez primera en el año 1978 para estudiar la interacción entre proteínas y ADN, pero después fue adaptada como un método de identificación de interacciones específicas a secuencias determinadas de moléculas de bajo peso molecular con el ADN. Asimismo, este método también puede utilizarse para determinar la afinidad de unión y las constantes de asociación y disociación de ligandos del ADN. El *footprinting* se ha utilizado para estudiar la especificidad de unión de moléculas tales como la equinomicina, la triostina A y el TANDEM. Hoy en día, es una de las técnicas más fiables para el estudio de interacciones DNA-ligando.

En este método un fragmento de doble cadena de ADN marcado (fluorescente o radioactivamente) en uno de los extremos de una de las hebras es cortado por un agente enzimático o químico de una manera tal que cada una de las bases del ADN es cortada en sólo una ocasión; esta muestra de fragmentos del ADN se corre en un gel de poliacrilamida, obteniendo señales homogéneas y seguidas, correspondientes a los fragmentos de ADN. Sin

embargo, si aplicamos la misma metodología a una cadena de ADN que posee alguna molécula intercalada veremos un hueco (la llamada "huella") donde debería haber bandas de ADN; este hueco corresponde a las bases entre las cuales está intercalado el ligando, dado que la molécula unida al ADN impide que el agente enzimático o químico corte los enlaces entre las bases (Figura 6).

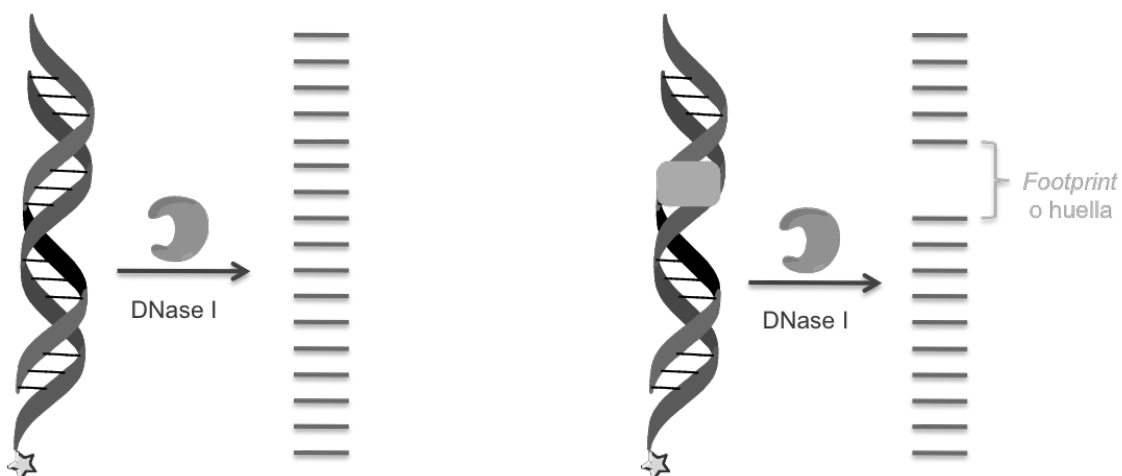


**Figura 6.** Representación esquemática del experimento de footprinting

|             |  |
|-------------|--|
| <b>MS1</b>  | 5'-CCTAGGTATACGCCGTTATGTGTACCGGCTAAAGGTTGACGTGATCAGCATCGCGTAGTTCCAATTGAGGGCAAGATAGGACCATATC<br>GTTAACCCGCACTTCTCAATACATTTCATGCAGGCCACCCAGACAAAACAGTAGAGTCGGAGCTTACGCCTAGG- 3'  |
| <b>MS2</b>  | 5'-GGATCCGCATTCGAGGCTGAGATGACAAAACAGACCCCACCGGACGTACTTACATAACTCTTCACGCCCTAATTGCTATACCAGGATAGA<br>ACGGGAGCTTAACCTTGATCGCGCTACGACTAGTGCAGTTGAAATCGGCCATGTGTATTGCCGATATGGATCC- 3' |
| <b>HexA</b> | 5'-GGATCCGGGATATCGATATGGGCCAAATTAGCTATAGATCTAGAATTCCGGACCGCGGTTAACGTTACCGTACCTAGGCCTG<br>CAGCTGCGCATGCTAGCGCTTAAGTACTAGTGCACGTGGCCATGGATCC- 3'                                 |
| <b>HexB</b> | 5'-GGATCCATGCATTAATTGAATATTGATCATGACGTCGACATGTACATATGTATATACGCGCGTACGCGTACGTAGCGCCTATAAGCTTGC<br>CAATTGCCGGCTAATTAGGGCCCTCGAGCTCGCGATGGCCGGATCC- 3'                            |

**Figura 7.** Secuencias de los sustratos universales de footprinting. Dado que todos los fragmentos se marcan en el extremo 3', sólo se muestra la hebra marcada.

No existe un agente de ruptura de ADN ideal, puesto que la DNasa I no puede romper los enlaces O3'-P de secuencias muy rígidas (regiones ricas en bases GC) o de surcos menores muy estrechos y la ruptura por radicales hidroxilo es muy laboriosa y lenta, además de que se ve afectada por la presencia de solventes orgánicos y que algunos compuestos no generan "huella" (del inglés *footprint*) usando esta metodología.

Como sustrato o muestras de ADN para el *footprinting* se utilizaron los sustratos "universales" MS1 y MS2, que contienen cada combinación de tetranucleótido posible, así como HexA y HexB, que con sus 64 hexanucléotidos simétricos distintos pueden dar una idea de la especificidad de pares de bases de casi todos los ligandos que se estudien (Figura 7).

Para el marcaje de ADN se utilizó  $^{32}\text{P}$  pues permite la detección de muy pequeñas cantidades de ADN una vez que se revela el gel, mejorando por mucho la sensibilidad de las técnicas que emplean fluorescencia.

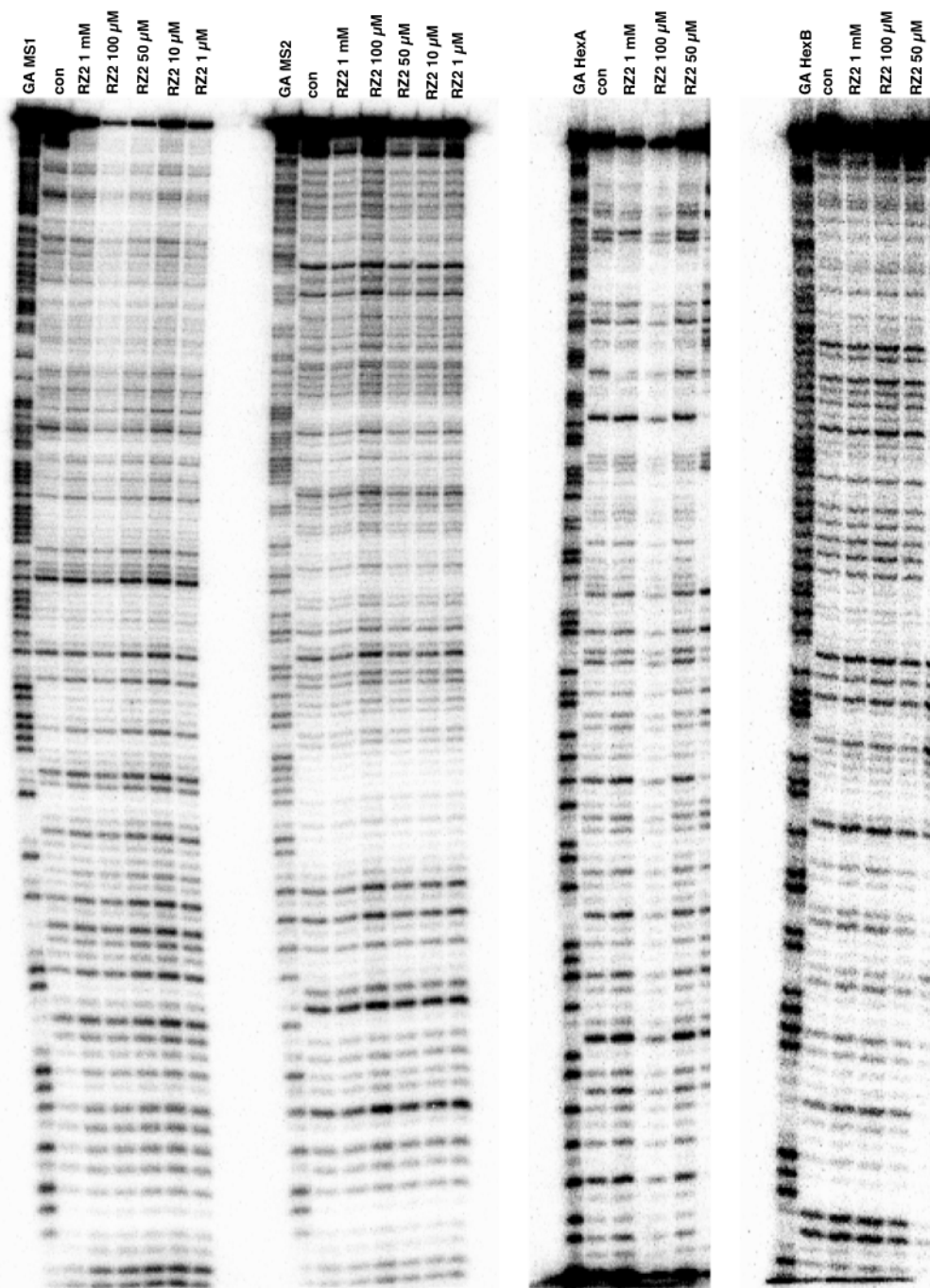


**Figura 8.** Geles de los experimentos de DNase I *footprinting* con el compuesto RZ2 usando todos los sustratos universales.

Desafortunadamente, ninguno de los análogos sintetizados generó alguna "huella" con alguno de los sustratos "universales" (Figuras 8 y 9). Dado que todos los controles positivos que se emplearon (equinomicina, triostina A, TANDEM y doxorrubicina) generaron las "huellas" o *footprints* esperadas, se puede afirmar que todos los experimentos fueron realizados de manera correcta. Por lo tanto, los resultados negativos son una clara corroboración de que los compuestos sintetizados no interaccionan con el ADN, así que su mecanismo de acción es distinto a el que exhibe la triostina A.

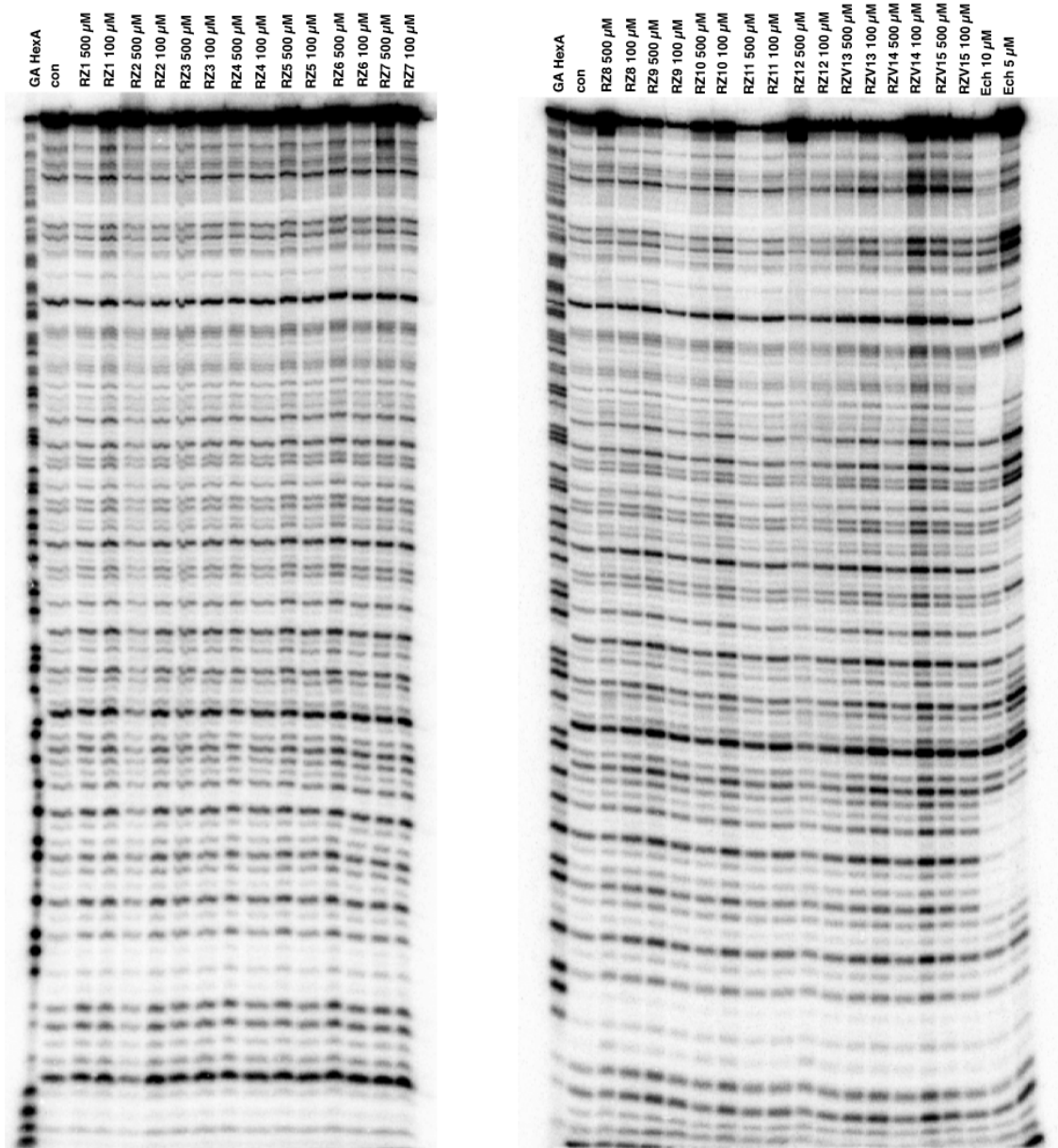


**Figura 9.** Digestión por la DNasa I del sustrato HexA en presencia de todos los compuestos sintetizados. La equinomicina fue usada como control positivo (Ech) y es el único compuesto que generó *footprints*.

Una vez obtenidos estos inesperados resultados que demuestran que los análogos de triostina A sintetizados no son bisintercaladores, se realizó un estudio conformacional del compuesto RZ2 utilizando simulaciones de dinámica molecular con el objetivo de estudiar con más detalle la conformación secundaria del péptido en medios acuosos, así como la distancia existente entre ambas quinoxalinas.

Se realizaron 5 simulaciones independientes a 298 °K. Se comenzó desde una estructura completamente abierta del péptido inmerso en una caja octahédrica de 5867 moléculas de agua.

Los resultados corroboran la formación de una lámina  $\beta$  antiparalela con un giro  $\beta$  formado entre los residuos D-Pro y Gly. El análisis también corrobora que la probabilidad de ocurrencia de esta conformación es mucho mayor que cualquier otra posible. Los confórmeros más poblados se ilustran en la Figura 10.

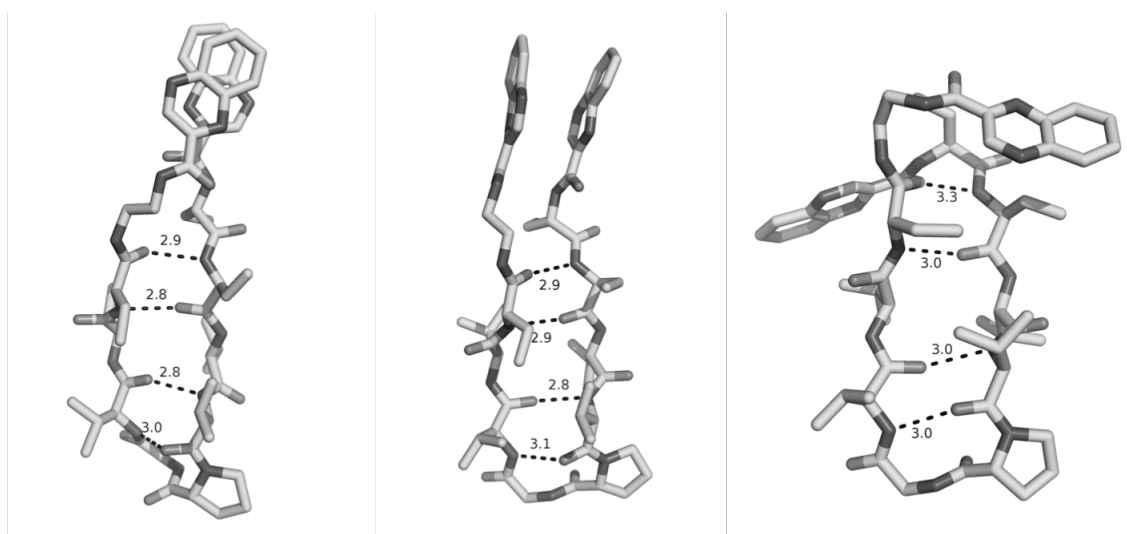


**Figura 10.** Confórmeros más poblados para el compuesto RZ2 de acuerdo a las simulaciones de dinámica molecular.

Adicionalmente, se realizaron simulaciones de intercambio de réplicas con un rango de temperaturas entre 298 °K y 310 °K. De nueva cuenta, el confórmero más poblado sigue siendo la lámina  $\beta$  antiparalela en todos los casos. Sin embargo, se observa una distancia entre los centros de ambas quinoxalinas de tan sólo 4 Å, y la tendencia de las quinoxalinas por permanecer juntas es constante en todas las simulaciones. Así, queda explicada la imposibilidad de los análogos sintetizados para bisintecalarse en el ADN, pues las quinoxalinas están demasiado juntas, si se compara con la distancia de 10.5 Å que existe entre las quinoxalinas de la triostina A. Con tan poca distancia entre los cromóforos es imposible el acomodo de los pares de bases entre ambos heterociclos.

Dado que se ha demostrado que moléculas bisintercalantes, como la tiocoralina, son también inhibidores de la topoisomerasa, se realizaron algunos ensayos con las topoisomerasas humanas I y II en presencia del compuesto RZ2, pero no se observó ningún resultado positivo significativo.

Se inició un estudio exhaustivo para determinar la vía de muerte de las células HeLa una vez que son tratadas con el compuesto más citotóxico de todos los análogos.

Primero se evaluó si RZ2 provoca necrosis por medio de dos experimentos. En el primero se evaluó la capacidad del compuesto para perturbar bicapas lipídicas, dado que éstas asemejan las membranas celulares. Para ello, se obtuvieron liposomas en los cuales se atrapó carboxifluoresceína, y éstos fueron incubados en presencia de RZ2 durante una hora, usándose melitina como control positivo. No se observó escape del fluoróforo, lo que asegura que la bicapa lipídica del liposoma permaneció intacta a pesar de la presencia del compuesto RZ2. En el segundo experimento se utilizó un sustrato fluorogénico que no puede internalizarse en células sanas; si las células sufren algún tipo de disrupción de membrana se liberan las proteasas que actúan sobre este sustrato y se genera una señal fluorescente. De manera semejante al experimento anterior, las células HeLa se incubaron con el compuesto RZ2 y con melitina como control positivo y se realizó en ensayo a distintos tiempos de incubación, desde 1 hasta 8 horas. La melitina provocó la aparición de señal fluorescente mientras que esto no se observó para el compuesto RZ2. Por lo tanto, se puede afirmar que este compuesto no ejerce su acción citotóxica por una vía necrótica.

Después se evaluó si el compuesto RZ2 provoca apoptosis en las células tumorales, y dado que no existe un único parámetro que defina al proceso apoptótico, se realizaron distintos experimentos para determinar de una manera fiable los cambios sugerentes de apoptosis.

Primero se evaluó la translocación de la fosfatidil serina en células expuestas a RZ2 durante 1, 2 y 3 días por medio del ensayo de anexina V / ioduro de propidio. Los resultados de citometría mostraron que menos del 20% de las células eran anexina V positivas después de 24 horas de tratamiento, pero a las 48 horas este porcentaje aumentó a más del 40% de las células y superó el 50% a las 72 horas.

Se evaluó también el porcentaje de fragmentación de ADN o población sub-G<sub>0/1</sub>. A las 24 horas de incubación con RZ2, menos del 5% de la población celular era sub-G<sub>0</sub>, pero a las 48 horas este porcentaje ya era mayor del 20% y a las 72 horas alcanzaba casi el 30%.

Se observó bajo el microscopio, después del marcaje nuclear con Hoechst 33528, que a las 48 horas de tratamiento las células ya presentaban fragmentación nuclear, pero este cambio no se hace evidente a las 24 horas de tratamiento.

Se realizó un ensayo para monitorear la actividad de las caspasas efectoras 3/7 por medio de la hidrólisis del sustrato fluorogénico Ac-DEVD-AFC, pero no se detectó un aumento significativo en la actividad de las DEVDasas, sino hasta después de 48 horas de tratamiento con RZ2.

También se detectaron los niveles intracelulares de caspasa 3 y PARP (otro indicador de apoptosis) por la metodología de Western blot. No se detectó un incremento significativo con respecto al control (células no tratadas) a las 24 horas de tratamiento. Sin embargo, los niveles de caspasa 3 aumentaron cerca de 25 veces a las 48 horas de tratamiento, y los niveles de PARP aumentaron 10 veces con respecto al control.

Con todos estos resultados se confirma que el compuesto RZ2 provoca apoptosis a las células HeLa, pero este proceso no se activa en primera instancia, sino que se hace evidente hasta después de 24 horas de exposición al compuesto RZ2. Entonces, la siguiente pregunta a responder fue: ¿qué pasa en las primeras 24 horas de tratamiento?

Para tratar de responder a esta incógnita, se estudió la distribución del ciclo celular en células tratadas con RZ2. Se observó un incremento significativo en la fase S, mientras que los niveles en G<sub>1</sub> disminuyeron desde el primer día de tratamiento, y los niveles en G<sub>2</sub> aumentaron a las 24 horas de incubación con RZ2, pero fueron disminuyendo para el segundo y tercer día, llegando casi a alcanzar el mismo porcentaje que al inicio del ensayo. Estos resultados sugieren que el compuesto RZ2 provoca un paro en la fase S del ciclo celular.

Se evaluaron los niveles de proteína p53 y su forma fosforilada Ser-15, pero no se observaron incrementos en su expresión, por lo que se postula que RZ2 causa apoptosis por medio de un mecanismo independiente de p53. También se demostró que el paro en el ciclo celular no se induce por la activación del gen p21.

Se estudió la implicación de la otra vía de muerte celular como respuesta a RZ2: autofagia. Para ello, se realizó la inmunodetección de las proteínas LC3 y p62. Los niveles de la primera se incrementaron más de diez veces después de 24 horas de incubación con el compuesto. Los niveles de p62 también aumentaron un poco y se mantuvieron elevados, sugiriendo un bloqueo en los siguientes pasos del proceso autófago después de la activación de LC3.

Los experimentos de microscopía confocal con el compuesto fluorescente RZ2CF y distintos marcadores fluorescentes de organelos, en particular LysoTracker Red, permitieron la colocalización del compuesto citotóxico con los organelos acídicos intracelulares, donde se hace evidente la acumulación del péptido unido a quinoxalinas.

Se evaluó si el compuesto RZ2 promueve la formación de cuerpos acídicos dentro de las células HeLa por medio de citometría de flujo. Los resultados muestran que el marcaje con Lysotracker Green casi se duplica en presencia de RZ2.

Para estudiar si RZ2 bloquea la formación de autophagolisosomas, se evaluó la expresión de LC3 por Western blot en presencia y ausencia del inhibidor de acidificación de organelos Baflomicina A<sub>1</sub> (Baf) en células tratadas con el compuesto citotóxico. Los niveles de LC3 aumentaron en presencia de Baf, por lo que se concluye que RZ2 induce la formación de autofagosomas sin bloquear la subsecuente fusión con los lisosomas.

En base al incremento observado en la expresión de p62, la resistencia de RZ2 frente a la catepsina B y la observación de que el compuesto RZ2CF se acumula en los cuerpos acídicos de la célula, se plantea que RZ2 bloquea la respuesta autofágica por una excesiva acumulación en el sistema endo/lisosomal.

Por otra parte, se estudiaron las perturbaciones en expresión de ARN de células HeLa tratadas con una baja concentración de RZ2 por medio de un microarreglo de expresión génica. El ARN fue extraído de células tratadas por 24 horas, es decir, antes de que se inicie el proceso apoptótico. Los resultados obtenidos después del análisis de datos muestran una sobreexpresión de los genes implicados en la respuesta a la innanición y en la respuesta de defensa, mientras que los genes implicados en la activación de p53 y en la activación de caspasas se expresaron menos. También se observó que muchas vías metabólicas estaban sobreexpresadas, lo que sugiere que RZ2 causa estrés metabólico a las células cancerígenas.

Finalmente, se evaluó el efecto del compuesto RZ2 en las mitocondrias, dado que son los organelos que regulan el metabolismo celular. Se observó una disminución en el potencial de membrana mitocondrial en las células tratadas con RZ2, así como una gran depolarización de las membranas mitocondriales. También se detectó una hiperproducción de aniones superóxido en las células tratadas.

El proceso de autofagia relacionado a la falta de nutrientes se asocia con un incremento en el estrés oxidativo de las células causado por el aumento de especies reactivas de oxígeno (ROS) y la liberación de citocromo c se asocia a la pérdida permanente del potencial de membrana de las mitocondrias con la subsecuente activación de caspasa 3. Por lo tanto, es muy factible que las células tumorales tratan de sobrevivir al estrés generado por la acumulación del compuesto RZ2 en los compartimentos acídicos intracelulares activando el proceso de autofagia. Sin embargo, este esfuerzo citoprotector se ve rebasado después de 24 horas y las células sufren una disfunción en la maquinaria lisosomal por el exceso de RZ2 acumulado, desencadenando la pérdida del potencial de membrana mitocondrial y a un aumento en la producción de ROS.

Entonces se da la activación de las caspasas efectoras y el proceso de muerte celular por apoptosis comienza.